

APPLICATION OF DIELECTRIC SPECTROSCOPY IN AN INDUSTRIAL BIOPROCESS
UTILIZING THE BACULOVIRUS EXPRESSION VECTOR SYSTEM

by

ALEXANDER BRIX

Diplom-Ingenieur Biotechnologie (FH), University of Applied Sciences Giessen-Friedberg,
Giessen, Germany, 2007

AN ABSTRACT OF A DISSERTATION

submitted in partial fulfillment of the requirements for the degree

DOCTOR OF PHILOSOPHY

Department of Chemical Engineering
College of Engineering

KANSAS STATE UNIVERSITY
Manhattan, Kansas

2011

Abstract

Large-scale insect cell culture utilizing the baculovirus expression vector system (BEVS) can be used to produce biopharmaceuticals such as vaccines and therapeutic proteins. Biopharmaceutical production processes are generally complex and sensitive to many process parameters and changes, but on-line monitoring in this area is relatively limited and the fundamental understanding of the intricate relationships between significant process parameters and the process outcome, especially on the multi-liter or multi-m³ scale, is rarely conclusive. Dielectric spectroscopy (DS), which is based on the frequency dependent measurement of the passive dielectric properties of materials, was applied to large-scale insect cell cultures infected with a baculovirus under low multiplicity of infection conditions to produce a recombinant protein of the virus-like particle class. DS not only allowed the qualitative monitoring of the infection and recombinant protein production process within the culture in real-time but also the detection of important culture events, e.g. the peak in baculovirus production/concentration. Additionally, DS seemed to be able to serve as a predictive tool for the overall recombinant protein yield early in the process. Partial Least Square models were successfully developed allowing monitoring of the cultures progress in terms of cell density, size, and even nutrient concentration replacing the need for discrete sampling and therefore reducing contamination risks. In summary, DS has been demonstrated to have the potential to increase bioprocess understanding and the repeatability of recombinant protein production in the BEVS but ultimately also to satisfy the increased requirements for process monitoring as delineated recently in the Process Analytical Technology initiative by the Food and Drug Administration.

APPLICATION OF DIELECTRIC SPECTROSCOPY IN AN INDUSTRIAL BIOPROCESS
UTILIZING THE BACULOVIRUS EXPRESSION VECTOR SYSTEM

by

ALEXANDER BRIX

Diplom-Ingenieur Biotechnologie (FH), University of Applied Sciences Giessen-Friedberg,
Giessen, Germany, 2007

A DISSERTATION

submitted in partial fulfillment of the requirements for the degree

DOCTOR OF PHILOSOPHY

Department of Chemical Engineering
College of Engineering

KANSAS STATE UNIVERSITY
Manhattan, Kansas

2011

Approved by:

Co-Major Professor
Peter H. Pfromm

Approved by:

Co-Major Professor
Peter Czermak

Copyright

ALEXANDER BRIX

2011

Abstract

Large-scale insect cell culture utilizing the baculovirus expression vector system (BEVS) can be used to produce biopharmaceuticals such as vaccines and therapeutic proteins. Biopharmaceutical production processes are generally complex and sensitive to many process parameters and changes, but on-line monitoring in this area is relatively limited and the fundamental understanding of the intricate relationships between significant process parameters and the process outcome, especially on the multi-liter or multi-m³ scale, is rarely conclusive. Dielectric spectroscopy (DS), which is based on the frequency dependent measurement of the passive dielectric properties of materials, was applied to large-scale insect cell cultures infected with a baculovirus under low multiplicity of infection conditions to produce a recombinant protein of the virus-like particle class. DS not only allowed the qualitative monitoring of the infection and recombinant protein production process within the culture in real-time but also the detection of important culture events, e.g. the peak in baculovirus production/concentration. Additionally, DS seemed to be able to serve as a predictive tool for the overall recombinant protein yield early in the process. Partial Least Square models were successfully developed allowing monitoring of the cultures progress in terms of cell density, size, and even nutrient concentration replacing the need for discrete sampling and therefore reducing contamination risks. In summary, DS has been demonstrated to have the potential to increase bioprocess understanding and the repeatability of recombinant protein production in the BEVS but ultimately also to satisfy the increased requirements for process monitoring as delineated recently in the Process Analytical Technology initiative by the Food and Drug Administration.

Table of Contents

Table of Contents.....	vi
List of Figures.....	ix
List of Tables.....	xix
Chapter 1 - Introduction.....	1
1.1 Research Motivation.....	1
1.2 Research Objective and Hypothesis.....	2
1.2.1 Hypothesis.....	2
1.3 Dissertation Outline.....	3
Chapter 2 - Background.....	5
2.1 The Baculovirus Expression Vector System for Recombinant Protein Production.....	6
2.2 Process Monitoring and Control.....	9
2.2.1 Methods of Monitoring.....	10
2.2.1.1 Cell and Biomass Concentration.....	10
2.2.1.2 Substrate and Metabolite Concentration.....	11
2.2.1.3 Product Concentration.....	12
2.3 Process Analytical Technology.....	12
2.4 Dielectric Spectroscopy as a Tool for Process Analytical Technology.....	13
2.4.1 Basic Theory of Dielectric Spectroscopy.....	14
2.4.1.1 Physical Principle and Applications.....	14
2.4.1.2 Mathematical Description.....	19
2.4.2 Applications.....	22
2.4.2.1 Mammalian Cell Culture.....	23
2.4.2.2 Dielectric Spectroscopy of Insect Cell Culture and Relationship to the Work Performed Here.....	24
Chapter 3 - Materials and Methods.....	27
3.1 Materials.....	27
3.1.1 Cell lines and Recombinant Baculovirus.....	27
3.1.2 Culture Medium, Antibiotics and Supplements.....	27

3.1.3	Bioreactor and Associated Instrumentation	27
3.1.4	Chemicals, Reagents and Antibodies.....	28
3.2	Creation of Sf-9 Clone Cell Working Cell Bank	29
3.3	Sf-9 Clone Cell Initiation and Scale-Up	30
3.4	Bioreactor Experiments	31
3.4.1	Bioreactor Preparation	33
3.4.2	Precultures for Cell Expansion	34
3.4.3	Infection at Low MOI.....	35
3.4.4	Medium Supplementation for Uninfected Sf-9 Clone Cell Growth	37
3.4.5	Bioreactor Decontamination and Cleaning.....	38
3.5	Dielectric Spectroscopy	38
3.6	Quantification of Medium Nutrient and Metabolite Concentrations	41
3.7	Quantification of Viable Cell Density, Cell Viability and Mean Cell Diameter	44
3.8	Quantification of Fraction of Infected Cells by Flow Cytometry.....	45
3.9	Quantification of Recombinant PCV2 ORF2 Baculovirus by Titration.....	47
3.10	Quantification of Recombinant PCV2 ORF2 Protein by ELISA	49
3.11	Error and Reproducibility Considerations	51
Chapter 4	- Results and Discussion	53
4.1	Precultures for Cell Expansion	53
4.1.1	Cell Culture Parameters	53
4.1.2	Dielectric Spectroscopy	61
4.1.3	Use of DS for Real-Time Determination of Viable Biovolume and Cell Density ...	70
4.1.4	Conclusions.....	77
4.2	Infection at Low MOI.....	80
4.2.1	Viable Cell Density, Viability and Viable Cell Diameter.....	81
4.2.2	Physiological Culture Parameters, Nutrients and Metabolites	89
4.2.3	Fraction of Infected Cells.....	96
4.2.4	Production of Recombinant PCV2 ORF2 Baculovirus	99
4.2.5	Production of Recombinant PCV2 ORF2 Protein	101
4.2.6	Dielectric Spectroscopy	106
4.2.7	Detection of Culture Events in Real-Time by Dielectric Spectroscopy	123

4.2.8	Recombinant PCV2 ORF2 Protein Yield Prediction.....	127
4.2.9	Infection Phase Modeling with Dielectric Spectroscopy Data	131
4.2.10	Conclusions.....	137
4.3	Medium Supplementation for Uninfected Sf-9 Clone Cell Growth	146
4.3.1	Conclusions.....	154
Chapter 5	- Conclusion and Outlook.....	155
References	159
Appendix A	- Composition of PCV2 ORF2 ELISA Buffers.....	173
Appendix B	- Precultures – Raw Data.....	174
Appendix C	- Precultures - Kinetics	176
Appendix D	- Infection at Low MOI - Raw Data.....	177
Appendix E	- Infection at Low MOI – Complete Plots	181
Appendix F	- Infection at Low MOI - Tests for Statistical Significance.....	197
Appendix G	- Infection at Low MOI – PLS Model Details	200
Appendix H	- Infection at Low MOI – Raw Data PLS Model Validation	210
Appendix I	- Medium Supplementation for Uninfected Sf-9 Clone Cell Cultures – Raw Data	211

List of Figures

Figure 1.1. Overall thesis structure and relationship to hypothesis.	3
Figure 2.1. Basic concept of recombinant protein production with the BEVS. The genetic code for a specific target protein, here PCV2 ORF2, is introduced into the genetic code of a recombinant baculovirus. This recombinant baculovirus is then used to infect insect cell cultures. Infected insect cells will produce both, new recombinant baculovirus and the desired target protein. Following the cell culture process itself are downstream processing and eventually formulation to make up e.g. a vaccine. The box confines the cell culture based production process itself and is in the focus of this work.	5
Figure 2.2. Observed dispersions in the permittivity(capacitance) for biological materials such as cell suspensions or tissues over a range of frequencies. Different dispersions are ascribed to specific phenomena. α : tangential flow of ions across the cell surface, β : charge build-up at the cell membrane, δ : rotation of macromolecular side-chains and bound water, γ : dipolar rotation of small molecules. From: 72.	15
Figure 2.3. Schematic representation of a cell suspension in a DS field. The highly conductive cytoplasm is surrounded by an essentially non-conductive membrane. The cell culture medium surrounding the cell is aqueous and conductive.	16
Figure 2.4. Schematic drawing of the β -dispersion observed for biological materials. The β -dispersion can be described with the characteristic parameters dielectric increment $\Delta\epsilon$, characteristic frequency f_c , and the Cole-Cole α . From: 12.	17
Figure 2.5. Capacitance ΔC , characteristic frequency f_c , and medium background capacitance C_∞ . From: 77.	18
Figure 2.6. Change of the characteristic frequency f_c with cell size. From: 5.	19
Figure 2.7. Linear correlation of $\Delta\epsilon$ with cell density for different types of cells. Here the relative permittivity is used. From: 72.	21
Figure 3.1. Schematic of Sf-9 clone cell initiation and scale-up. Cells were passaged every three days (with the exception of the initial 75 ml culture which was passaged after four days). Two of the last three 1000 ml cultures were then used for planting of 7.5 L working volume bioreactor precultures.	31

Figure 3.2. Applikon BioClave 20 L bioreactors with ADI 1030 BioController and ADI 1035 BioConsole. The red circle indicates location of the DS pre-amplifier and probe.	32
Figure 3.3. FOGALE nanotech iBiomass 465 pre-amplifier and probes. The two electrode pairs for applying the alternating electrical field and measuring resulting response are shown. Modified from: 108.....	39
Figure 3.4. Effect of cell size on β -dispersion at constant viable biovolume. Measurement in the f_c region (Biomass signal, FOGALE frequencies) ensures cell-size independent estimations of the viable biovolume. From: 108.....	40
Figure 3.5. Sensor principle of the YSI 2700 Select Biochemistry Analyzer. The substrate (or analyte) diffuses through the first polycarbonate membrane and is oxidized by an immobilized oxidase. The produced H_2O_2 diffuses through a cellulose acetate membrane and is oxidized at the platinum anode of the sensor. The resulting electron flow is linearly proportional to the analyte concentration. From: 109.....	42
Figure 4.1. Viable cell density post planting in the 13 precultures. Cells started growing without apparent lag-phase immediately post planting and reached a viable cell density of approximately 2.00×10^6 cells ml^{-1} after two days of growth. Trendline is intended to guide the eye only.	54
Figure 4.2. Mean viable cell diameter post planting in the 13 precultures. Mean viable cell diameters were around $18.00 \mu m$ but no major change was observed during the two-day growth phase and. Trendline is intended to guide the eye only.	55
Figure 4.3. Culture medium pH post planting in the 13 pre-cultures. Initial pH values ranged from approximately 6.4 to 6.5 and decreased slightly to approximately 6.3 during the two-day growth phase. Trendline is intended to guide the eye only.	56
Figure 4.4. Medium D-glucose concentration post planting in the 13 pre-cultures. Initial D-glucose concentrations were approximately 32.0 mmol L^{-1} and decreased to approximately $30.00 \text{ mmol L}^{-1}$ during the two-day growth phase. Trendline is intended to guide the eye only.	57
Figure 4.5. Medium L-glutamine concentration post planting in the 13 pre-cultures. Initial L-glutamine concentrations were usually above 5.00 mmol L^{-1} and decreased to approximately 2.00 to 3.51 mmol L^{-1} . Precultures #11 and 12 showed slightly lower	

L-glutamine concentrations because of older medium used. Trendline is intended to guide the eye only.	58
Figure 4.6. Medium L-lactate concentration post planting in the 13 pre-cultures. Initial L-lactate concentrations were slightly above 1.00 mmol L ⁻¹ and increased continuously during the two-day growth phase to approximately 2.00 mmol L ⁻¹ . Trendline is intended to guide the eye only.	59
Figure 4.7. Medium L-glutamate concentration post planting in the 13 pre-cultures. Initial concentrations were approximately 7.00 mmol L ⁻¹ and increased continuously during the two-day growth phase to approximately 8.50 mmol L ⁻¹ . Trendline is intended to guide the eye only.	60
Figure 4.8. Dielectric increment $\Delta\epsilon$ post planting in the 13 precultures. Initial values of $\Delta\epsilon$ were approximately 3.0 pF cm ⁻¹ and increased continuously during the two-day growth phase to a range from approximately 11.0 to 22.0 pF cm ⁻¹	62
Figure 4.9. Specific cell membrane capacitance C_m post planting in the 13 precultures. Values for C_m generally ranged from approximately 1.0 to 1.5 $\mu\text{F cm}^{-2}$ and did not exhibit any major changes during the two-day growth phase.	63
Figure 4.10. Characteristic frequency f_c post planting in the 13 precultures. Initial values were around 700 kHz and decreased slightly to approximately 600 kHz during the two-day growth phase. Deviations from this are generally attributed to technical issues.	64
Figure 4.11. Cole Cole α post planting in the 13 precultures. Initial values of approximately 0.10 decreased and spread slightly during the two-day growth phase to a range of approximately 0.08 to 0.10.	65
Figure 4.12. Biomass signal post planting in the 13 precultures. Initial values were approximately 1.0 pF cm ⁻¹ and continuously increased to approximately 3.0 to 6.0 pF cm ⁻¹ during the two-day growth phase.	67
Figure 4.13. Suspension conductivity σ_s post planting in the 13 precultures. Values ranged from approximately 15.3 to 15.4 mS cm ⁻¹ throughout the two-day growth phase. Spikes observed could generally be attributed to changes in the culture temperature.	68
Figure 4.14. Intracellular conductivity σ_i post planting in the 13 precultures. Values generally ranged from approximately 4.0 to 7.0 mS cm ⁻¹ during the two-day growth phase and did not exhibit major changes.	69

Figure 4.15. Linear correlation viable biovolume vs. $\Delta\varepsilon$ post planting for uninfected Sf-9 clone cells.	72
Figure 4.16. Linear correlation viable biovolume vs. Biomass signal post planting for uninfected Sf-9 clone cells.....	72
Figure 4.17. Correlation viable cell density vs. $\Delta\varepsilon$ post planting for uninfected Sf-9 clone cells.	74
Figure 4.18. Correlation viable cell density vs. Biomass signal post planting for uninfected Sf-9 clone cells.....	75
Figure 4.19. Probe/Pre-Amp set dependency of obtained correlation between $\Delta\varepsilon$ and the viable cell density. Deviations can be observed at higher cell densities of approximately 2.0×10^6 cells ml^{-1} . If cell densities are further increased, an even stronger deviation is expected.	76
Figure 4.20. Correlation viable cell density vs. $\Delta\varepsilon$ post planting.	79
Figure 4.21. Viable cell density post infection at the three different MOI compared to an uninfected control culture. Initial values were approximately 1.0×10^6 cells ml^{-1} . The viable cell density increased for up to 72 h post infection depending on the MOI. Decreasing maximum viable cell densities were observed with increasing MOI with peak values of approximately 3.0 , 2.2 , and 1.2×10^6 cells ml^{-1} for MOI 0.01, 0.10, and 1.00, respectively. Afterwards the viable cell density decreased continuously until the end of the process. Trendlines are intended to guide the eye only.	82
Figure 4.22. Cell viability post infection at the three different MOI compared to an uninfected control culture. Cell viability dropped continuously from approximately 95 % starting after at least 48 h post infection. Cell viabilities below 10 % (the defined harvest criterion) were reached after approximately 168 (MOI 1.00 and 0.10) and 192 h (MOI 0.01) post infection. Trendlines are intended to guide the eye only.	84
Figure 4.23. Mean viable cell diameter post infection at the three different MOI compared to an uninfected control culture. Mean diameters increased continuously from approximately $18.0 \mu\text{m}$ immediately post infection to up to approximately $24.0 \mu\text{m}$. The higher the MOI the faster the increase occurred and the earlier a peak was reached. Afterwards the mean diameter decreased continuously until the end of the process. Trendlines are intended to guide the eye only.	86

Figure 4.24. Viable biovolume post infection at the three different MOI compared to an uninfected control culture. Initial values were approximately $4.0 \times 10^9 \mu\text{m}^3 \text{ml}^{-1}$ and increased for up to 72 h post infection depending on the MOI. Decreasing maximum viable biovolumes were observed with increasing MOI. Afterwards the viable biovolume decreased continuously until the end of the process. Trendlines are intended to guide the eye only. 88

Figure 4.25. Culture medium pH post infection at the three different MOI compared to an uninfected control culture. Initial pH was approximately 6.3 and decreased slightly during the first 24 to 48 h post infection down to 6.2 before increasing again and peaking between 6.3 and 6.4 at 48 to 96 h post infection. Thereafter the pH decreased continuously until the end of the process. Final pH at the time of harvest values decreased with MOI. Trendlines are intended to guide the eye only. 89

Figure 4.26. Medium D-glucose concentration post infection at the three different MOI compared to an uninfected control culture. Initial concentrations were approximately 31.0 mmol L^{-1} and decreased continuously throughout the culture. Decreasing final D-glucose concentrations were found with decreasing MOI with values ranging from approximately 25.0 to 15.0 mmol L^{-1} . Trendlines are intended to guide the eye only. 91

Figure 4.27. Medium L-glutamine concentration post infection at the three different MOI compared to an uninfected control culture. Initial concentrations were approximately 4.5 mmol L^{-1} and decreased continuously throughout the culture. Depletion of this nutrient was assumed to have occurred approximately between 48 and 72 h post infection, depending on the MOI. The detection limit for this analysis is approximately 0.7 mmol L^{-1} and therefore no concentrations below this level could reliably measured. Trendlines are intended to guide the eye only. 92

Figure 4.28. Medium L-lactate concentration post infection at the three different MOI compared to an uninfected control culture. Initial concentrations were approximately 1.5 mmol L^{-1} and increased to up to approximately 2.5 mmol L^{-1} during the first 24 to 48 h post infection. This was followed by a decrease lasting until approximately 72 to 96 h post infection and another subsequent continuous increase until the end of the process. A lower MOI seems to cause a higher final L-lactate concentration. Trendlines are intended to guide the eye only. 94

Figure 4.29. Medium L-glutamate concentration post infection at the three different MOI compared to an uninfected control culture. Initial concentrations were approximately 8.0 mmol L^{-1} and increased to up to approximately 9.0 mmol L^{-1} until the end of the process for MOI 0.10 and 1.00. Cultures infected at MOI showed a slightly different profile with a slight decrease in L-glutamate during the first 24 h post infection before another increase and decrease up to 120 h post infection. Afterwards the L-glutamate concentration increased continuously until the end of the process and reached comparable levels to cultures infected at MOI 0.10 and 1.00. Trendlines are intended to guide the eye only. 95

Figure 4.30. Fraction of infected cells post infection at the three different MOI. A higher initial MOI resulted in faster infection kinetics and eventually earlier complete infection of the culture at approximately 48 to 72 h post infection. 97

Figure 4.31. Comparison of theoretical Poisson model vs. experimental and literature data for the fraction of infected cells at 24 hours post infection (primary infection). Experimental data from this work is comparable to the theoretical model as well as literature. 98

Figure 4.32. Recombinant PCV2 ORF2 baculovirus concentration post infection at the three different MOI. A higher initial MOI resulted in earlier recombinant PCV2 ORF2 baculovirus production. Maximum concentrations were reached at different times ranging from approximately 48 to 96 for all MOI at approximately $8.0 \log_{10} \text{ TCID}_{50} \text{ ml}^{-1}$. Trendlines are intended to guide the eye only. 100

Figure 4.33. Recombinant PCV2 ORF2 protein concentrations post infection at the three different MOI. A higher initial MOI resulted in earlier recombinant PCV2 ORF2 protein production. Maximum concentrations were generally reached at the end of the process. Infection at all MOI was capable of producing PCV2 ORF2 protein at a volumetric yield of approximately 4.0 RP after 168 to 216 h post infection but variability increased greatly with decreasing MOI (see Appendix E -). Trendlines are intended to guide the eye only. 102

Figure 4.34. Dependency of harvest recombinant PCV2 ORF2 protein concentration on MOI. Variability in the harvest PCV2 ORF2 concentration decreased greatly with increasing MOI. Values shown are mean \pm standard deviation based on the three replicates performed at each MOI. 103

Figure 4.35. Dependency of the specific recombinant PCV2 ORF2 protein productivity per observed maximum viable biovolume on MOI. Mean specific yields were approximately

2.5 times higher at MOI 1.00 than at 0.01. Values shown are mean \pm standard deviation based on the three replicates performed at each MOI.....	104
Figure 4.36. Dependency of the specific recombinant PCV2 ORF2 protein productivity per observed maximum viable cell density on MOI. Mean specific yields were approximately 3 times higher at MOI 1.00 than at 0.01. Values shown are mean \pm standard deviation based on the three replicates performed at each MOI.....	105
Figure 4.37. Dielectric increment $\Delta\epsilon$ post infection at the three different MOI. $\Delta\epsilon$ increased immediately post infection from below 10.0 pF cm ⁻¹ to values as high as approximately 55.0 pF cm ⁻¹ after approximately 48 to 72 h post infection. Highest peak values were generally reached at MOI 0.10 but the time of the peak was delayed with decreasing MOI. $\Delta\epsilon$ decreased continuously afterwards until the end of the process.....	107
Figure 4.38. Specific membrane capacitance C_m post infection at the three different MOI. Values ranged from approximately 0.6 to 2.0 $\mu\text{F cm}^{-2}$ during the first 120 h post infection but did not show any distinct differences at different MOI. Late in the process, some cultures showed strong increases in C_m but it remains unclear if this is indeed a true representation of the reality.	108
Figure 4.39. Characteristic frequency f_c post infection at the three different MOI. f_c generally decreased slightly from approximately 600 kHz during the first 48 to 72 h post infection and was followed by another subsequent increase once a local minimum had been reached. The time of the minimum was delayed with decreasing MOI and different absolute minimum values were reached. Some of the cultures showed another strong increase in f_c late in the process but the exact reason for this remains unknown.....	111
Figure 4.40. Suspension conductivity σ_s post infection at the three different MOI. Initial values measured for σ_s were approximately 15.4 mS cm ⁻¹ and generally decreased post infection until a minimum was reached at approximately 72 to 84 h post infection. This was followed by an increase in σ_s until the end of the process.	113
Figure 4.41. Intracellular conductivity σ_i post infection at the three different MOI. Initial values determined for σ_i ranged from approximately 3.0 to 5.0 mS cm ⁻¹ but no major changes were observed during the first 72 h post infection. Late in the process, some cultures showed strong increases in σ_i but it remains unclear if this is indeed a true representation of the reality.	114

Figure 4.42. Cole-Cole α post infection at the three different MOI. α decreased immediately post infection from slightly below 0.10 to approximately 0.80 during the first 24 to 36 h post infection for all MOI. Afterwards a strong increase up to approximately 0.11 between 54 to 84 h post infection was detected which generally occurred the earlier the higher the MOI. Afterwards α first decreased again, which was followed by another increase up to a local peak. Thereafter α eventually continuously decreased until the end of the process. 116

Figure 4.43. Biomass signal post infection at the three different MOI. The Biomass signal increased immediately post infection from approximately 2.5 pF cm⁻¹ up to a maximum value of approximately 12.0 pF cm⁻¹. Generally, decreasing maximum Biomass signals were observed for increasing MOI and the peak occurred earlier. Distinct plateau phases could be observed in especially the MOI 0.01 culture. After the respective peak, the Biomass signal decreased continuously until the end of the process..... 118

Figure 4.44. Linear correlation viable biovolume vs. $\Delta\epsilon$ post infection. 121

Figure 4.45. Linear correlation viable biovolume vs. Biomass signal post infection. 121

Figure 4.46. Comparison of $\Delta\epsilon$ with the time of complete infection in the culture at the three different MOI. Complete infection was detected around the peak in $\Delta\epsilon$ and is indicated by the red vertical lines. 124

Figure 4.47. Comparison of Biomass Signal with the time of peak recombinant baculovirus concentration at the three MOI. The peak in recombinant baculovirus concentration was achieved at approximately the occurrence of the peak in the Biomass signal and is indicated by the red vertical lines. 125

Figure 4.48. Correlation specific recombinant PCV2 ORF2 yield vs. specific Biomass signal at the time of signal peak based on viable biovolume. 128

Figure 4.49. Correlation specific recombinant PCV2 ORF2 yield vs. specific Biomass signal at the time of signal peak based on viable cell density. 128

Figure 4.50. Model validation for volume fraction of viable cells P. 134

Figure 4.51. Model validation for viable cell density. 134

Figure 4.52. Model validation for average cell diameter. 135

Figure 4.53. Model validation for medium glutamine concentration. 135

Figure 4.54. Viable cell density post infection at the three different MOI compared to an uninfected control culture. Initial values were approximately 1.0 x 10⁶ cells ml⁻¹. The viable

cell density increased for up to 72 h post infection depending on the MOI. Decreasing maximum viable cell densities were observed with increasing MOI with peak values of approximately $3.0, 2.2,$ and 1.2×10^6 cells ml^{-1} for MOI 0.01, 0.10, and 1.00, respectively. Afterwards the viable cell density decreased continuously until the end of the process.

Trendlines are intended to guide the eye only.	138
Figure 4.55. Fraction of infected cells post infection at the three different MOI. A higher initial MOI resulted in faster infection kinetics and eventually earlier complete infection of the culture at approximately 48 to 72 h post infection. Trendlines are intended to guide the eye only.	139
Figure 4.56. Dependency of harvest recombinant PCV2 ORF2 protein concentration on MOI. Variability in the harvest PCV2 ORF2 concentration decreased greatly with increasing MOI. Values shown are mean \pm standard deviation based on the three replicates performed at each MOI.....	140
Figure 4.57. Dependency of the specific recombinant PCV2 ORF2 protein productivity per observed maximum viable cell density on MOI. Mean specific yields were approximately 3 times higher at MOI 1.00 than at 0.01. Values shown are mean \pm standard deviation based on the three replicates performed at each MOI.	141
Figure 4.58. Comparison of Biomass Signal with the time of peak recombinant baculovirus concentration at the three MOI. The peak in recombinant baculovirus concentration was achieved at approximately the occurrence of the peak in the Biomass signal and is indicated by the red vertical lines.	142
Figure 4.59. Correlation specific recombinant PCV2 ORF2 yield vs. specific Biomass signal at the time of signal peak based on viable cell density.	143
Figure 4.60. Model validation for volume fraction of viable cells P.	144
Figure 4.61. Model validation for average cell diameter.	144
Figure 4.62. $\Delta\epsilon$ and Biomass signal from the uninfected control culture in the low MOI study. The first plateau occurred at approximately the same time L-glutamine was depleted in the culture medium.	147
Figure 4.63. Comparison of the Biomass signal for a L-glutamine supplemented culture with a control culture without any supplementation. The supplemented culture does not show the same plateau phase as the control culture around 48 h post planting.	149

Figure 4.64. Comparison of $\Delta\epsilon$ for a L-glutamine supplemented culture with a control culture without any supplementation.	150
Figure 4.65. Comparison of the viable cell density for an L-glutamine supplemented culture with a control culture without any supplementation. The supplemented culture shows increased cell growth reaching an approximately 45 % higher maximum viable cell density at 72 h post planting. Trendlines are intended to guide the eye only.	151
Figure 4.66. Schematic of a proposed feed-rate control based on DS measurements in-line of a bioreactor.	153
Figure 5.1. Comparison of Biomass signals for a supplemented infected culture (MOI 0.10, L-glutamine and L-cystein supplementation) with a control culture without any supplementation. The supplemented culture seems to be extended slightly and exhibits a higher Biomass signal peak.	157
Figure E.1. Viable cell density post infection.	181
Figure E.2. Viability post infection.	182
Figure E.3. Mean viable cell diameter post infection.	183
Figure E.4. Viable biovolume post infection.	184
Figure E.5. pH post infection.	185
Figure E.6. D-glucose post infection.	186
Figure E.7. L-glutamine post infection.	187
Figure E.8. L-lactate post infection.	188
Figure E.9. L-glutamate post infection.	189
Figure E.10. Fraction of infected cells post infection.	190
Figure E.11. Recombinant PCV2 ORF2 baculovirus concentration post infection.	191
Figure E.12. Recombinant PCV2 ORF2 protein concentration post infection.	192
Figure E.13. $\Delta\epsilon$ post infection.	193
Figure E.14. f_c post infection.	194
Figure E.15. Cole-Cole α post infection.	195
Figure E.16. Biomass signal post infection.	196

List of Tables

Table 3.1. Bioreactor dimensions and controller set-points.	32
Table 3.2. Overview of performed low MOI experiments and utilized precultures.	36
Table 3.3 Vi-CELL XR “cell type” settings used in this work. “Sf-9 clone” settings were used for uninfected cells and until day 5 post infection. Afterwards “Sf-9 clone low viability” was used.	45
Table 3.4. EPICS-XL settings for the fluorescence channels used in this work.	46
Table 4.1. Summary of the measured cell culture parameters for uninfected Sf-9 clone cell growth in precultures. Given are mean values \pm one standard deviation.	61
Table 4.2. Pearson correlation coefficients for viable biovolume and dielectric spectroscopy signals of uninfected Sf-9 clone cells.	71
Table 4.3. Pearson correlation coefficients for viable cell density and dielectric spectroscopy signals for uninfected Sf-9 clone cells.	73
Table 4.4. Summary of the measured cell culture parameters for uninfected Sf-9 clone cell growth in precultures. Given are mean values \pm one standard deviation.	78
Table 4.5. Overview of performed Low MOI experiments and utilized precultures.	81
Table 4.6. Pearson correlation coefficients for viable biovolume and dielectric spectroscopy signals in infected cultures.	120
Table 4.7. Performance of calibration models.	132
Table 4.8. Model predictive power (RMSEP).	136
Table 4.9. Model predictive power (RMSEP).	145
Table B.1. Raw data precultures – off-line analyses.	174
Table B.2. Raw data precultures – dielectric spectroscopy.	175
Table C.1. Kinetics precultures.	176
Table D.1. Raw data infection at low MOI – off-line analyses (1 of 2).	177
Table D.2. Raw data infection at low MOI – off-line analyses (2 of 2).	178
Table D.3. Raw data infection at low MOI – dielectric spectroscopy (1 of 2).	179
Table D.4. Raw data infection at low MOI – dielectric spectroscopy (2 of 2).	180
Table F.1. t-test for parameter RP.	197
Table F.2. t-test for parameter specific RP per viable biovolume.	198

Table F.3. t-test for parameter specific RP per viable cell.....	199
Table H.1. Raw data PLS model validation – off-line analyses.	210
Table H.2. Raw data PLS model validation – dielectric spectroscopy.	210
Table I.1. Raw data medium supplementation for uninfected Sf-9 clone cell cultures – off-line analyses.	211
Table I.2. Raw data medium supplementation for uninfected Sf-9 clone cell cultures – dielectric spectroscopy.....	211

Chapter 1 - Introduction

1.1 Research Motivation

The baculovirus expression vector system (BEVS) is widely used for the production of recombinant proteins ranging from antibodies over enzymes to virus like particles (VLP)¹. VLP can be used as active agents in vaccines since they are generally immunostimulating but non-pathogenic in the target host. Biopharmaceutical production processes are generally complex and sensitive to many process parameters and changes. On-line monitoring in this area is relatively limited and the fundamental understanding of the intricate relationships between significant process parameters and the process outcome especially on the multi-liter or multi-m³ is rarely conclusive. In 2004, the Food and Drug Administration (FDA) introduced the Process Analytical Technology (PAT) initiative to tackle this problem². Described as a tool for designing, analyzing, and controlling processes through timely measurements of critical parameters to ensure the final product quality, it introduced more stringent requirements for bioprocess monitoring and control.

Dielectric spectroscopy (DS), which is based on the frequency dependent measurement of the passive dielectric properties of materials, has been suggested as a technique supporting the PAT goals^{3,4}. Initial application of DS in bioprocessing was mainly in the brewing industry but the technique is emerging as a useful tool in biopharmaceutical research and production for both, adherent and suspended cells⁵⁻¹¹. DS is usually used to monitor the viable cell density on-line but could potentially also provide more insight into more intricate properties like the physiological state of the cells⁵. The possible use of DS as an on-line tool to gain insight into intricate processes of a cell culture infected by a virus and producing a recombinant protein are subject of the work presented here.

For the specific case of application of DS in insect cell cultures and the BEVS only a few reports can be found in the literature¹¹⁻¹⁵. Because of instrument limitations, frequency scanning was not applied until recently and only limited use of the obtained spectra was prevalent. Maybe most importantly reports of monitoring of infected insect cells generally focused on synchronous infections at a high virus to cell ratio (multiplicity of infection, MOI). This is usually not preferred in the large scale BEVS processes due to the large amount of costly virus seed

required. The focus on high MOI potentially leads to deviations between laboratory work and industrial processes due to the significant impact of small changes in parameters like cell to virus ratio or the time of infection¹. There is also only limited data available that links the obtained DS data to the cell's physiological state, the infection progress, and parameters like the medium nutrient limitations. The work presented here attempts to advance the DS technique towards monitoring of large-scale cell culture of insect cells under low MOI conditions exploring not only the current state of the culture but attempting to predict the success of product formation already at an early stage.

1.2 Research Objective and Hypothesis

This PhD research project focused on the application of DS in an industrial bioprocess at the multi-liter bioreactor scale utilizing the BEVS to produce a recombinant protein of the VLP class that serves as the immunostimulating agent in a vaccine. Monitoring the process with the DS and connecting the DS data with information gathered by off-line analyses will advance the understanding of the processes itself and its potential deviations in the low MOI range. This will be accomplished by utilizing a newly developed DS instrument specialized for the use in the biopharmaceutical field together with a range of analyses performed off-line to quantify key bioprocess parameters. It is anticipated that this will allow the application of DS on-line on a routine basis in industrial scale bioprocesses based on the BEVS to not only follow the process and detect important events but also identify deviations from the normal and their causes and even to supply predictive capability for the success or failure of a given batch cell culture. Eventually DS along with the information derived in this work will contribute to satisfy the increased requirements for on-line process monitoring as delineated in the PAT initiative by the FDA.

1.2.1 Hypothesis

The data from dielectric spectroscopy applied on-line to large scale insect cell cultures infected with a baculovirus to produce recombinant protein can give real time information on the physiological state of the culture, and ultimately can be used to predict future success or failure of the intricate culture/infection/protein expression process at low initial multiplicities of infection.

1.3 Dissertation Outline

A roadmap to the work presented here and the relation to the hypothesis is given in Figure 1.1. The need for a reproducible cell culture system that can then be interrogated via DS requires a significant ramp-up. This is reflected in a substantial amount of work that was done prior to applying DS to cell cultures to support the hypothesis (above).

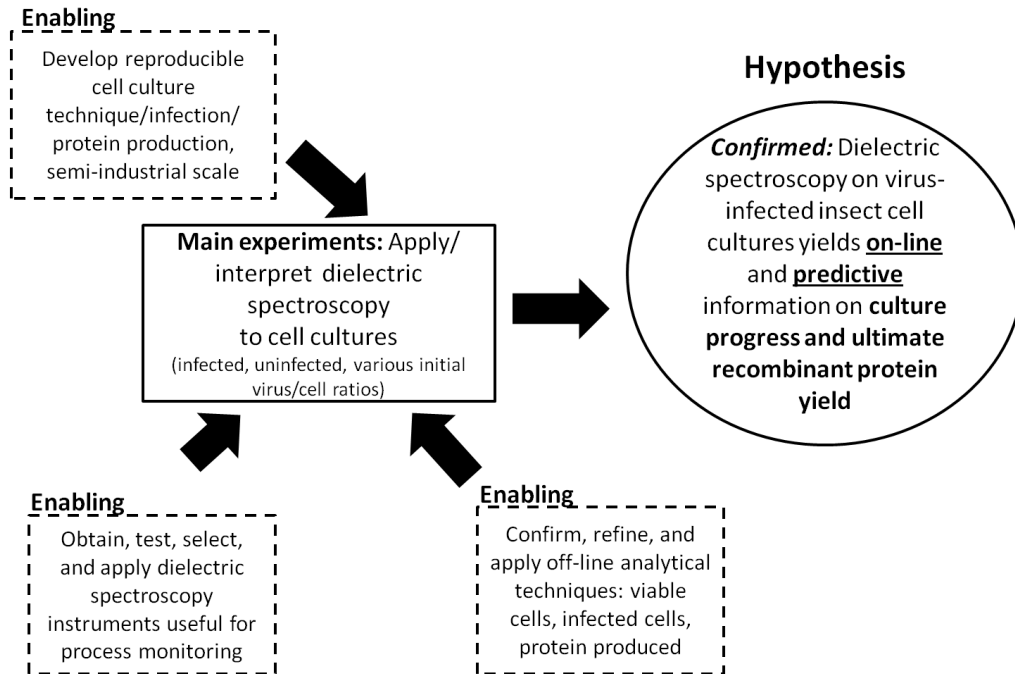


Figure 1.1. Overall thesis structure and relationship to hypothesis.

Chapter 2 describes the use of the baculovirus expression vector system for the production of recombinant proteins and highlights properties, advantages, and challenges. In addition it introduces the reader to the concept of virus like particles as an immunostimulating agent in vaccines. A short summary of the properties of the porcine circovirus type 2 and its associated diseases and impact in the swine producing industry is given. The chapter also explains the need for process monitoring and control in biopharmaceutical processes and the new emerging concept of process analytical technology as introduced by the Food and Drug Administration. Dielectric Spectroscopy is presented as a tool with capabilities supporting the PAT initiative and the basic theory of DS is described. Additionally the current applications in

the cell culture technology in both research and industry is summarized for both, mammalian and insect cell cultures.

Chapter 3 presents the materials and methods. Methods range from insect cell culture initiation and scale up to several off-line analyses performed for bioreactor samples. The different types of studies performed at the multi-liter bioreactor scale are also presented including preparation and post process decontamination and cleaning. The use and configuration of the dielectric spectroscopy instrument and probes is presented.

Chapter 4 shows results obtained from the different dielectric spectroscopy studies performed at the multi-liter bioreactor scale. The DS data is related to the off-line methods. Based on these results different potential applications of the dielectric spectroscopy in the industrial scale routine production of recombinant proteins utilizing the baculovirus expression vector system are presented.

Chapter 5 summarizes the major findings and gives an outlook on potential research in this field to foster deeper understanding of the dielectric spectroscopy in the BEVS and its promising applications in the industry.

Chapter 2 - Background

The large-scale production of biologically potent materials such as vaccines is perhaps one of the most challenging frontiers for biochemical engineering. The requirements for consistency and purity of the product that is to be injected directly into the tissue or bloodstream of a human or animal are exceptional due to the potentially catastrophic outcome should the material be of unreliable potency, or should it contain undesirable components. The basic concept of a cell culture based vaccine production system that relies on a virus to import the genetic information for production of a target particle (recombinant protein in this work) into the living insect cell is shown in Figure 2.1. The specific system used in this work will be described in detail below.

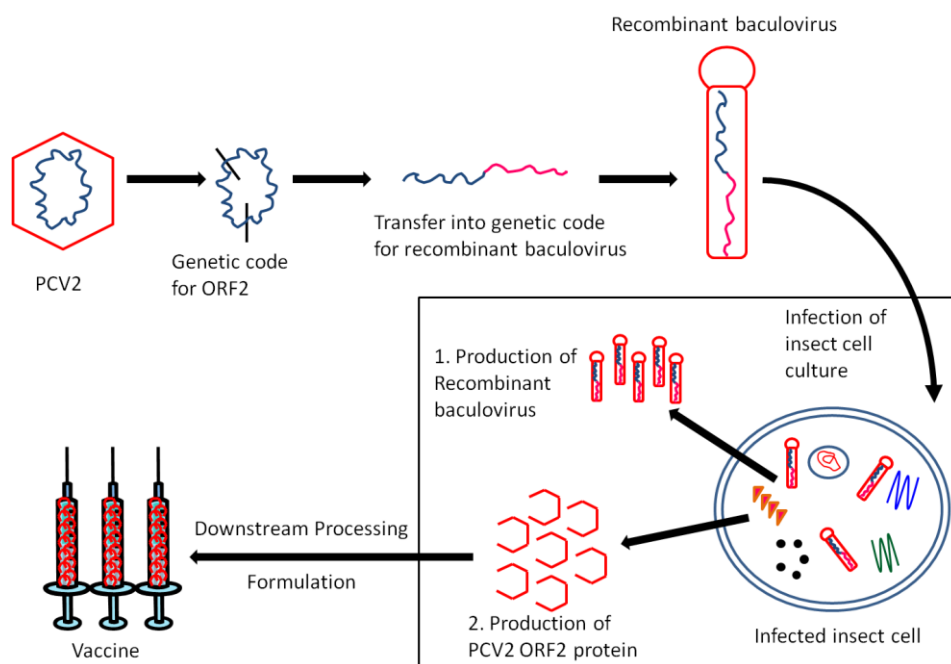


Figure 2.1. Basic concept of recombinant protein production with the BEVS. The genetic code for a specific target protein, here PCV2 ORF2, is introduced into the genetic code of a recombinant baculovirus. This recombinant baculovirus is then used to infect insect cell cultures. Infected insect cells will produce both, new recombinant baculovirus and the desired target protein. Following the cell culture process itself are downstream processing and eventually formulation to make up e.g. a vaccine. The box confines the cell culture based production process itself and is in the focus of this work.

This work establishes dielectric spectroscopy (DS) as a powerful tool to monitor a system as shown in Figure 2.1 above throughout the process of producing a target protein. This extends even to prediction of the final process success at an early stage in the culture. This may have a significant impact on process economics since a given culture can be terminated early on without expending more resources. The fundamentals of DS are described in detail below. The principle of DS is to take advantage of the response of living cells to a rapidly alternating electrical field. Both concentration and electrical potentials are maintained by the organism's metabolism across the membrane of a living cell. The storage and release of electrical energy depending on the frequency of an externally applied field is used in DS to derive information on the system where the system can range from suspension of unicellular organisms to an entire human.

2.1 The Baculovirus Expression Vector System for Recombinant Protein Production

The baculovirus expression vector system is nowadays generally considered to be one of the most common and widely used systems for the production of recombinant proteins^{1, 16, 17}. First established in the 1980s¹⁸ it utilizes a host insect cell line such as *Spodoptera frugiperda* (Sf-9 or Sf-21) or *Trichoplusia ni* (BTI-Tn-5B1-4) derived cell lines into which the genetic code for the desired recombinant protein is transduced by infection with a recombinant baculovirus. Most commonly used baculovirus vectors are based on the *Autographa californica* multiple nucleopolyhedrovirus (AcMNPV), a lytic DNA virus with a double stranded circular genome condensed within a rod-shaped nucleocapsid¹⁹. Foreign genes are usually introduced into non-essential baculovirus genes encoding for occlusion body proteins, which are under the control of the strong polyhedrin and p10 promoters. This allows a recombinant protein expression at levels up to 50 % of the total host cellular protein^{1, 16, 20}.

Insect cell cultures are usually grown at 27 to 28 °C at which cells double approximately every 24 hours. The optimum pH is reported to be in the range of 6.2 to 6.9 and maintained by a phosphate buffer system. The pH is often left uncontrolled in insect cell cultures due to the high buffer capacity of the cells^{1, 21}. Insect cell culture medium usually contains relatively high levels of carbohydrates and free amino acids because of a high tolerance of the cells before switching to

a wasteful overflow metabolism and is similar in cost to medium used in mammalian cell culture processes. Insect cells seem to be more shear sensitive than mammalian cells and therefore shear force protecting agents like Pluronic F68 are often added to the medium¹. One of the main advantages in addition to the potential high target protein yield of insect cell culture based bioprocesses is that the innately adherent cell lines could be adapted to suspension culture which allows a simplified recombinant protein production at a large scale. Other advantages of insect cells include improved posttranslational modifications over bacteria and yeast, a broad range of recombinant target proteins to be produced, safety and the relatively ease of handling. Insect cells are generally capable of posttranslational modifications like glycosylation, fatty acid acetylation, phosphorylation and disulfide bond formation but patterns are not necessarily equivalent to those of mammalian cell lines^{1, 17, 22}. Thousands of different proteins have been expressed with the baculovirus expression vector system ranging from antibodies over enzymes to virus like particles that serve as vaccines, and even multi-protein complexes¹. Overall the baculovirus expression vector system is often seen as a good compromise between the fast and relatively inexpensive bacterial expression systems which often do not provide acceptable protein folding and posttranslational modifications, and mammalian cell culture based processes which produce correctly folded and modified proteins but have relatively low yields and high costs²³.

Main parameters to be considered in the BEVS for large-scale production of recombinant proteins are the cell and virus concentration and the physical status of the cell at the time of infection. Due to the lytic nature of the baculovirus there is a limited time and number of protein molecules each cell can produce before lysis and it is important to optimize infection kinetics to ensure sufficient nutrient supply and maximize the yield. The time of infection in a culture is therefore a very important parameter to consider^{1, 24}. Two different strategies are generally applied in the BEVS to produce recombinant proteins. The first is the infection of the culture with an amount of virus particles which is enough to infect all cells immediately (synchronous infection). While this promotes reproducibility, it requires substantial amounts of virus seed stocks because a multiplicity of infection (MOI, the ratio of virus particles to cells) of 5 or higher is required to achieve this. A second strategy utilizes an infection at a very low MOI (often below 1) and therefore is dependent on subsequent production of new virus particles to

completely infect the culture and induce recombinant protein expression in the cells. This approach is generally preferred in large-scale industrial processes since it requires significantly lower amounts of virus seed. On the other hand, small deviations in characteristics like cell density or time of infection may be amplified in such a process causing variability in the process outcome. Therefore a good understanding of the process kinetics is desirable to develop efficient and robust large-scale production processes¹.

In this work, the baculovirus expression vector system was used to produce a virus like particle resembling the main viral capsid protein of the type 2 porcine circovirus. The porcine circovirus is a very small non-enveloped DNA virus with a single stranded circular genome of 1.7 kb^{25, 26} and belongs to the genus *Circovirus* in the family *Circoviridae*^{27, 28}. It was first observed 1974 as contaminant in a continuous porcine kidney cell line (PK-15) but isolates did not affect the health of challenged pigs^{26, 29, 30}. In the 1990s a new infectious disease initially called postweaning multisystemic wasting syndrome (PMWS) to describe the clinical symptoms found in herds was reported in Canada but subsequently detected around the world^{25, 31, 32}. The disease can be characterized by wasting, paleness of the skin, enlargement of the lymph nodes, respiratory distress, occasional diarrhea and icterus^{25, 26} and commonly affects piglets four to twelve weeks old. Symptoms usually develop in an affected herd over a period of time³³ and even though PMWS is a low morbidity disease with only 5 to 30 % of the animals in a herd showing clinical signs at the same time^{34, 35}, it has a high case mortality. In acute outbreaks the overall mortality in a herd can be 10 % or higher³⁶. Due to this, economical losses are high and have a significant impact on pig producers worldwide. Common and essential infectious agent identified was the porcine circovirus but analyses revealed significant genetic differences between the strain found in herds showing postweaning multisystemic wasting syndrome and the strain derived earlier from PK-15 cell cultures. To distinguish between the two the non-pathogenic is usually referred to as porcine circovirus type 1 (PCV1) while the one associated with postweaning multisystemic wasting syndrome is called porcine circovirus type 2 (PCV2)^{26, 29, 37}. Retrospective analyses of samples detected porcine circovirus type 2 as early as 1969²⁹ but the exact role of the virus in postweaning multisystemic wasting syndrome remains unclear. Infection with the virus does not always produce the disease suggesting that other host-dependent factors or co-infections with other pathogens might be of importance. In addition

PCV2 has been linked with a variety of other diseases including porcine dermatitis and nephropathy syndrome, porcine respiratory disease complex and others^{26, 27}. Because of the abundance of symptoms and diseases related to porcine circovirus type 2 and with PMWS only representing a fraction of those the term porcine circovirus associated disease (PCVAD) was introduced in 2006 to describe any PCV2-associated disease²⁹.

The genome of PCV2 contains three major open reading frames (ORFs) which encode for different virus proteins. While ORF1 and ORF3 encode for replication-associated and apoptotic proteins, respectively, the major viral capsid protein with a size of approximately 30 kDa is encoded by ORF2 which is the main immunostimulating agent in infected animals^{25, 27, 38, 39}.

This fact was utilized in the development of a BEVS based process for the cell culture based production of the ORF2 protein as the immunostimulating antigen in a vaccine against PCV2 in swine. The genetic code contained in ORF2 was introduced into an AcMNPV and allows expression of the PCV2 ORF2 protein under the strong polyhedrin promoter. Once expressed in the cell the ORF2 seems to self-assemble and form virus like particles³⁸. In this specific case, a specialized suspension insect cell line derived from Sf-9 cells (from now on referred to as Sf-9 clone) is used as the biological host to express the protein.

2.2 Process Monitoring and Control

Monitoring and characterization of bioprocesses is very important and essential in developing an understanding of the relationships between process parameters and the process outcomes such as a specific product. This is generally required by regulatory agencies for validation and documentation⁴⁰. Main parameters monitored in a bioprocess include cell density, culture medium conditions (temperature, pH, pO₂ or D.O., pCO₂.) as well as medium metabolite concentrations (carbohydrates, amino acids, waste byproducts) and product concentration and quality. But while many processes ideally require a timely and accurate measurement of these parameters for the control of e.g. feeding or perfusion rates to accomplish maximum productivity⁵, both, the availability of real-time monitoring techniques as well as the fundamental

understanding of the relationships between process parameters and process outcome, are limited. Small changes in a seemingly innocuous process parameter can have a significant impact on the process and even growth rates can often not be predicted from the available knowledge of the organism or controlled easily⁴¹. Improved process monitoring could accelerate process development as well as help achieve the efficient and consistent production of high quality product⁴².

2.2.1 Methods of Monitoring

Currently, key parameters routinely monitored in bioprocess are the temperature, pH, dissolved gas (O₂ and CO₂), cell and virus concentration as well as concentrations of culture medium metabolites. Other parameters are concentration of electrolyte and trace minerals, conductivity, and viscosity. It is expected that more parameters will emerge in the future as the availability of monitoring techniques and process understanding expands⁴³. Four different categories of bioprocess monitoring are recognized: in-line, on-line, at-line and off-line. For both, in-line and on-line, the analysis is performed directly interfaced to the process or within a recirculation loop of liquid from the process, respectively, without the need of discrete sampling. At-line and off-line both describe an analysis performed on a sample taken from the process. In the case of at-line the analysis is performed in close physical proximity to the process itself while off-line describes an analysis in a separated location⁴⁴.

The following chapters describe common available methods for cell and biomass concentration determination as well as quantification of metabolite and product concentrations.

2.2.1.1 Cell and Biomass Concentration

The cell or biomass concentration (both viable and non-viable) is generally considered as one of, if not the most important parameter in bioprocesses and therefore accurate and real-time measurements are highly desired⁴⁵.

Different in-line and on-line methods are currently available to measure cell density and cell size distribution in real-time. Most of them are based on optical methods and image analysis and can provide additional information about cell morphology but they generally require a well-

mixed and representative cell suspension for reasonably accurate estimations of the state of a cell culture. Examples include different types of in-situ microscopy, focused beam reflectance and particle vision measurement^{5,44}. Other examples for optical methods are optical density measurements, acoustics, laser light-, Raman-, and fluorescence spectroscopy⁴⁴. Infrared and laser turbidity have also been applied for this purpose⁵. A common disadvantage of optical sensors is their vulnerability to fouling and changes in culture medium turbidity, light dispersion, cell debris or other interferences^{5,44}. The options for the in-line monitoring of immobilized cell cultures on micro-carriers or in a fixed bed have been very limited. Today several optical methods (light absorbance and/or scattering, real-time imaging) as well as the measurement of the culture medium density enable estimates of the cell or biomass concentration under those conditions⁴⁶.

A range of commercial analyzers is available for the direct determination of the cell or biomass concentration at-line and off-line, e.g. Cedex (Roche Applied Science) or Vi-Cell XR (Beckman Coulter) which are based on an automated trypan blue staining and image analysis⁴⁷. Disadvantages of at-line or off-line methods are the risk of contamination due to the sampling and the delay until availability of the result⁴⁴. Methods including the quantification of DNA⁴⁸⁻⁵⁰ or the use of available data of the dissolved oxygen, glucose or lactate concentration in the culture medium have been used to calculate the cell or biomass concentration indirectly⁴⁴.

Another very important parameter related to the cell or biomass concentration is the viability as it additionally represents the state of the culture. Estimation of this parameter is usually performed utilizing one of the available permeability, functional, reproductive or morphological assays⁵¹.

2.2.1.2 Substrate and Metabolite Concentration

Concentrations of substrates and metabolites (glucose, glutamine, lactate, glutamate, oxygen, carbon dioxide) can be measured using probes, enzymatic kits (photometric) and bioanalyzers (electrochemical) or chromatographic methods (HPLC, Ion chromatography). Examples for the measurement of glucose concentrations off-line and on-line include

potentiometric⁵², flow injection analysis^{53, 54} and fluorescence⁵⁵ based sensors but challenges regarding stability, calibration and validation remain⁵⁶. Near and mid infra-red have been used to measure glucose, glutamine, glutamate, proline, lactic acid, ammonia, and dissolved carbon dioxide in-line of bioprocesses but background interferences complicate analysis^{44, 57, 58}. Another example is the use of Raman spectroscopy⁵⁹.

Measurements of substrate or metabolite concentrations can be used for an indirect estimation of the cell and biomass concentration, e.g. by concluding from the cells oxygen uptake rate in perfusion cultures to the viable biomass present⁶⁰.

2.2.1.3 Product Concentration

A specific protein (as in the work presented here) or molecule may be the desired product of a bioprocess. Quantifications are commonly performed off-line by HPLC or ELISA, but in-line sensors, e.g. based on Raman spectroscopy, also have also been applied, depending on the type of the product^{59, 61-64}.

2.3 Process Analytical Technology

The Process Analytical Technology (PAT) initiative was introduced by the FDA within the “GMP-Initiative for the 21st Century” in 2004 and has been supported by authorities around the world since then^{2, 64}. PAT is usually described as a tool for designing, analyzing, and controlling pharmaceutical manufacturing through timely measurements of critical quality and performance parameters with the goal of ensuring final product quality. The FDA states that “quality cannot be tested into products, it should be built-on or should be by design” and categorizes the tools to be applied within the PAT framework as 1. multivariate tools for design, data acquisition, and analysis, 2. process analyzers, 3. process control tools, 4. continuous improvement, and knowledge management tools^{2, 65, 66}. Combining these tools is hoped to result in a better process understanding and consistent and improved yields, but also minimization of waste, prevention of rejects and reprocessing, and overall cost reduction and product real-time releases².

Bioprocesses are notoriously sensitive to even small changes in sometimes seemingly innocuous process parameters because these can lead to significant variations in growth or productivity due to sometimes unknown processes or dependencies. Current real-time in-line or on-line monitoring is often limited to temperature, pH, and dissolved oxygen with limited ability to detect or control those small changes in a culture especially at large scale (multi-liter to multi-m³). With the PAT initiative increased requirements for bioprocess monitoring were implemented to improve the understanding and eventually control of bioprocesses³.

Several key technologies were suggested by the FDA to support the PAT initiative including near infra-red spectroscopy, UV-VIS, NMR, MS, HPLC, fluorescence measurements, and imaging technology^{2, 57, 64, 66, 67}. In addition to these, DS is considered to be a promising tool and has been the focus of recent work^{3, 4}. The work presented here extends the use of DS to process monitoring and predictive capabilities for virus infected insect cell cultures under low MOI conditions.

2.4 Dielectric Spectroscopy as a Tool for Process Analytical Technology

Bioprocesses are used for the production of specific products ranging from a molecule to whole organisms. DS is considered to be a promising tool for the real-time in-line and on-line monitoring of such processes. It allows non-invasive and non-destructive continuous monitoring of suspension as well as adherent cell cultures⁵. Breweries have been using DS to monitor yeast concentration and budding^{68, 69} but the technique has now evolved into applications in the cell culture technology. Examples include the application in bacterial, yeast, mammalian, and insect cell cultures⁵⁻¹¹.

While application of DS as a timely and accurate method to determine cell and biomass concentration in-line and on-line of bioprocesses within the framework of PAT has already been discussed in the literature^{5, 45, 57} it also has potential to allow more detailed insight into the cells physiological state. The extension of DS to monitor the progress of a cell culture after infection with a virus and perhaps even predictive capabilities towards the target product is the hypothesis that is pursued in the work presented here.

2.4.1 Basic Theory of Dielectric Spectroscopy

DS is based on the measurement of the passive dielectric properties of a material or system. An alternating electrical field of potentially varying frequency is applied to the material placed in between or around two electrodes and the electrical response measured. Materials ranging from cement paste over yeast suspensions in breweries and now cell cultures have been investigated utilizing DS. The technique is well established to interrogate interfacial electrochemical phenomena in corrosion⁷⁰. Even selected tissues or the entire human body can be subjected to DS to derive information on body composition etc.⁷¹.

2.4.1.1 Physical Principle and Applications

In cell culture technology and bioprocesses the materials investigated by DS are usually suspensions or adherent cells in the cell culture medium. The medium is an electrically conductive solution or suspension containing low molecular solutes (salts, nutrients), cell debris, and virus particles as in the work presented here. Depending on the frequency of the alternating electrical field applied, biological material exhibits specific responses in terms of energy storage (capacitance) or dissipation (conductance) and the lag in those responses in time (relative to the applied signal) can be detected. A simple mechanical analog is a spring which stores energy (extension) and releases this energy (contraction) without lag. However, if a dashpot is added, say, in parallel to the spring, or in some other configuration, the response to an applied becomes much more complex, depending on the dashpot's properties and the configuration. Responses of cell suspensions to DS are usually only constant in a specific frequency range and tend to decrease or increase in a series of characteristic steps, called dispersions, for capacitance and conductance, respectively, with increasing frequency. Figure 2.2 shows the four observed dispersions observed for cell suspensions or biological tissues in regard to the capacitance (permittivity).

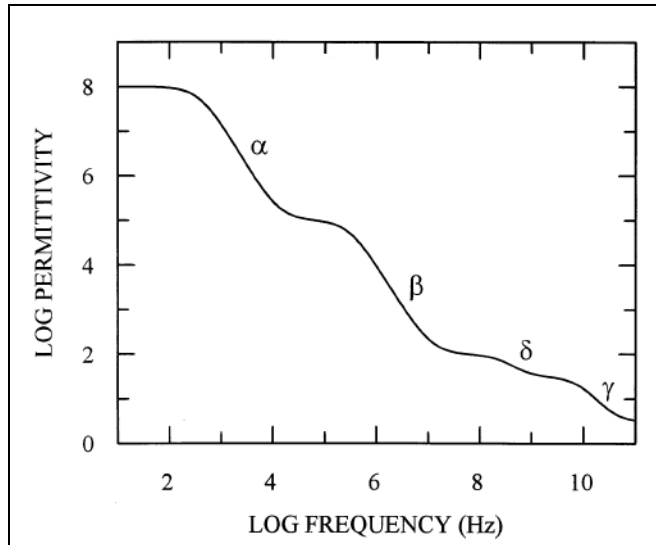


Figure 2.2. Observed dispersions in the permittivity(capacitance) for biological materials such as cell suspensions or tissues over a range of frequencies. Different dispersions are ascribed to specific phenomena. α : tangential flow of ions across the cell surface, β : charge build-up at the cell membrane, δ : rotation of macromolecular side-chains and bound water, γ : dipolar rotation of small molecules. From: 72.

The dispersions are caused by the subsequent loss of specific polarization processes when the frequency increases. The α -dispersion is ascribed to tangential flow of ions across the cell surface, the β - dispersion to charge build-up at the cell membranes, the δ -dispersion to the rotation of macromolecular side-chains and bound water and the γ -dispersion to the dipolar rotation of small molecules like water⁷².

The dielectric properties of cells in suspension are rather complex because they consist of layers of materials with significantly different properties⁷². Depending on the cell type, surface structures like pili or glycoproteins are present and an electrical double layer is formed between the negatively charged cell surface and the surrounding aqueous culture medium that contains highly mobile anions and cations from salts etc. The latter is regarded as highly conductive mainly due to salts. If a cell wall is present, it adds another layer of complicated porous structures with large amounts of polysaccharides integrated which change their properties depending on the ion concentration in the surrounding medium. The cells cytoplasm surrounding membrane is usually a thin lipid bilayer and has channel-, receptor-, and pump proteins

integrated for ion exchange and other functions. In addition, cells maintain an electrical membrane potential. Because transport of ions is highly regulated, the cell membrane is usually assumed to be essentially non-conductive. The cytoplasm on the other hand is generally regarded as highly conductive because it contains various amounts of salts, proteins, nucleic acids and other small molecules. In addition, intracellular membranous structures are often present⁷². Figure 2.3 shows this schematically.

Changes in the physiological state of a cell will often be reflected in changes of the parameters discussed above in some way and therefore also in dielectric properties of cells. DS allows determining specific values representing the physiological state, e.g. the membrane capacitance C_m , the membrane conductance G_m or the intracellular conductivity σ_i . Those values are dependent on the folding and permeability of the membrane, and the mobility of the ions within the cell's cytoplasm⁷³⁻⁷⁵.

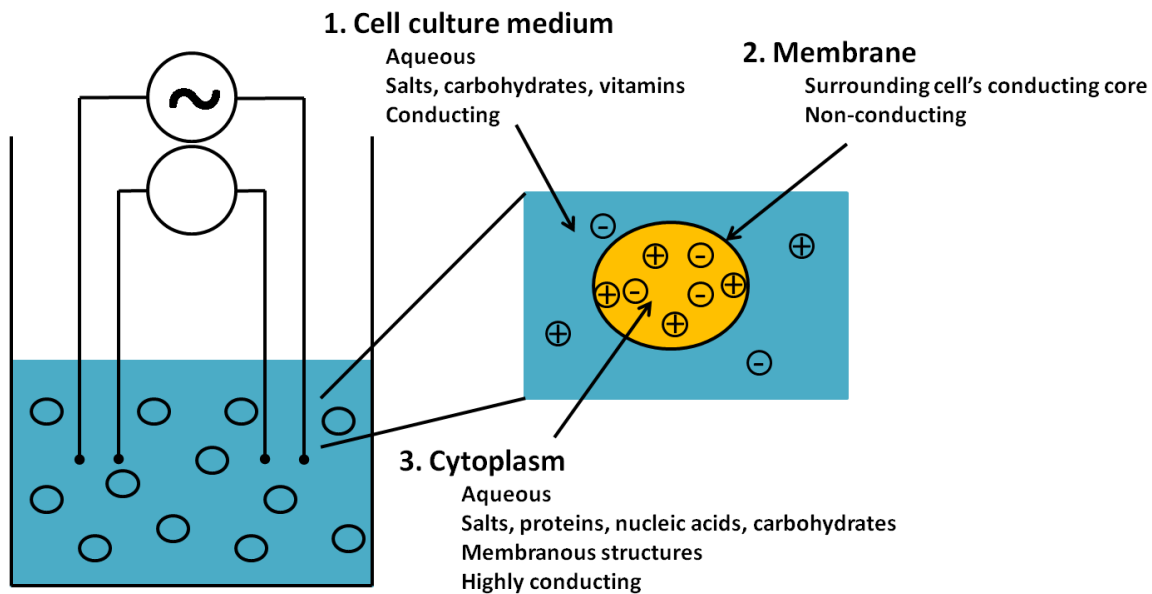


Figure 2.3. Schematic representation of a cell suspension in a DS field. The highly conductive cytoplasm is surrounded by an essentially non-conductive membrane. The cell culture medium surrounding the cell is aqueous and conductive.

DS in cell cultures and bioprocesses with the goal of estimating cell or biomass concentrations is usually performed in the β -dispersion range of 0.1 – 10 MHz and is therefore causing the build-up of charge differences across the cells essentially non-conducting lipid-based cell membrane, and polarization⁷⁶. Suspended cells are basically acting as capacitors within the conductive culture medium⁹. Figure 2.4 shows the generally observed decrease in measured capacitance with increasing frequency known as β -dispersion. At low frequencies the polarization process is slow and results in a high measured capacitance. With increasing frequency the polarization and measured capacitance decreases because less and less ions are able to migrate to the cell membrane to build up charge and eventually only the medium background capacitance is measured. The shape of the β -dispersion is dependent on the cell type and shape which can be characterized by three characteristic parameters dielectric increment $\Delta\epsilon$, characteristic frequency f_c and Cole-Cole α and can be described by the Cole-Cole equation (see Equation 1)⁷⁷⁻⁷⁹. ϵ_∞ describes the background (medium) permittivity measured on the high frequency plateau.

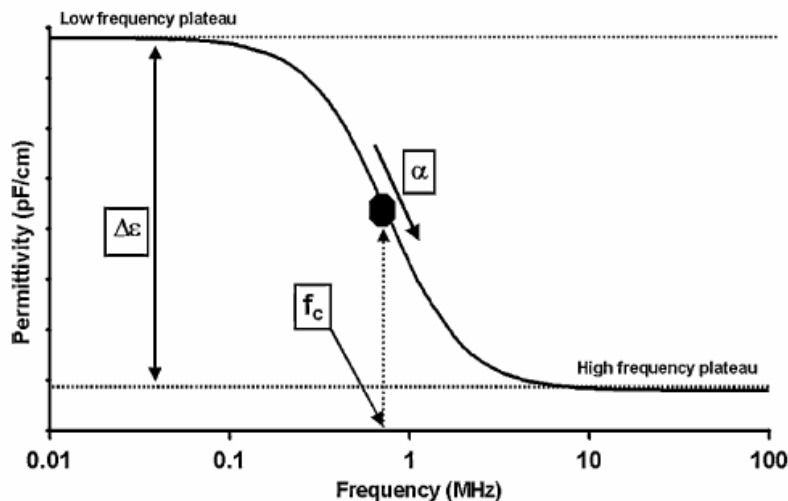


Figure 2.4. Schematic drawing of the β -dispersion observed for biological materials. The β -dispersion can be described with the characteristic parameters dielectric increment $\Delta\epsilon$, characteristic frequency f_c , and the Cole-Cole α . From: 12.

$$\varepsilon(f) = \frac{\Delta\varepsilon \left(1 + \left(\frac{f}{f_c} \right)^{(1-\alpha)} \sin \left(\alpha \frac{\pi}{2} \right) \right)}{\left(1 + \left(\frac{f}{f_c} \right)^{2(1-\alpha)} + 2 \left(\frac{f}{f_c} \right)^{(1-\alpha)} \sin \left(\alpha \frac{\pi}{2} \right) \right)} + \varepsilon_\infty$$

According to theory, those values are dependent on specific parameters of the cell suspension even when the physiological state does not change. The dielectric increment $\Delta\varepsilon$ is dependent on the volume of the cells and increases with an increasing fraction of cells in a suspension. The characteristic frequency f_c , defined as the frequency at 50 % of the permittivity difference between the low and high frequency plateau, decreases with an increasing cell size because of the change in time it takes to polarize the cells. The Cole-Cole α is thought to increase with the width of the cell size distribution^{77, 78, 80}. These relationships are shown in Figure 2.5 and Figure 2.6.

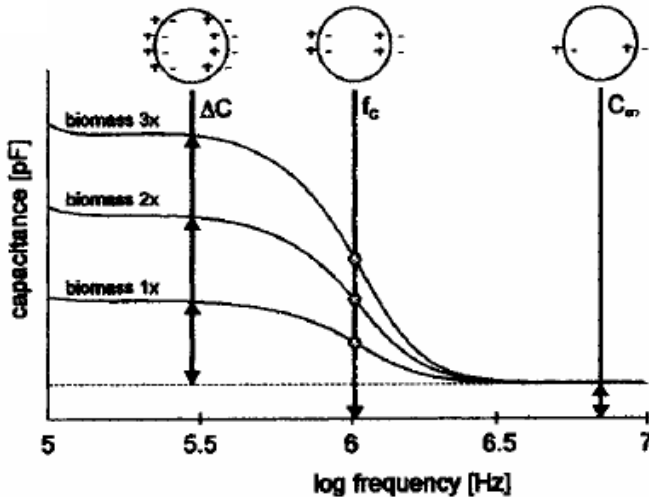


Figure 2.5. Capacitance ΔC , characteristic frequency f_c , and medium background capacitance C_∞ . From: 77.

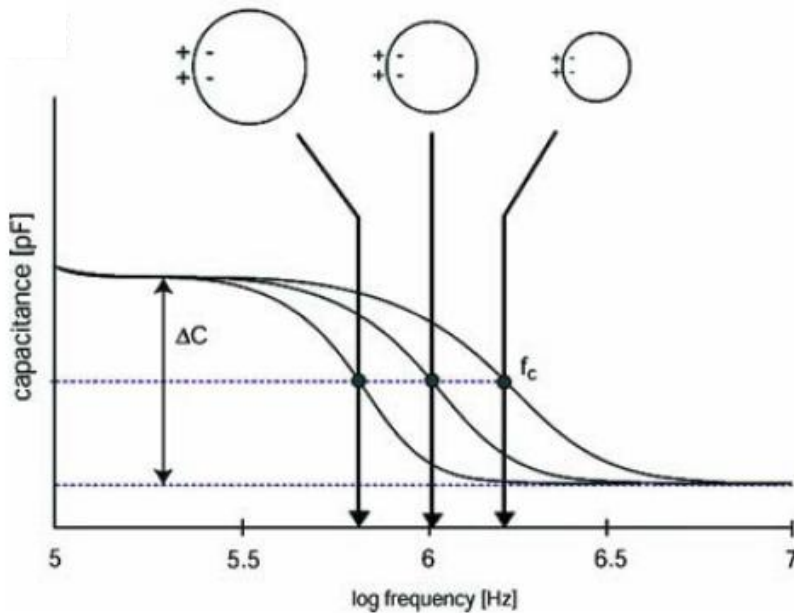


Figure 2.6. Change of the characteristic frequency f_c with cell size. From: 5.

It is important to note that the measured capacitance of viable cells with an intact membrane in suspension is very high compared to non-viable cells with either a leaky or even broken membrane. Cell debris, gas bubbles and other media components essentially do also not contribute directly to the DS measurement or can be compensated for by subtracting out the background capacitance at the high frequency plateau^{6, 7, 46}. This means that it is theoretically also possible to use DS for the measurement of cells growing adherently, e.g. on micro-carriers⁸¹. Usually lower capacitance and shifted f_c signals are observed for adherent cells compared to those in suspension^{82, 83}.

2.4.1.2 Mathematical Description

The treatment of the rather complex biological cell as a simple conductive spherical core with a thin shell of a low conductivity membrane lead to the development of several relatively simple so called shell models describing the dielectric properties successfully within the radio frequency range⁷². Models for single⁸⁴ and multiple⁸⁵ shells as well as ellipsoidal shapes were developed⁸⁶.

DS as it is applied in cell culture and bioprocesses is based on the measurement of the frequency dependent capacitance C in F and conductance G in S of the cell system at hand, usually in the frequency range of 0.1 -10 MHz where the β -dispersion phenomenon can be observed. Both macroscopic variables depend on the system measured but also perhaps on the probe geometry and interactions at the probe interface with the surrounding medium. Often C and G are converted into their probe independent parameters permittivity ε in $F\ m^{-1}$ and conductivity σ in $S\ m^{-1}$ by using

$$\varepsilon = C \times k \quad \text{Equation 2}$$

$$\sigma = G \times k \quad \text{Equation 3}$$

where k in m^{-1} is the electrode constant⁷². Based on the single shell model for representation of a cell Schwan found that the dielectric increment $\Delta\varepsilon$ or the change therein was correlated by

$$\Delta\varepsilon = \frac{9 \times r \times P \times C_m}{4} \quad \text{Equation 4}$$

where r is the cell radius in m, P the volume fraction of the cells in the suspension measured (dimensionless) and C_m the specific membrane capacitance in $F\ m^{-2}$ ⁷². Here P is given by

$$P = \frac{4}{3} \times \pi \times r^3 \times N \quad \text{Equation 5}$$

where N is the cell density in cells m^{-3} and a spherical cell shape is assumed. This predicts a linear correlation of $\Delta\varepsilon$ increasing with the volume fraction P and the cell density N . This has been widely confirmed and examples are given exemplary in Figure 2.7.

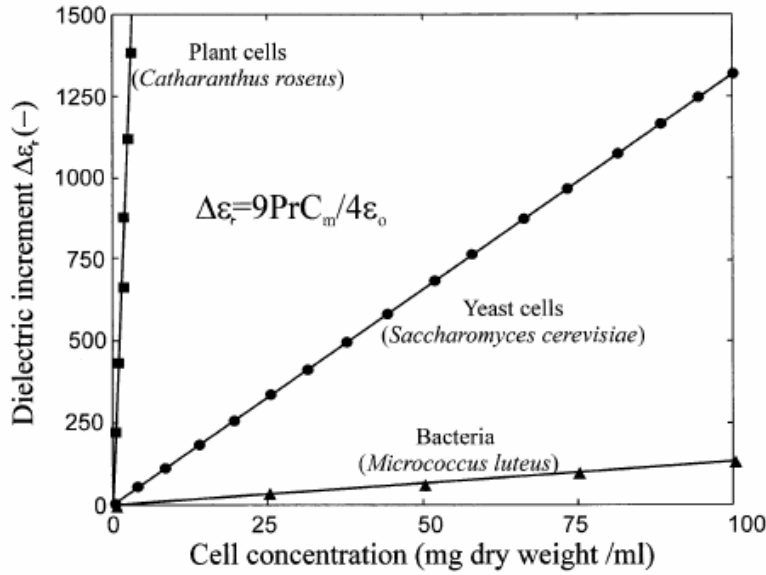


Figure 2.7. Linear correlation of $\Delta\epsilon$ with cell density for different types of cells. Here the relative permittivity is used. From: 72.

Additionally it was found, that the characteristic frequency f_c can be described with

$$f_c = \frac{1}{2 \times \pi \times r \times C_m \times \left(\frac{1}{\sigma_i} + \frac{1}{2 \times \sigma_e} \right)} \quad \text{Equation 6}$$

where σ_i and σ_e are the intracellular and medium conductivity in $S m^{-1}$, respectively⁸⁷.

The medium conductivity can be obtained from the actually measured suspension conductivity by using the Bruggeman equation⁸⁸

$$\sigma_e = \frac{\sigma_s}{(1 - P)^{1.5}} \quad \text{Equation 7}$$

The relationships above depend not only on the cell number (concentration/density) or size, but also on more intricate parameters like the specific membrane capacitance C_m or the intracellular conductivity σ_i . These are indicators for the physiological state of a cell. It is therefore clear, that DS might be used to theoretically investigate some aspects of the

physiological state of a cell but often complex mathematical correlations to compensate for extraneous influences on the parameters based on information obtained by off-line sample analysis for reference is required akin to a calibration for the cell suspension of interest^{9, 12, 46, 77, 79}.

2.4.2 Applications

While the focus of this work is the application of DS in industrial bioprocesses and the use as a tool for PAT, it should be mentioned, that this technique has been widely applied for research on cells outside of the biopharmaceutical production area itself. DS helped to detect the existence of the cellular membrane early in the 20th century⁸⁹ but has also been used to describe differentiation processes of mesenchymal stem cells⁹⁰ or to assess cell adhesion and morphological changes of several other cell lines^{82, 91-96}. Cell death due to apoptosis, necrosis or induced by cytotoxic agents has also been monitored with DS⁹⁷⁻¹⁰⁰ as well as the inhibitory effect of a protein kinase on 3T3 fibroblast cells¹⁰¹. Another example is the monitoring of tissue growth within a micro-porous polymer scaffold¹⁰² but detecting and monitoring of infection processes in mammalian cells has also been reported¹⁰³. DS has also been proposed for the detection of living organisms in extreme organisms such as Martian soil¹⁰⁴.

The literature gives several examples of the application of DS in biopharmaceutical production processes. The focus is generally on the monitoring of cell or biomass concentration, and cell death caused by physical or chemical stresses or virus infection but other areas of interest may include changes in cell size and morphology or cell metabolism. The immobilization process of adherently growing cells is of interest and can be followed with DS. Limitations generally occur in cases where the measurement has to be performed within specialized geometries such as hollow fiber modules¹⁰⁵. Examples for both, mammalian and insect cell cultures, are presented.

2.4.2.1 Mammalian Cell Culture

Several different mammalian cell lines have been monitored with DS. Many of the publications focus on CHO cells in various types of reactors and process modes for both, suspension and adherent cells. DS was successful in determining viable cell densities for two different suspension cell lines as well as in detecting depletion of specific nutrients, e.g. glutamine, in the culture medium of batch and fed-batch processes¹⁰⁶. In the same work the characteristic frequency f_c could be correlated to the oxygen uptake rate and so to metabolic activity. Later research confirmed the influence of the nutrient concentrations on the intracellular conductivity of the cells⁷³. Models derived from the capacitance spectra (linear, Cole-Cole, PLS) were able to predict cell related parameters like cell density, volume, mean size and oxygen uptake rate in batch, fed-batch and perfusion cultures. It was noticed that correlations weakened when cells entered the stationary and death phase of their growth cycle, presumably due to changes in the physiological state and thereby the dielectric properties of the cells^{77, 88}. It was possible to correlate the capacitance to the size, their membrane area, and changes in the physiological state represented by nucleotide triphosphates or protein content and the glutamine consumption rate in a hybridoma suspension cell culture. In addition, the immobilization progress for adherent cells could also be followed by monitoring changes in the capacitance. Capacitance values for adherent cells were generally much lower than for cells in suspension due to a lower specific membrane capacitance C_m ⁹. Another example are adherently growing Vero cells producing rabies virus¹⁰⁷. Batch and perfusion cultures exhibited the predicted linear relationship between viable cell density during the growth and virus production phase. Additionally cell lysis and changes in the specific membrane capacitance C_m and the intracellular conductivity σ_i could be followed through changes in the characteristic frequency f_c .

As stated above, the dielectric properties of cells often change during the stationary and death phase. It is often assumed that the cell's membrane loses its integrity or changes its permeability during these phases which decreases the capacitance (or permittivity) signals measured. Generally, the capacitance measured overall decreases during cell death due to cell lysis but it is unclear how different types of cell death such as apoptosis, or traumatic cell death, impact the dielectric properties specifically. In addition to the actual cell death, other events like

osmotic or shear stress, virus infection or intercalation of solvents into the membrane could be monitored applying DS⁷⁴.

2.4.2.2 Dielectric Spectroscopy of Insect Cell Culture and Relationship to the Work Performed Here

The baculovirus expression vector system is one of the most common and widely used systems for the production of recombinant proteins^{1, 16, 17}. Nevertheless, research on the application of DS in insect cell cultures is relatively scarce.

In 1999 capacitance measurements of both, uninfected and baculovirus infected insect cells, here *Spodoptera frugiperda* Sf-9, was apparently reported for the first time¹¹. Experiments were performed in a 3.5 L (total volume) bioreactor and it was found that measurements correlated well with the viable biovolume of uninfected cells and after synchronous infection (MOI 10). Cell size changes accounted for most of the increase seen in the permittivity post infection. Temporary cell size leveling approximately 18 – 24 hours post infection could also be detected with the measurements as well as the onset of cell lysis. The highest product concentration (β -galactosidase) corresponded to an accelerated decrease in permittivity late in the death phase.

The same research group extended their research on DS in insect cell cultures by monitoring high cell density fed-batch cultures up to 5.2×10^7 cells ml⁻¹ for uninfected and 1.7×10^7 cells ml⁻¹ for infected cultures¹³. The focus of this research was the evaluation of different feeding strategies to enhance cell growth and productivity and the usefulness of DS under those conditions was confirmed. In addition, the CO₂ evolution rate as one physiological parameter during growth and infection was correlated to DS measurements of Sf-9 and High-5 cells¹⁵. The peak in CO₂ evolution coincided with a plateau in the DS signal and the release of virus particles into the medium. The peak was delayed approximately 40 h for low MOI infection of 0.001 compared to infection at an MOI of 10. It was suggested, that DS could be used as a tool to detect the time of harvest.

The work cited above performed DS measurements only at one fixed frequency. More sophisticated DS at multiple frequencies has been reported more recently. One study compared the frequency-dependent permittivity signal to different off-line biovolume measurements for Sf-9 cells infected at a MOI of 10 in a 1.2 L bioreactor culture¹². It was found that correlations for biovolume measurements obtained by Vi-CELL XR and CASY 1 correlated well throughout the whole infected culture (MOI 10). In addition, changes in the characteristic frequency f_c could be explained with a concurrently changing cell diameter, but it was proposed that cell membrane properties also had an influence on this parameter. A second study applied DS in a large scale (40 L) production process for recombinant adeno-associated vectors (rAAV) and three different baculoviruses (total MOI 3)¹⁴. It was possible to optimize the process by determination of the optimum time of harvest in real-time by detecting a specific second maximum in the permittivity signal at the time of the maximum product yield.

Summarized, literature reporting the application of DS in insect cell cultures and the BEVS is very limited with only five publications available. Synchronous infections at a high MOI were the main focus of the early research in 1999 and 2000 with only one publication reporting the application of DS using a low MOI (MOI 0.001). Generally, important parameters such as time of infection and cell density at infection changed significantly from experiment to experiment. Variations in these parameters can have a significant effect on the BEVS process and it was therefore difficult to compare the results presented in a “normalized” way. Additionally, due to instrument limitations, measurements were generally only performed at a single fixed frequency and information gathered was therefore limited. More recent research performed in 2007 applied DS measurements at multiple frequencies, the so-called frequency scanning, but again focused on high MOI infections. Obtained DS spectra were used for a qualitative assessment of the process progress, but no attempt was made to use the data for modeling or even yield prediction. Except in one report, all experiments were performed at a relatively small scale (working volumes of less than 3.5 L).

The work presented here attempts to advance the DS technique towards monitoring of large-scale cell culture of insect cells and the BEVS under low MOI conditions exploring not only the current state of the culture but attempting to predict the success of product formation

already at an early stage. A standardized approach in terms of cell state, age, and density at the time of infection was taken to reduce the number of unidentified factors potentially affecting the process. A range of off-line analyses was performed to relate the DS data with culture progress and state. The high number of experiments performed additionally allowed an evaluation of the robustness of DS and the instrument used in this work, something of high importance for the potential application in industrial-scale routine production.

Chapter 3 - Materials and Methods

3.1 Materials

3.1.1 Cell lines and Recombinant Baculovirus

Suspension *Spodoptera frugiperda* (Sf-9 clone) insect cells were used as the biological host for the recombinant protein production with the BEVS in this work. A recombinant baculovirus carrying the gene for the PCV2 ORF2 target protein was used to infect the cells and trigger recombinant protein production. Adherent *Spodoptera frugiperda* Sf-9 insect cells were used in the end-point dilution assay for the quantification of recombinant baculovirus in culture samples. Both cell lines and the recombinant baculovirus were kindly provided by Boehringer Ingelheim Vetmedica, St. Joseph, MO.

3.1.2 Culture Medium, Antibiotics and Supplements

Sf-9 clone spinner flask cultures for cell scale-up as well as bioreactor cultures were cultivated in EX-CELL 420 (serum-free, with L-glutamine, SAFC Biosciences, Lenexa, KS). A sterile 200 mM L-glutamine solution (in saline, suitable for cell culture, SAFC Biosciences, Lenexa, KS) was used in the supplementation experiments. Dimethyl sulfoxide (sterile-filtered, biotechnology performance certified, Sigma-Aldrich, St. Louis, MO) was used as additional cryo-protectant in the preparation of the working cell bank. Sf-9 cultures were also maintained in EX-CELL 420 medium but supplemented with 5 vol-% of fetal bovine serum (Sigma-Aldrich, St. Louis, MO) and gentamicin sulfate as antibiotic (sterile-filtered, endotoxin- and hybridoma-tested, Sigma-Aldrich, St. Louis, MO).

3.1.3 Bioreactor and Associated Instrumentation

Experiments in this work were carried out in two BioClave 20 L stirred tank reactors (Applikon Biotechnology, Foster City, CA). Each bioreactor was equipped with two upwards directed pitched-blade impellers (3 blades, 45°). A set of ADI 1030 BioController and ADI 1035 BioConsole was used to control temperature, agitation, and dissolved oxygen while pH was monitored but not controlled. Dissolved oxygen was measured using polarographic OxyProbe

sensors (Broadley James, Irvine, CA) and pH was measured with a FermProbe gel electrode (Broadley James, Irvine, CA). Dissolved oxygen was controlled by aeration of the culture with air or oxygen using an L-shaped sparger located under the lower impeller. Dielectric spectroscopy was performed in-line of the bioreactors with the iBiomass 465 instrument (FOGALE nanotech, Nimes, France).

3.1.4 Chemicals, Reagents and Antibodies

Several chemicals were used in the preparation of ELISA buffers. They included sodium carbonate (Na_2CO_3 , ACS grade), sodium bicarbonate (NaHCO_3 , ACS grade), dibasic sodium phosphate (Na_2HPO_4 , ultrapure) (all Sigma-Aldrich, St. Louis, MO), sodium chloride (NaCl , ACS grade), monobasic potassium phosphate (KH_2HPO_4 , ACS grade), and potassium chloride (KCl , UPS grade) (all J.T. Baker, Phillipsburg, NJ). Tween 20 (cell culture tested, Sigma-Aldrich, St. Louis, MO), 10 N hydrochloric acid (NF grade) and non-fat dry milk (Best Choice, Kansas City, KS) were also used for this purpose. Deionized water was used to make up these buffers (Boehringer Ingelheim Vetmedica, St. Joseph, MO). A TMB microwell peroxidase substrate system (KPL, Gaithersburg, MD) and normal rabbit serum (Jackson ImmunoResearch, West Grove, PA) were additional reagents used in this assay. Methanol (biotech grade, 99.93 %) and acetone (histological grade, ≥ 99.5 %) were used as a fixative in the end-point dilution assay for recombinant baculovirus quantification. Sigmacote (silicone solution in heptane) was used to siliconize spinner flasks to reduce cell attachment (all Sigma-Aldrich, St. Louis, MO). Phosphate buffered saline (powder, pH 7.4, biotechnology performance certified, Sigma-Aldrich, St. Louis, MO or liquid, pH 7.4, Invitrogen, Carlsbad, CA) and bovine serum albumin ($\geq 98\%$, lyophilized powder, Sigma-Aldrich, St. Louis, MO) were additionally used in this work for various purposes.

Several different antibodies were used in this work. A single anti-baculovirus envelope gp64 protein phycoerythrin-labeled antibody (eBioscience, San Diego, CA) was used in the quantification of the fraction of infected cells. An anti-baculovirus envelope gp64 protein antibody (eBioscience, San Diego, CA) together with a fluorescein-labeled goat anti-mouse IgG (H+L) antibody (KPL, Gaithersburg, MD) was used in the end-point dilution assay for recombinant baculovirus quantification. Three different antibodies were used in the ELISA assay

for the quantification of recombinant PCV2 ORF2 protein. Here a swine anti-PCV2 ORF2 polyclonal antibody was used as a capture antibody while a monoclonal antibody against PCV2 ORF2 served as a detection antibody (both provided by Boehringer Ingelheim Vetmedica, St. Joseph, MO). A goat anti-mouse IgG (H+L) antibody conjugated with horseradish peroxidase (Jackson ImmunoResearch, West Grove, PA) was also used.

3.2 Creation of Sf-9 Clone Cell Working Cell Bank

Bioprocesses for the production of recombinant proteins are generally dependent on biological factors, e.g. the quality of the cells used, but it is often difficult to obtain a good measure of what this so-called quality really is and by what it is affected. Often cell productivity changes over the lifetime and passaging of a culture and therefore their use is generally limited within a specific passage range in the industrial biopharmaceutical production, e.g. 20 to 50 post initiation of a new working stock culture the master cell bank. To minimize the effects of variations in the biological system used in this work, it was decided to prepare a new Sf-9 clone cell working cell bank and to initiate and scale-up a new culture for each bioreactor-scale experiment. This prevents significant deviations in the passage number of cells used for the bioreactor experiments and ensures a consistent biological system as good as possible.

For this, a total of approximately 5 L of *Spodoptera frugiperda* Sf-9 clone cell culture (passage 31) was dispensed into multiple sterile 250 ml centrifuge beakers and centrifuged at 200 g and 4 °C for 5 minutes (Avanti J-25I, Beckman Instruments, Palo Alto, CA). The supernatant was discarded and approximately 5 ml of cold EX-CELL 420 medium was added to each beaker. The cells in each beaker were resuspended and collected in a sterile Erlenmeyer flask. Cold EX-CELL 420 medium and dimethyl sulfoxide (final concentration approximately 9 vol-%) were added to dilute the cells further and as a cryo-protectant, respectively. The cell suspension was then dispensed into pre-chilled (4 °C) 2 ml vials at a fill volume of 1.5 ml. Subsequently the vials with the cell suspension were gradually cooled down by holding them at -20 °C and -70 °C for approximately 3 and 39 hours, respectively, before placing them into long term storage tanks under liquid nitrogen. The final viable cell density was determined to be 4.56×10^7 cells ml⁻¹.

3.3 Sf-9 Clone Cell Initiation and Scale-Up

For each Sf-9 clone cell initiation two vials of the Sf-9 clone cell working cell bank were retrieved from the liquid nitrogen storage tank and thawed at room temperature. Once the content of the vials was thawed it was mixed by pipetting up and down once and then added to a 250 ml spinner flask with approximately 75 ml of pre-warmed (27 °C) EX-CELL 420 medium and incubated in a walk-in incubator on a stirrer plate (passage 32). Incubation conditions for this initial and all subsequent Sf-9 clone cell spinner flask cultures during scale-up were $27 \pm 2^\circ\text{C}$ and 100 RPM (P2005, Bellco Biotechnology, Vineland, NJ) with all caps loosened to allow gas exchange. After four days of initial incubation, the cell culture was sampled and a cell count performed. Based on the results of the cell count the cell culture was then adjusted to a working volume of approximately 150 ml at a viable cell density of approximately 1.00×10^6 cells ml^{-1} by, if required, removal of old cell suspension and addition of fresh pre-warmed (27 °C) EX-CELL 420 medium. This and every subsequent culture during scale-up was then incubated for three days (passage 33) before the sampling and passaging procedure was repeated. Scale-up was done through subsequent passaging into a 1000 ml spinner flask at a target working volume of 350 ml (passage 34), a 3000 ml low-profile spinner flask at a target working volume of 1000 ml (passage 35), and eventually three 3000 ml low-profile spinner flasks at a target working volume of 1000 ml (passage 36). Target planting viable cell density in each case was 1.00×10^6 cells ml^{-1} . The last three spinner flasks cultures were incubated for another three days before usually used for bioreactor-scale experiments. In rare occasions the cultures had to be passaged one more time (passage 37), before they were used due to unforeseen delays but it was assumed that this did not affect the bioreactor-scale experiment significantly. Figure 3.1 schematically shows the cell initiation and scale-up process. Spinner flasks used were siliconized after each third use to reduce cell attachment to the glass walls.

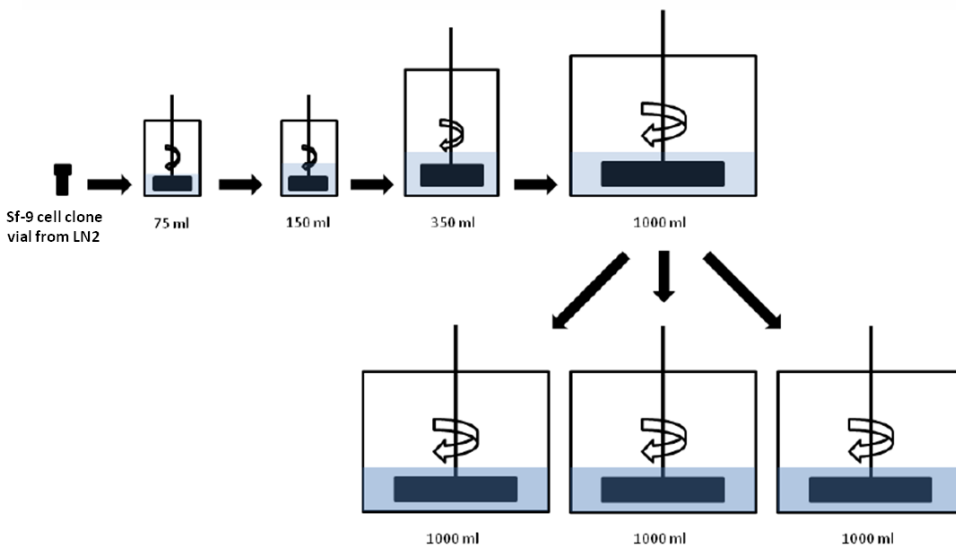


Figure 3.1. Schematic of Sf-9 clone cell initiation and scale-up. Cells were passaged every three days (with the exception of the initial 75 ml culture which was passaged after four days). Two of the last three 1000 ml cultures were then used for planting of 7.5 L working volume bioreactor precultures.

3.4 Bioreactor Experiments

All experiments performed in this work were conducted in bioreactors to ensure a consistent, monitored and, most importantly, controlled environment for the cell cultures ensuring, e.g. a sufficient oxygen supply. Two autoclavable BioClave 20 L stainless steel bioreactors (15 L working volume, see Figure 3.2) were used in this work. The vessels were monitored and controlled by a set of Applikon ADI 1030 BioController and ADI 1035 BioConsole, respectively. The bioreactors dimensions and their configuration are shown in Table 3.1.

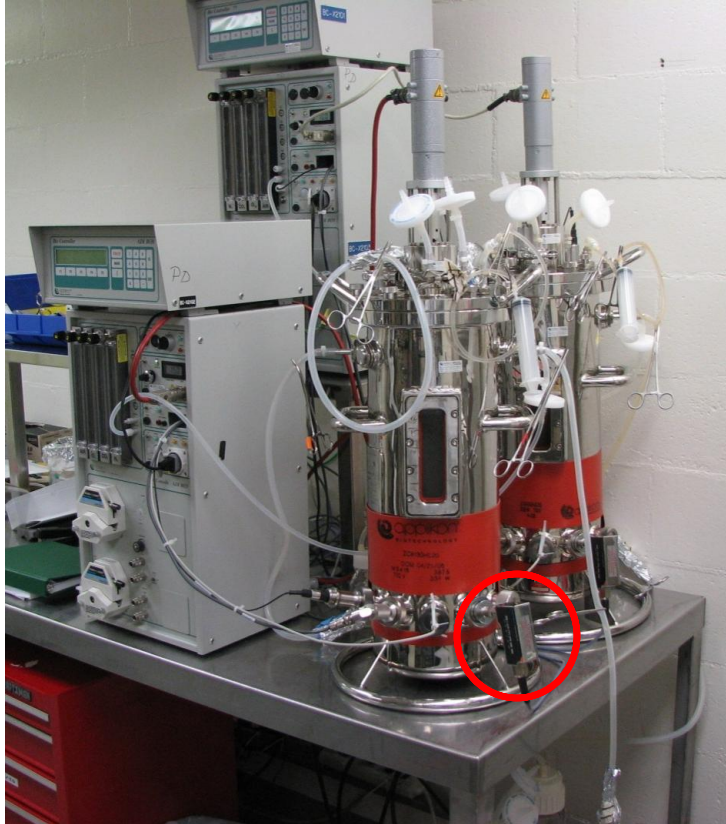


Figure 3.2. Applikon BioClave 20 L bioreactors with ADI 1030 BioController and ADI 1035 BioConsole. The red circle indicates location of the DS pre-amplifier and probe.

Table 3.1. Bioreactor dimensions and controller set-points.

	Applikon BioClave20
Type	Stirred tank reactor
Total Volume in L	20
Working Volume in L	15
Overall Height H in mm	715
Internal Diameter D in mm	210
H/D Total Volume	3
H/D Working Volume	2.1
Impeller Type	Pitched-blade, 3 x 45°, upward
Number of Impellers	2
Impeller Diameter d in mm	100
D/d	2.1
Temperature in °C	27 ± 2 °C
Agitation in RPM	100
Dissolved Oxygen in %	40
pH	Monitored
Sparger type	L-sparger below lowest impeller
Aeration in SLPM	0.1 Air + 1.0 O ₂
Aeration in vvm	0.07

Details on each study and experiment are given below. Because all experiments were conducted at a working volume of approximately 15 L and therefore required a relatively large amount of Sf-9 clone cells, an additional cell expansion step had to be included after cell scale up in spinner flasks. This was accomplished by allowing another cell growth step directly in the 20 L bioreactors at a working volume of approximately 7.5 L. When the required cell density was reached this so called preculture was then simply back diluted with fresh medium to meet the 15 L working volume scale for any subsequent experiment. The additional cell growth in the controlled environment of the bioreactor also served as an additional quality control phase for the uninfected cells.

3.4.1 Bioreactor Preparation

Before each bioreactor experiment, the pH-, dissolved oxygen-, and dielectric spectroscopy probes were visually inspected for any damage and replaced if necessary. Additionally the electrolyte for the dissolved oxygen probe was replaced and the probe polarized for at least 6 hours before calibration was performed. Probe calibrations or functionality checks were performed with pH buffer 4.01 and 7.00 (Thermo Fisher Scientific, Beverly, MA) and pure nitrogen and air, respectively. The dielectric spectroscopy pre-amplifier and probe was checked with the iBiomass simulator and internal procedures by the software. Once checks and calibrations had been performed satisfactorily, the three probes were installed into the vessel. Every addition port of the vessel was equipped with an appropriate quick-connect and 0.2 μm filter. The quick-connects themselves were wrapped in blue autoclave paper and aluminum foil. The vessel's vent ports were also equipped with 0.2 μm filters. The sampling line was equipped with a Luer-lock connector and bagged in an autoclave bag. For sterilization, approximately 75 ml of deionized water was added to the 20 L bioreactor to support steam production inside the vessel during autoclaving. The bioreactor was then autoclaved at 122.5 °C for 30 minutes, usually the day before starting the scheduled experiment (91422 ARB2, Getinge, Rochester, NY). Once the autoclave cycle was completed, the vessel was removed from the autoclave and allowed to cool down to approximately room temperature before reconnecting the probes to the controller and iBiomass pre-amplifier and instrument, respectively. Approximately 6.5 L of EX-CELL 420 was then added aseptically to the vessel and the vessel temperature and agitation

controls set to their respective set points (see Table 3.1) and allowed to stabilize over-night. Additionally air sparging was set to a low level and started to allow oxygen saturation for subsequent D.O. probe calibration the next day. Specific procedures undertaken for the dielectric spectroscopy probes are described below in Chapter 3.5.

3.4.2 Precultures for Cell Expansion

The main purpose of the precultures was further cell expansion after the spinner flask scale for support of the experiments performed at 15 L working volume. Several off-line analyses were performed to evaluate and quantify the Sf-9 clone cell growth process and its metabolic behavior under the given conditions. Dielectric spectroscopy was utilized to monitor the growth process in-line and in real-time and to establish correlations with the viable biovolume and cell density taking into account process and probe variations. Combining both eventually allowed a deeper insight into the physiological state of the cells.

Once bioreactor preparation as described above was completed, a medium sample was taken from the bioreactor for pH offset and the medium dissolved oxygen concentration control was started. The preculture was planted at a cell target concentration of 0.50×10^6 viable cells ml^{-1} (at the final working volume of 7.5 L) with Sf-9 clone cells from a scale up spinner flask culture. The working volume of the culture was adjusted to approximately 7.5 L by addition of EX-CELL 420 medium immediately post planting. The cells were then grown for approximately two days until the culture achieved a viable cell density of approximately 2.00×10^6 viable cells ml^{-1} . Samples for off-line analyses were taken from the bioreactor approximately every 24 hours starting immediately post planting.

A total of 13 precultures were grown in order to support subsequent experiments at the 15 L working volume scale. At the end of each preculture specific characteristic parameters were calculated to obtain a measurement of the quality of these cells, including the specific growth rate μ in h^{-1} , the cell doubling time t_D in h and metabolite utilization rates q_i in $\text{mmol cell}^{-1} \text{ s}^{-1}$. Equation 8 to Equation 10 show how these parameters were obtained.

$$\mu = \frac{\ln X_2 - \ln X_1}{t_2 - t_1} \quad \text{Equation 8}$$

$$t_D = \frac{\ln 2}{\mu} \quad \text{Equation 9}$$

$$q_i = \frac{\mu}{\left(\frac{X_2 - X_1}{c_{i,2} - c_{i,1}}\right)} \quad \text{Equation 10}$$

with viable cell density X in cells ml^{-1} , process time t in h, and nutrient/metabolite concentration c in mmol L^{-1} .

3.4.3 Infection at Low MOI

The Infection at Low MOI study focused on investigating the differences between and deviations within the recombinant PCV2 ORF2 protein production process in the range of MOI 0.01 to 1.00 and was performed in the 20 L bioreactor at a working volume of approximately 15 L. Industrial scale bioprocesses based on the BEVS system usually are operated in this range of MOI to reduce the amount of costly virus seed required. On the downside, small MOI and/or variations in viable cell density are easily amplified in such situations, potentially leading to undesirable process variations¹. For this study three replicates at each MOI were performed with all other parameters (bioreactor and biological) kept constant to assure comparable results. Sf-9 clone cells grown in the precultures described above in Chapter 3.4.2 were utilized in these experiments. Experiment order was randomized to reduce potential bias of undetected factors affecting the experiments. One additional culture with no

addition of virus seed was performed to serve as an uninfected control. Table 3.2 gives an overview of the experiments performed in this study.

Table 3.2. Overview of performed low MOI experiments and utilized precultures.

Preculture #	Used for Low MOI Experiment #
1	MOI 0.10 #1
2	MOI 0.01 #1
3	MOI 1.00 #1
4	MOI 0.10 #2
5	MOI 1.00 #2
6	MOI 0.01 #2
8	MOI 0.01 #3
9	MOI 0.10 #3
10	MOI 1.00 #3
11	Uninfected Control

Once the preculture had grown to a viable cell density of approximately 2.00×10^6 viable cells ml^{-1} EX-CELL 420 medium was added to back-dilute the culture to a target viable cell density of 1.00×10^6 viable cells ml^{-1} at a target working volume of approximately 15 L. Medium addition was done in steps to avoid lowering the culture temperature below 25 °C. For infection of the culture the recombinant PCV2 ORF2 baculovirus seed was removed from the -70 °C storage, thawed in a water bath at 27 °C (Precision, Winchester, VA) and added to the culture together with approximately 150 ml of pre-warmed EX-CELL 420 medium. The seed volume required for infection at the specific target multiplicity of infection was calculated accordingly to the procedures in our lab using Equation 11. Predetermined seed titer was $8.1 \pm 0.5 \log_{10}$ TCID50 ml^{-1} . TCID50 stands for 50 % Tissue Culture Infective Dose and describes the concentration of virus particles that infects 50 % of the inoculated cultures. It is known to the author that this underestimates the “real MOI” slightly compared to a MOI calculation based on plaque forming units (pfu). Nevertheless, with the pre-established error of the TCID50-based virus quantification method of $\pm 0.5 \log_{10}$ TCID50 ml^{-1} the difference is not significant. Where applicable this is indicated.

$$Volume\ virus\ seed\ (ml) = \frac{Total\ viable\ cells \times MOI}{Seed\ titer} \quad \text{Equation 11}$$

Samples for off-line analyses were taken from the bioreactor approximately every 24 hours starting immediately post infection until the harvest criterion (cell viability $\leq 10\%$) was achieved, usually after approximately 168 to 216 hours post infection (day 7 to 9 post infection), depending on the multiplicity of infection. Bioreactor decontamination and cleaning was then performed as described below in Chapter 3.4.5.

3.4.4 Medium Supplementation for Uninfected Sf-9 Clone Cell Growth

During the bioreactor cultures performed in the low MOI study described above it was observed, that one of the main metabolites, namely L-glutamine, was rapidly depleted in the culture medium in both, uninfected and infected cultures. Since the depletion happened relatively early in the cultures, usually after 48 to 72 hours, this could have had a significant negative impact on the respective cultures in terms of cell growth or recombinant PCV2 ORF2 baculovirus and protein production. Spent medium analysis of samples from additional unrelated experiments confirmed this observation and provided even more insight into possible metabolite limitations (data not shown). Interestingly, DS signals also exhibited specific behaviors around the time of L-glutamine depletion in the culture medium as described below in Chapter 4.2. Based on these observations an additional set of medium supplementation experiments for uninfected Sf-9 clone cells were designed to address and investigate this issue.

This study consisting of a total of two bioreactor experiments was performed in the 20 L bioreactors at a working volume of approximately 15 L. Sf-9 clone cells grown in the precultures described above in Chapter 3.4.2 were utilized in these experiments. Once the preculture had grown to a viable cell density of approximately 2.00×10^6 viable cells ml^{-1} EX-CELL 420 medium was added to back-dilute the culture to a target viable cell density of 1.00×10^6 viable cells ml^{-1} at a target working volume of approximately 15 L. Medium addition was done in steps to avoid dropping the culture temperature below 25 °C.

One of the two performed cultures was a replicate of the uninfected control culture from the low MOI study described in Chapter 3.4.3, while the second culture was fed multiple times with a 200 mM L-glutamine solution during the experiment in order to prevent depletion. This culture was supplemented every time the L-glutamine concentration in the media had dropped

below approximately 2.0 mmol L^{-1} and L-glutamine levels were brought back up to approximately 6.0 mmol L^{-1} . It was taken care not to exceed this level to avoid any other potential side effects on the cells metabolism. Samples for off-line analyses were taken from the cultures at an increased frequency (approximately every 8 h) starting from approximately 24 h into the process to obtain more information about changes in the culture during the observed L-glutamine depletion. Both cultures were contaminated late in the process during the stationary phase of the growth cycle and were therefore terminated. Because insect cells are usually passaged or infected during the exponential phase of the growth cycle, this did not compromise the usefulness of the obtained data and information. Bioreactor decontamination and cleaning was then performed as described below in Chapter 3.4.5.

3.4.5 Bioreactor Decontamination and Cleaning

Once the respective bioreactor experiment had been finished, the cell culture broth was harvested into a sterile carboy and decontaminated using a sodium hypochlorite solution. For bioreactor decontamination, approximately 5 L of deionized water were then added to the 20 L bioreactor and the vessel autoclaved as described earlier. Following cool down to approximately room temperature, the vessel was drained and all filters removed from any tubing and addition ports. Subsequent cleaning in place (CIP) was performed by refilling the vessel with approximately 19 L of deionized water with 0.5 % of a potassium hydroxide based cleaning in place solution. The vessel was heated up to $50 \text{ }^{\circ}\text{C}$ and held at this temperature for a minimum of 3 hours. The vessel was then allowed to cool-down to room temperature, usually over-night, drained and rinsed three times with deionized water to remove any chemical residuals. All probes were then removed and stored according to the instructions.

3.5 Dielectric Spectroscopy

Dielectric spectroscopy was performed with the iBiomass 465 instrument (FOGALE nanotech, Nimes, France). Measurements were made directly in-line of the bioreactors with sterilizable probes connected to a pre-amplifier and eventually one of four channels of the

instrument. These probes have two pairs of electrodes at their tip. Figure 3.3 shows the pre-amplifier and probe as well as the electrode configuration at the probe's tip.

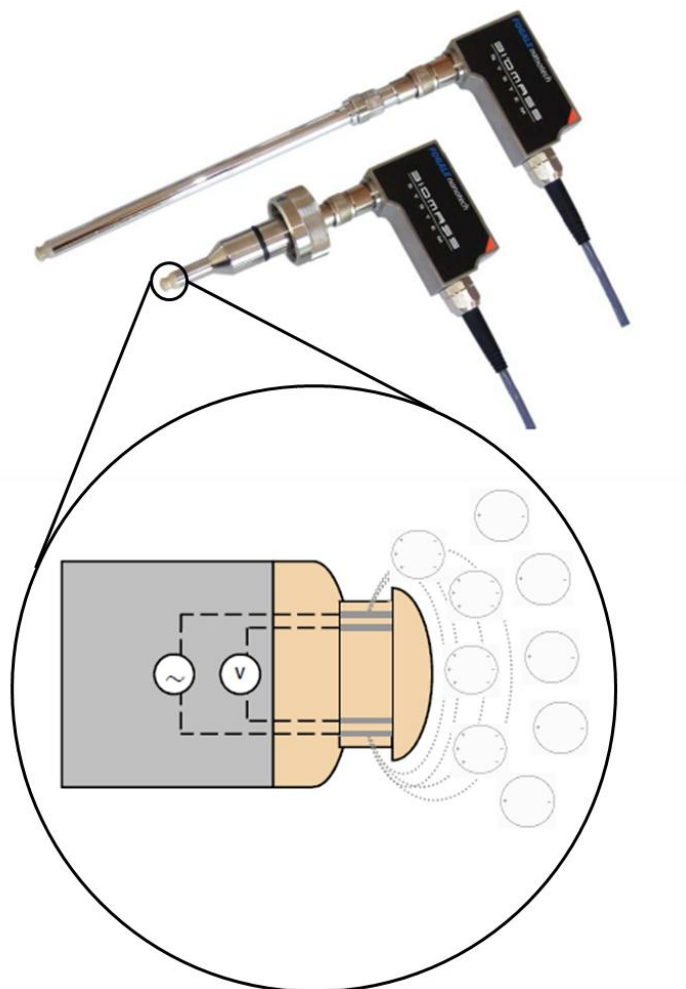


Figure 3.3. FOGALE nanotech iBiomass 465 pre-amplifier and probes. The two electrode pairs for applying the alternating electrical field and measuring resulting response are shown. Modified from: 108.

One electrode pair was used to apply an alternating electrical field to the culture medium surrounding the probe's tip while the second pair was used to measure the response. The instrument principally functions as a capacitance and conductance meter by utilizing a bridge circuit with a variable reference capacitor and resistor. These measurements were performed at a total of 17 frequencies evenly distributed over a log-scale between 300 to 10000 kHz, the so-

called frequency scan. In addition to the raw capacitance measurements at these frequencies, further proprietary processing and modeling within the instrument's software also provided the user with the three characteristic β -dispersion parameters dielectric increment $\Delta\epsilon$, characteristic frequency f_c and Cole-Cole α . The so-called Biomass signal based on the dual-frequency method and the low-frequency conductivity of the culture were provided also. The Biomass signal is often used for viable biovolume estimation because due to the nature of its measurement it is believed to be independent, or at least less influenced, by changes in viable cell radius. In other words, whereas $\Delta\epsilon$ would exhibit significant differences in two measurements of the same volume fraction of viable cells P with two different cell sizes r , the Biomass signal would give the same absolute value. This behavior is presented schematically in Figure 3.4. Both, the dielectric increment $\Delta\epsilon$ as well as the Biomass signal were given by the instrument as permittivities rather than capacitances.

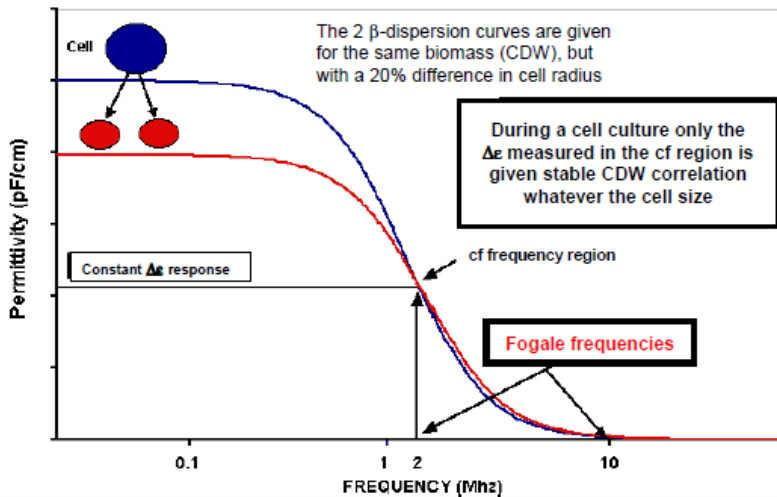


Figure 3.4. Effect of cell size on β -dispersion at constant viable biovolume. Measurement in the f_c region (Biomass signal, FOGALE frequencies) ensures cell-size independent estimations of the viable biovolume. From: 108.

Measurements with the instrument could be performed in up to four channels simultaneously. Before installation of the dielectric spectroscopy probes into the bioreactor and use during an experiment the performance of the pre-amplifier and the probe itself was verified

with the simulator tip and internal procedures. The simulator tip basically simulates a sensor measurement and the instrument verifies the functionality based on the obtained measurements. Once vessel sterilization, cool-down and initial medium addition was accomplished, two manual cleaning cycles were applied to the probe. The cleaning consists of applying proprietary predefined voltages to the probe. After medium temperature and signal stabilization the Biomass signal and frequency scan measurements were zeroed to adjust for the medium background. Data recording was started immediately before planting of the cultures into the bioreactors and set to an acquisition time of 30 minutes. For the dual-frequency Biomass measurement the “Animal Cell Culture” mode (1000 kHz measurement frequency, 10000 kHz background frequency, signal integration “high” (5 minutes)) was chosen to ensure a measurement at a frequency slightly higher than the f_c observed for the cells in preliminary experiments to obtain a signal independent of the cell radius. At the time of harvest the recording was stopped and the data retrieved from the instruments storage for subsequent analysis. Once decontamination and cleaning of the vessel had been performed as described earlier in 3.4.5 the dielectric spectroscopy probes were stored dry capped in the provided holder.

3.6 Quantification of Medium Nutrient and Metabolite Concentrations

The YSI 2700 Select Biochemistry Analyzer (YSI, Yellow Springs, Ohio) was utilized to quantify culture medium concentrations of four major insect cell culture metabolites, namely D-glucose, L-glutamine, L-lactate and L-glutamate. The sensor principle is based upon membrane-immobilized oxidase enzymes coupled with an electrochemical probe and is shown in Figure 3.5.

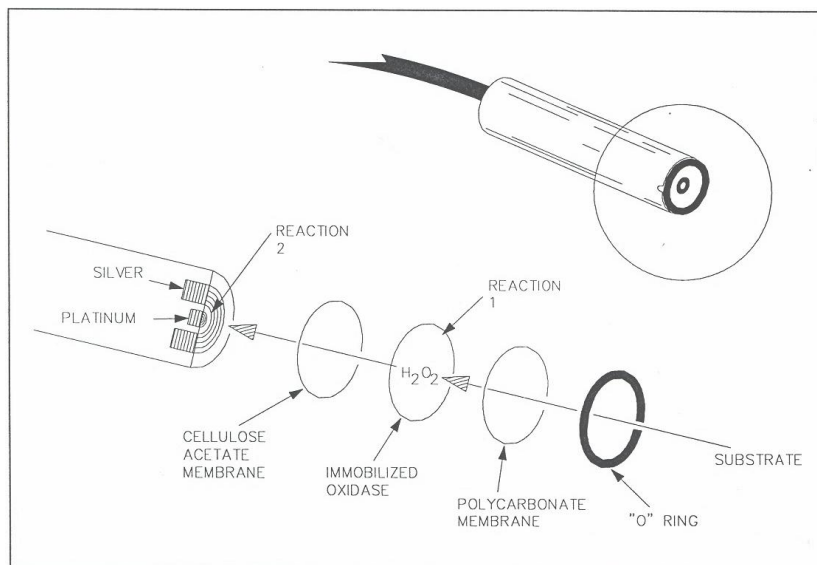
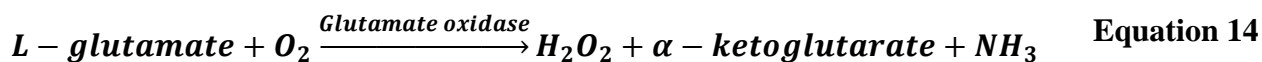
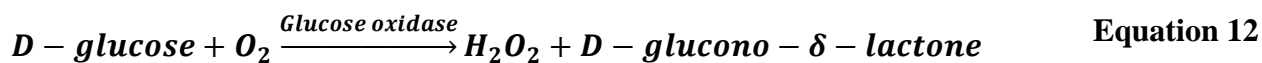
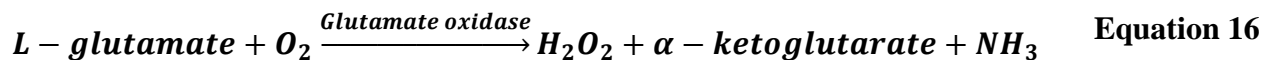


Figure 3.5. Sensor principle of the YSI 2700 Select Biochemistry Analyzer. The substrate (or analyte) diffuses through the first polycarbonate membrane and is oxidized by an immobilized oxidase. The produced H_2O_2 diffuses through a cellulose acetate membrane and is oxidized at the platinum anode of the sensor. The resulting electron flow is linearly proportional to the analyte concentration. From: 109.

The probe's face is covered with a three-layer membrane containing the immobilized oxidase and is exposed to the buffer-filled sample chamber¹⁰⁹. Each analyte requires a specific oxidase enzyme and so membrane. Once the sample is injected into the sample chamber the analyte diffuses through the first polycarbonate membrane and is rapidly oxidized according to the reactions shown below. As a result, H_2O_2 is produced.



To determine the amount of L-glutamine in a sample, two enzymes are co-immobilized in one membrane.



The produced H₂O₂ subsequently diffuses through a cellulose acetate membrane and is oxidized at the platinum anode of the probe. The cellulose acetate membrane serves as a barrier for other chemical compounds with a molecular weight above approximately 200 g mol⁻¹ potentially interfering with the oxidation and contributing to the sensor current. This reaction produces an electron flow, which is linearly proportional to the steady state H₂O₂ concentration, and thus the analyte concentration in the sample, in absence of mass transfer limitations.



Analytes were quantified in pairs in two dual-channel instruments equipped for either D-glucose and L-lactate or L-glutamine and L-glutamate analysis. This allowed the simultaneous measurement of the latter two in cell culture samples containing both analytes by subtraction of the quantified “free L-glutamate” from the “total L-glutamate” detected on the L-glutamine channel (see reactions above).



The instrument performance was verified before each analysis with provided standards of known analyte concentration. In case performance was outside of established ranges the membrane on the affected channel was replaced. The analysis with the YSI 2700 Select Biochemistry Analyzer has an accuracy of ± 5 % of the measured concentration¹⁰⁹.

3.7 Quantification of Viable Cell Density, Cell Viability and Mean Cell Diameter

The Vi-CELL XR analyzer (Beckman Coulter, Brea, CA) was utilized to determine total and viable cell density, cell viability and mean total and viable cell diameter of a Sf-9 clone cell culture sample. This instrument performs an automated analysis based on the trypan blue dye exclusion method and utilizes video imaging of a flow through cell. Trypan blue is usually incapable of entering a viable cell through the cell membrane because of its high molecular weight (961 g mol^{-1}) and negative charge and viable cells therefore appear “unstained” on the flow through cell images. Cells with a damaged membrane however will take up the dye and therefore appear “stained”. However, it should be noted that the trypan blue exclusion method tends to overestimate cell viability^{110, 110}. Differences of 20 to 30 % cell viability compared to other methods have been reported^{111, 112}. For analysis with the Vi-CELL XR analyzer approximately 1 ml of well-mixed cell culture sample was dispensed into a sample cup, the sample information entered into the software and the analysis started. The instrument automatically mixed the sample with the trypan blue dye and analyzed 50 images taken of the flow through cell in order to obtain the parameters mentioned above. Two different instrument settings, called “cell type”, were used for analysis. Cell culture samples with cell viabilities above approximately 50 % were analyzed with the standard Sf-9 clone setting. Because these settings did not yield reliable results for samples with cell viabilities below approximately 50 % and a lot of cell debris, a second “Sf-9 clone low viability” setting was used in these cases. But while this setting allowed a better estimation of cell density and viability, as determined by visual inspection of the obtained flow cell images, mean total and viable cell diameters were usually estimated significantly higher than before. The analysis with the Vi-CELL XR instrument has an accuracy of $\pm 10 \%$ of the measured cell density Table 3.3 gives an overview of the used analyzer settings.

Table 3.3 Vi-CELL XR “cell type” settings used in this work. “Sf-9 clone” settings were used for uninfected cells and until day 5 post infection. Afterwards “Sf-9 clone low viability” was used.

	Cell type setting	
	Sf-9 clone	Sf-9 clone low viability
Minimum cell diameter	8 μm	5 μm
Maximum cell diameter	30 μm	40 μm
Minimum circularity	0.3	0.3
Dilution factor	1	1
Cell brightness	70 %	80 %
Cell sharpness	150	150
Viable cell spot brightness	40 %	70 %
Viable cell spot area	30 %	20 %
Decluster degree	High	Low
Aspirate cycles	1	1
Trypan blue mixing cycles	2	2

3.8 Quantification of Fraction of Infected Cells by Flow Cytometry

To follow the infection process in the cultures post infection a flow cytometric technique was utilized in this work. A monoclonal antibody against the baculovirus envelope protein gp64 labeled with the fluorochrome phycoerythrin (excitation 488 nm, emission 575 nm) allowed the direct identification of infected cells within a sample using an EPICS XL flow cytometer (Beckman Coulter, Miami, FL). The gp64 protein is essential for virus infectivity and spread in a culture and is expressed on the surface of infected insect cells as early as 6 h post infection¹¹³⁻¹¹⁵.

Daily routine decontamination and cleaning procedures of the Beckman Coulter EPICS XL flow cytometer were performed before and after each set of samples. Twice filtered (0.2 μm) 3 % sodium hypochlorite solution was run (300 s) once through the instrument followed by three times twice filtered (0.2 μm) deionized water. When a large number of events (> 50) was detected during any of the runs, this procedure was repeated. Additionally vacuum line maintenance was performed at the end of each analysis with twice filtered (0.2 μm) deionized water. The performance of the instrument was verified daily by using Flow Check fluorospheres after the initial decontamination and cleaning procedure. 5000 events were collected and acceptance limits were > 90 % of events in the forward and side scatter box, > 99 % of events in each channel gate and a coefficient of variance < 2 % in each channel.

For sample preparation, the culture volume equivalent to a total number of 1.00×10^6 viable cells was dispensed into each of two centrifuge tubes and centrifuged at 500 g and 4 °C for 5 minutes (Labnet Z 382K, Hermle, Wehingen, Germany). Subsequently, the supernatant was discarded. The sample was washed twice by resuspension of the pellet in 500 µl of cold (4 °C) phosphate buffered saline (pH 7.4) with 0.2 % of bovine serum albumin (to reduce unspecific binding) followed by centrifugation as described above. One of the samples was then resuspended in 100 µl of a labeled anti-baculovirus envelope gp64 protein solution. Monoclonal antibody (0.125 µg per sample) was used as recommended by the manufacturer and confirmed by titration experiments¹¹⁶. The remaining sample was resuspended in 100 µl of cold (4 °C) phosphate buffered saline (pH 7.4) with 0.2 % of bovine serum albumin to serve as a negative control. The samples were then incubated in the dark at 4 °C for 30 minutes. Following the incubation the samples were centrifuged as described above and the supernatant discarded. The samples were then washed twice in PBS as described above and subsequently resuspended in 1 ml of cold (4 °C) phosphate buffered saline (pH 7.4) with 0.2 % of bovine serum albumin for analysis on Channel 2 (575 nm) of the EPICS XL flow cytometer. The FL2 fluorescence of the negative control sample was used as a cut-off with events having a higher fluorescence being defined as phycoerythrin-stained and therefore baculovirus infected. Events (30000) were collected for each sample and results were reported as percentage below and above the set cut-off (software EXPO 32 ADC, Applied Cytometry Systems, Sheffield, UK). Only viable cells as determined by forward and side scatter discrimination were considered because dead cells tend to bind antibodies unspecifically¹¹⁷. Table 3.4 shows important instrument settings for this analysis. These settings allowed inclusion of the whole cell population post infection despite significant differences in cell size and granularity.

Table 3.4. EPICS-XL settings for the fluorescence channels used in this work.

Channel	Volts	Gain
FS	20	1.00
SS	625	2.00
FL2 (PE)	567	1.00

3.9 Quantification of Recombinant PCV2 ORF2 Baculovirus by Titration

An antibody-based end-point dilution assay was used to quantify the recombinant PCV2 ORF2 baculovirus concentration in bioreactor experiment samples. Stock cultures of adherent Sf-9 cells were routinely passaged in tissue culture flasks to provide the cells needed for the actual titrations performed in 96-well plates. Both procedures are described below. Per scheduled assay day, 22 samples plus 2 accompanying reference samples were analyzed.

Sf-9 Cell Stock Cultures

Tissue culture flasks with a viable *Spodoptera frugiperda* Sf-9 cell sheet of seven days of age were selected and examined visually under the microscope (CK2, Olympus, Melville, NY) for cell confluence and adherence. If determined to be acceptable, the old growth media was discarded and the cells dislodged by aspirating and dispensing approximately 10 ml of EX-CELL 420 medium with 5 % fetal bovine serum against the cell sheet. If cells remained attached another 10 ml of EX-CELL 420 medium with 5 % fetal bovine serum was added to the tissue culture flask and the cells dislodged by gently tapping the side of the tissue culture flask. Cell suspensions from both dislodging steps and multiple tissue culture flasks were pooled into a sterile container, mixed and a cell count performed using the Vi-CELL XR analyzer as described above. New tissue culture flasks (175 cm², BD Falcon, Franklin Lakes, NY) were planted at a viable cell density of 1.00×10^7 cells per flask in 100 ml of EX-CELL 420 medium with 5 % fetal bovine serum and $50 \mu\text{g ml}^{-1}$ gentamicin sulfate. The cells were incubated at 27 ± 2 °C in a humidified incubator (Nuair, Plymouth, MN) for seven days before this procedure was repeated.

Planting of 96-Well Tissue Culture Plates

The 96-well plates (flat bottom, BD Falcon, Franklin Lakes, NY) for the titration assay were planted one to four hours before actual initiation of the titrations. The number of plates planted depended on the number of assays scheduled. Firstly the same steps as described above for the Sf-9 cell stock cultures were performed. Using the determined viable cell count a cell suspension with a viable cell density of 5.00×10^5 cells ml⁻¹ was prepared in EX-CELL 420 medium with $50 \mu\text{g ml}^{-1}$ gentamicin sulfate. The 96-well plates were then planted with 0.1 ml of this cell suspension per well and incubated in a humidified incubator at 27 ± 2 °C for up to four

hours. This resulted in a 30 – 50 % confluent cell sheet at the time of the titration initiation described below.

Titration and Inoculation of 96-Well Tissue Culture Plates

The samples to be analyzed were retrieved from the $-70\text{ }^{\circ}\text{C}$ freezer and thawed at room temperature. In the meantime, so-called 96-deep well dilution blocks were prepared by adding $1350\text{ }\mu\text{l}$ of EX-CELL 420 medium with $50\text{ }\mu\text{g ml}^{-1}$ gentamicin sulfate to each well. $150\text{ }\mu\text{l}$ of each sample and a baculovirus concentration reference was then pipetted into the designated wells in row A of the dilution blocks. Using a multi-channel pipette a ten-fold dilution series was prepared by transferring $150\text{ }\mu\text{l}$ from the wells in row A to row B and so forth down to row H. Before each transfer, the contents of each well were mixed by pipetting up and down for five times. Pipette tips were changed after each transfer. Once this was accomplished, the 96-well tissue culture plates planted earlier were removed from the incubator and inoculated with 0.1 ml of the prepared dilutions. Overall one 96-well tissue culture plate was used per sample with ten replicate wells (columns 2 to 11) per dilution. Columns 1 and 12 were used as negative controls and inoculated with 0.1 ml of EX-CELL 420 medium with $50\text{ }\mu\text{g ml}^{-1}$ gentamicin sulfate. The baculovirus concentration reference was run on one separate plate per assay day. The plates were then covered with the lid provided and incubated in a humidified incubator at $27 \pm 2\text{ }^{\circ}\text{C}$ for six days.

Fixing and Staining

At the end of the six-day incubation, the inoculated 96-well tissue culture plates were removed from the incubator and the media of each well discarded. $100\text{ }\mu\text{l}$ of cold 50:50 methanol/acetone solution was then added to each well and incubated at room temperature for 10 ± 2 minutes to fix the plates. Subsequently, $50\text{ }\mu\text{l}$ of 1:300 diluted anti-baculovirus envelope gp64 protein was added to each well, the plates covered with the accompanying lid and incubated in a humidified incubator at $37 \pm 2\text{ }^{\circ}\text{C}$ for 50 minutes. At the end of the incubation, the plates were removed from the incubator and the antibody solution discarded from each well. Each well was then washed with $100\text{ }\mu\text{l}$ of room temperature phosphate buffered saline twice. After this $50\text{ }\mu\text{l}$ of the 1:100 diluted fluorescein labeled goat anti-mouse IgG (H + L) antibody was added to each well. The plates were covered again and incubated in a humidified incubator

at 37 ± 2 °C for 50 minutes. At the end of the incubation, the plates were removed from the incubator and the antibody solution discarded from each well. Each well was washed with 100 μ l of phosphate buffered saline and the liquid discarded. As a last step 50 μ l of phosphate buffered saline was added to each well, the plates were covered with the lid, wrapped in aluminum foil, and transferred to the fluorescent microscope for reading and interpretation.

Reading and Interpretation of Titrations

Utilizing the fluorescent microscope (Eclipse TE2000U, Nikon Instruments, Melville, NY), wells of the 96-well tissue culture plates were observed for positive fluorescence. A well was scored positive when immunofluorescent positive cells due to baculovirus were observed in any area of the well. The number of positive wells over the ten wells inoculated per dilution was recorded. The Reed-Muench 50 % end-point formula was used to calculate the baculovirus concentration as \log_{10} TCID₅₀ ml⁻¹. For a valid test, two criteria had to be met. Firstly, the negative control wells on each 96-well tissue culture plate (columns 1 and 12) showed no positive fluorescence typical of baculovirus. Secondly, the reference titer fell within ± 0.5 \log_{10} TCID₅₀ ml⁻¹ of the established average titer for this specific reference. Both criteria were met for all performed titrations. Previously established error for this method exhibited is ± 0.5 \log_{10} TCID₅₀ ml⁻¹.

3.10 Quantification of Recombinant PCV2 ORF2 Protein by ELISA

An indirect-sandwich enzyme-linked immunosorbent assay was utilized to quantify the recombinant PCV2 ORF2 protein concentration in bioreactor experiment samples. Concentrations were reported as relative potency (RP) to a reference sample with a known (but confidential) PCV2 ORF2 protein concentration as calculated by the software RelPot 4.0. Per scheduled assay day, 10 samples were analyzed. For buffer compositions, see Appendix A - .

As a first step, the swine anti-PCV2 ORF2 polyclonal antibody (capture antibody) was diluted 1:6000 in carbonate coating buffer and 100 μ l of this solution was added to all wells of a 96-well plate (Microlon 600, Greiner Bio-One, Montroe, NC). Up to five plates were coated at a time to allow analysis of up to ten samples. The plates were then sealed and stacked. The stack

was capped with an empty 96-well plate and incubated at 37 ± 2 °C for 17 to 24 hours, usually overnight.

After the initial incubation, all plates were washed three times with 250 µl of washing buffer per well utilizing an automated plate washer (EL_x 405, BioTek Instruments, Winooski, VT). After the last wash, the plates were inverted and tapped onto a paper towel to remove residual liquid. 250 µl of blocking solution were then added to each well, the plates sealed and incubated at 37 ± 2 °C for 1 hour \pm 5 minutes. The plates were not stacked during this or any subsequent incubation.

The frozen sample vials as well as the reference and a negative control were retrieved from the -70- °C freezer and thawed at room temperature. Separate 96-deep well sample dilution plates (polypropylene, Nunc, Roskilde, Denmark) were prepared by addition of 200 µl of diluent solution to each well except for columns 1 to 3 in row H and all of row A. The samples, references, and controls were diluted 1:30 in diluent solution in separate test tubes and 300 µl of this dilution added to the corresponding wells in row A of the previously prepared dilution plates. Using a multichannel pipette the contents of row A were then mixed by pipetting up and down for five times before 100 µl were transferred to row B. This was continued down to row G with changing pipette tips after each transfer.

Following the incubation with the blocking solution step, the plates were washed again as described above. Starting at row H 100 µl of each well were then transferred from the prepared dilution plates to the corresponding well on the actual 96-well test plates. Pipette tips were changed after the first liquid transfer (row H) but the same set of pipette tips were used for all subsequent transfers up to row A. Prior to each transfer the contents of each well on the dilution plates were mixed by pipetting up and down for three times. The plates were sealed and incubated at 37 ± 2 °C for 1 hour \pm 5 minutes.

This incubation was followed by another washing step as described above. 100 µl of a 1:300 dilution of the monoclonal antibody to PCV2 ORF2 (detection antibody) in diluent

solution were then added to each well. The plates were sealed and incubated at 37 ± 2 °C for 1 hour \pm 5 minutes.

Following the incubation, the plates were then washed again as described above. 100 μ l of a 1:10000 dilution of the goat anti-mouse (H+L)-HRP (conjugate antibody) in conjugate solution (1 % normal rabbit serum in diluent solution) were added to each well. The plates were sealed and incubated at 37 ± 2 °C for 45 ± 5 minutes.

This incubation was followed by another final washing step as described above. Equal volumes of the two components (3,3',5,5'-tetramethylbenzidine and H₂O₂) of a microwell peroxidase substrate system were mixed immediately prior to use and 100 μ l of this solution was added to each well. The plates were incubated at room temperature for 15 minutes \pm 15 seconds. The reaction was stopped by addition of 100 μ l of a 1 M HCl solution to each well. Subsequently the absorption of each well at 450 nm was read with an automated ELISA plate reader (Wave_x 340, BioTek Instruments, Winooski, VT). For a valid test, three criteria had to be met. Firstly, the absorbance of the positive control (wells C1, C2, and C3) had to be ≥ 0.838 . Secondly, the average absorbance of the negative control (wells H1, H2, and H3) had to be ≤ 0.200 . Thirdly, the analysis with the software RelPot 4.0 (USDA, APHIS) had to result in valid co-parallel lines or a valid reported RP value. All three criteria were met for all performed analysis.

3.11 Error and Reproducibility Considerations

Analytical techniques and methods used in the field of cell culture technology have considerable variability or errors associated with them. Methods and instruments used in this work for example included an automated cell density analyzer (Vi-CELL XR) and a membrane-based electrochemical biochemistry analyzer for medium component quantification (YSI Select 2700), as well as a bioassay for the quantification of a recombinant baculovirus (end-point dilution assay) or an immunosorbent assay (ELISA) for the quantification of a recombinant target protein. Errors of 10 % or higher (e.g. error of $\pm 0.5 \log_{10}$ TCID₅₀ ml⁻¹ for virus quantification) are commonly seen with these methods or instruments and are accepted in the

field of cell culture technology. While this alone often already poses a significant challenge for data interpretation, sample preparation adds another layer of potential variability in addition to the assay error. Small variations or delays in the processing of a discrete sample taken from a bioreactor can for example change the obtained results significantly, e.g. for cell viability. While every effort was made in this work to reduce the variability in sample preparation, the reader should be aware that the overall random error generally will exceed the specified instrument/assay error. This becomes especially important for cases where specific parameters were calculated based on multiple error-associated values, e.g. the specific recombinant protein productivity per viable cell. Error propagation was used to capture the impact of multiple error-prone parameters on a final result as comprehensively as possible.

Chapter 4 - Results and Discussion

4.1 Precultures for Cell Expansion

The main purpose of the precultures was further cell expansion after the spinner flask scale for support of the experiments performed at 15 L working volume. Several off-line analyses were performed to evaluate and quantify the Sf-9 clone cell growth process and its metabolic behavior under the given conditions. Dielectric spectroscopy was utilized to monitor the growth process in-line and in real-time and to establish correlations with the viable biovolume and cell density taking into account process and probe variations. Combining both eventually allowed a deeper insight into the physiological state of the cells.

As described in Chapter 3.4.2 the 20 L bioreactors were inoculated with a viable cell density of approximately 0.50×10^6 cells ml^{-1} at a working volume of 7.5 L. Culture conditions were controlled at 27.0 °C, 100 rpm and 40 % dissolved oxygen concentration. The cells were allowed to grow for two days with sampling for off-line analyses approximately every 24 hours. A total of 13 of cultures was performed. Since the cells grown in these cultures were to be used in subsequent experiments they were not allowed to reach the stationary phase in their cell growth cycle to avoid potential detrimental effects on those experiments. Raw data collected is presented in Appendix B - .

4.1.1 Cell Culture Parameters

Most of the cultures showed a slightly lower initial planting viable cell density than targeted which is probably due to a systematic error in the initial medium addition process, despite the use of a scale to verify the amount of medium added to the vessel. Initial viable cell densities ranged from 0.33 to 0.50×10^6 cells ml^{-1} . Nevertheless, the initial viable cell density proved to be very consistent within the 13 precultures and resulted in immediate cell growth without any major lag phase, as shown in Figure 4.1. At the end of the two-day cell growth phase all precultures had reached a viable cell density of approximately 2.00×10^6 cells ml^{-1} and were therefore ready for back dilution and use for subsequent experiments. Additionally, all 13

cultures showed viabilities well above 90 % during this two-day cell growth phase (data not shown).

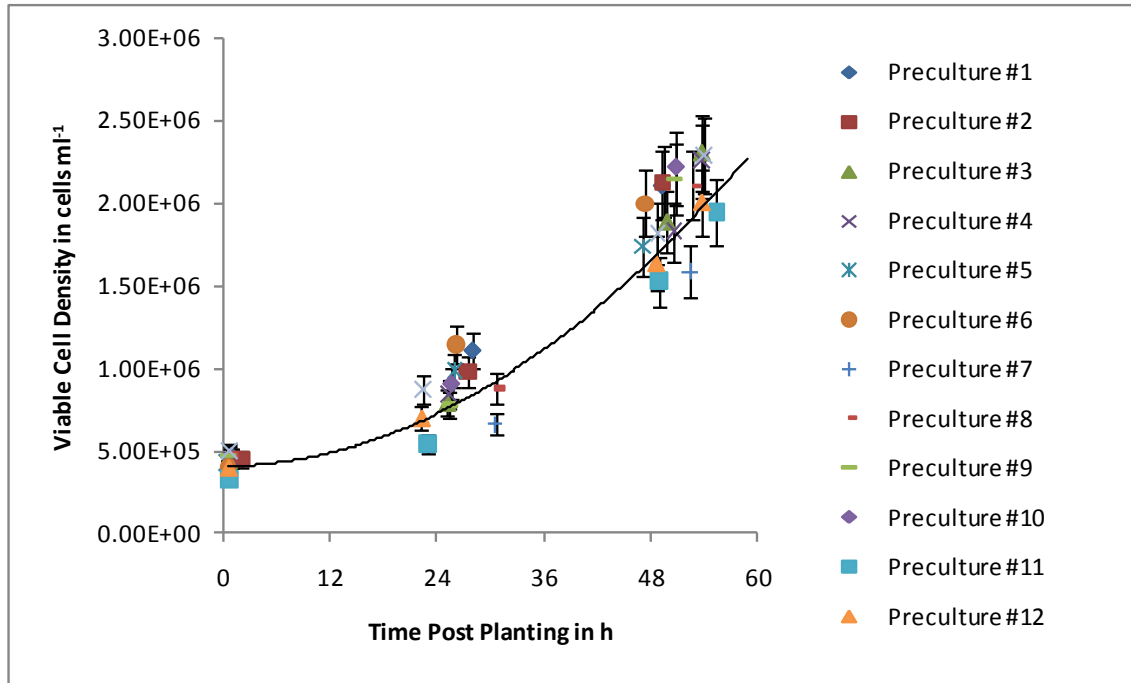


Figure 4.1. Viable cell density post planting in the 13 precultures. Cells started growing without apparent lag-phase immediately post planting and reached a viable cell density of approximately 2.00×10^6 cells ml⁻¹ after two days of growth. Trendline is intended to guide the eye only.

Based on the data for all 13 precultures the average specific growth rate μ and the cell doubling time t_D were calculated with Equation 8 and Equation 9. The specific growth rate μ was estimated to be $0.031 \pm 0.002 \text{ h}^{-1}$, while the cell doubling time t_D was $22.2 \pm 1.4 \text{ h}$. These values are in accordance with literature available for Sf-9 insect cell cultures, reporting ranges for μ and t_D of about 0.029 to 0.035 h^{-1} and 20 to 24 h , respectively¹¹⁸⁻¹²⁰.

Figure 4.2 gives an overview over the mean viable cell diameters profiles for all 13 precultures. Initial viable cell diameters ranged from 17.00 to $18.66 \mu\text{m}$ with values stabilizing between 17.83 and $18.53 \mu\text{m}$ at the end of the two-day growth phase. No major changes over

time or differences between precultures were observed. This, together with the cell viability values, also indicated consistent precultures suitable for the subsequent experiments.

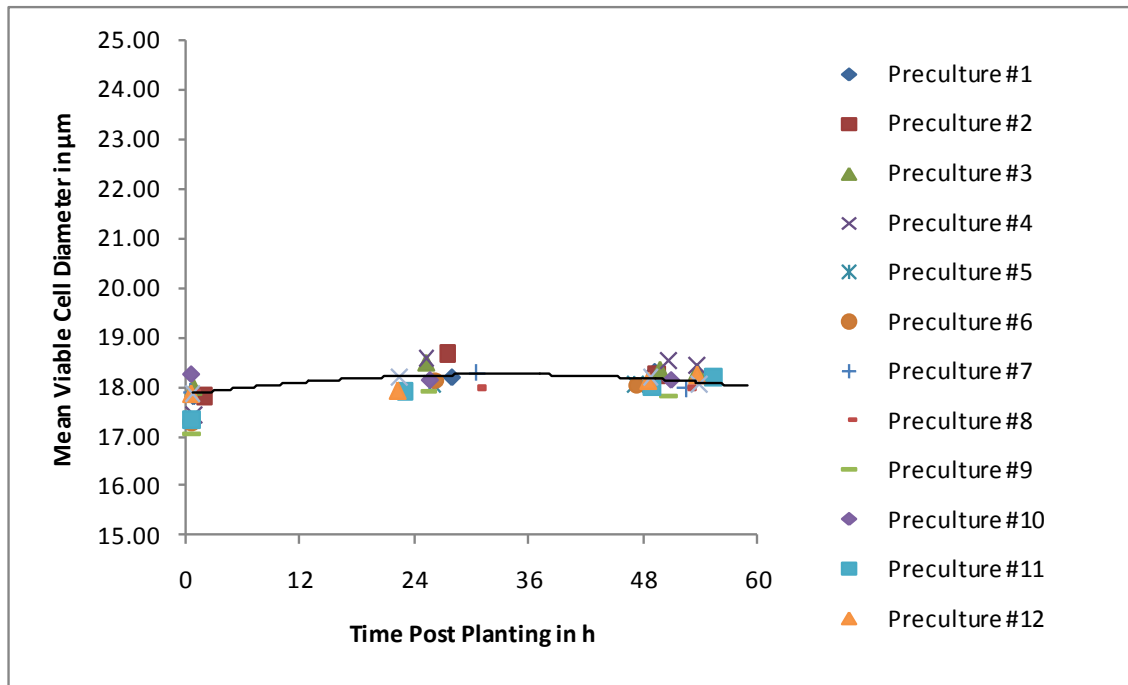


Figure 4.2. Mean viable cell diameter post planting in the 13 precultures. Mean viable cell diameters were around 18.00 µm but no major change was observed during the two-day growth phase and. Trendline is intended to guide the eye only.

Reported literature values for the mean cell diameter of uninfected *Spodoptera frugiperda* insect cells are generally slightly lower than values found in this work and range from approximately 12 to 15 µm^{13, 15, 120}. These values were mostly obtained for a different cell clone, Sf-9, and they were also obtained with a Coulter Counter, which is based on a different (electric) analysis principle. It is possible that the Sf-9 clone cell clone used in this work is either simply slightly larger in terms of diameter or the different analysis principle of the Coulter Counter produced systematically lower values and “underestimates” the cell diameter compared to the Vi-CELL XR analysis and the specific image analysis settings used in this work. In addition, generally the total mean viable cell diameter is reported in the literature, which takes into account viable and dead cells. In this work only the mean viable cell diameter was used and reported. It is known to the author that dead cells usually have a slightly smaller cell diameter

than viable cells if analyzed with the Vi-CELL XR analyzer. Therefore, the mean total cell diameter will usually be lower than the mean viable cell diameter of the same sample but in this work the difference was less than 2 % for the case of uninfected Sf-9 clone cells and therefore this is probably not the main contributor to the difference observed.

The pH was left uncontrolled during the precultures but it was monitored with an in-line probe directly immersed into the cell culture broth. Initial pH values ranged from 6.39 to 6.55 but generally dropped slightly to 6.21 to 6.39 at the end of the two-day growth phase (see Figure 4.3). The pH is often left uncontrolled in insect cell cultures because these cells are supposed to have a very high buffer capacity themselves²¹. Additionally the EX-CELL 420 medium used in this work has a 8.4 mM phosphate buffer system integrated to help keeping the pH in acceptable range¹²¹. The optimum pH range for insect cell cultures is reported to be about 6.2 to 6.9¹ which covers the values observed in this work.

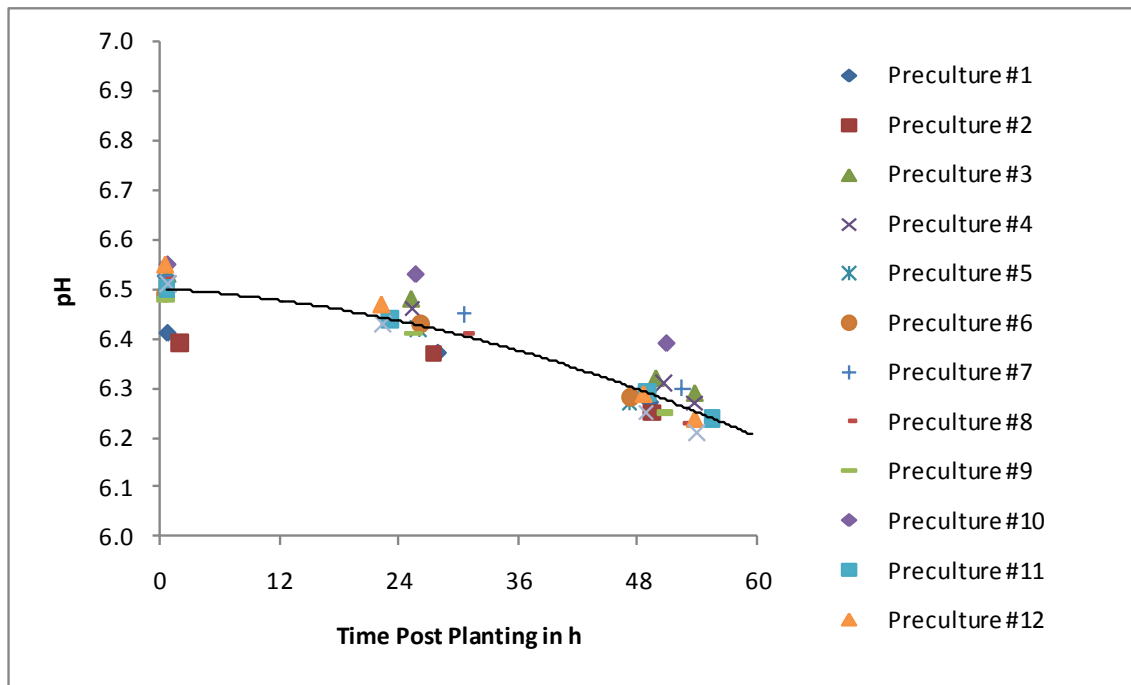


Figure 4.3. Culture medium pH post planting in the 13 pre-cultures. Initial pH values ranged from approximately 6.4 to 6.5 and decreased slightly to approximately 6.3 during the two-day growth phase. Trendline is intended to guide the eye only.

The medium concentrations of the four metabolites D-glucose, L-glutamine, L-lactate and L-glutamate were measured off-line in whole cell culture broth samples with the YSI 2700 Select Biochemistry Analyzer. These analyses are prone to an error of 5 % as specified by the instrument manufacturer¹⁰⁹.

Initial medium D-glucose concentrations ranged from 31.42 to 33.86 mmol L⁻¹ and continuously fell to 28.70 to 31.19 mmol L⁻¹ during the two-day growth phase, as can be seen in Figure 4.4. The uninfected Sf-9 clone cells used D-glucose during their growth phase but the measured decrease this nutrient's medium concentration was barely significant.

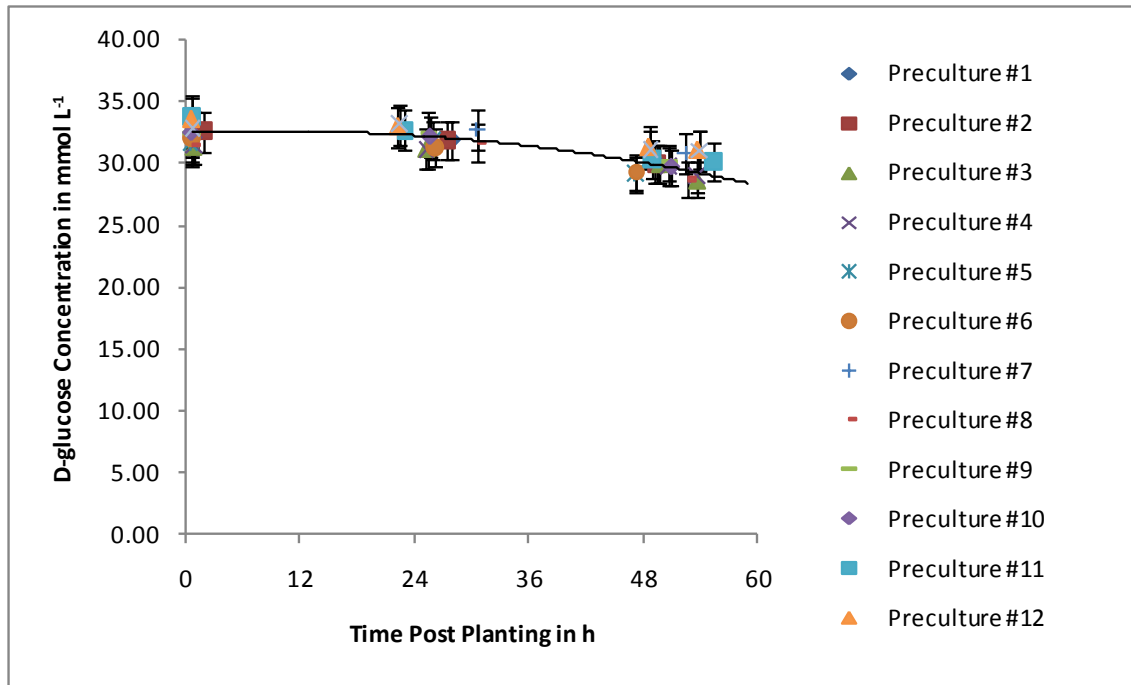


Figure 4.4. Medium D-glucose concentration post planting in the 13 pre-cultures. Initial D-glucose concentrations were approximately 32.0 mmol L⁻¹ and decreased to approximately 30.00 mmol L⁻¹ during the two-day growth phase. Trendline is intended to guide the eye only.

The specific D-glucose utilization rate q_{Glc} was estimated to be $(-1.38 \pm 0.29) \times 10^{-14} \text{ mmol cell}^{-1} \text{ s}^{-1}$, which is comparable to Sf-9 cell data available in the literature where a value of $-2.4 \times 10^{-14} \text{ mmol cell}^{-1} \text{ s}^{-1}$ is reported¹²⁰.

A more significant decrease in medium concentration due to utilization by the uninfected Sf-9 clone cells could be observed for L-glutamine. Figure 4.5 shows that initial concentrations of this nutrient ranged from 4.05 to 5.83 mmol L⁻¹ and continuously decreased to 1.41 to 3.51 mmol L⁻¹ during the two-day growth phase. The significantly lower medium L-glutamine concentrations for pre-cultures #11 to #13 can be explained by the fact, that these experiments were performed with EX-CELL 420 medium, which had been stored longer before usage. Since L-glutamine is instable in a liquid environment, even at 4 °C, it had degraded over the prolonged storage time.

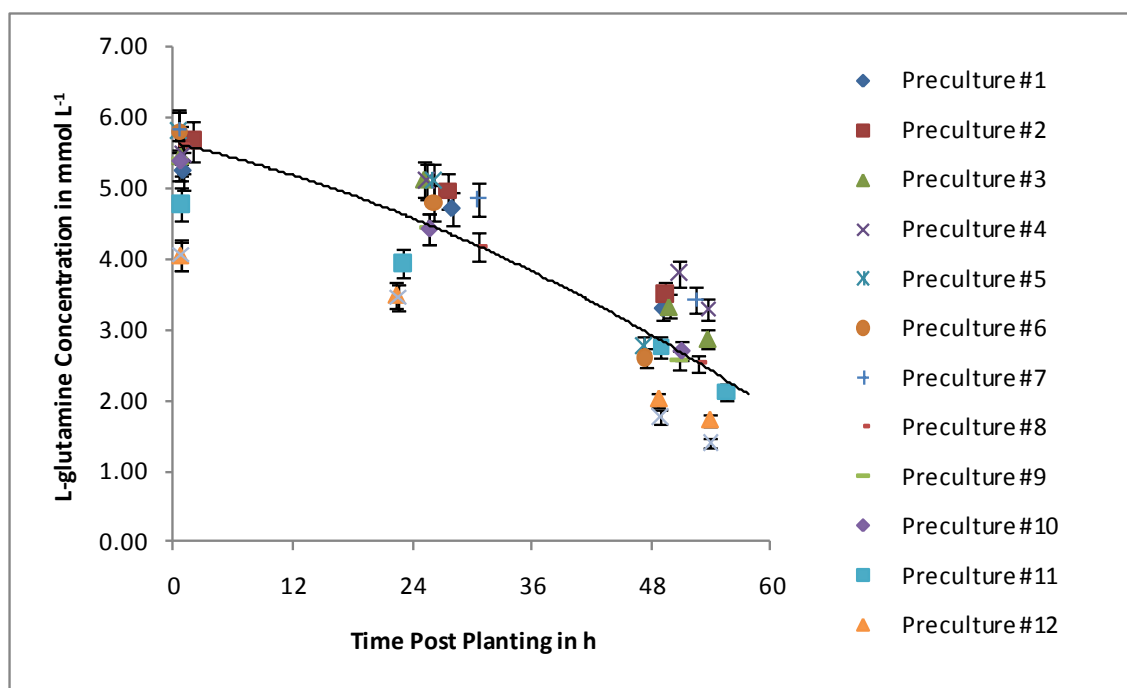


Figure 4.5. Medium L-glutamine concentration post planting in the 13 pre-cultures. Initial L-glutamine concentrations were usually above 5.00 mmol L⁻¹ and decreased to approximately 2.00 to 3.51 mmol L⁻¹. Precultures #11 and 12 showed slightly lower L-glutamine concentrations because of older medium used. Trendline is intended to guide the eye only.

The specific L-glutamine utilization rate q_{Glc} was estimated to be $(-1.39 \pm 0.29) \times 10^{-14} \text{ mmol cell}^{-1} \text{ s}^{-1}$, which is comparable to Sf-9 cell data available in the literature where values slightly above $-1.0 \times 10^{-14} \text{ mmol cell}^{-1} \text{ s}^{-1}$ are reported^{120, 122}.

In contrast to the first two medium components measured, the two metabolites L-lactate and L-glutamate continuously built up as byproducts in the culture medium during the two-day growth phase of the pre-cultures. Figure 4.6 gives an overview of the medium L-lactate concentration for the 13 pre-cultures. Initial medium L-lactate concentrations ranged from 0.98 to 1.14 mmol L^{-1} and continuously increased to 1.55 to 2.39 mmol L^{-1} over the course of the two-day growth phase.

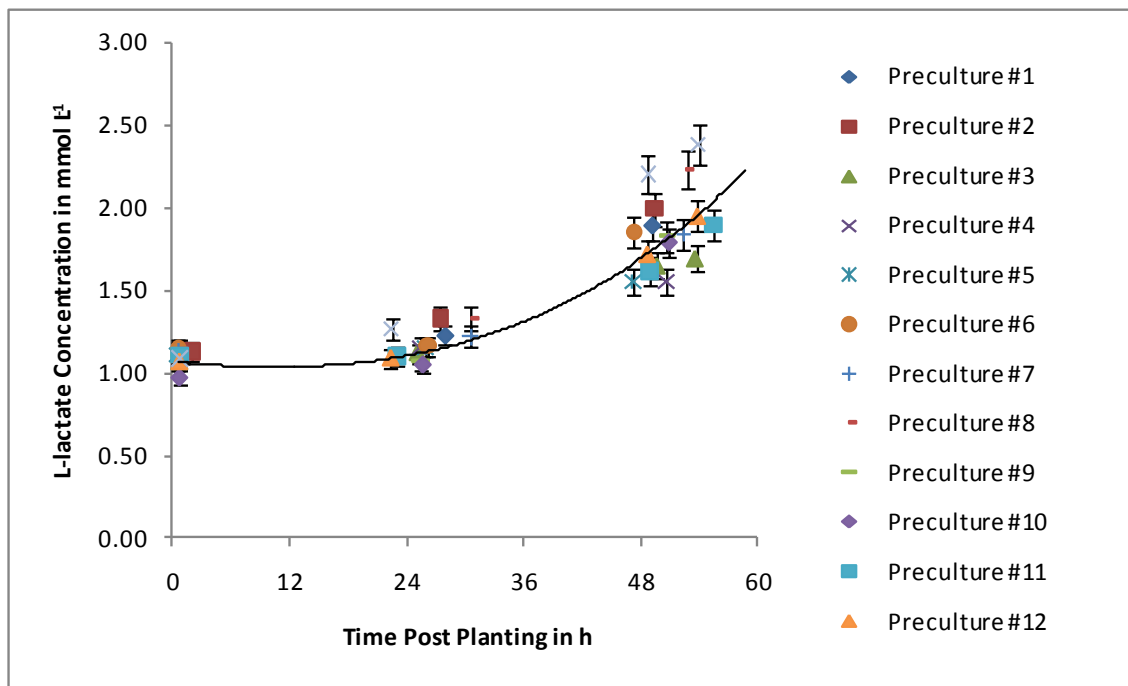


Figure 4.6. Medium L-lactate concentration post planting in the 13 pre-cultures. Initial L-lactate concentrations were slightly above 1.00 mmol L^{-1} and increased continuously during the two-day growth phase to approximately 2.00 mmol L^{-1} . Trendline is intended to guide the eye only.

The specific L-lactate production rate q_{Lac} was estimated to be $(4.25 \pm 0.81) \times 10^{-15} \text{ mmol cell}^{-1} \text{ s}^{-1}$. Literature states that L-lactate is generally toxic for insect

cell cultures at higher levels but usually does not accumulate during exponential growth of *Spodoptera frugiperda* cells when oxygen limitation is not an issue^{120, 123, 124}. This seems to be in contrast to the findings of this work but the production rate and the concentrations reached in this work are very low and well below any toxic level, respectively.

The same trend could be observed for L-glutamate and is shown in Figure 4.7. Initial medium concentrations of this metabolite ranged from 6.64 to 7.46 mmol L⁻¹ and continuously increased to 8.10 to 8.71 mmol L⁻¹ during the two-day growth phase.

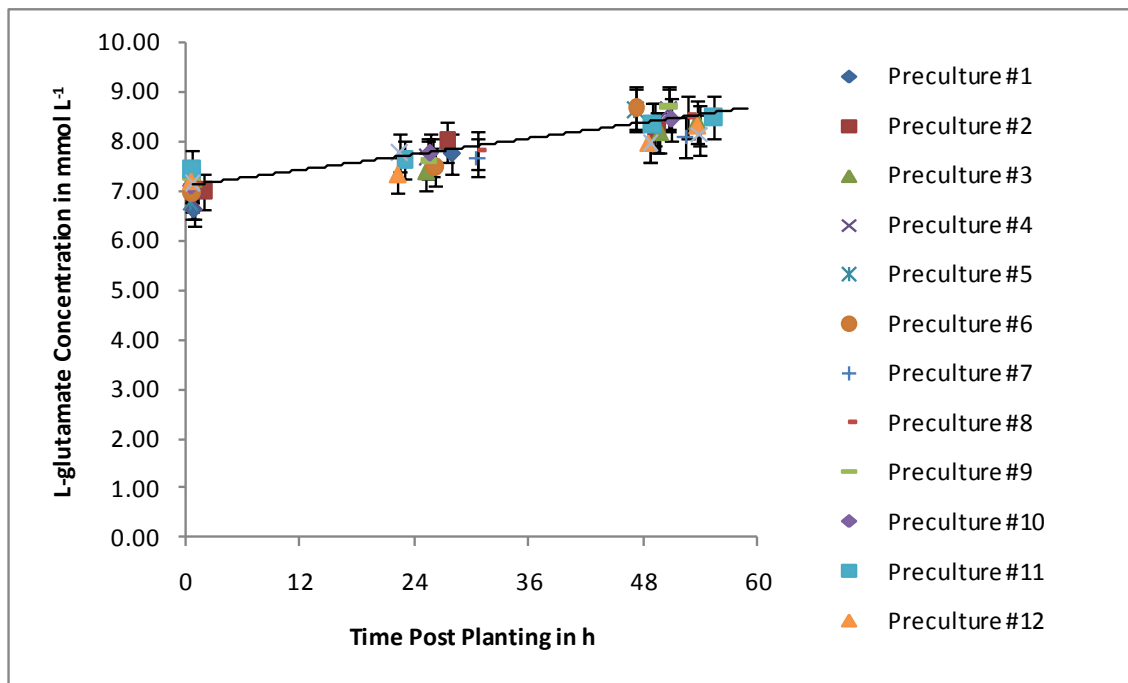


Figure 4.7. Medium L-glutamate concentration post planting in the 13 pre-cultures. Initial concentrations were approximately 7.00 mmol L⁻¹ and increased continuously during the two-day growth phase to approximately 8.50 mmol L⁻¹. Trendline is intended to guide the eye only.

The specific L-glutamate production rate q_{Glu} was estimated to be $(7.13 \pm 1.98) \times 10^{-15} \text{ mmol cell}^{-1} \text{ s}^{-1}$. Interestingly, available literature usually states that L-glutamate is a nutrient rather than a metabolite for *Spodoptera frugiperda* cell cultures and therefore is consumed by the cells at a rate of $1.94 \times 10^{-15} \text{ mmol cell}^{-1} \text{ s}^{-1}$ rather than produced.

On the other hand L-glutamate can be produced if a carbon source, e.g. D-glucose, and ammonia are present in excess¹²², which may be the case here.

Table 4.1 summarizes the findings for the uninfected Sf-9 clone cell growth in the two-day precultures and values found in the literature. See Appendix C - for the complete data set.

Table 4.1. Summary of the measured cell culture parameters for uninfected Sf-9 clone cell growth in precultures. Given are mean values \pm one standard deviation.

	Estimated	Literature	Reference
μ in h^{-1}	0.031 ± 0.002	0.029 to 0.035	118-120
t_D in h	22.2 ± 1.4	20 to 24	118-120
q_{Glc} in $\text{mmol cell}^{-1} \text{s}^{-1}$	$(-1.38 \pm 0.29) \times 10^{-14}$	-2.4×10^{-14}	120
q_{Gln} in $\text{mmol cell}^{-1} \text{s}^{-1}$	$(-1.39 \pm 0.29) \times 10^{-14}$	-1.0×10^{-14}	120, 122
q_{Lac} in $\text{mmol cell}^{-1} \text{s}^{-1}$	$(4.25 \pm 0.81) \times 10^{-15}$	No accumulation	120, 123, 124
q_{Glu} in $\text{mmol cell}^{-1} \text{s}^{-1}$	$(7.13 \pm 1.98) \times 10^{-15}$	-1.94×10^{-15}	122

4.1.2 Dielectric Spectroscopy

Dielectric spectroscopy was performed with the FOGALE iBiomass 465 instrument during the two-day preculture growth phase. These measurements yielded the raw capacitance values at 17 frequencies in the range of 300 to 10000 kHz and the three model derived β -dispersion parameters dielectric increment $\Delta\epsilon$, characteristic frequency f_c and Cole-Cole α . Additionally the Biomass signal based on a dual frequency measurement and the suspension conductivity were obtained. Data was recorded every 30 minutes. Observed major deviations in the data could usually be attributed to technical problems.

Initial values for the dielectric increment $\Delta\epsilon$, obtained after a short stabilization phase due to suspension mixing and temperature adjustments, ranged from 2.21 to 4.06 pF cm^{-1} . $\Delta\epsilon$ then immediately and continuously increased nearly exponentially until the end of the two-day growth phase, as shown in Figure 4.8. Final values for $\Delta\epsilon$ ranged from 10.92 to 22.35 pF cm^{-1} . It has to be noted, that the $\Delta\epsilon$ profile for preculture #9 temporarily deviated from the near exponential profile evolution and exhibited more or less constant values for extended periods of time. The signal could usually be recovered for limited time after applying a cleaning cycle but this improvement was generally not permanent and had to be repeated multiple times until the end of

the two-day growth phase. The reason for this behavior is unknown, but an unknown technical issue is believed to be the cause for this.

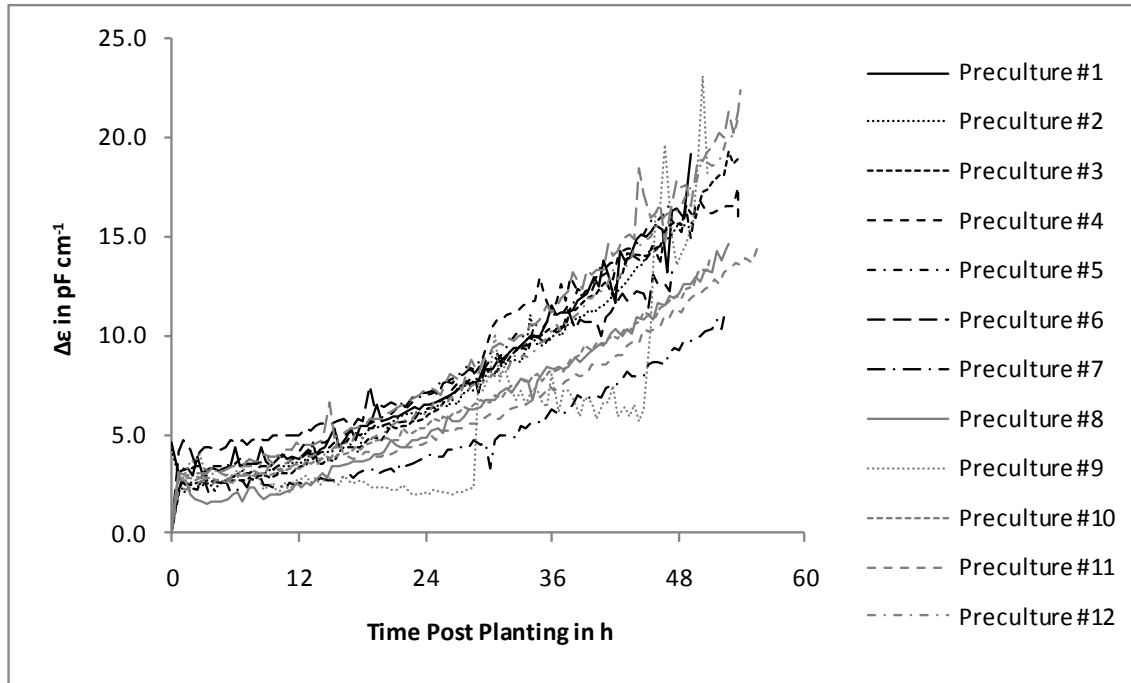


Figure 4.8. Dielectric increment $\Delta\epsilon$ post planting in the 13 precultures. Initial values of $\Delta\epsilon$ were approximately 3.0 pF cm^{-1} and increased continuously during the two-day growth phase to a range from approximately 11.0 to 22.0 pF cm^{-1} .

$\Delta\epsilon$ is directly related to the volume fraction of viable cells P (viable biovolume) as described in Equation 4 and Equation 5 assuming a spherical cell shape. The general profile of $\Delta\epsilon$ can therefore be attributed to the observed cell growth and therefore increase in biovolume post planting as described earlier. The data here also supports the assumption made earlier that the cultures exhibited only a minor lag phase of a few hours maximum before actually starting to grow exponentially.

According to Equation 4 additional parameters possibly affecting $\Delta\epsilon$ are the cell radius r and the specific cell membrane capacitance C_m . As shown in Figure 4.2 the mean viable cell diameter did only change very slightly during the preculture growth phase and therefore probably did not affect $\Delta\epsilon$ much. C_m was not measured directly in this study but can be

calculated based on Equation 4 using the viable cell density and size obtained by off-line measurements for each sample. C_m profiles obtained by this calculation are shown in Figure 4.9.

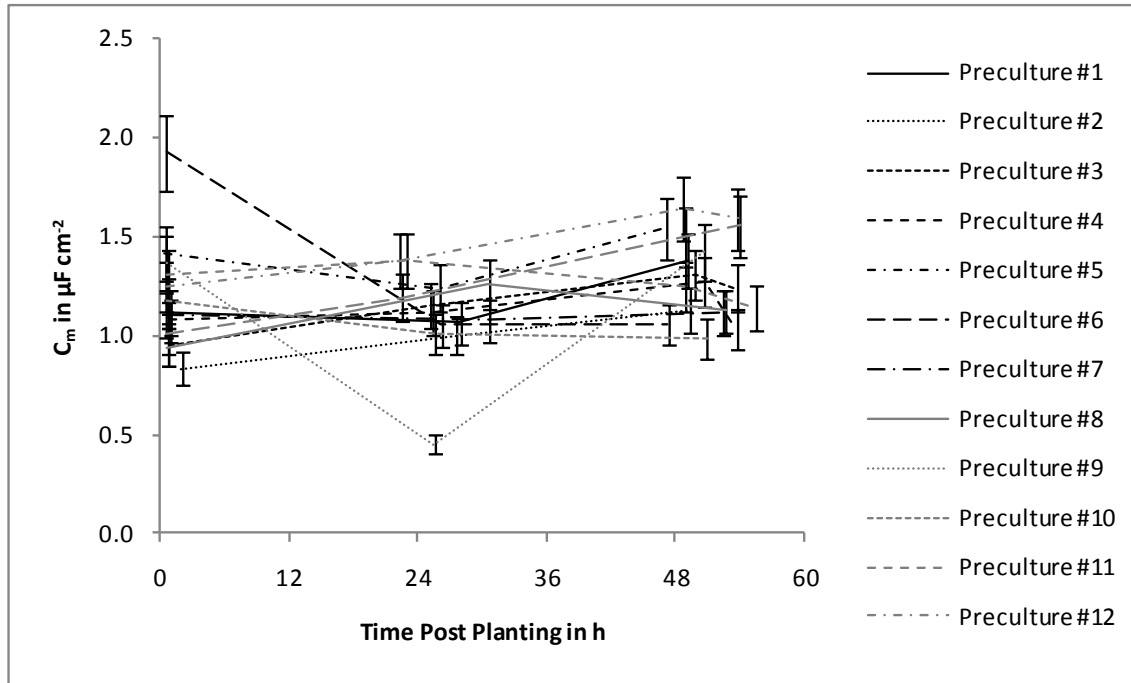


Figure 4.9. Specific cell membrane capacitance C_m post planting in the 13 precultures. Values for C_m generally ranged from approximately 1.0 to 1.5 $\mu\text{F cm}^{-2}$ and did not exhibit any major changes during the two-day growth phase.

Calculated initial values for C_m for the uninfected precultures ranged from 0.83 to 1.41 $\mu\text{F cm}^{-2}$ and generally increased slightly during the experiment. At the end of the growth phase C_m ranged from 0.98 to 1.59 $\mu\text{F cm}^{-2}$. The two calculated values for C_m at approximately 0.6 h and 26 h post planting for precultures #6 and #9, respectively, fall out of these ranges. In the case of preculture #6, this can be explained with an unreasonable high $\Delta\epsilon$ observed at a very low volume fraction of viable cells, while in case of preculture #9 a technical issue with unknown cause caused the $\Delta\epsilon$ signal to be lower than expected for the observed volume fraction of viable cells. The specific cell membrane capacitance C_m is generally interpreted to be dependent on the level of folding of the cellular membrane^{73, 74} and was originally thought to be a cell biological constant with a value of approximately $(1.0 \pm 0.5 \mu\text{F cm}^{-2})$ ^{73, 87, 125, 126}. Recent research suggests that this assumption is not entirely true and C_m can indeed be influenced by

cell viability, physiological state, virus infection or during overexpression of cation channels. Data specifically for *Spodoptera frugiperda* cells is scarce and only one publication states values in the range of 0.8 to 0.9 $\mu\text{F cm}^{-2}$ for uninfected Sf-9 cells¹²⁷, but these values are also not obtained directly by measurements on the cells but rather calculated based on dielectric spectroscopy measurements and a simplified dielectric cell model. In this work, C_m was found to be $1.2 \pm 0.2 \mu\text{F cm}^{-2}$ (mean \pm one standard deviation) during the two-day cell growth phase in the precultures. Because no major changes in the C_m profiles were observed it can be assumed that no major physiological changes have occurred during the two-day preculture growth phase.

The second β -dispersion parameter provided by the instrument was the characteristic frequency f_c . Profiles for this parameter are shown in Figure 4.10. Initial values for f_c ranged from 630 to 787 kHz and overall decreased slightly to 553 to 660 kHz during cell growth.

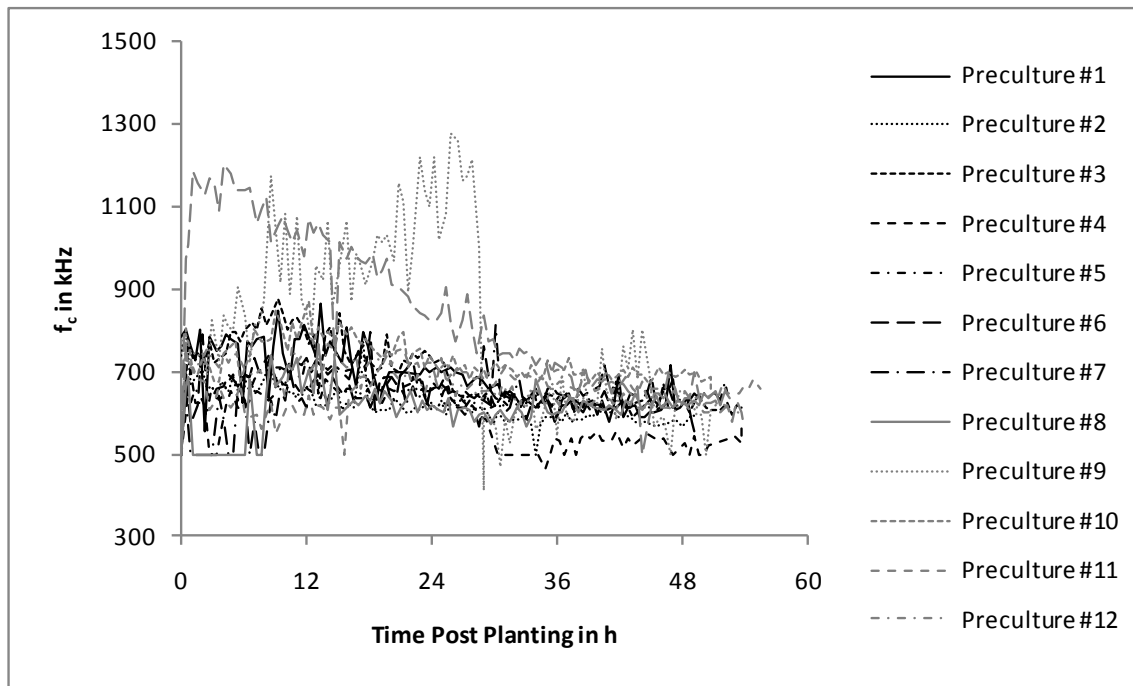


Figure 4.10. Characteristic frequency f_c post planting in the 13 precultures. Initial values were around 700 kHz and decreased slightly to approximately 600 kHz during the two-day growth phase. Deviations from this are generally attributed to technical issues.

The characteristic frequency f_c did not exhibit major changes during the uninfected precultures but seemed to increase slightly immediately post planting before starting to decrease again as soon as 12 h post planting. According to Equation 6 f_c is directly influenced by the cell radius r , specific cell membrane capacitance C_m and the intracellular and medium conductivities σ_i and σ_e , respectively. Since a slight increase in viable cell radius was observed during preculture cell growth this may have contributed to the observed slight decrease in f_c .

Third and last β -dispersion parameter obtained with the instrument was the Cole-Cole α . Initial values for α ranged from 0.100 to 0.102 and spread out to a range from 0.080 to 0.104 during cell growth (see Figure 4.11). In addition, most of the values seemed to decrease slightly during this period.

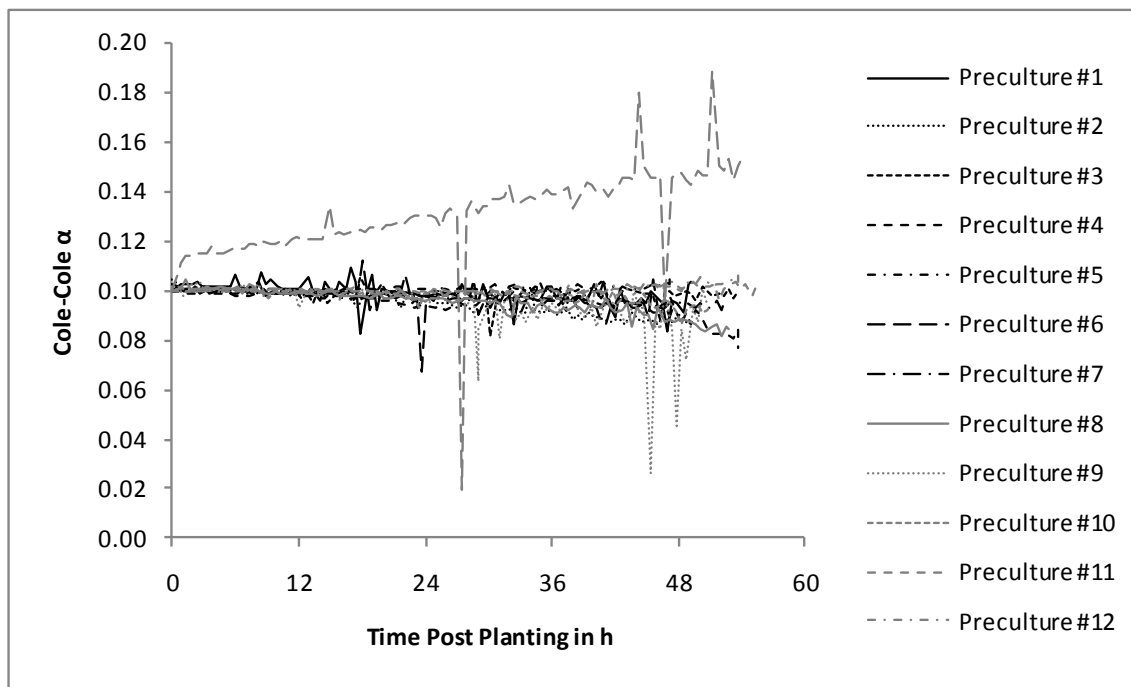


Figure 4.11. Cole Cole α post planting in the 13 precultures. Initial values of approximately 0.10 decreased and spread slightly during the two-day growth phase to a range of approximately 0.08 to 0.10.

The parameter Cole-Cole α is an empirical value describing the decrease in capacitance (or permittivity) measured with increasing frequency. The parameter α can assume values

between 0 and 1 where 0 describes a very steep and 1 an infinitely shallow fall in capacitance. In cell culture applications α is generally interpreted as a measurement of viable cell size distribution and believed to increase when the cell size distribution widens^{12, 80} and values observed are typically between 0.1 and 0.2¹²⁸. But the physical origin of this parameter is continuously disputed and may indeed also be influenced by several other effects including morphology of extracellular spaces, the mobility of membranous proteins and the fractal nature of dielectric relaxation¹²⁸⁻¹³¹. Decreasing and widening values for α observed during the uninfected preculture cell growth cannot be explained with changes or trends in the cell size distribution since no significant changes were observed in those values (data not shown).

In addition to the three β -dispersion parameters, two additional parameters were measured by the instrument. The first was the Biomass signal, which was based on the dual frequency method. The Biomass signal was obtained by measuring the capacitance (permittivity) at a frequency close to the specific f_c of the cell culture system utilized (here 1000 kHz), the so called working frequency, and subtracting the capacitance (permittivity) obtained at a very high frequency (here 10000 kHz). The latter adjusts the measurement for changes in the medium background capacitance (permittivity) over time¹⁰⁸.

Profiles for the Biomass signal are shown in Figure 4.12. Initial values, taken after a short stabilization phase for suspension mixing and temperature adjustments, ranged from 0.59 to 1.44 pF cm⁻¹ and started to increase in a close to exponential fashion immediately post planting. Final values at the end of the growth phase ranged from 2.95 to 5.82 pF cm⁻¹.

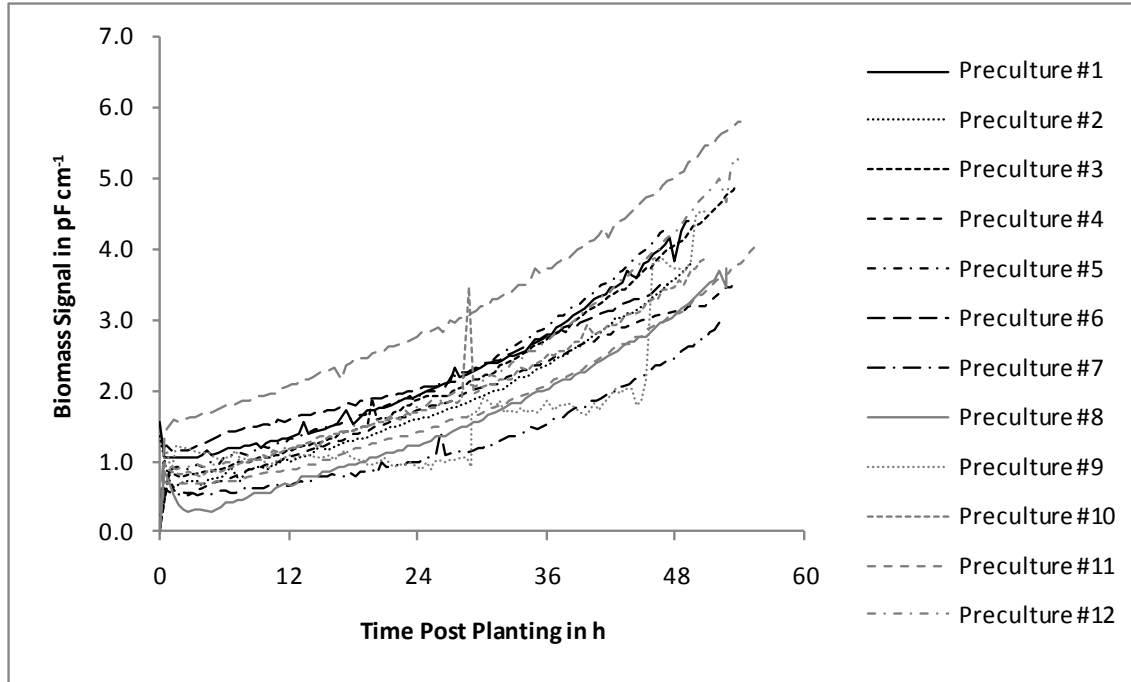


Figure 4.12. Biomass signal post planting in the 13 precultures. Initial values were approximately 1.0 pF cm^{-1} and continuously increased to approximately 3.0 to 6.0 pF cm^{-1} during the two-day growth phase.

The Biomass signal is often used for viable biovolume estimation because due to the nature of its measurement, it is believed to be independent, or at least less influenced, by changes in viable cell radius. As with $\Delta\epsilon$, the general Biomass signal increase immediately post planting can be attributed to viable cell growth and so increases in the viable biovolume.

The last parameter provided by the instrument was the suspension conductivity σ_s for which profiles are shown in Figure 4.13. Initial values for σ_s , taken after a short stabilization phase for suspension mixing and temperature adjustments, ranged from 15.21 to 15.45 mS cm^{-1} . σ_s did not significantly change during two day cell growth ranged from 15.24 to 15.45 mS cm^{-1} at the end of the precultures. In addition observed shifts in the profiles from process to process are generally statistically not significant because the error for this measurement is at least 1 % as stated by the manufacturer. Exceptions were phases of small culture medium temperature changes and readjustments, as can be seen from approximately 24 to 34 h post planting in

precultures #1 and #2. These deviations were generally caused by changes in the room temperature and subsequent changes and readjustments of the culture temperature.

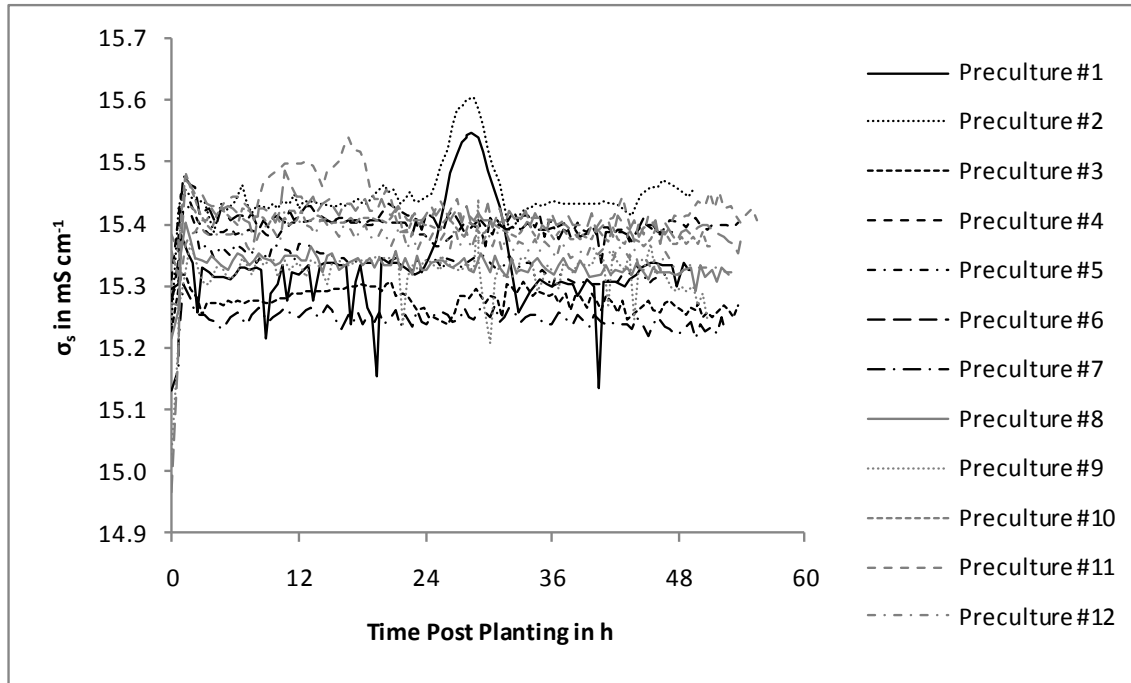


Figure 4.13. Suspension conductivity σ_s post planting in the 13 precultures. Values ranged from approximately 15.3 to 15.4 mS cm⁻¹ throughout the two-day growth phase. Spikes observed could generally be attributed to changes in the culture temperature.

At this point, the intracellular conductivity σ_i can be calculated because r and C_m are already known and σ_e is given by Equation 7. σ_i profiles obtained by this calculation are shown in Figure 4.14. Generally, the calculated σ_i values ranged from 3.66 to 7.11 mS cm⁻¹ at the beginning of the culture and did not change much during the two-day preculture growth phase. Values obtained at the end of the cultures showed nearly the same range, from 3.80 to 6.68 mS cm⁻¹. Again precultures #6 and #9 showed two values, the same as in the case of C_m , deviating from these ranges. This can be explained by the simple fact that C_m directly affects the calculation of σ_i and deviations in the first will consequently be found in the latter.

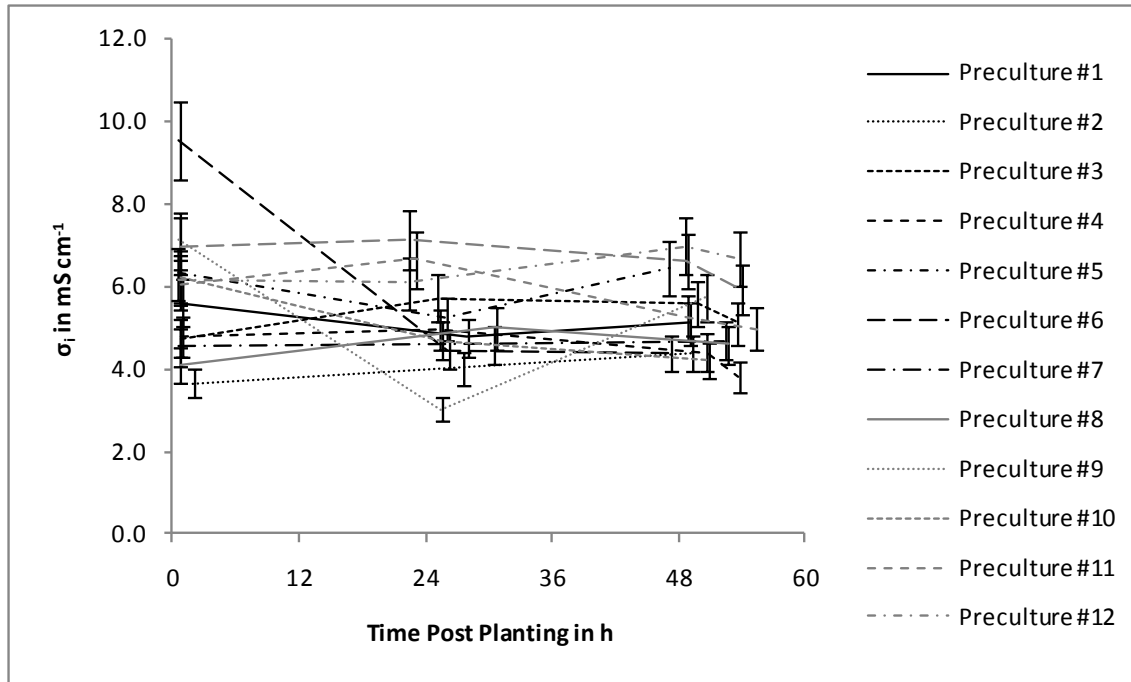


Figure 4.14. Intracellular conductivity σ_i post planting in the 13 precultures. Values generally ranged from approximately 4.0 to 7.0 mS cm^{-1} during the two-day growth phase and did not exhibit major changes.

σ_i is generally interpreted as the ability of the cell's interior to conduct electrical current and changes are presumably due to different ion concentrations within the cell^{73, 75}. Until recently studies often treat σ_i as independent on the physiological state^{73, 125, 132, 133} but it is well known that this value can indeed change in apoptotic and necrotic cells, when morphological changes are induced or when the cell membrane conductance is increased, i.e. by treatment with antibiotics¹³⁴⁻¹³⁸. To the knowledge of the author, no literature values for σ_i in *Spodoptera frugiperda* derived cells have been published. In mammalian cell cultures σ_i usually falls somewhere in between 2 and 9 mS cm^{-1} with some researchers suggesting an even narrower range of 3 to 5 mS cm^{-1} ^{173, 75, 125, 139, 140}. Overall σ_i was found to be $5.4 \pm 1.2 \text{ mS cm}^{-1}$ (mean \pm one standard deviation) during the exponential cell growth phase in uninfected Sf-9 clone cell precultures.

4.1.3 Use of DS for Real-Time Determination of Viable Biovolume and Cell Density

Traditionally the main use of DS is the determination of viable biovolume or cell density in-line and in real-time^{5, 45, 57}. Eliminating the need for time-consuming off-line analyses and the sterility risk associated with the sampling procedure is a great benefit of the DS application in industrial bioprocesses. Specifically for the BEVS system employed in this work, an accurate determination of the cell density at the time of infection is rather important to minimize the effects of an inconsistent MOI as much as possible. The data DS obtained during the uninfected cell growth of Sf-9 clone cells in the thirteen precultures was used to establish calibrations with the viable biovolume and cell density as determined by off-line analyses.

Based on the theory the capacitance and permittivity measured correlate linearly to the volume fraction of the viable cells P (viable biovolume) in the cell culture suspension. To verify this theory the viable cell densities and mean viable cell diameters obtained for every sample during the two-day cell growth in the precultures were used to calculate the viable biovolume, assuming a spherical cell shape. This value was then paired with its raw capacitance values at each of the 16 remaining frequencies after adjusting for the medium background capacitance by subtracting the capacitance value measured at 10000 kHz. In addition, $\Delta\epsilon$ and the Biomass signal were also used to obtain correlations. The Pearson correlation coefficient r was then calculated for each combination to obtain a measure of linearity of the correlation. Results are shown in Table 4.2. A total of 44 data points was used in this analysis.

Table 4.2. Pearson correlation coefficients for viable biovolume and dielectric spectroscopy signals of uninfected Sf-9 clone cells.

Signal	Pearson r
Delta ϵ	0.957
Biomass	0.938
C(300 kHz)	0.907
C(373 kHz)	0.923
C(465 kHz)	0.932
C(578 kHz)	0.936
C(720 kHz)	0.938
C(897 kHz)	0.937
C(1117 kHz)	0.935
C(1391 kHz)	0.925
C(1732 kHz)	0.907
C(2156 kHz)	0.868
C(2684 kHz)	0.846
C(3342 kHz)	0.794
C(4161 kHz)	0.709
C(5181 kHz)	0.640
C(6451 kHz)	0.514
C(8031 kHz)	0.407

Generally, capacitance measurements obtained at frequencies below 3000 kHz provided reasonable good correlations with the best correlations obtained for $\Delta\epsilon$ and the Biomass signal. Estimated Pearson correlation coefficients for these signals were 0.957 and 0.938, respectively. The best linear correlation based on the raw capacitance measurements at single frequencies was obtained at 720 kHz with a Pearson r of 0.938. Figure 4.15 and Figure 4.16 show the correlations obtained for $\Delta\epsilon$ and the Biomass signal versus the viable biovolume.

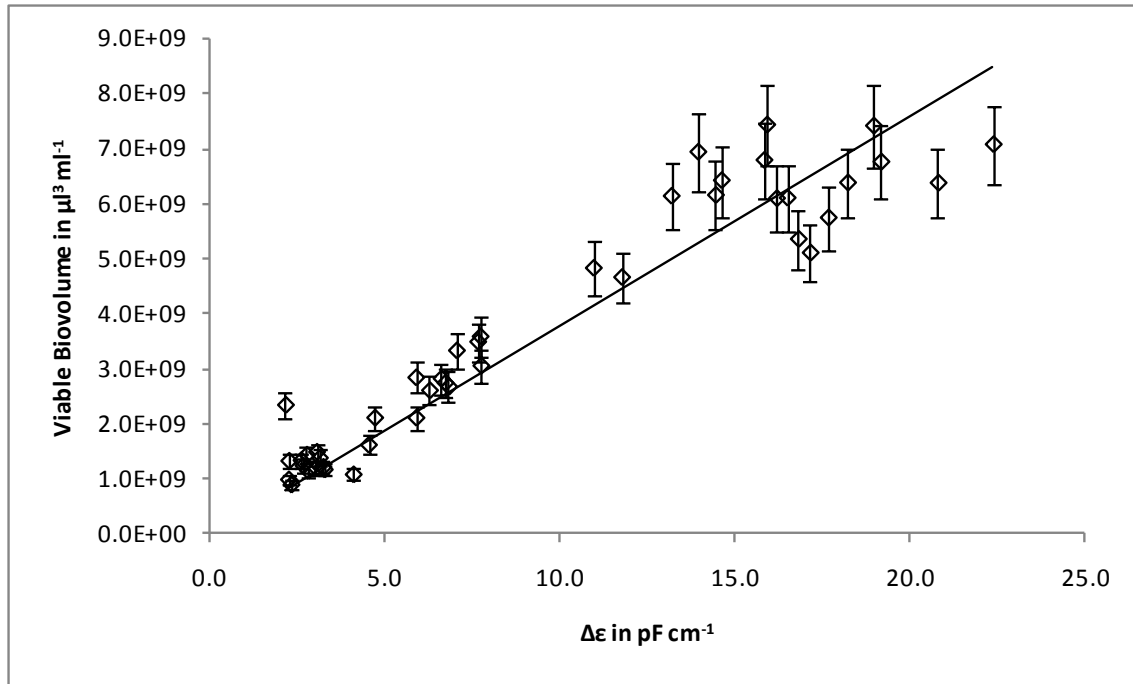


Figure 4.15. Linear correlation viable biovolume vs. $\Delta\epsilon$ post planting for uninfected Sf-9 clone cells.

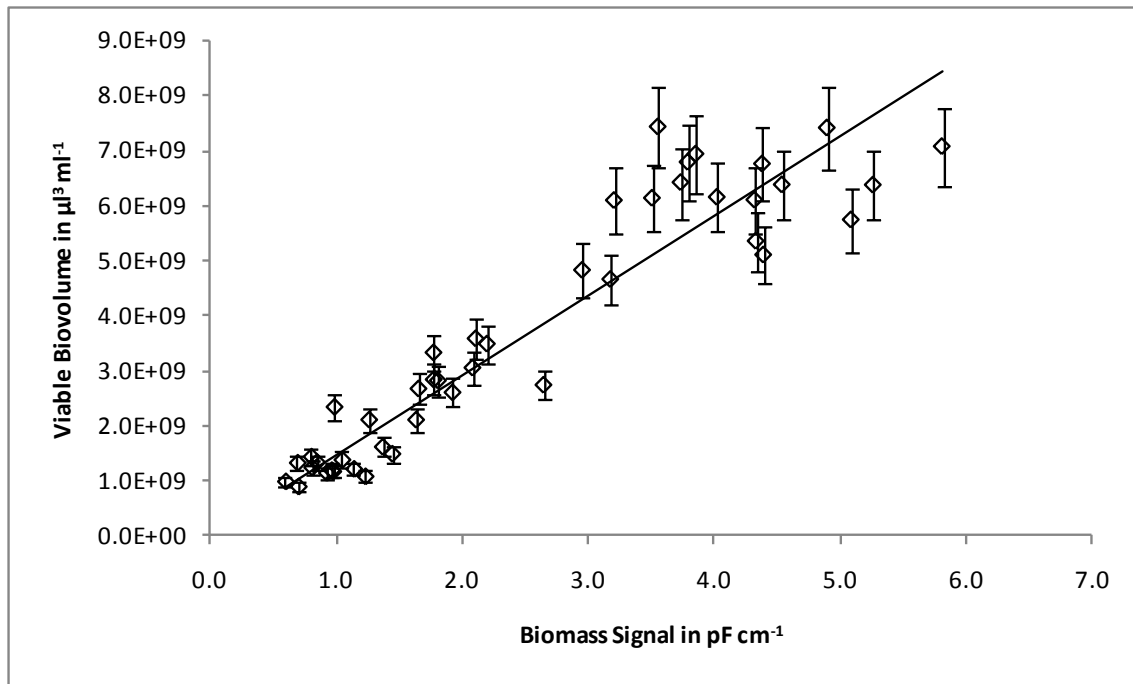


Figure 4.16. Linear correlation viable biovolume vs. Biomass signal post planting for uninfected Sf-9 clone cells.

The two linear correlations obtained can be described by the equations

$$\text{Viable biovolume } (\Delta\epsilon) = \left(3.80 \times 10^8 \times \Delta\epsilon \frac{\text{cm}}{\text{pF}} \right) \frac{\mu\text{l}^3}{\text{ml}} \quad \text{Equation 19}$$

and

$$\text{Viable biovolume}(\text{Biomass}) = \left(1.46 \times 10^9 \times \text{Biomass} \frac{\text{cm}}{\text{pF}} \right) \frac{\mu\text{l}^3}{\text{ml}} \quad \text{Equation 20}$$

The parameter viable biovolume is generally not used in insect cell culture technology. Instead, the parameter viable cell density is usually preferred. Therefore, the same procedure as described above was repeated with viable cell density instead of biovolume values. Results of this analysis are shown in Table 4.3.

Table 4.3. Pearson correlation coefficients for viable cell density and dielectric spectroscopy signals for uninfected Sf-9 clone cells.

Signal	Pearson r
Delta ε	0.958
Biomass	0.943
C(300 kHz)	0.911
C(373 kHz)	0.926
C(465 kHz)	0.935
C(578 kHz)	0.940
C(720 kHz)	0.942
C(897 kHz)	0.941
C(1117 kHz)	0.939
C(1391 kHz)	0.930
C(1732 kHz)	0.912
C(2156 kHz)	0.875
C(2684 kHz)	0.854
C(3342 kHz)	0.804
C(4161 kHz)	0.716
C(5181 kHz)	0.647
C(6451 kHz)	0.520
C(8031 kHz)	0.412

Again, capacitance measurements obtained below 3000 kHz generally provided reasonable good correlations with the best correlations obtained for $\Delta\epsilon$ and the Biomass signal. For these signals the determined Pearson correlation coefficients were 0.958 and 0.943, respectively. The best linear correlation based on the raw capacitance measurements at single frequencies was once again obtained at 720 kHz with a Pearson r of 0.942. This can be explained by the fact, that the viable cell diameter and size distribution did not exhibit any major changes during the preculture growth phase. Therefore, the calculated viable biovolume is linearly correlated to the viable cell density with very high significance. In fact, the relationship between these two values has a Pearson correlation coefficient of 0.998. This fact is also represented in the characteristic frequency f_c and Cole-Cole α , which are somewhat dependent on the viable cell size and size distribution. Both parameters did only shown minor changes during the cell growth in the precultures. Figure 4.17 and Figure 4.18 show the correlations obtained for $\Delta\epsilon$ and the Biomass signal versus the viable cell density.

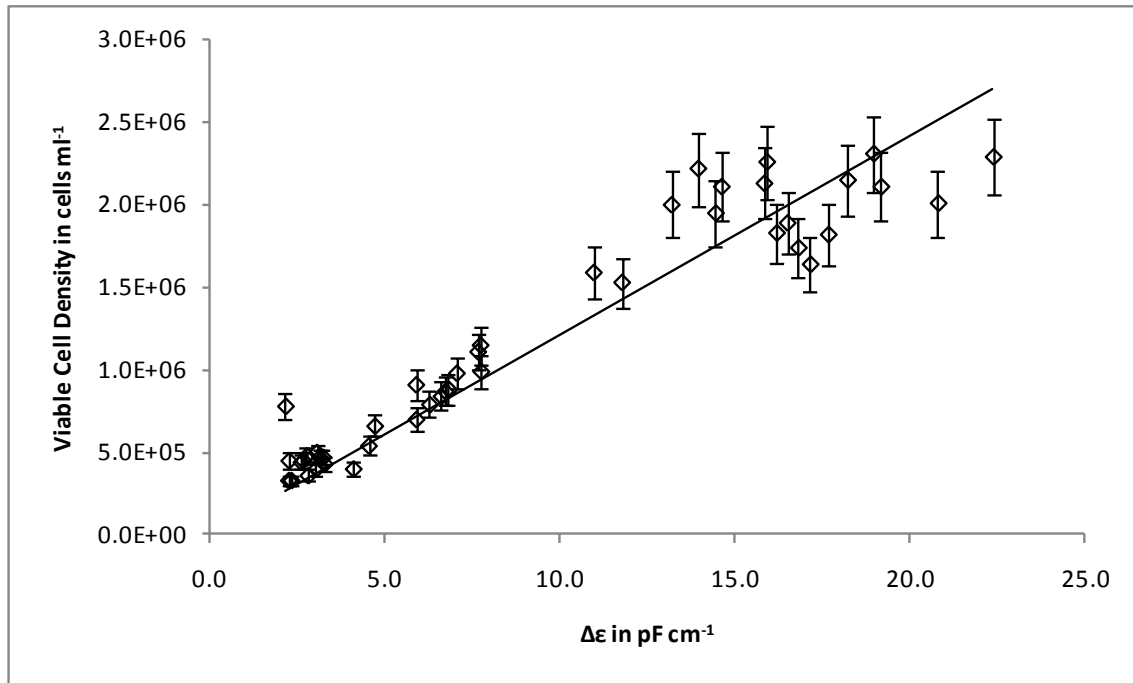


Figure 4.17. Correlation viable cell density vs. $\Delta\epsilon$ post planting for uninfected Sf-9 clone cells.

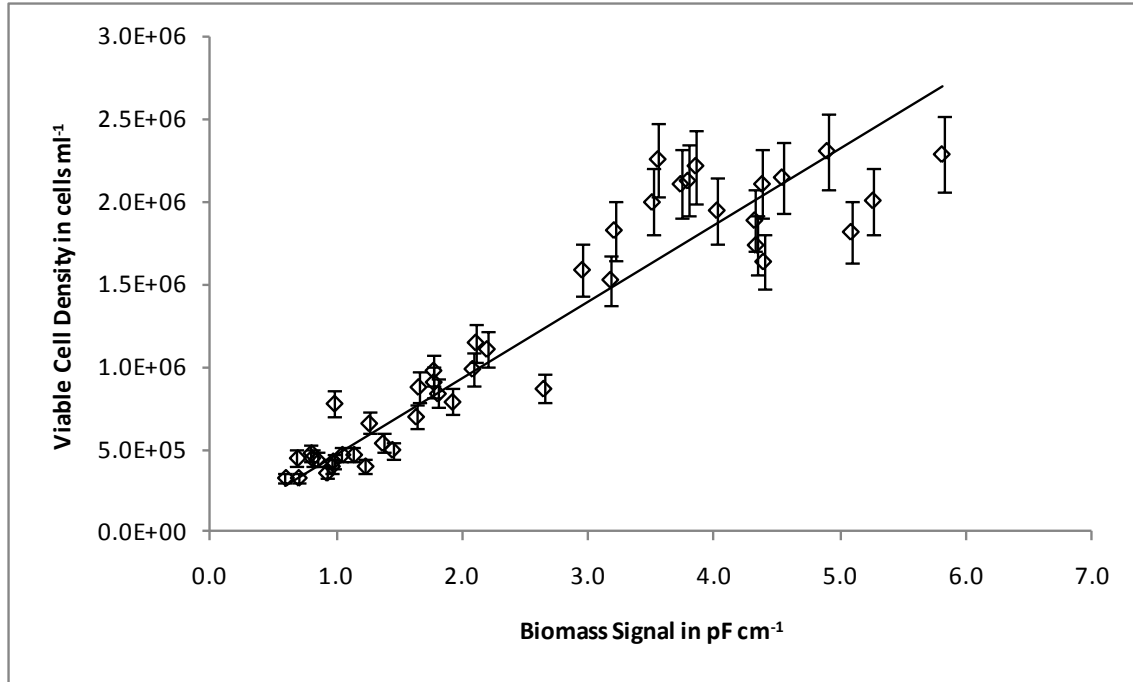


Figure 4.18. Correlation viable cell density vs. Biomass signal post planting for uninfected Sf-9 clone cells.

The two linear correlations obtained can be described by the equations

$$\text{Viable cell density } (\Delta\varepsilon) = \left(1.21 \times 10^5 \times \Delta\varepsilon \frac{\text{cm}}{\text{pF}} \right) \frac{\text{cells}}{\text{ml}} \quad \text{Equation 21}$$

and

$$\text{Viable cell density } (\text{Biomass}) = \left(4.64 \times 10^5 \times \text{Biomass} \frac{\text{cm}}{\text{pF}} \right) \frac{\text{cells}}{\text{ml}} \quad \text{Equation 22}$$

Overall, the obtained correlations between dielectric spectroscopy measurements and their respective viable biovolume and cell density values for both probes used in all 13 precultures are acceptable based on the Pearson correlation analysis and show a good reproducibility.

This result suggests that the application of dielectric spectroscopy could replace the manual sampling for cell density determination in routine insect cell production processes during cell expansion. This would eliminate the effort and sterility risks associated with the manual sampling process and additionally and very importantly, the estimation of the viable cell density at the actual time of infection could be greatly improved. This would subsequently lead to more consistent “real MOI” and so recombinant protein expression. Usually in routine production, a viable cell density estimated is already outdated for hours once the virus seed is added to the bioreactor. This is because of the long procedures performed in between sampling and virus addition like thawing of the virus seed, dispensing or sterilization of the addition lines. It has to be noted that the obtained correlations for each single probe/amplifier combination are slightly different and deviating more the higher the viable biovolume or cell density in the suspension (see Figure 4.19).

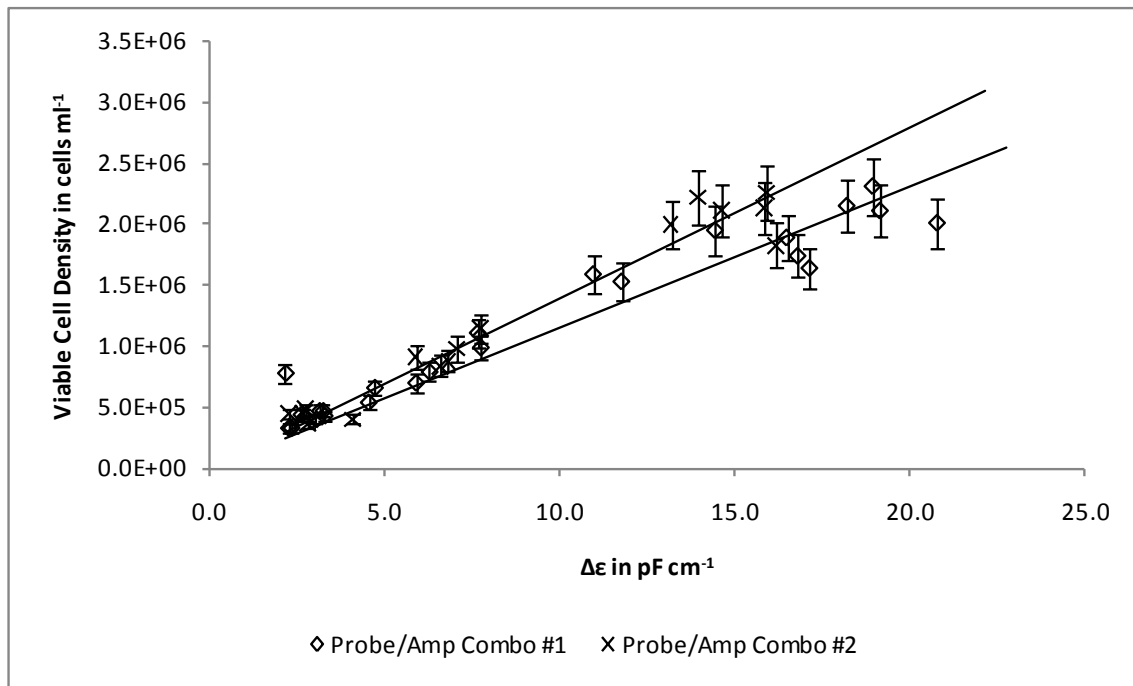


Figure 4.19. Probe/Pre-Amp set dependency of obtained correlation between $\Delta\epsilon$ and the viable cell density. Deviations can be observed at higher cell densities of approximately 2.0×10^6 cells ml^{-1} . If cell densities are further increased, an even stronger deviation is expected.

This was of less impact in the ranges investigated here, shows, could become more important when viable biovolume or cell density are increased beyond what was measured here. Therefore, the use of different correlation equations for each might be beneficial in terms of accuracy. Such a behavior is expected for correlations obtained with the macroscopic and probe geometry dependent raw capacitance values, but should ideally not be the case with for the intrinsic permittivity data ($\Delta\epsilon$ and the Biomass). On the other hand using different correlation equations for each single probe increases the overall complexity in routine production and therefore might be abandoned due to the relatively good results even for the overall correlations. To the knowledge of the author, the probe/amp combination dependency of the real-time determination of viable cell density or biovolume has not been of a big concern in literature.

Another very important fact to consider is that these correlations are based solely on viable cell densities between approximately 0.50×10^6 and 2.50×10^6 cells ml^{-1} . Strictly speaking, the obtained correlations are not valid outside this range but could be extended once additional data outside this range is available from additional experiments or even routine production processes. In addition, the correlations were obtained with cells in the exponential growth phase. It is known from literature and own experiments that the same linear correlations fail once the cell culture reaches the stationary phase and later, even if the cell size does not change significantly. Most probable explanation for this is a change in the dielectric properties of the cells when shifting from exponential growth to the stationary phase and later to the death phase. Since insect cell cultures are ideally passaged or infected during the exponential growth phase, this should not be an issue in routine industrial application of dielectric spectroscopy.

4.1.4 Conclusions

The thirteen precultures served as additional cell expansion step between the spinner flask scale and the bioreactor experiments performed at the 15 L working volume scale. Off-line sampling and analysis of standard cell culture parameters like viable cell density or medium nutrient/metabolite concentrations allowed estimation of cell growth related kinetics for comparison with literature. Eventually a judgment of the overall robustness of the growth process and the health of the cells was possible. The application of DS in these cultures

additionally allowed evaluating the applicableness of this technique towards real-time estimation of viable biovolume and cell density as well as gaining more insight into the cell's physiological state.

It was found, that the *Spodoptera frugiperda* Sf-9 clone cell clone used in this work overall performed comparably in terms of growth to Sf-21 and Sf-9 cells as reported in the literature. Also, D-glucose and L-glutamine were utilized at comparable rates but were never depleted during the two-day cell growth in the precultures. Interestingly, L-lactate and L-glutamate both accumulated in the culture medium during growth. This is contrary to findings in the literature where it was reported, that L-lactate generally does not accumulate under non oxygen-limited conditions. Also, L-glutamate was reported to be utilized rather than be produced. Overall, the growth process was reproducible and cell health, as determined by evaluating the different parameters and kinetics obtained, was deemed acceptable for subsequent experiments at the 15 L working volume scale. Table 4.4 summarizes the findings.

Table 4.4. Summary of the measured cell culture parameters for uninfected Sf-9 clone cell growth in precultures. Given are mean values \pm one standard deviation.

	This work	Literature	Reference
μ in h^{-1}	0.031 ± 0.002	0.029 to 0.035	118-120
t_D in h	22.2 ± 1.4	20 to 24	118-120
q_{Glc} in $\text{mmol cell}^{-1} \text{s}^{-1}$	$(-1.38 \pm 0.29) \times 10^{-14}$	-2.4×10^{-14}	120
q_{Gln} in $\text{mmol cell}^{-1} \text{s}^{-1}$	$(-1.39 \pm 0.29) \times 10^{-14}$	-1.0×10^{-14}	120, 122
q_{Lac} in $\text{mmol cell}^{-1} \text{s}^{-1}$	$(4.25 \pm 0.81) \times 10^{-15}$	No accumulation	120, 123, 124
q_{Glu} in $\text{mmol cell}^{-1} \text{s}^{-1}$	$(7.13 \pm 1.98) \times 10^{-15}$	-1.94×10^{-15}	122

DS was successfully implemented into the Sf-9 clone cell growth process. Combining the DS data with the parameters obtained off-line allowed establishing calibrations for the real-time estimation of viable biovolume and cell density in-line of subsequent processes without the need of sampling. An example of one of the correlations is shown in Figure 4.20. Utilization of different probe/pre-amp combinations in multiple processes overall yielded robust results but using a specific calibration for each combination may be beneficial in terms of accuracy. It should be noted that preparation and the so-called zeroing of the probes have to be done in a consistent way and in the culture medium at process temperature, respectively, to avoid deviations.

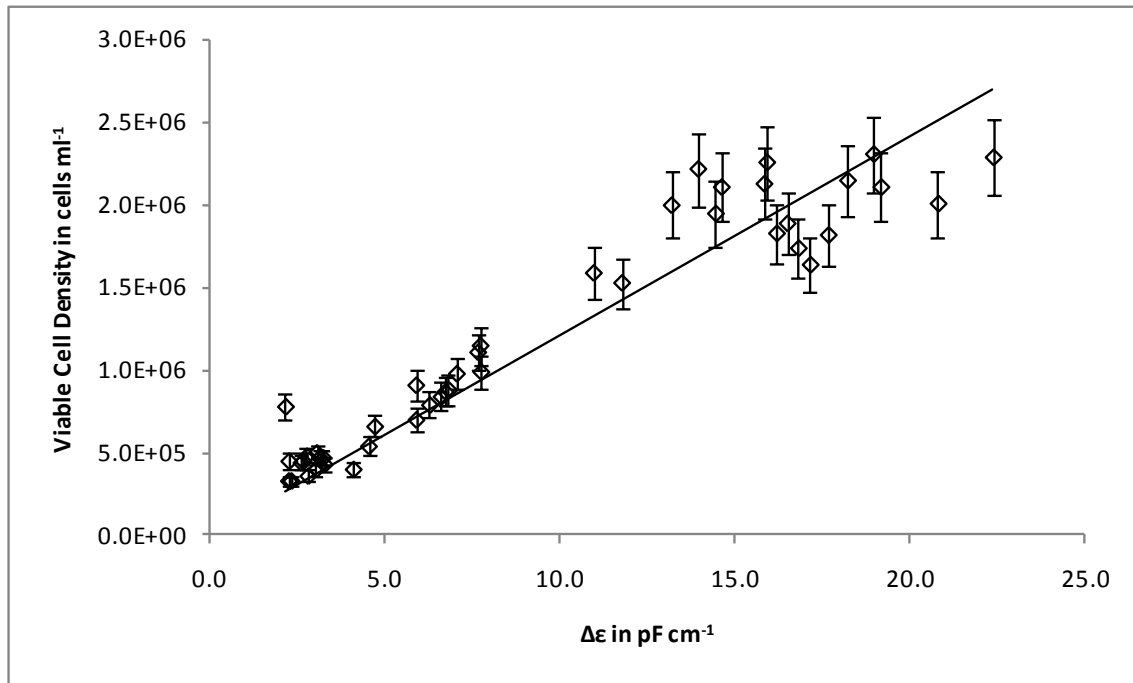


Figure 4.20. Correlation viable cell density vs. $\Delta\epsilon$ post planting.

With the obtained calibrations, DS does not only eliminate the contamination risk associated with the usually required sampling procedure but also reduces the time and effort required to follow cell growth while providing data in real-time and continuously. Infections in the large scale could be performed at more consistent “real MOI” because of elimination of the delay between initial sampling and medium or virus addition traditionally hours later. This will lead to more repeatable recombinant protein production processes, which potentially could have a large impact on a variety of important parameters like capacity planning and the overall cost of the recombinant protein production.

4.2 Infection at Low MOI

Reports of monitoring of infected insect cells and the BEVS generally focused on synchronous infections at a high MOI. This is usually not preferred in the large scale BEVS processes due to the large amount of costly virus seed required. The focus on high MOI potentially leads to deviations between laboratory work and industrial processes due to the significant impact of small changes in parameters like cell to virus ratio or the time of infection¹. Additionally only limited data that links the obtained DS data to the cell's physiological state, the infection progress, and parameters like the medium nutrient limitations is available. Here DS was applied to a range of low MOI experiments under standardized conditions to advance the technique into this field and to follow or even predict the process and its outcome.

Eleven different experiments according to the experimental plan described in Table 4.5 were performed. In essence, the only parameter varied in these experiments was the multiplicity of infection while efforts were made to keep other parameters unchanged (engineering and biological) to assure comparable results. Sf-9 clone cells grown in the precultures described earlier (see Chapter 4.1) at a working volume of approximately 7.5 L were diluted back by the addition of fresh EX-CELL 420 medium to a target viable cell density of 1.00×10^6 viable cells ml^{-1} at approximately 15.0 L working volume. Immediately afterwards the culture was infected with the appropriate amount of recombinant PCV2 ORF2 baculovirus. To cover the range of comparably low MOI usually utilized in industrial scale baculovirus expression vector system bioprocesses, the target MOI were 0.01, 0.10 and 1.00. Bioreactor parameters post infection were the same as post planting with an agitation rate of 100 RPM, an aeration rate of 1.00 SLPM and a dissolved oxygen concentration of 40 %. Experiments were performed in triplicates at each MOI to observe repeatability of the process. Additionally all experiments were performed in a randomized order to reduce potential bias of undetected factors affecting the experiments. One additional culture with no addition of virus seed was performed to serve as an uninfected control.

Table 4.5. Overview of performed Low MOI experiments and utilized precultures.

Preculture #	Used for Low MOI Experiment #
1	MOI 0.10 #1
2	MOI 0.01 #1
3	MOI 1.00 #1
4	MOI 0.10 #2
5	MOI 1.00 #2
6	MOI 0.01 #2
8	MOI 0.01 #3
9	MOI 0.10 #3
10	MOI 1.00 #3
11	Uninfected Control

With few exceptions, the data recorded for the three replicate processes performed at each MOI was consistent and comparable. Therefore, only one process at each MOI is shown in the following plots to ensure clarity of the plots. Additionally, the recorded data for an uninfected control culture is shown in each plot for comparison. With few exceptions, the data recorded for the three replicate processes performed at each MOI was consistent and comparable. Therefore, only one process at each MOI is shown in the following plots to ensure clarity of the plots. Plots with the complete set of experiments can be found in Appendix E - . Raw data collected is presented in Appendix D - .

4.2.1 Viable Cell Density, Viability and Viable Cell Diameter

The three parameters viable cell density, viability and mean viable cell diameter were determined off-line with the Beckman Coulter Vi-CELL XR analyzer utilizing the “Sf-9 clone” or, from day 5 post infection on, “Sf-9 clone low viability” settings as described in Chapter 3.7. The latter setting had to be used once samples contained significant amounts of dead cells and cell debris to avoid erroneous detection of these as viable cells.

Viable cell density profiles are shown in Figure 4.21. All cultures showed a slightly higher viable cell density at the time of infection than targeted. This is probably due to a systematic error in the medium addition process, despite utilizing a scale to verify the amount added to the vessel. Nevertheless, the viable cell density at the time of infection proved to be very consistent at around 1.25×10^6 viable cells ml^{-1} . During the first few days post infection the viable cell density generally increased significantly. Depending on the MOI, the maximum

viable cell density was reached between 24 and 72 h post infection with values ranging from 1.19×10^6 to 3.72×10^6 viable cells ml^{-1} . Generally, the maximum viable cell density observed decreased with increasing MOI. The respective maximum was also reached earlier for cultures infected at higher MOI. Once this maximum had been reached, the viable cell density continuously decreased until the end of the process. In comparison, the uninfected control culture showed an even higher maximum viable cell density than all infected cultures with 4.61×10^6 viable cells ml^{-1} reached after approximately 130 h culture time.

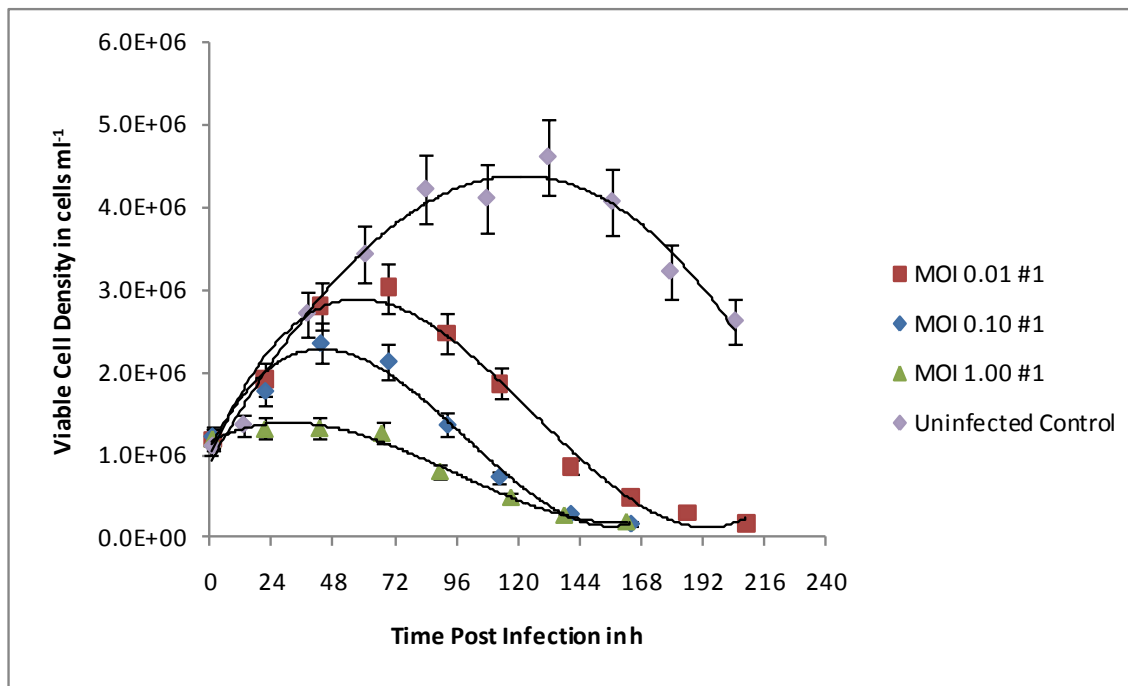


Figure 4.21. Viable cell density post infection at the three different MOI compared to an uninfected control culture. Initial values were approximately 1.0×10^6 cells ml^{-1} . The viable cell density increased for up to 72 h post infection depending on the MOI. Decreasing maximum viable cell densities were observed with increasing MOI with peak values of approximately 3.0 , 2.2 , and 1.2×10^6 cells ml^{-1} for MOI 0.01, 0.10, and 1.00, respectively. Afterwards the viable cell density decreased continuously until the end of the process. Trendlines are intended to guide the eye only.

The general differences observed in the viable cell density profiles for the infected Sf-9 clone cell cultures post infection can directly be explained with the three MOI utilized. Once a

Spodoptera frugiperda insect cell is infected by a baculovirus it stops dividing and starts replicating the virus, and in this case, additionally expressing the recombinant PCV2 ORF2 protein^{141, 142}. While an MOI of 1.00 at least theoretically ensures enough virus particles to infect each cell, this is not the case at the two lower MOI of 0.10 and 0.01. The cells left uninfected after the virus seed addition continue to replicate until they are infected during the so-called secondary infection by virus particles already produced and released by the relatively few cells that had originally been infected during the primary infection. It has been reported that the production and release of budded baculovirus peaks at around 17 to 20 h post infection¹⁴¹, which left significant time for uninfected cells to divide, especially at the two lower MOI in this work. This interpretation is supported by flow cytometric analyses performed in this work, where significantly different infection kinetics could be observed depending on the MOI. Basically, the lower the MOI the longer it took until a complete infection of the culture was achieved (see below, Figure 4.30). These differences in the infection kinetics eventually resulted in the observed differences in the viable cell density profiles. In contrast to this, the uninfected control culture showed a steady increase in viable cell density until approximately 131 h into the process. No arrest in cell division due to baculovirus infection occurred here so that this culture just went through the normal growth cycle phases.

All cultures showed cell viabilities well above 90 % at the time of infection. The cell viability remained stable above 90 % for at least 48 h post infection before starting to decrease, as can be seen in Figure 4.22. A viability of 10 % or below, the specified harvest criteria for this process, was reached after approximately 186 h post infection (day 7) at MOI 1.00 and 0.10 or 216 h post infection (day 9) at MOI 0.01. It was found previously that such a harvest criteria allowed recovery of more than 90 % of the total produced recombinant PCV2-ORF2 protein from the supernatant after simple removal of cells and cell debris¹⁴³. Employing this strategy therefore greatly reduces the downstream processing efforts compared to an earlier harvest, which would require target protein extraction from the still intact cells in some fashion. On the downside, it lengthens the production process by a few days. The uninfected control culture showed a much slower decrease in viability with still 49.0 % of the cells remaining viable after approximately 216 hours (day 9). A viability of less than 10 % was eventually achieved after 384 h (day 16, data not shown).

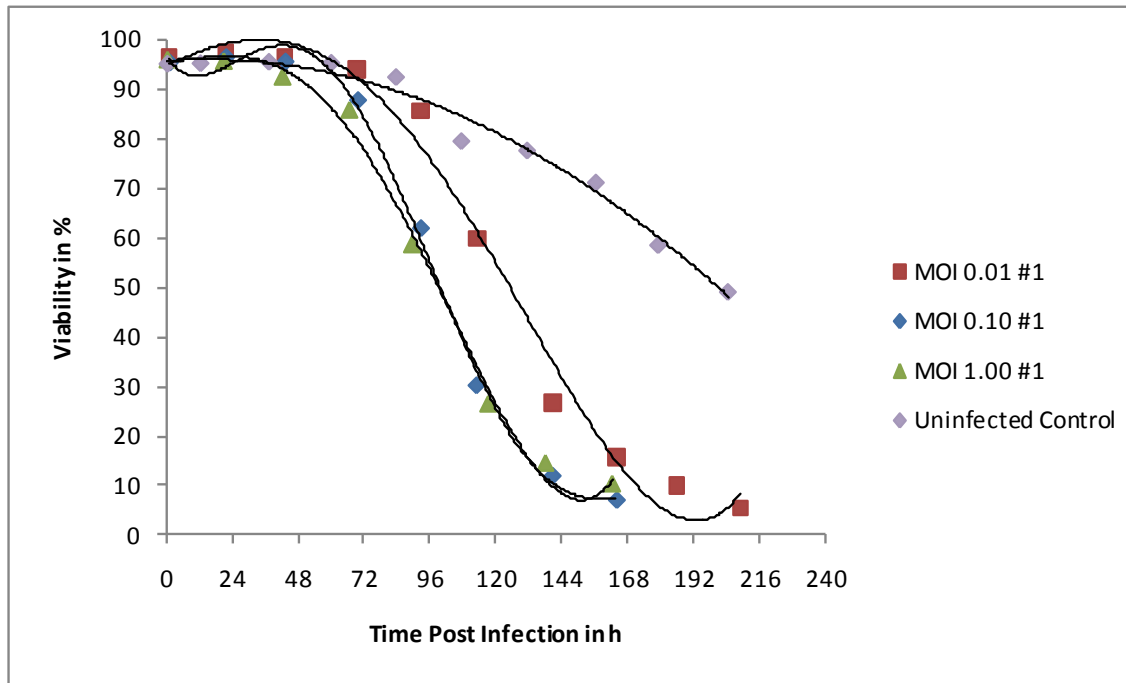


Figure 4.22. Cell viability post infection at the three different MOI compared to an uninfected control culture. Cell viability dropped continuously from approximately 95 % starting after at least 48 h post infection. Cell viabilities below 10 % (the defined harvest criterion) were reached after approximately 168 (MOI 1.00 and 0.10) and 192 h (MOI 0.01) post infection. Trendlines are intended to guide the eye only.

The first drop in cell viability could usually be observed after all cells had been infected by the recombinant PCV2 ORF2 baculovirus (as determined by flow cytometric analysis, see Figure 4.30) and cell division had been largely arrested. The lytic nature of the baculovirus is likely responsible for the observed accelerated decrease in viability with increasing MOI¹⁹. With more cells initially infected, the subsequent infection kinetics were expected to be faster which subsequently led to an earlier onset of the cell lysis. Cell viability remained higher and dropped slower in the uninfected control culture because not lytic baculovirus was contributing to cell death.

In addition to the observed cell division arrest, another characteristic response of a *Spodoptera frugiperda* insect cell culture to the infection with a (recombinant) baculovirus is the

swelling of the viable cells^{11, 15, 141}. This response can be easily followed by measuring the mean viable cell diameter (here with Vi-CELL XR). Figure 4.23 shows the profiles for the mean viable cell diameter post infection. All cultures showed mean viable cell diameters between 17.74 and 18.35 μm at the time of infection, comparable to the values observed for the uninfected cell in the precultures. Immediately post infection the mean viable cell diameter started to increase. Maximum values were reached either on day 3 post infection for cultures infected at MOI 1.00 and 0.10 or on day 4 post infection for cultures infected at MOI 0.01. Maximum values ranged from 21.16 to 23.83 μm with higher maximum values generally observed for cultures infected at a higher MOI. Afterwards the mean viable cell diameter seemed to decrease again continuously until the time of the harvest. The shift in the mean viable cell diameter observed after approximately 120 h post infection (day 5) is an artifact due to the switch in image analysis settings and not caused by actual changes in the cell culture. While it is not possible to compare absolute values from this point in the culture with values obtained before, the continuous decrease in the mean viable cell diameter was still detected. The uninfected control culture showed a similar initial mean viable cell diameter, which did not increase significantly throughout the process.

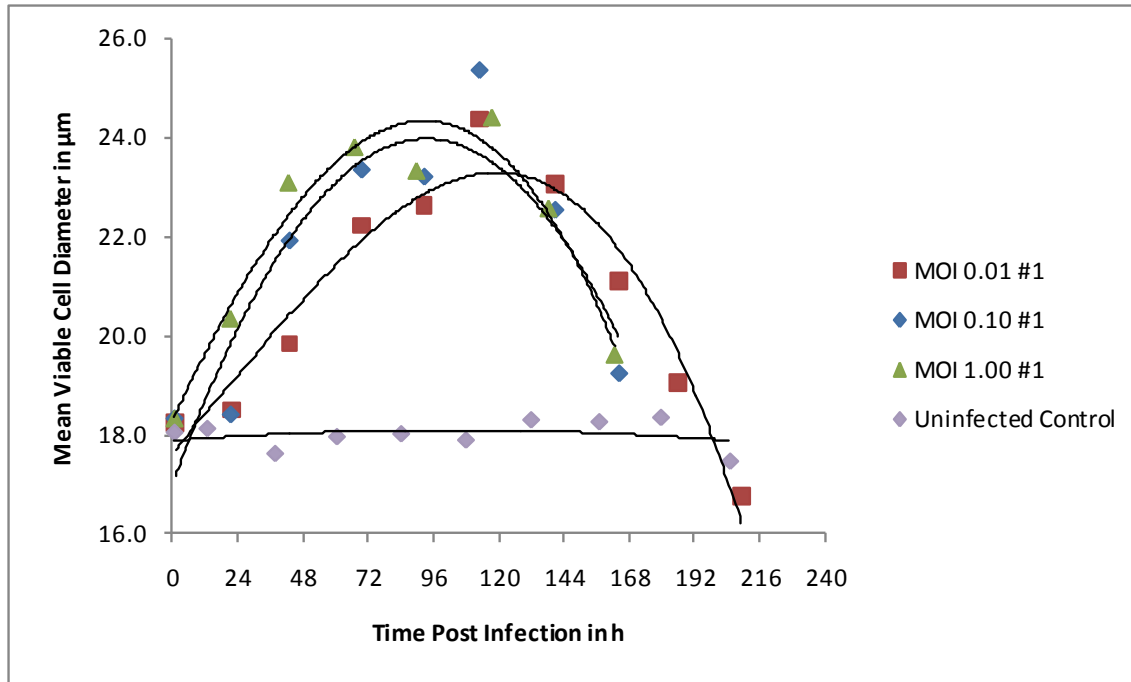


Figure 4.23. Mean viable cell diameter post infection at the three different MOI compared to an uninfected control culture. Mean diameters increased continuously from approximately 18.0 μm immediately post infection to up to approximately 24.0 μm. The higher the MOI the faster the increase occurred and the earlier a peak was reached. Afterwards the mean diameter decreased continuously until the end of the process. Trendlines are intended to guide the eye only.

The observed cell swelling is attributed to nuclear hypertrophy and rearrangements within the cytoskeleton as well as virus and recombinant protein production directly^{11, 15, 141}. The mean viable cell diameter changed significantly post infection for cultures infected at all three MOI, but time of start and peak of this increase was quite different between the three MOI. Usually the lower the MOI, the later the mean viable cell diameter started increasing with the peak also occurring later. This goes hand in hand with the slower infection kinetics discussed above. With the first significant decreases in cell viability, the mean viable cell diameter also decreased. Cells that had undergone an early infection and subsequent cell swelling lysed at this point, leaving cells infected later and therefore still early in the swelling process behind, therefore decreasing the mean viable cell diameter.

Based on the Vi-CELL XR measurements for viable cell density and mean viable cell diameter, the viable biovolume per unit of cell suspension was calculated assuming a spherical cell shape. Figure 4.24 shows the profiles for this parameter. The initial biovolume at the time of infection ranged from 3.46 to $4.53 \times 10^9 \mu\text{m}^3 \text{ml}^{-1}$ cell suspension and started to increase immediately post infection. After reaching a maximum value, which ranged from 8.01 to $17.43 \times 10^9 \mu\text{m}^3 \text{ml}^{-1}$ depending on the MOI, the viable biovolume decreased continuously until the end of the process. Generally, the maximum values observed were the higher the lower the MOI but occurred around 72 h post infection for all three MOI. The shift in the viable biovolume observed after approximately 120 h post infection (day 5) is an artifact due to the switch in image analysis settings and not caused by actual changes in the cell culture. While it is not possible to compare absolute values from after this point in the culture with values obtained before, the continuous decrease in the viable biovolume was still detected. The uninfected control culture showed a similar initial viable biovolume and peaked after approximately 96 h (day 4) at $1.29 \times 10^{10} \mu\text{m}^3 \text{ml}^{-1}$ cell suspension. It has to be noted that the error range for this parameter is at least 10 % (10 % error for viable cell density estimation plus an unknown error for mean viable cell diameter).

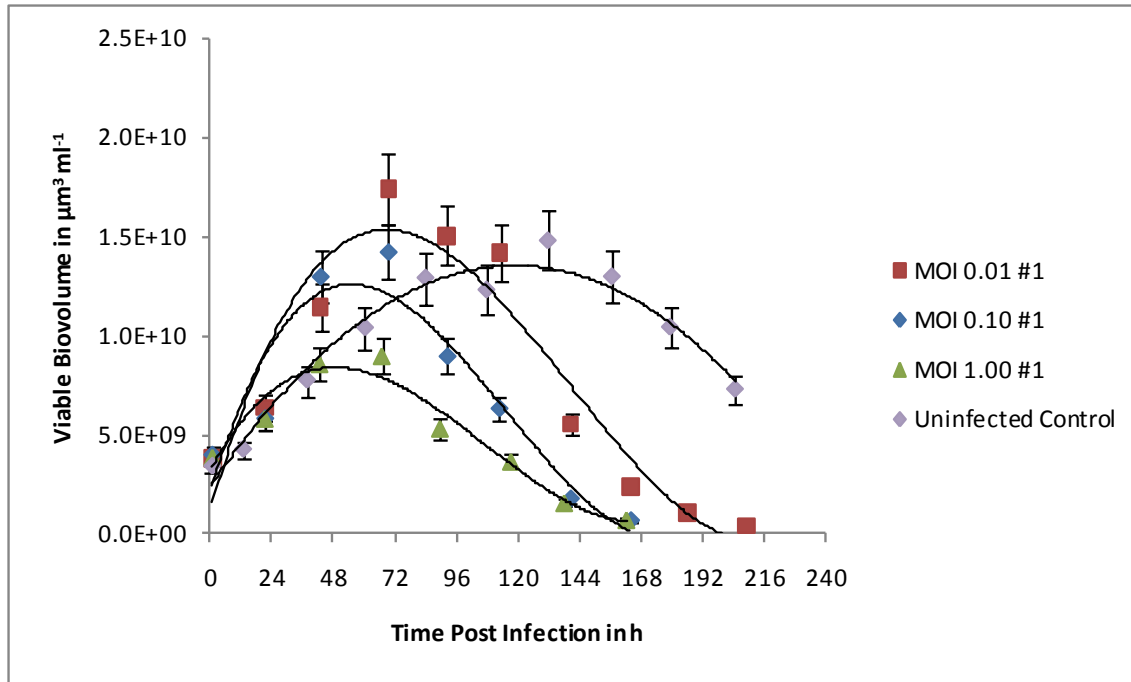


Figure 4.24. Viable biovolume post infection at the three different MOI compared to an uninfected control culture. Initial values were approximately $4.0 \times 10^9 \mu\text{m}^3 \text{ml}^{-1}$ and increased for up to 72 h post infection depending on the MOI. Decreasing maximum viable biovolumes were observed with increasing MOI. Afterwards the viable biovolume decreased continuously until the end of the process. Trendlines are intended to guide the eye only.

The trends observed for the viable biovolume are apparently caused by the same kinetics and effects post infection the viable cell density and mean viable cell diameter were subjected to. Therefore the observed differences generally go along with the observations and interpretations made for those parameters. But interestingly, the peak in viable biovolume occurs at about the same time, 72 h (day 3) post infection, despite the fact that the viable cell density and diameter profiles had shown significant differences between different MOI.

4.2.2 Physiological Culture Parameters, Nutrients and Metabolites

The pH was left uncontrolled during the experiments but it was monitored with an in-line probe directly immersed into the cell culture broth. Significant changes in pH could be observed post infection, as can be seen in Figure 4.25. Initial readings post infection were in the range of 6.28 to 6.42 and generally slightly higher than before the back dilution with fresh EX-CELL 420 medium. The pH then dropped slightly during the first one or two days post infection before increasing again for the next one or two days. After this, the pH in all cultures started to decrease continuously and generally reached its minimum value at the time of harvest. pH values on the harvest day ranged from 5.67 to 6.02. The uninfected control culture showed a comparable behavior in pH during the first 72 h but afterwards the pH stayed above 6.2 and did not decrease as strongly as observed for the infected cultures.

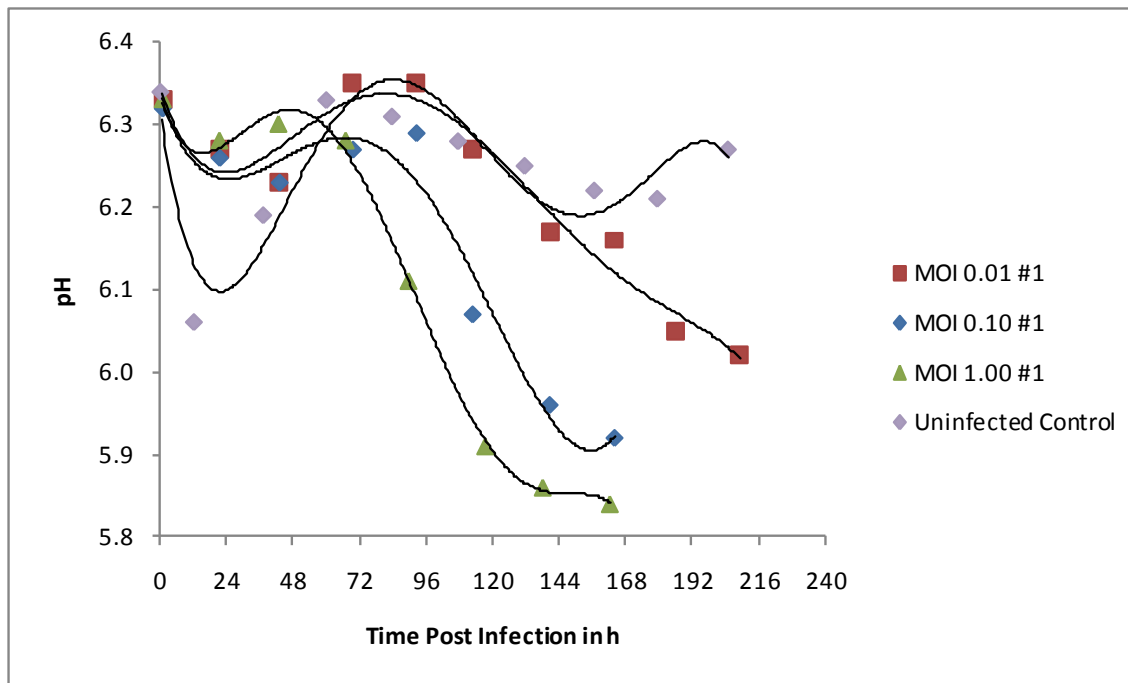


Figure 4.25. Culture medium pH post infection at the three different MOI compared to an uninfected control culture. Initial pH was approximately 6.3 and decreased slightly during the first 24 to 48 h post infection down to 6.2 before increasing again and peaking between 6.3 and 6.4 at 48 to 96 h post infection. Thereafter the pH decreased continuously until the end of the process. Final pH at the time of harvest values decreased with MOI. Trendlines are intended to guide the eye only.

The pH is often left uncontrolled in insect cell cultures because these cells are said to have a very high buffer capacity themselves²¹. Additionally the EX-CELL 420 medium used in this work has a 8.4 mM phosphate buffer system integrated to help keeping the pH in acceptable range¹²¹. The observed changes in pH could directly be related to changes in the L-lactate concentration in the culture medium. As expected, increasing L-lactate concentrations during the experiments led to a decreasing pH and the other way around (also see Figure 4.28). The optimum pH range for insect cell cultures is reported to be about 6.2 to 6.9¹ but cultures in this work usually exhibited significantly lower values, especially later in the process during cell lysis. The lowest pH could be observed for the highest MOI. Interestingly the cultures did not seem to be negatively affected by the lower pH values in terms of recombinant baculovirus and protein production (see below), presumably these were observed late in the process after infection, and protein production had already been accomplished to a major portion.

Figure 4.26 gives an overview of the D-glucose medium concentrations post infection. Initial D-glucose concentrations ranged from 30.69 to 31.75 mmol L⁻¹ and generally decreased post infection. Final values reached at the end of each process ranged from 6.55 to 25.81 mmol L⁻¹ with generally lower values reached the lower the MOI. Nevertheless, D-glucose was not depleted in any infected culture, therefore a limitation of the culture is not likely. The uninfected control culture showed a comparable initial D-glucose concentration of 33.86 mmol L⁻¹ but in this case D-glucose was depleted at around 205 h (day 9) into the process, during the cultures death phase.

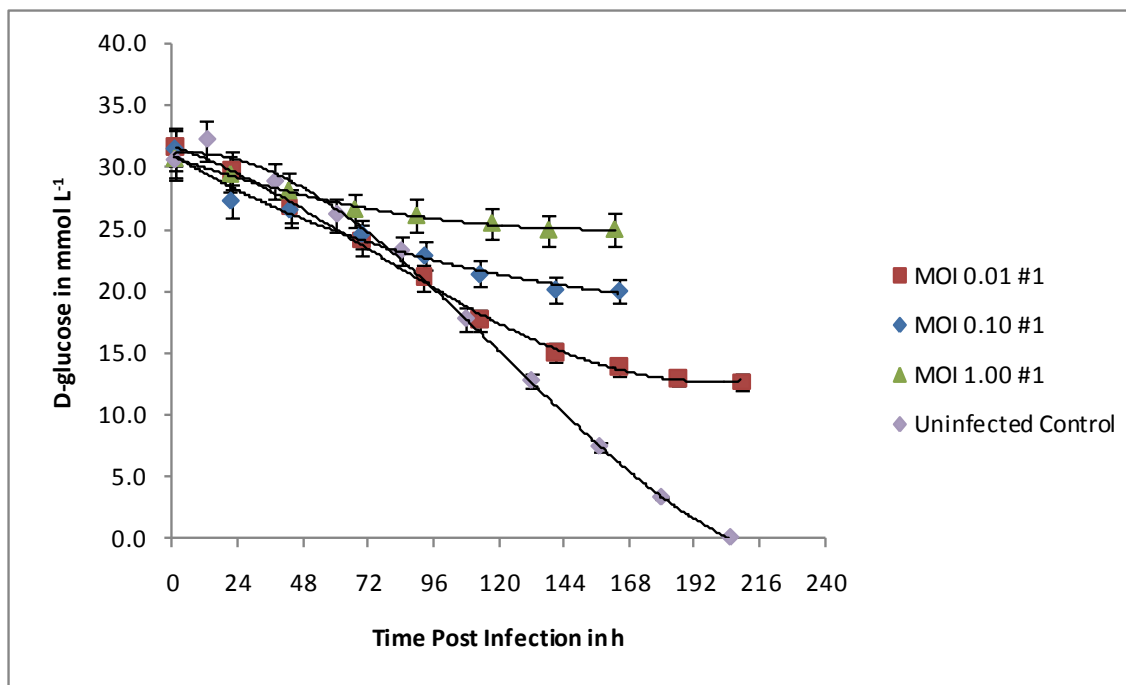


Figure 4.26. Medium D-glucose concentration post infection at the three different MOI compared to an uninfected control culture. Initial concentrations were approximately 31.0 mmol L⁻¹ and decreased continuously throughout the culture. Decreasing final D-glucose concentrations were found with decreasing MOI with values ranging from approximately 25.0 to 15.0 mmol L⁻¹. Trendlines are intended to guide the eye only.

The observed decrease in medium D-glucose post infection is in line with previous reports that describe D-glucose as the main carbon source in *Spodoptera frugiperda* cells for energy production^{122, 144, 145}. Based on the measured medium D-glucose concentrations it can be assumed, that a limitation in this nutrient did not occur during any of the cultures infected at one of the three MOI. In contrast to this, D-glucose was depleted in the uninfected control culture at around 205 h (day 9) because there were still significant amounts of viable cells consuming this nutrient at that time.

Figure 4.27 shows the medium concentration profiles obtained for L-glutamine. Initial concentrations ranged from 3.96 to 4.69 mmol L⁻¹ and generally rapidly decreased post infection. Due to interference with the EX-CELL 420 medium, the lower detection limit for this analysis is about 0.70 mmol L⁻¹. Therefore it was assumed that even with analyses never resulting in a

measured value of 0.00 mmol L^{-1} , L-glutamine was depleted in the media around 48 to 72 h post infection, depending on the culture and MOI used. Usually a higher MOI led to a later depletion of L-glutamine in the medium. Some cultures showed a slight increase in L-glutamine concentration late in the process again, presumably due to cell lysis and release of intracellular L-glutamine into the medium, but concentrations always stayed well below 1.50 mmol L^{-1} . The uninfected control culture showed a significantly lower initial L-glutamine concentration of 3.07 mmol L^{-1} which was depleted at around 60 h into the process. The lower initial concentration in L-glutamine can be attributed to the fact that the medium used for this process was stored longer before usage and the instable L-glutamine therefore degenerated slightly during this prolonged storage time.

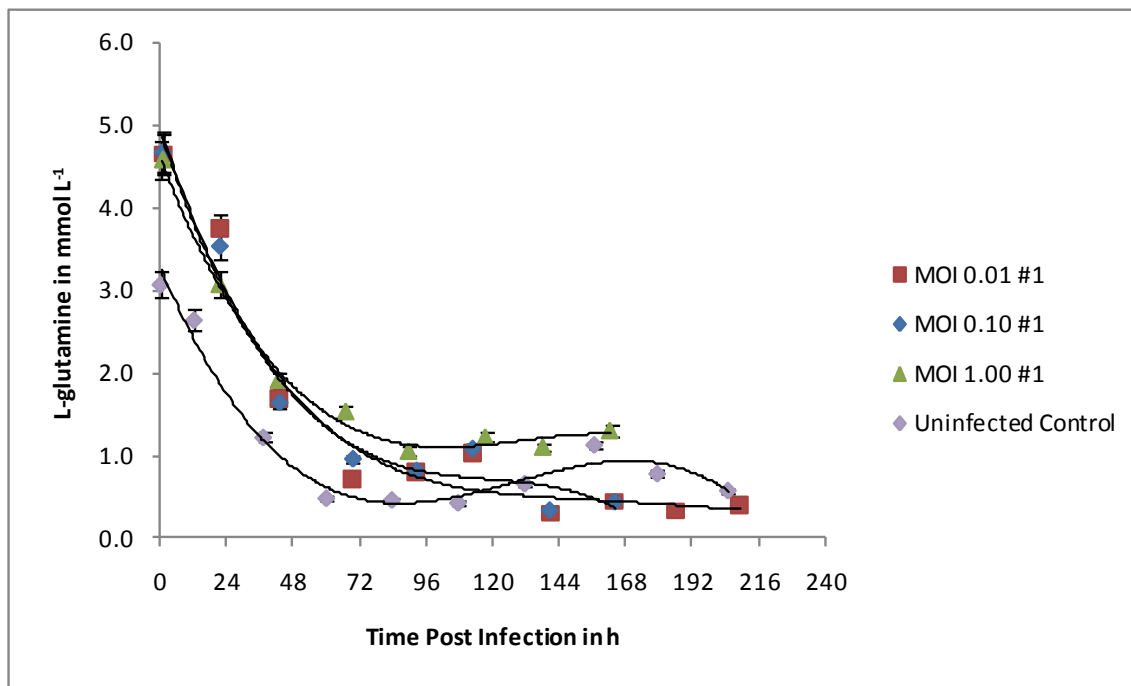


Figure 4.27. Medium L-glutamine concentration post infection at the three different MOI compared to an uninfected control culture. Initial concentrations were approximately 4.5 mmol L^{-1} and decreased continuously throughout the culture. Depletion of this nutrient was assumed to have occurred approximately between 48 and 72 h post infection, depending on the MOI. The detection limit for this analysis is approximately 0.7 mmol L^{-1} and therefore no concentrations below this level could reliably measured. Trendlines are intended to guide the eye only.

Like D-glucose, L-glutamine is also a major nutrient in *Spodoptera frugiperda* insect cell cultures and was rapidly consumed in the experiments. The depletion of this nutrient occurred with higher MOI, presumably because overall less viable cells were consuming L-glutamine in this case than compared to the low MOI experiments, where substantial cell growth occurred even after infection. The same was observed for the uninfected control culture, where L-glutamine was depleted around 60 h into the process.

Profiles for medium L-lactate concentrations are shown in Figure 4.28. Initial concentrations immediately post infection ranged from 1.35 to 1.69 mmol L⁻¹. The concentration then increased for at least one day before decreasing again to an overall minimum value generally below 1.00 mmol L⁻¹ on day 3 or 4 post infection, presumably due to oxidization by the cells¹²³. From this point on the L-lactate concentration increased steadily again until the end of each process. Final concentrations ranged from 2.29 to 4.97 mmol L⁻¹. The uninfected control culture showed a comparable initial L-lactate concentration of 1.11 mmol L⁻¹ and also showed a slight immediate increase up to concentration of 1.90 mmol L⁻¹ after approximately 55 h. From that point on the L-lactate concentration decreased until approximately 157 h and 0.03 mmol L⁻¹ before starting to increase again and reaching a concentration of 0.82 mmol L⁻¹ after approximately 216 h.

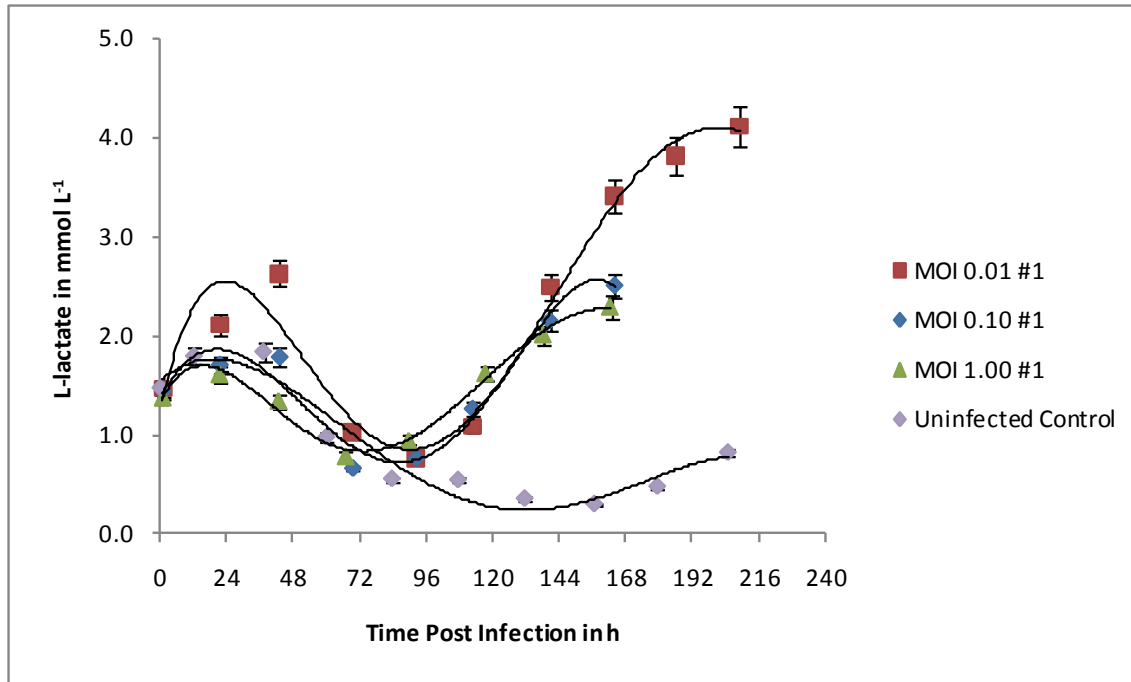


Figure 4.28. Medium L-lactate concentration post infection at the three different MOI compared to an uninfected control culture. Initial concentrations were approximately 1.5 mmol L^{-1} and increased to up to approximately 2.5 mmol L^{-1} during the first 24 to 48 h post infection. This was followed by a decrease lasting until approximately 72 to 96 h post infection and another subsequent continuous increase until the end of the process. A lower MOI seems to cause a higher final L-lactate concentration. Trendlines are intended to guide the eye only.

Initial L-glutamate concentrations ranged from 7.46 to 8.43 mmol L^{-1} . Depending on the MOI utilized cultures followed slightly different profiles (see Figure 4.29). Cultures infected with an MOI of 0.01 showed an initial slight increase in L-glutamate until day 2 post infection. Then values decreased again down to a minimum at around day 5 post infection before steadily increasing until the end of the process. Cultures infected with an MOI of 0.10 generally showed an L-glutamate concentration increase post infection until the end of the experiments without a distinguished minimum as described for MOI 0.01 cultures. Cultures infected with an MOI of 1.00 also showed an increase right from the start but values leveled off at around day 3 post infection without any further increase. However, it has to be noted that some of these observations are barely significant due to the error associated with this analysis. Final

concentrations ranged from 8.12 to 9.57 mmol L⁻¹. The uninfected control culture showed a comparable initial L-glutamate concentration of 7.83 mmol L⁻¹ with values slightly increasing during the first 38 h. From that point on the L-glutamate concentration decreased again with a final value of 4.39 mmol L⁻¹ after approximately 205 h.

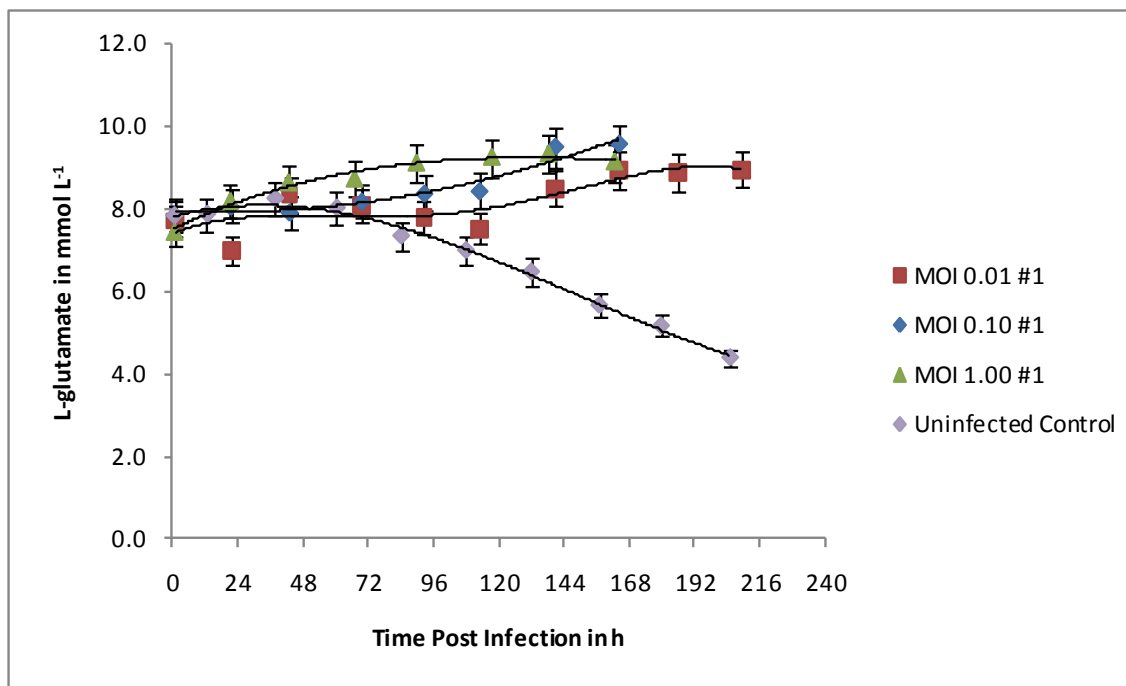


Figure 4.29. Medium L-glutamate concentration post infection at the three different MOI compared to an uninfected control culture. Initial concentrations were approximately 8.0 mmol L⁻¹ and increased to up to approximately 9.0 mmol L⁻¹ until the end of the process for MOI 0.10 and 1.00. Cultures infected at MOI showed a slightly different profile with a slight decrease in L-glutamate during the first 24 h post infection before another increase and decrease up to 120 h post infection. Afterwards the L-glutamate concentration increased continuously until the end of the process and reached comparable levels to cultures infected at MOI 0.10 and 1.00. Trendlines are intended to guide the eye only.

Profiles in medium L-glutamate concentrations for all three MOI seemed to differ slightly but differences observed were generally barely significant. Interestingly, the profile for the uninfected control culture somewhat resembled the data for the MOI 0.01 experiments, further confirming the fact that these cultures behaved mainly like uninfected cultures during the first

days post infection due to the very low initial virus concentration. During the later days the uninfected control continuously utilized L-glutamate while in the case of any infected culture L-glutamate was released into the medium.

4.2.3 Fraction of Infected Cells

Figure 4.30 shows the profiles obtained for the fraction of infected cells post infection at the different MOI. The percentage of infected cells for each of the three MOI showed different profiles but were relatively consistent within each MOI. The first main difference was found to be the initial percentages estimated immediately after infection. Generally, a higher MOI meant a higher initial percentage of infected cells. Values here ranged from 0.09 at MOI 0.01 to 14.15 % at MOI 1.00. While essentially all cells were infected eventually, as defined by percentages above 90 %, the time post infection at which this occurred was quite different at each MOI. While cultures infected at MOI 0.01 showed a relatively slow increase in the fraction of infected cells post infection and were eventually completely infected at around 72 h post infection, a faster increase observed at MOI 0.10 and 1.00. In those cases, a complete infection was already achieved at around 48 h post infection. Because samples were only analyzed in approximately 24 h intervals, no further differentiation between the point of complete infection at these two MOI could be made. But it is obvious from the profiles, that the culture infected at the higher MOI of 1.00 should have reached the point of complete infection earlier, already indicated 24 h post infection, where between 32.97 and 52.94 % of the cells were infected, compared to only 3.89 to 7.25 % in MOI 0.10 cultures.

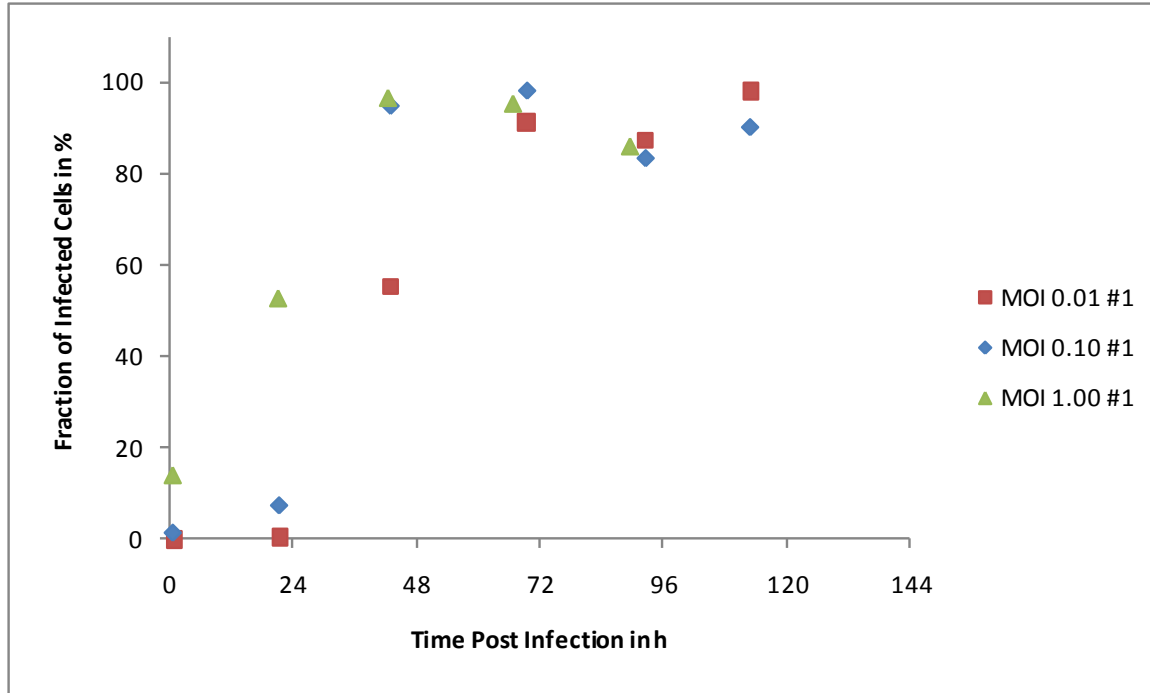


Figure 4.30. Fraction of infected cells post infection at the three different MOI. A higher initial MOI resulted in faster infection kinetics and eventually earlier complete infection of the culture at approximately 48 to 72 h post infection.

The rate of infection and the fraction of initially infected cells is a direct function of the MOI and as expected results obtained in this work showed significantly different profiles for the three MOI. Infection at a lower MOI led to lower fractions of infected cells early in the process and complete infection of the culture was delayed. The Poisson probability distribution can be used to model the baculovirus infection process and predict the fraction of initially infected cells as a function of the MOI^{24, 146-148}. Experimental values obtained in this work were compared to the theoretical predictions by the Poisson distribution (Equation 23) for the situation that each cell was infected by at least one baculovirus.

$$P(w, MOI) = \frac{MOI^w}{w!} \times e^{-MOI} \quad \text{Equation 23}$$

Data used in this comparison was from approximately 24 h (day 1) post infection, since it was assumed, that at this time the initially added virus particles had completed infection but no

significant subsequent infection by newly produced virus particles (secondary infection) had taken place yet¹⁴⁹. This assumption could be verified by the fact that very little infectious virus particles had been produced until 24 h post infection for any MOI (see below, Figure 4.32). Results of this comparison are shown in Figure 4.31. Additional data extracted from literature and converted to a TCID50-based MOI is added to the plot for comparison¹⁴⁹. Experimental values shown are mean values of the three replicates performed at each MOI \pm one standard deviation and the assay error for the fraction of infected cells and MOI, respectively.

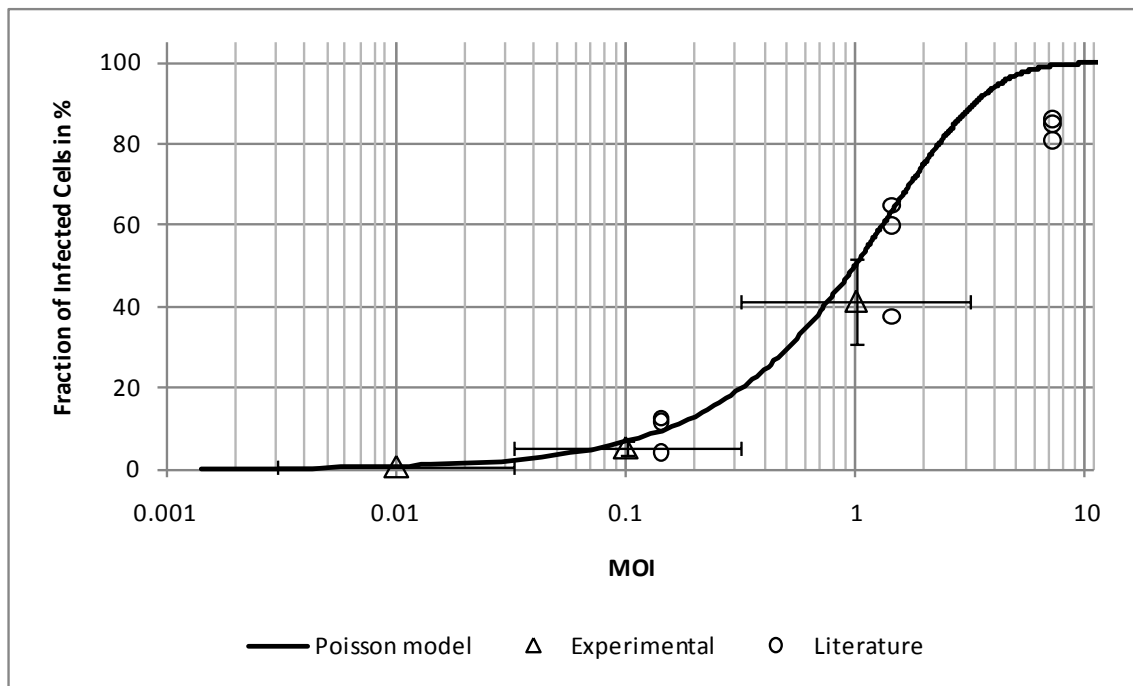


Figure 4.31. Comparison of theoretical Poisson model vs. experimental and literature data for the fraction of infected cells at 24 hours post infection (primary infection). Experimental data from this work is comparable to the theoretical model as well as literature.

Calculated mean experimental values were generally lower than estimated by the Poisson model but not significantly different when the 95 % confidence interval was taken into account. This was mainly due to the rather large error for the baculovirus titration of $\pm 0.5 \log \text{TCID ml}^{-1}$. This caused a wide range of possible “real MOI” around the targeted MOI at which the cultures could have actually been infected, as shown with the horizontal error bars. Additionally

suboptimal culture conditions at the time of infection could also have influenced the amount of infective virus particles available, e.g. by retaining in surface foam or suboptimal pH conditions. While it was out of the scope of this work, if desired more sophisticated models can be used if one wants to obtain more detailed information about the subsequent infection processes over time at the comparably low MOI utilized here. The literature gives several examples of this¹⁴⁹⁻¹⁵³.

In summary, the relationship of MOI and the progress of infection early in the culture (24 H) as given by the proposed Poisson model was confirmed here. In industrial practice, a tradeoff is often necessary between the use of costly virus and the time required to achieve a complete infection and subsequent product formation.

4.2.4 Production of Recombinant PCV2 ORF2 Baculovirus

Upon infection with a recombinant baculovirus and if the target protein gene is controlled under one of the very late promoters, e.g. the polyhedrin promoter, the insect cell initially produces new virus particles before eventually shifting to recombinant protein production. To follow the baculovirus production kinetics at the different MOI the baculovirus concentration was measured in whole culture samples stored at -70 °C with an end-point dilution assay.

Recombinant baculovirus concentrations for all three MOI showed overall similar profiles and were consistent within each MOI (see Figure 4.32). Generally, the recombinant baculovirus concentration initially remained relatively constant with no significant differences in concentration for the first 24 h post infection, but only the data for cultures infected at MOI 1.00 may indicate a slight increase during this time. Different starting recombinant baculovirus concentrations immediately after infection were due to the different MOI used. The recombinant baculovirus concentration then continuously increased to reach its specific maximum concentration and remained constant within the error range of the assay once this concentration was reached. Maximum concentrations ranged from 7.63 to 8.50 log₁₀ TCID₅₀ ml⁻¹. Noticeably the time of reaching this maximum concentration is different for the three MOI. Generally, the maximum recombinant baculovirus concentration was reached earlier the higher the MOI, more

specifically it took approximately 96, 72, and 48 h post infection to reach this point in the process for the MOI 0.01, 0.10, and 1.00, respectively.

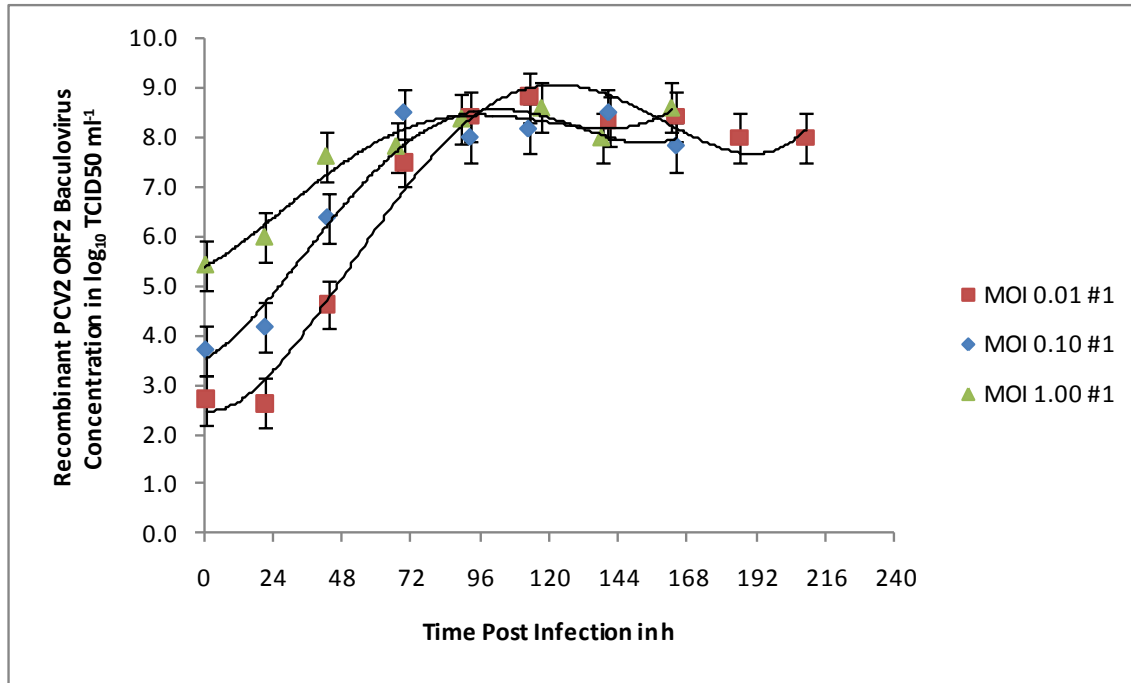


Figure 4.32. Recombinant PCV2 ORF2 baculovirus concentration post infection at the three different MOI. A higher initial MOI resulted in earlier recombinant PCV2 ORF2 baculovirus production. Maximum concentrations were reached at different times ranging from approximately 48 to 96 for all MOI at approximately 8.0 log₁₀ TCID₅₀ ml⁻¹. Trendlines are intended to guide the eye only.

The described differences in the infection kinetics can also explain the observed differences in the production of recombinant baculovirus post infection. Generally, the lower the MOI cultures were infected with the later the peak in recombinant baculovirus concentration was observed. The release of budded virus usually occurs from approximately 6 to 8 h post infection and peaks around 17 to 20 h post infection¹⁴¹. Lower initial virus concentrations will lead to less immediately infected cells - as confirmed above – and therefore less new virus particles will be produced early in the process by these cultures. But subsequent infection processes will lead to an ever-increasing fraction of infected cells over time, which produce the recombinant baculovirus, and eventually lead to a complete infection. Recombinant baculovirus

concentrations generally peaked around 24 h after the time point when virtually all cells had been infected. This is in agreement with the 17 to 20 h of time needed from the time of infection to the peak in virus production. Interestingly no significant differences could be observed between the maximum recombinant baculovirus concentrations obtained after infection at the three different MOI.

4.2.5 Production of Recombinant PCV2 ORF2 Protein

The relative PCV2 ORF2 protein concentration for all three MOI showed overall similar profiles and is shown in Figure 4.33. The first time protein was detected at approximately 96, 72, and 48 h post infection for cultures infected at MOI 0.01, 0.10, and 1.00, respectively. From this point on the protein concentration increased continuously (with some fluctuations due to assay variation) to reach a maximum at the end of the process. The final PCV2 ORF2 protein concentrations ranged from 2.2 to 4.8 RP. It has to be noted, that even taking the large error range of the assay into consideration the PCV2 ORF2 antigen expression seemed to be more consistent within each MOI the higher the MOI was. Especially the data for cultures infected at MOI 0.01 showed a rather wide spread of the three data sets and significant differences in harvest concentrations determined. This spread seemed to narrow for MOI 0.10 and especially 1.00 (see Appendix E -).

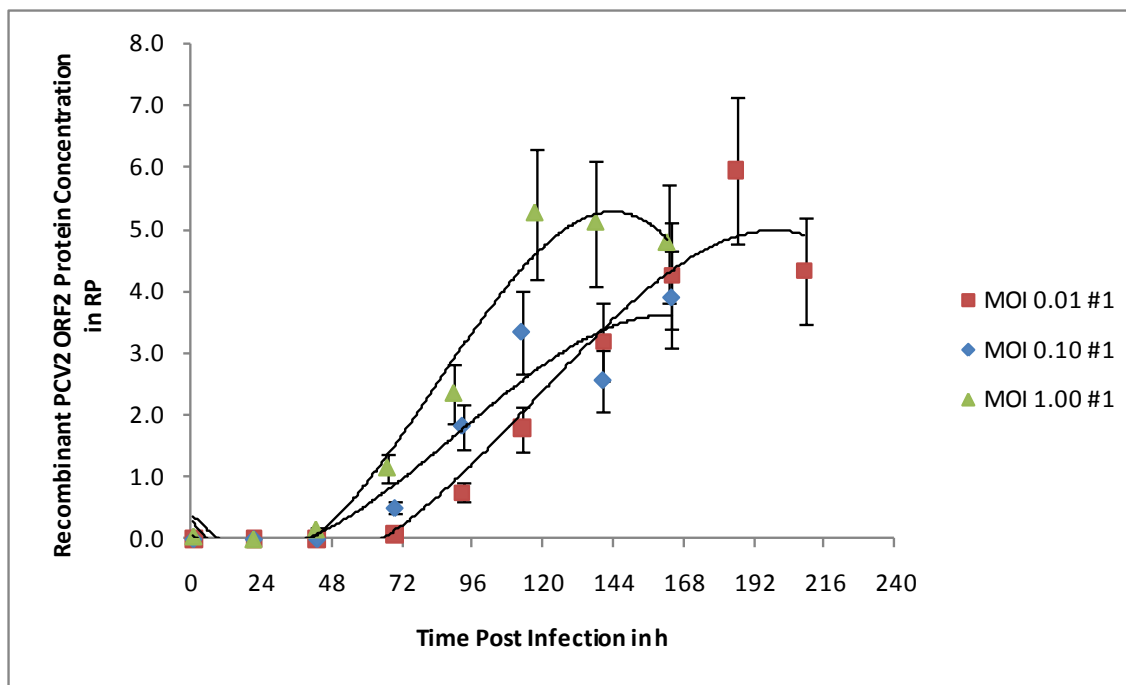


Figure 4.33. Recombinant PCV2 ORF2 protein concentrations post infection at the three different MOI. A higher initial MOI resulted in earlier recombinant PCV2 ORF2 protein production. Maximum concentrations were generally reached at the end of the process. Infection at all MOI was capable of producing PCV2 ORF2 protein at a volumetric yield of approximately 4.0 RP after 168 to 216 h post infection but variability increased greatly with decreasing MOI (see Appendix E -). Trendlines are intended to guide the eye only.

Overall, the same trends could be observed in the profiles for the recombinant PCV2 ORF2 protein concentration but a lower MOI generally led to a slower increase in the PCV2 ORF2 protein concentration. Because the expression of the PCV2 ORF2 gene is regulated under the very late polyhedrin promoter, production started approximately around 15 to 20 h post infection^{20, 152}. Consequently, the first significant amounts of the PCV2 ORF2 protein could be detected approximately 24 h after a major fraction of the cells had been infected. Figure 4.34 shows the overall trend observed. Harvest PCV2 ORF2 protein concentration seemed to increase with MOI but statistical analysis revealed that the differences observed are not significantly different ($p > 0.05$ in all cases, by using a t-test assuming unequal variances, see Appendix F -). Nevertheless, the consistency of PCV2 ORF2 harvest concentrations improves greatly with increasing MOI (from 33 to 3 % standard deviation). This behavior is presumably due to the fact that even small deviations in the viable cell density and amount of virus added, both together

eventually constituting the “real MOI”, but also in the time of infection, are amplified in situations below MOI 0.10 and may lead to fluctuations¹. Nevertheless, MOIs as low as 3×10^{-5} have been used to successfully produce recombinant protein with the baculovirus expression vector system¹⁵⁴.

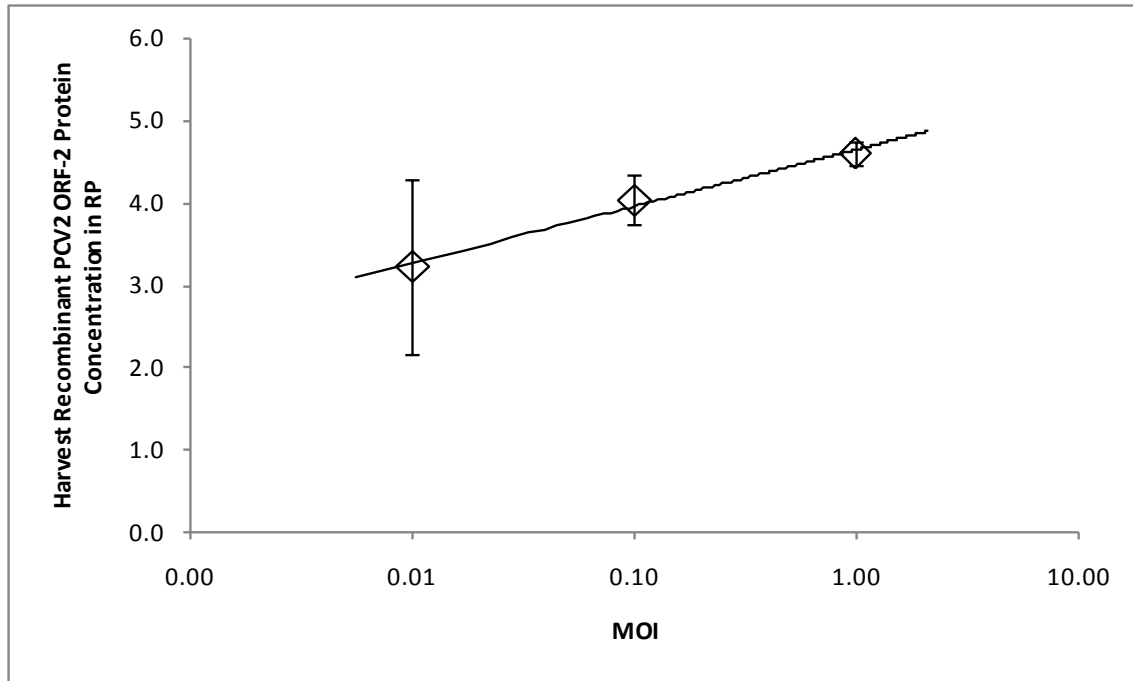


Figure 4.34. Dependency of harvest recombinant PCV2 ORF2 protein concentration on MOI. Variability in the harvest PCV2 ORF2 concentration decreased greatly with increasing MOI. Values shown are mean ± standard deviation based on the three replicates performed at each MOI.

In addition to the overall volumetric recombinant PCV2 ORF2 protein yield of the process, the specific productivity per unit of viable biovolume or cells is an important parameter to consider. While eventually the volumetric concentration of recombinant protein at the time of harvest may be the most important factor in the routine vaccine production, the specific yield has important implications for downstream processes and the overall effectivity of the process in terms of yield and cost compared to the raw materials and work invested. To obtain a measure of the mean specific yield of a respective culture the harvest PCV2 ORF2 protein concentration was divided by the observed maximums of viable biovolume and cell density during that respective culture. Figure 4.35 and Figure 4.36 show the calculated specific yields.

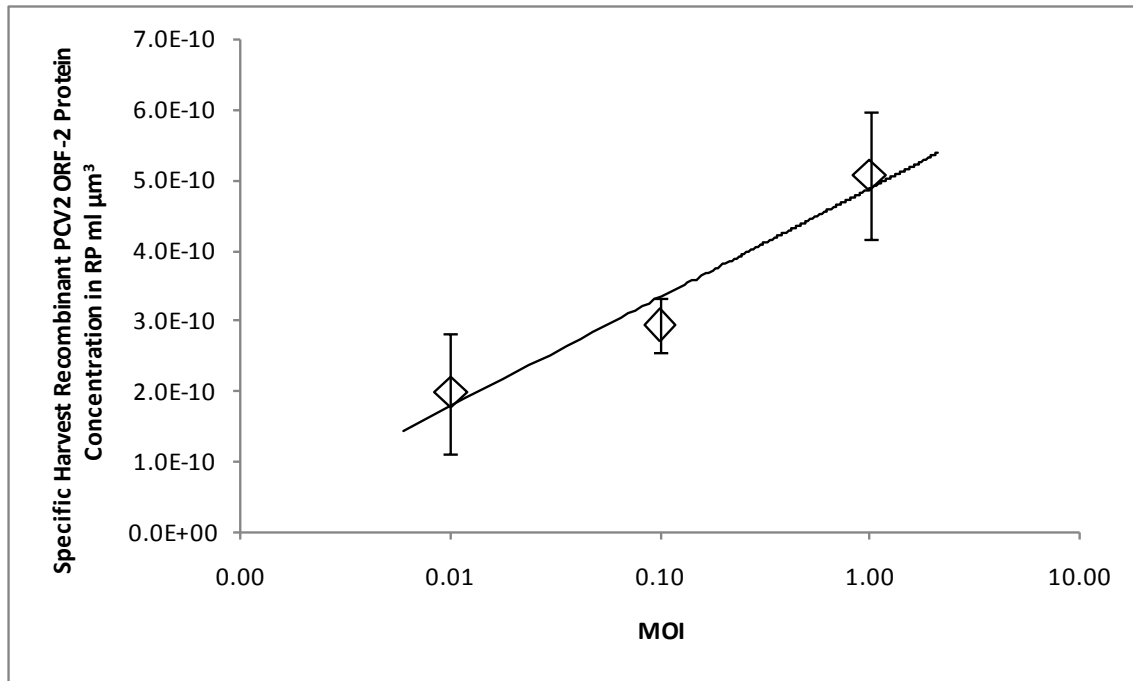


Figure 4.35. Dependency of the specific recombinant PCV2 ORF2 protein productivity per observed maximum viable biovolume on MOI. Mean specific yields were approximately 2.5 times higher at MOI 1.00 than at 0.01. Values shown are mean \pm standard deviation based on the three replicates performed at each MOI.

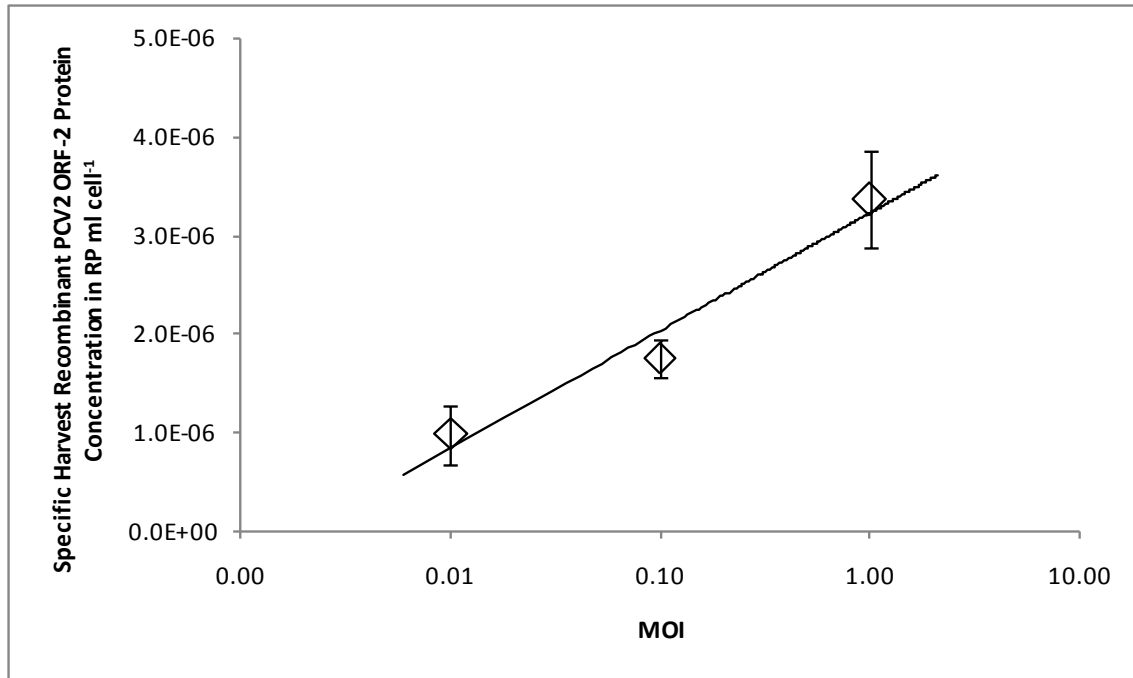


Figure 4.36. Dependency of the specific recombinant PCV2 ORF2 protein productivity per observed maximum viable cell density on MOI. Mean specific yields were approximately 3 times higher at MOI 1.00 than at 0.01. Values shown are mean \pm standard deviation based on the three replicates performed at each MOI.

A rather large discrepancy could also be observed for the specific PCV2 ORF2 protein yields for the three different MOI. Generally, a strong dependence of the specific yields on the MOI could be observed. It was found (by using a t-test assuming unequal variances, see Appendix F -), that the means at all MOI were statistical significantly different with $p < 0.05$, except between MOI 0.01 and 0.10 ($p = 0.09$ and 0.07 for the biovolume and cell correlation, respectively). Mean specific yields at MOI 1.00 were up to three times higher than at MOI 0.01 with mean values increasing from 9.9 to 33.7×10^{-7} RP ml μm^3 or 2.0 to 5.1×10^{-10} RP ml cell. This indicates a more effective intracellular PCV2 ORF2 production process with increasing MOI. This may be facilitated by the fact that the cultures at higher MOI replicate less post infection and therefore all available resources, in terms of nutrients and the intracellular apparatus, can be channeled into the recombinant baculovirus and eventually protein production.

4.2.6 Dielectric Spectroscopy

With few exceptions, the data recorded for the three replicate processes performed at each MOI was consistent and comparable. Therefore, only one process at each MOI is shown in the following plots to ensure clarity of the plots. Additionally, the recorded data for an uninfected control culture is shown in each plot for comparison.

Figure 4.37 gives an overview of the dielectric increment $\Delta\epsilon$ profiles post infection at the three MOI utilized in this work. Initial $\Delta\epsilon$ values ranged from about 5.00 to 8.00 pF cm⁻¹ and generally increased immediately post infection for infection at all three MOI, peaked and then started to decrease again. Peak values were generally reached earlier the higher the MOI, occurring from approximately 48 to 74 h post infection. Interestingly the shape of the increase for the three different MOI was also different. $\Delta\epsilon$ values for MOI 0.01 and 0.10 showed a slower increase during the first 24 h post infection than observed for MOI 1.00. In addition, MOI 0.01 data also showed a small plateau phase from around 48 h post infection before increasing again. Peak values reached were approximately 42.00, 55.00, and 38.00 pF cm⁻¹ for infection at MOI 0.01, 0.10, and 1.00, respectively. Once $\Delta\epsilon$ had reached its specific peak value, it decreased continuously until the culture was terminated. This decrease is relatively slow for another 24 to 48 h – depending on the experiment - before a drop-off in the signal could be observed and the signal then fell rapidly thereafter. $\Delta\epsilon$ for the uninfected control culture was relatively similar to the MOI 0.01 process during the first 48 h of the process and also exhibited the mentioned plateau in $\Delta\epsilon$ around the same time. But the plateau observed in the uninfected control culture was much more prominent and lasted about 24 h longer than in the infected culture. Following the plateau $\Delta\epsilon$ started to increase again slowly in the control culture until reaching a secondary plateau around 120 h into the process, followed by another but slower subsequent increase. $\Delta\epsilon$ never really peaked or exhibited the subsequent decrease observed in the infected cultures.

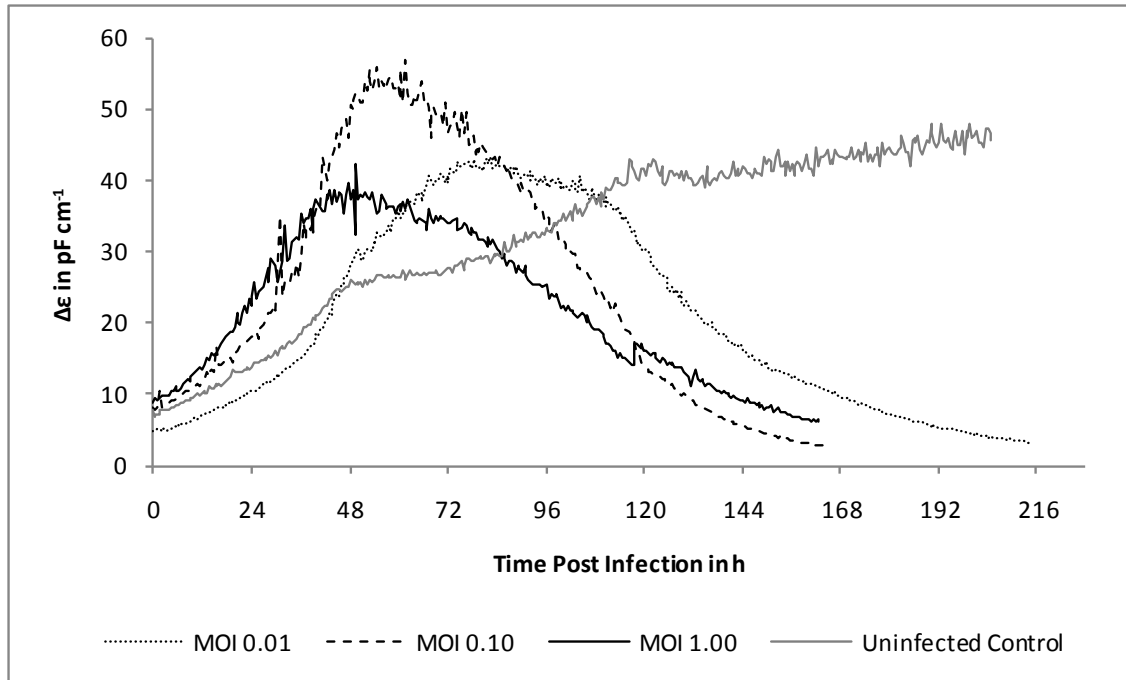


Figure 4.37. Dielectric increment $\Delta\epsilon$ post infection at the three different MOI. $\Delta\epsilon$ increased immediately post infection from below 10.0 pF cm^{-1} to values as high as approximately 55.0 pF cm^{-1} after approximately 48 to 72 h post infection. Highest peak values were generally reached at MOI 0.10 but the time of the peak was delayed with decreasing MOI. $\Delta\epsilon$ decreased continuously afterwards until the end of the process.

$\Delta\epsilon$ is directly related to the volume fraction of viable cells P or viable biovolume, which increased significantly immediately post infection. But other than in the case of the uninfected cells described earlier, this time the viable cell diameter also changed during the process and therefore additionally affected $\Delta\epsilon$. In the case of MOI 1.00 cell size changes in the viable cell diameter were observed as early as 24 h post infection while it took approximately 48 h until significant changes were observed in cultures infected at MOIs 0.10 and 0.01. Therefore, significant influences on the viable cell size on $\Delta\epsilon$ can be excluded until these points post infection but not thereafter. While the volume fraction of viable cells (viable biovolume) determined off-line usually peaked around 72 h post infection, this was not always the case for $\Delta\epsilon$. For MOI 0.10 and 1.00 $\Delta\epsilon$ peaked significantly earlier, approximately 60 and 48 h post infection, respectively. This might be rationalized with the influence of the viable cell size on $\Delta\epsilon$ as described earlier. In the cases of MOI 0.10 and 1.00, the viable cell size changed and leveled

off earlier during the process and therefore may have contributed to this observation. Nevertheless, it has to be taken into account, that off-line samples for the determination of the viable biovolume were only taken approximately every 24 h so that slight time shifts for the respective peaks may be explained by this. Additionally the change in the settings from approximately 120 h (day 5) post infection may have lead to deviations in the biovolume calculations late in the process because these settings usually estimated the viable cell diameter to be higher.

Another factor possibly affecting $\Delta\epsilon$ is the specific cell membrane capacitance C_m . In this work, C_m was not measured directly but could be calculated based on Equation 4 using the viable cell density and size obtained by off-line measurements (Vi-CELL XR) for each sample point. C_m profiles obtained by this calculation are shown in Figure 4.38.

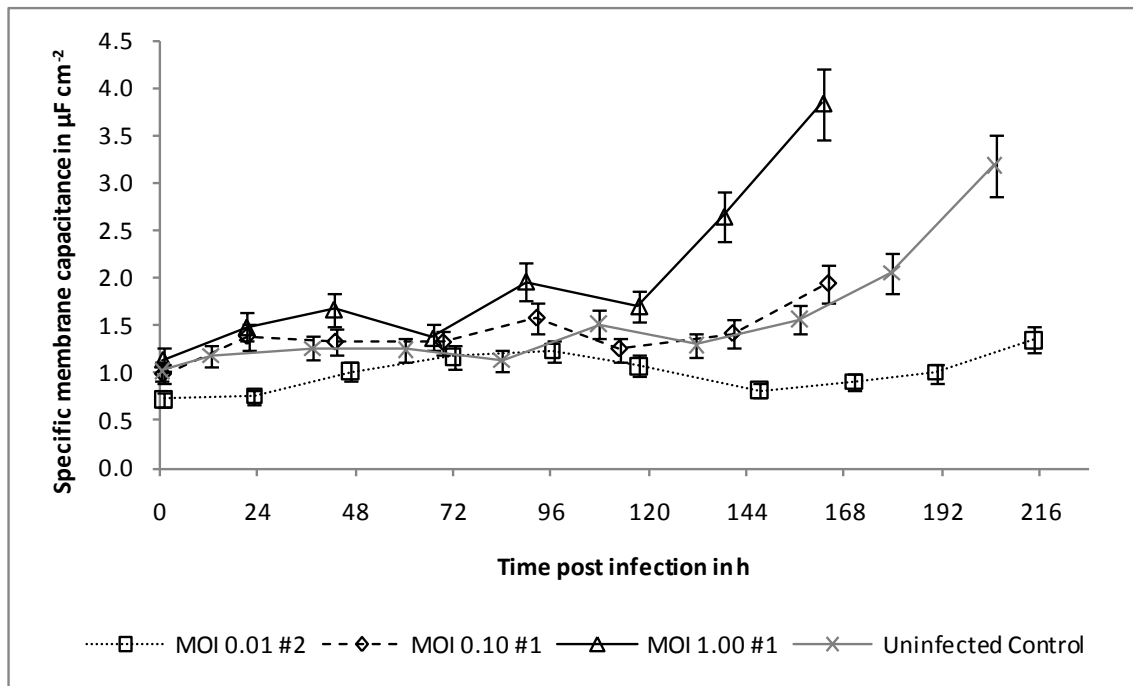


Figure 4.38. Specific membrane capacitance C_m post infection at the three different MOI. Values ranged from approximately 0.6 to 2.0 $\mu\text{F cm}^{-2}$ during the first 120 h post infection but did not show any distinct differences at different MOI. Late in the process, some cultures showed strong increases in C_m but it remains unclear if this is indeed a true representation of the reality.

Calculated values for C_m ranged from 0.61 to 2.03 $\mu\text{F cm}^{-2}$ during the first approximately 120 h post infection but did not show any distinct differences or trends between the three different MOI. After this, some of the cultures showed strong increases in C_m but at this point it remains unclear why this is the case. Often it is assumed that cell death goes along with a decrease in C_m due a loss in membrane structure and rounding. Such a behavior has been reported in the literature^{138, 155-157}. But other contradictory literature actually reports an increasing C_m during cell death, presumably due to increased folding of the membrane when the cells shrink and cell components leak out or other membrane properties change^{158, 159}. Trends observed for C_m are in accordance with the latter. The switch in the Vi-CELL XR settings after approximately 120 h (day 5) post infection and the observed changes also seem unreasonable to explain this behavior. The specific cell membrane capacitance C_m is generally interpreted to be dependent on the level of folding of the cellular membrane^{73, 74} and was originally thought to be a cell biological constant with a value of approximately $1.00 \pm 0.5 \mu\text{F cm}^{-2}$ ^{73, 87, 125, 126}. Recent research suggests that this assumption is not entirely true and C_m can indeed be influenced by cell viability, physiological state, virus infection and release or during overexpression of cation channels^{12, 73, 139}. Data specifically for *Spodoptera frugiperda* derived cells is scarce and only one publication reports values for C_m in the range of 0.55 to 0.85 $\mu\text{F cm}^{-2}$ for infected Sf-9 cells (no MOI given, but presumably higher than in this work due to observed immediate arrest in cell division post infection). But these values were also not obtained directly by measurements but rather calculated based on dielectric spectroscopy measurements and a simplified dielectric cell model¹²⁷. Interestingly, in the work cited the specific membrane capacitance C_m increased during the first 20 h post infection and then again dropped later in the process, a behavior that was not observed in this work.

The calculations above are assuming that the theoretical relationship stated in Equation 4 is valid even in the case of cell death. It had been developed based on the so-called single shell model, representing the cell as a conductive core surrounded by a non-conductive shell. Successful staining of the cells with trypan blue late in the process (by Vi-CELL XR) suggests, that the membrane permeability indeed increased, in case of a non-permeable membrane trypan blue should not have been able to enter the cell. While usually not done when using DS in cell

culture technology, the use of a modified relationship based on a shell model with a highly conductive shell is suggested for such situations⁸⁷ and described in Equation 24

$$\Delta\varepsilon = \frac{9 \times P \times r \times C_m}{4 \times \left[1 + r \times G_m \times \left(\left(\frac{1}{\sigma_i} \right) + \left(\frac{1}{2 \times \sigma_e} \right) \right) \right]^2} \quad \text{Equation 24}$$

where G_m is the membrane conductance in S. This modified relationship takes the membrane conductance G_m into account and therefore may be better suited to describe the behavior of $\Delta\varepsilon$ late in the process. An increase in G_m , as suggested by the decreasing viability determined with trypan blue staining, would further contribute to a typically observed decrease in $\Delta\varepsilon$. Because neither C_m nor G_m was directly measured in this work, no further statement about the behavior of those two parameters can be made at this point. Further research is required to address this issue.

The second β -dispersion parameter provided by the instrument was the characteristic frequency f_c , which is thought to be influenced by the cell radius r , the specific cell membrane capacitance C_m , and the intracellular and medium conductivities σ_i and σ_e , respectively (see Equation 6). Profiles for this parameter are shown in Figure 4.39. The characteristic frequency f_c for the three MOI started at around 600 kHz for all MOI but showed slightly different profiles during the process. In the case of infection at MOI 0.01 the signal initially increased slightly for about 30 h post infection followed by a decrease and a minimum reached at around 72 h post infection. From that point on f_c continuously increased until the end of the process. Data for MOI 0.10 generally also showed a slight increase in characteristic frequency post infection until about 30 h post infection from which point on a decrease could be observed also. A minimum in f_c could be observed at around 60 h post infection after which the characteristic frequency started to increase again until approximately 100 h post infection. In contrast to the observations for MOI 0.01 and 0.10, f_c for experiments performed with MOI 1.00 started to decrease immediately post infection. Again, a minimum in the signal was reached at approximately 48 h post infection and followed by a subsequent increase until the end of the process. Noticeably the increase slowed down at around approximately 72 h but picked up again at approximately 96 h post

infection. The shift in f_c observed at around 120 h post infection for the culture infected at MOI 1.00 was due to a technical issue and does not represent any actual change in the culture. In contrast to the changes observed in case of an infection with the recombinant PCV2 ORF2 baculovirus, the characteristic frequency in the uninfected control culture remained relatively constant during the first 56 h, but then increased slightly during the next 20 h. Afterwards f_c approximately remained constant until the end of the process. Overall, f_c was usually slightly higher than in the infected cultures, with exception of the first 30 h where the signal was close to the values observed for MOI 0.01.

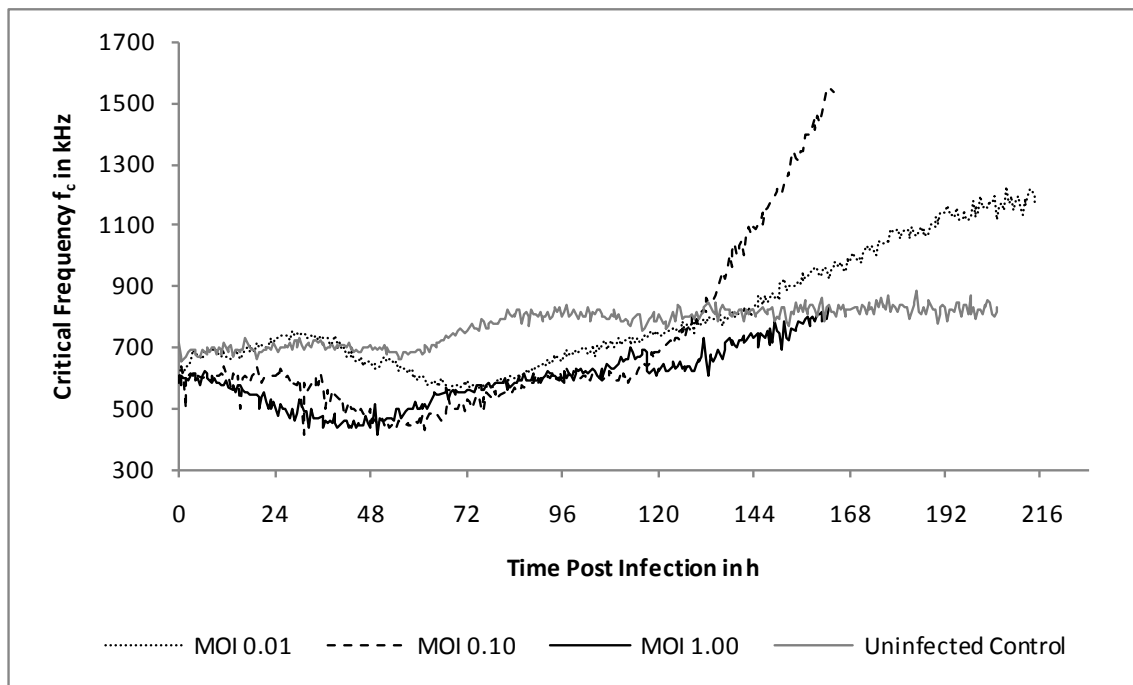


Figure 4.39. Characteristic frequency f_c post infection at the three different MOI. f_c generally decreased slightly from approximately 600 kHz during the first 48 to 72 h post infection and was followed by another subsequent increase once a local minimum had been reached. The time of the minimum was delayed with decreasing MOI and different absolute minimum values were reached. Some of the cultures showed another strong increase in f_c late in the process but the exact reason for this remains unknown.

In contrast to the uninfected cell growth in the precultures described earlier, the infected Sf-9 clone cell cultures all showed significant changes in the characteristic frequency f_c post

infection. The characteristic frequency f_c is, according to Equation 6, directly influenced by the cell radius r , the specific cell membrane capacitance C_m and the intracellular and medium conductivities σ_i and σ_e , respectively. The observed early decrease in f_c post infection generally occurred once the average viable cell diameter started to increase due to cell baculovirus infection induced swelling. This decrease occurred delayed for cultures infected at lower MOI because of the previously discussed overall slower infection progress and so viable cell diameter changes. The same was true for the observed minimum between approximately 48 and 72 h post infection. While the decrease in f_c due to an increase in the viable cell diameter is in accordance with the underlying theories, the minimum observed in the characteristic frequencies did not always occur at the same time as the peak observed in viable cell diameter. For example, for cultures infected at MOI 0.01 the minima in f_c occurred before the actual peak in viable cell diameter was observed, at 72 and 96 h post infection, respectively. Additionally the observed subsequent increase in f_c occurred for all MOI generally earlier than a respective decrease in average viable cell diameter was observed. Overall similar values and a similar profile for f_c during a synchronous infection at a much higher MOI of 10 of *Spodoptera frugiperda* Sf-9 cells was observed before, but deviations in f_c from the cell size profile in that study could also not be explained conclusively¹². It has to be mentioned again, that sampling in this work was only performed every 24 h and therefore may not be able to represent changes at the exact time they happened in the cultures. As stated above, other parameters affecting f_c are the specific cell membrane capacitance C_m and the intracellular and medium conductivities σ_i and σ_e respectively. As shown before C_m did not change significantly during the first 120 h post infection, and therefore presumably did not have a great influence on f_c during this time.

The suspension conductivity profiles for each MOI were relatively similar and are shown in Figure 4.40. Generally, immediately after infection and after a short stabilization phase due to the medium addition and subsequent temperature adjustments, the suspension conductivity started to decrease. At some point during the process, σ_s then reached a minimum with values ranging from 15.16 to 15.36 mS cm⁻¹. The time of occurrence of this minimum varied from approximately 84 h to 72 h post infection for MOI 0.01 to 1.00, respectively. From this point on σ_s started to increase again until the end of the specific process. Observed spikes in the profiles were generally due to slight temperature changes of the culture, which in turn were caused by

changes in the room temperature. In contrast to this, the suspension conductivity profile for the uninfected control cultured showed a constant decrease during the process while flattening out after approximately 150 h. The temporary decrease observed between 150 h and 180 h appears to be an artifact and could not be related to a culture medium temperature decrease within this time.

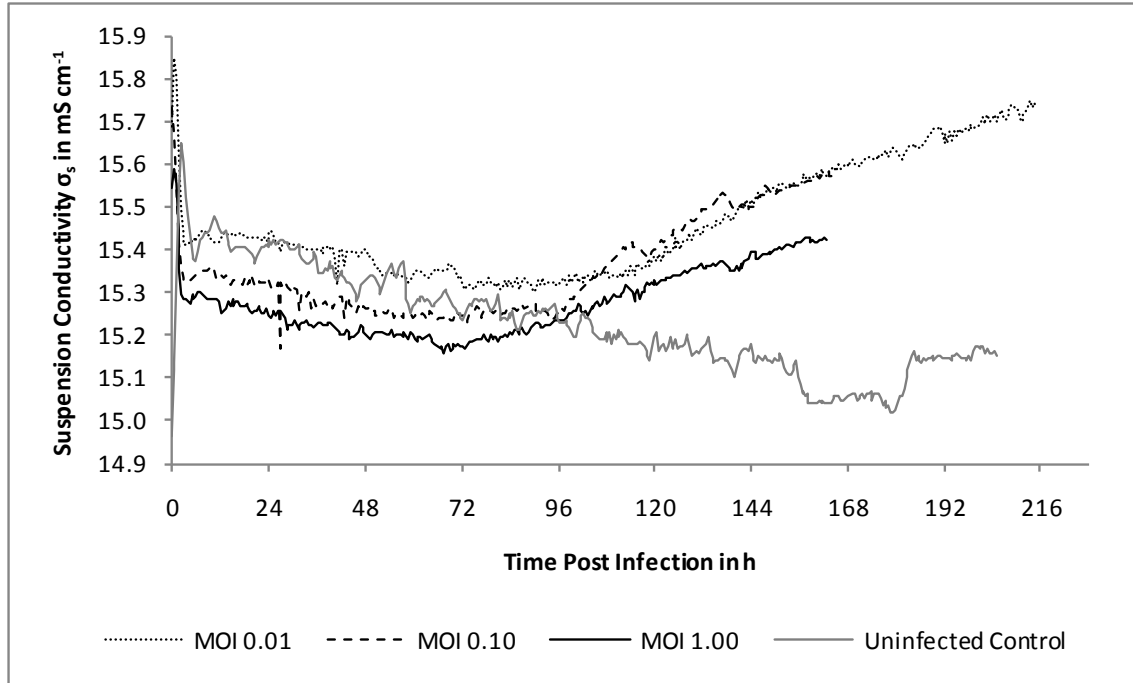


Figure 4.40. Suspension conductivity σ_s post infection at the three different MOI. Initial values measured for σ_s were approximately 15.4 mS cm^{-1} and generally decreased post infection until a minimum was reached at approximately 72 to 84 h post infection. This was followed by an increase in σ_s until the end of the process.

Most probable explanation for the observed suspension conductivities profiles are the increase, and later decrease, in viable biovolume. As cells divided and swell post infection, the fraction of volume they take up in each unit of the suspension, the viable biovolume, increased. Because the viable biovolume essentially hinders the conduction of charges throughout its fraction due to the non-conductive cell membrane, former conductive “material” was replaced by non-conductive “material” and the measured σ_s decreased. The opposite was true later in the process when σ_s increased again. The viable biovolume decreased significantly and caused a decrease in non-conductive material per unit volume of cell suspension. Therefore, σ_s increased

again. Additionally the take up and release of charged particles from the medium by the cells could have theoretically contributed to the observed changes. Calculated profiles for σ_e , using Equation 7, only showed minor variations and therefore this can be assumed to only have had minor effect on σ_s (data not shown). The same is true for the effect on the characteristic frequency f_c . But the latter can also be affected by the intracellular conductivity σ_i and while σ_i was not measured directly in this work, at this point it can be calculated using and Equation 6. Obtained profiles can be seen in Figure 4.41.

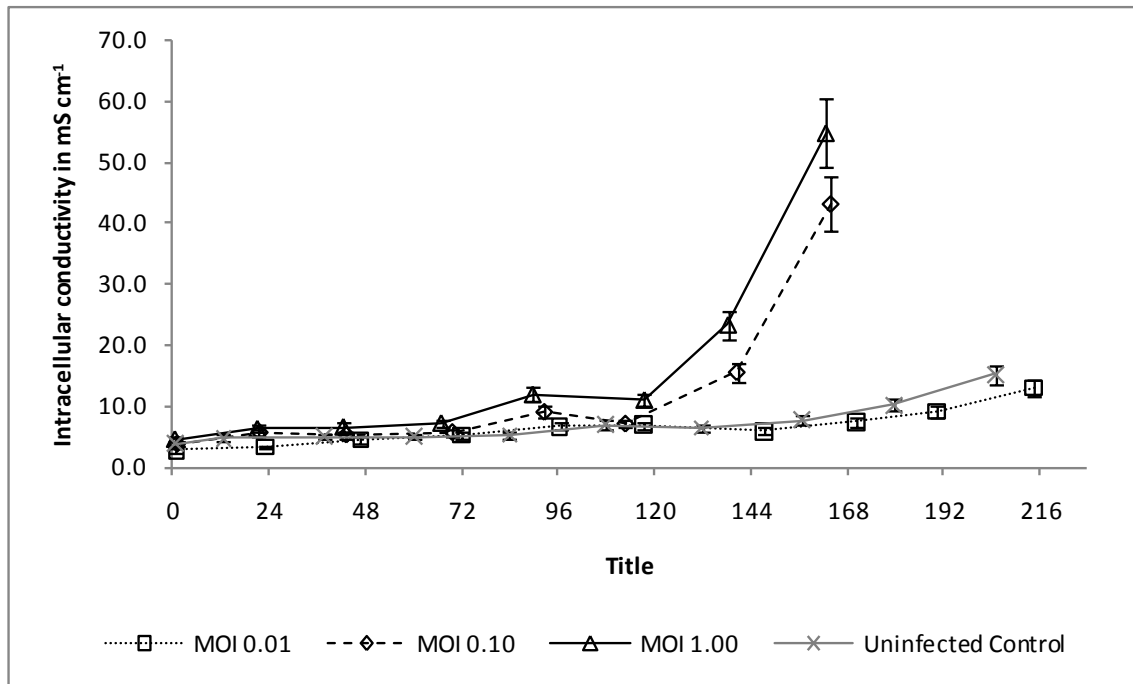


Figure 4.41. Intracellular conductivity σ_i post infection at the three different MOI. Initial values determined for σ_i ranged from approximately 3.0 to 5.0 mS cm^{-1} but no major changes were observed during the first 72 h post infection. Late in the process, some cultures showed strong increases in σ_i but it remains unclear if this is indeed a true representation of the reality.

Generally, the calculated σ_i values ranged from 2.79 to 5.44 mS cm^{-1} immediately post infection and seemed to slightly increase for most of the cultures over time. Approximately from 72 h post infection significant differences in the profiles could be observed with some cultures showing a rather strong further increase, while a few remained relatively constant before

eventually also strongly increasing very late in the process. The switch in the Vi-CELL XR settings after approximately 120 h (day 5) post infection may explain the observed unreasonable strong increases thereafter. σ_i is generally interpreted as the ability of the cell's interior to conduct electrical current and changes are presumably due to different ion concentrations within the cell^{73, 75}. Until recently studies often treat σ_i as independent on the physiological state^{73, 125, 132, 133} but it is well known that this value can indeed change in apoptotic and necrotic cells, when morphological changes are induced and when cell membrane conductance is increased, i.e. by treatment with antibiotics¹³⁴⁻¹³⁸. To the knowledge of the author, no literature values for σ_i in *Spodoptera frugiperda* cells have been published. In mammalian cell cultures σ_i usually falls somewhere in between 2 and 9 mS cm⁻¹ with some researchers suggesting an even narrower range of 3 to 5 mS cm⁻¹^{173, 75, 125, 139, 140}. Values calculated in this work fell in this range for the majority of the time but especially extreme values observed late in the processes seem to be rather unreasonable. They were caused by very high values obtained for the characteristic frequency f_c late in these processes but the reason for this behavior in f_c is not fully understood at this point. None of the investigated parameters affecting f_c , mainly the viable cell radius r , C_m , and σ_e , supported this kind of increase.

The Cole-Cole α showed slightly different profiles for infections at the three MOI, as shown in Figure 4.42. Immediately post infection α dropped slowly from slightly below 0.10 to about 0.08 for infection at all three MOI. After an minimum was reached between 24 and 36 h post infection α increased again to a peak of about 0.11 between 54 to 84 h post infection. This peak was generally reached the earlier the higher the MOI. Subsequently α decreased before increasing once again to another local peak. After this secondary peak was reached α continuously decreased until the end of the process at all three MOI. The shift in α around 120 h post infection is due to a technical issue and not cell culture related. The uninfected control culture showed a different profile for the Cole-Cole α . While starting at approximately the same value immediately post infection, α increased up to around 0.11 at about 50 h post infection and then continuously decreased until the end of the process to approximately 0.08, showing less of the observed changes than the infected cultures.

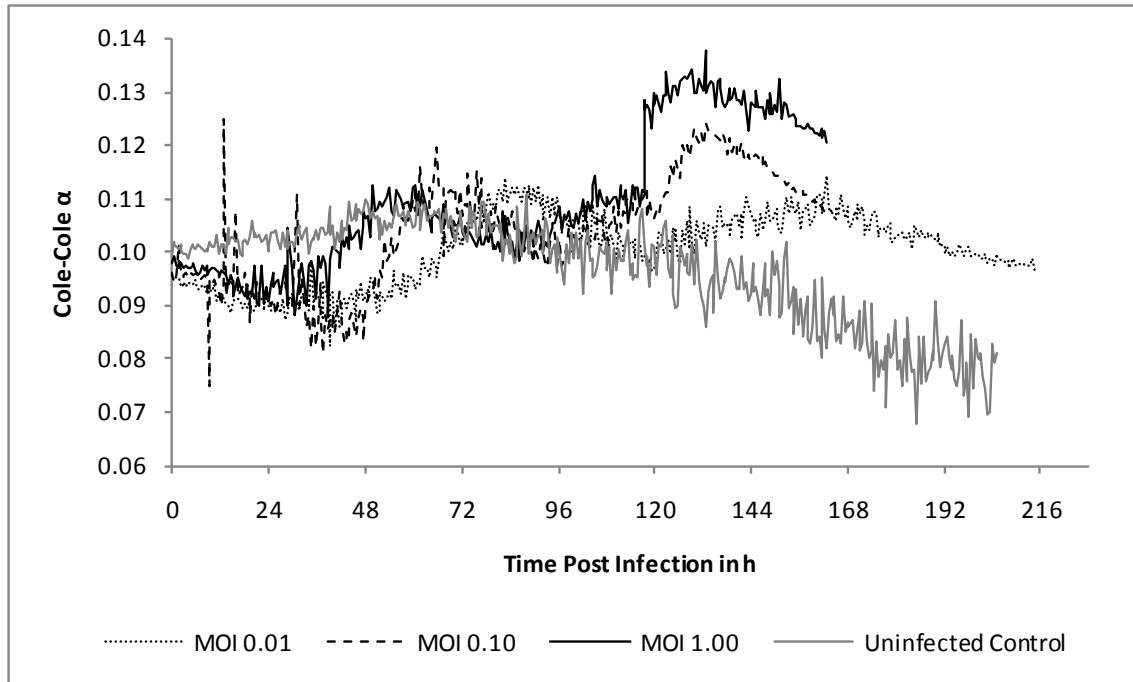


Figure 4.42. Cole-Cole α post infection at the three different MOI. α decreased immediately post infection from slightly below 0.10 to approximately 0.08 during the first 24 to 36 h post infection for all MOI. Afterwards a strong increase up to approximately 0.11 between 54 to 84 h post infection was detected which generally occurred the earlier the higher the MOI. Afterwards α first decreased again, which was followed by another increase up to a local peak. Thereafter α eventually continuously decreased until the end of the process.

The parameter Cole-Cole α is an empirical value describing the decrease in capacitance measured with increasing frequency. The parameter α can assume values between 0 and 1 where 0 describes a very steep and 1 an infinitely shallow fall in capacitance. In cell culture applications α is generally interpreted as a measurement of viable cell size distribution and shape believed to increase when the cell size distribution widens^{12, 80} with values observed typically between 0.1 and 0.2¹²⁸. But the physical origin of this parameter is continuously under discussion and may indeed also be influenced by several other effects including morphology of extracellular spaces, the mobility of membranous proteins and the fractal nature of dielectric relaxation¹²⁸⁻¹³¹. Vi-CELL XR data for the viable cell size distribution did not support the observed changes in α . The measurements performed may have been too insensitive but also other factors, as discussed

above, could have caused the changes in Cole-Cole α . Overall the Cole-Cole α was judged to be inconclusive in this work.

In addition to the three β -dispersion parameters and the suspension conductivity, the Biomass signal, based on the dual frequency method, was recorded by the instrument. The Biomass signal was obtained by measuring the capacitance (permittivity) at a frequency close to the specific f_c of the cell culture system utilized (here 1000 kHz), the so called working frequency, and subtracting the capacitance (permittivity) obtained at a very high frequency (here 10000 kHz). The latter adjusts the measurement for changes in the medium background capacitance (permittivity) over time¹⁰⁸. Figure 4.43 shows the Biomass signal evolution post infection.

The Biomass signal, thought to be a cell size independent measure of the viable biovolume, generally increased immediately post infection for all MOI but peak values reached were different and shifted in time. More specifically, initial Biomass values observed were around 2.00 pF cm⁻¹ and peak values were generally higher but reached later the lower the MOI. For example, in experiments utilizing a MOI of 1.00 the maximum value of about 8.00 pF cm⁻¹ was reached around 72 h post infection, while this was the case at 80 and 100 h post infection for MOI 0.10 and 0.01, respectively. In these two cases, the maximum values observed were about 10.00 and 12.00 pF cm⁻¹. Interestingly the shape of the increase for the three different MOI was also quite different, indicating different evolutions in the viable biovolume. The signal for MOI 0.01 showed a rapid increase directly from the beginning but at around 50 h post infection a distinct plateau could be observed. The signal for MOI 0.10 also showed a plateau at around the same time but it was generally less prominent. In the case of MOI 1.00, there was no real plateau phase detectable and the signal increased at a more or less constant rate to the specific peak value. Once the Biomass signal had reached its specific peak value it decreased continuously until the end of the process. While the signals for MOI 0.01 and 0.10 first showed a comparably fast decrease before slowing down, the decrease for MOI 1.00 was relatively constant until the end of the process. The Biomass signal recorded for the uninfected control culture resembled the MOI 0.01 profile somewhat, especially during the first 96 h of the process. In addition, the same distinct plateau in the signal could be observed around 48 h into the process. From 96 h into the

process the signal for the uninfected control culture continued to increase without ever peaking during the process but also showed a secondary plateau around 120 h into the process. After about 205 h a Biomass value of approximately 16.00 pF cm^{-1} was reached.

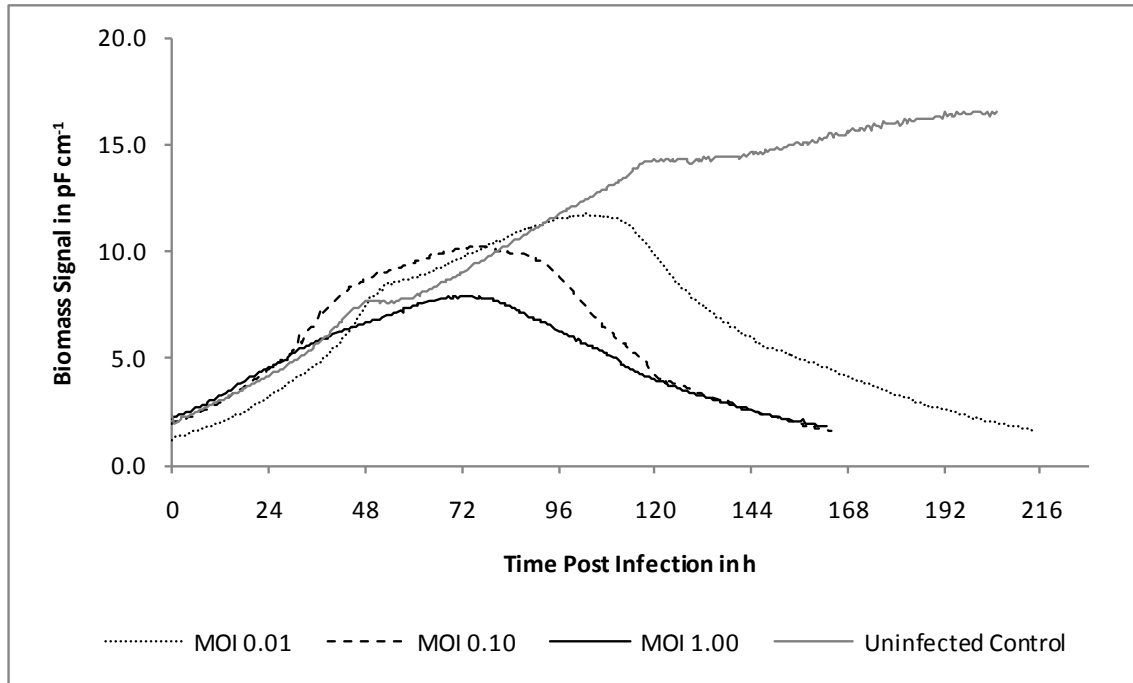


Figure 4.43. Biomass signal post infection at the three different MOI. The Biomass signal increased immediately post infection from approximately 2.5 pF cm^{-1} up to a maximum value of approximately 12.0 pF cm^{-1} . Generally, decreasing maximum Biomass signals were observed for increasing MOI and the peak occurred earlier. Distinct plateau phases could be observed in especially the MOI 0.01 culture. After the respective peak, the Biomass signal decreased continuously until the end of the process.

The Biomass signal is often used for viable biovolume estimation because due to the nature of its measurement, it is believed to be independent, or at least less influenced, by changes in cell size. As with $\Delta\epsilon$, the general increase in the Biomass signal starting immediately post infection can be attributed to an increase in the volume fraction of viable cells (viable biovolume). Interestingly the Biomass signal also showed some plateaus during the initial increase up the respective peaks. These plateaus were particularly visible for experiments at MOI 0.01 but still detectable at MOI 0.10. In both cases the plateau phase started at around 48 h post

infection. In the case of MOI 1.00, no plateau was observed. Since no samples were taken during, immediately before, and after these plateaus, no specific explanation for their occurrence can be given at this point. Assuming the Biomass signal to be a true representation of the viable biovolume, possible explanations include a temporarily leveling-off of the viable cell count, viable cell diameter or both. The peak in the Biomass signal generally occurred approximately at the same time as the peak in the calculated viable biovolume. Some deviations from this could be observed in the case of MOI 0.01 where the peak in the Biomass signal occurred delayed, up to approximately 24 h, compared to the viable biovolume. But again, due to the sampling frequency data at the actual sampling point may not represent the real maxima actually achieved during the process and therefore slightly differ.

The dielectric spectroscopy measurements obtained by the FOGALE iBiomass 465 instrument were used to generate correlations to estimate cell culture related variables on-line and in real-time. Based on the theory, the capacitance and permittivity measured correlate linearly to the volume fraction of the viable cells (viable biovolume) in the cell culture suspension. To verify this theory the viable cell densities and mean viable cell diameters obtained for every sample during cell growth were used to calculate the viable biovolume, assuming a spherical cell shape. This value was then paired with its raw capacitance values at each of the 16 frequencies adjusted for the medium background capacitance by subtracting the value measured at 10000 kHz. In addition, the polarization adjusted Biomass and $\Delta\epsilon$ signals were also used. The Pearson correlation coefficient r was then calculated for each combination to obtain a measure of linearity of the correlation. Therefore the data of all nine processes, a total of 78 data points, was used in this analysis. Results are given in Table 4.6.

Table 4.6. Pearson correlation coefficients for viable biovolume and dielectric spectroscopy signals in infected cultures.

Signal	Pearson r
Delta ϵ	0.902
Biomass	0.904
C(300 kHz)	0.853
C(373 kHz)	0.878
C(465 kHz)	0.894
C(578 kHz)	0.903
C(720 kHz)	0.907
C(897 kHz)	0.905
C(1117 kHz)	0.900
C(1391 kHz)	0.890
C(1732 kHz)	0.879
C(2156 kHz)	0.867
C(2684 kHz)	0.834
C(3342 kHz)	0.804
C(4161 kHz)	0.780
C(5181 kHz)	0.751
C(6451 kHz)	0.705
C(8031 kHz)	0.625

Generally, signals at frequencies below 3000 kHz provided reasonable good correlations. Determined Pearson correlation coefficients for the $\Delta\epsilon$ and Biomass signals were 0.902 and 0.904, respectively and the obtained correlations are shown in Figure 4.44 and Figure 4.45. The best linear correlation based on the raw capacitance measurements at single frequencies was obtained at 720 kHz with 0.907. As expected with the observed viable cell size changes, the correlation based on the cell size independent Biomass signal provided better slightly better results than the correlation with the $\Delta\epsilon$ signal. Nevertheless, the latter is still quite acceptable. The correlations obtained for these infected cultures are of a slightly lower quality than for the uninfected cells in the precultures (Pearson correlation coefficient of 0.957 and 0.938). In addition to the added variability due to viable cell size changes, the cells presumably underwent changes in their dielectric properties due to infection, virus, and recombinant protein production, and cell lysis later in the process. Additionally cells that might be determined as “dead” with off-line measurements like the trypan blue staining in the Vi-CELL RX, may still contribute to the dielectric signals measurements. Such a behavior was described earlier in the literature and also seems to be apparent here ^{7, 46}.

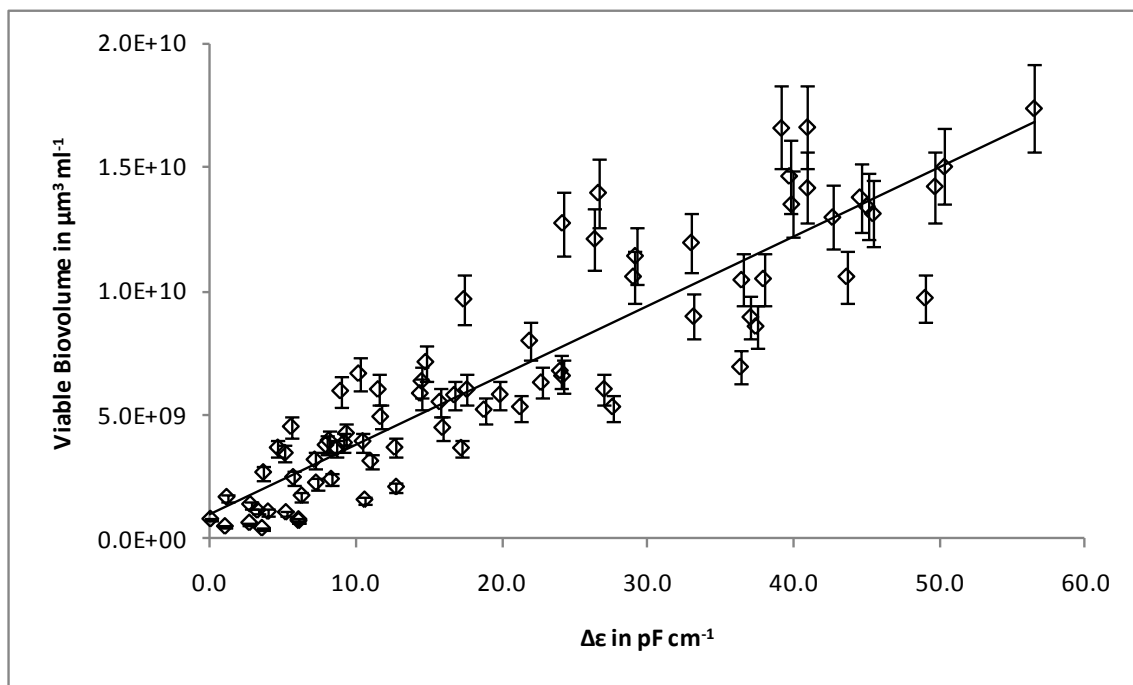


Figure 4.44. Linear correlation viable biovolume vs. $\Delta\epsilon$ post infection.

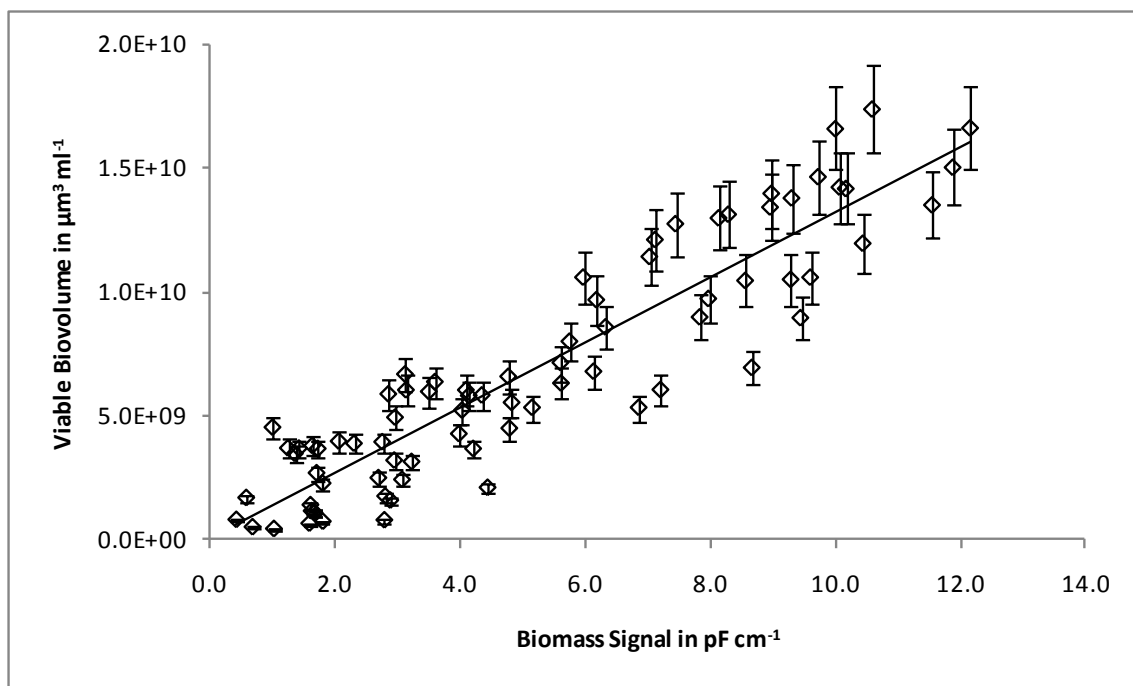


Figure 4.45. Linear correlation viable biovolume vs. Biomass signal post infection.

The two linear correlations obtained can be described by the equations

$$\mathbf{Viable\ biovolume}(\Delta\epsilon) = \left(3.13 \times 10^8 \times \Delta\epsilon \frac{\mathbf{cm}}{\mathbf{pF}} \right) \frac{\mu\mathbf{m}^3}{\mathbf{ml}} \quad \mathbf{Equation\ 25}$$

and

$$\mathbf{Viable\ biovolume}(Biomass) = \left(1.32 \times 10^9 \times Biomass \frac{\mathbf{cm}}{\mathbf{pF}} \right) \frac{\mu\mathbf{m}^3}{\mathbf{ml}} \quad \mathbf{Equation\ 26}$$

Correlations with the viable cell density were of much lower quality in general. Correlations obtained for the $\Delta\epsilon$ and Biomass signals had Pearson correlation coefficients of 0.684 and 0.714, respectively, while the best correlation at a single frequency was again obtained at 720 kHz with a Pearson correlation coefficient of 0.707. Therefore, a use of these for the estimation of viable cell density post infection is not suggested.

Overall, the results obtained are of significantly lower quality than for the uninfected cells in the precultures. For the viable biovolume the observed changes in viable cell diameter significantly reduced the quality of the linear correlation with $\Delta\epsilon$, as was expected based on the theoretic dielectric cell model. For the correlation with the Biomass signal a lesser reduction in quality was found, which may still be acceptable. Therefore, the claim of better representation of the “true” volume fraction of viable cells P (viable biovolume) seems to be justified. However, while it had been possible to estimate viable cell densities directly with a linear relationship during the uninfected cell growth, this is not possible anymore with a sufficient accuracy post infection. Reasons for this are the change in viable cell diameter post infection and presumably changes in the dielectric properties of the cells. Samples late in the process may also suffer from less accurate estimations of viable cell density and mean viable cell diameter. Overall, the quality of the correlations is not high enough for the reliable use in routine vaccine production. Therefore, a multivariate modeling approach was taken to account for the changes in multiple variables. While such a model will be more complicated in terms of the equation(s) obtained, it

should provide estimations for more variables at the same time, e.g. also viable cell diameter, and provide these with a lower error. More details on this approach are given in Chapter 4.2.9.

4.2.7 Detection of Culture Events in Real-Time by Dielectric Spectroscopy

The infection of *Spodoptera frugiperda* insect cell cultures at MOIs below 1.00 generally means that the process is strongly dependent on subsequent (secondary) infection by newly produced virus particles and shows significant differences in regards to kinetics and yields achieved post infection. This was confirmed by the experiments performed in this work. While the infection at MOIs between 0.01 and 1.00 also led to significantly different profiles in the dielectric spectroscopy signals depending on the MOI, specific observations in the dielectric spectroscopy signals could be related to important events in the cultures throughout the whole range of investigated MOI making them a potentially very useful tool for the routine monitoring of industrial scale bioprocesses utilizing the baculovirus expression vector system.

The dielectric increment $\Delta\epsilon$ increased immediately post infection, presumably due to the increase in viable biovolume through an increase of viable cell density and in the individual cell volume. At some point post infection $\Delta\epsilon$ peaked and decreased again subsequently. The time of the peak ranged from approximately 48 to 74 h post infection and occurred the earlier the higher the MOI. Off-line analyses showed, that at approximately the same time the culture was “completely” infected with fractions of infected cells around 95 %, signaling the end of the infection process in the cultures. This is shown in Figure 4.46. Slight deviations could be observed for cultures infected at MOI 0.10, where the peak in $\Delta\epsilon$ occurred slightly later than the detected “complete” infection, but the difference was only a few hours. Additionally, because samples for off-line analyses were only taken approximately every 24 h, the precise time of complete infection in the cultures may not coincide with the time of sampling.

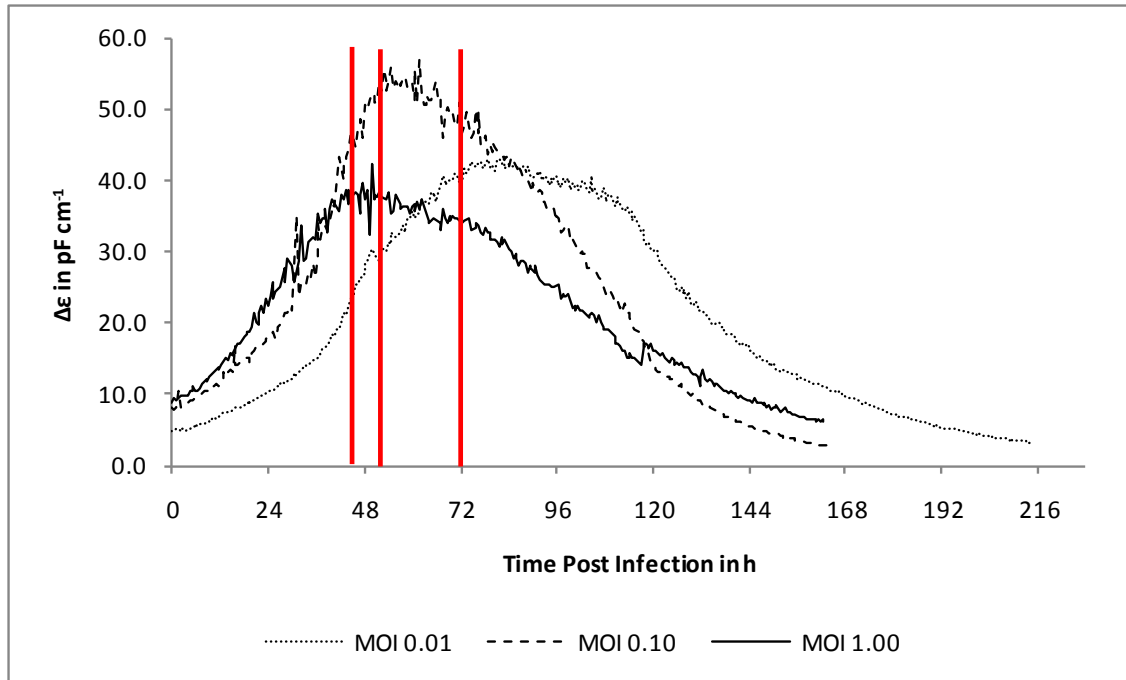


Figure 4.46. Comparison of $\Delta\epsilon$ with the time of complete infection in the culture at the three different MOI. Complete infection was detected around the peak in $\Delta\epsilon$ and is indicated by the red vertical lines.

Another dielectric spectroscopy signal, the Biomass signal, could also be used to detect another specific event in the cultures. Like $\Delta\epsilon$, the Biomass signal increased immediately post infection, but peaks were reached slightly later at approximately 72 to 100 h post infection, depending on the MOI. The Biomass signal generally tracked the viable biovolume post infection and peaked at the same time as this with some minor deviations observed and described earlier. In addition, the peak in the Biomass signal also coincided with the recombinant baculovirus concentration reaching its maximum value in the specific process before leveling off thereafter. This comparison is shown in Figure 4.47. Again, slight deviations caused by the sampling frequency need to be considered.

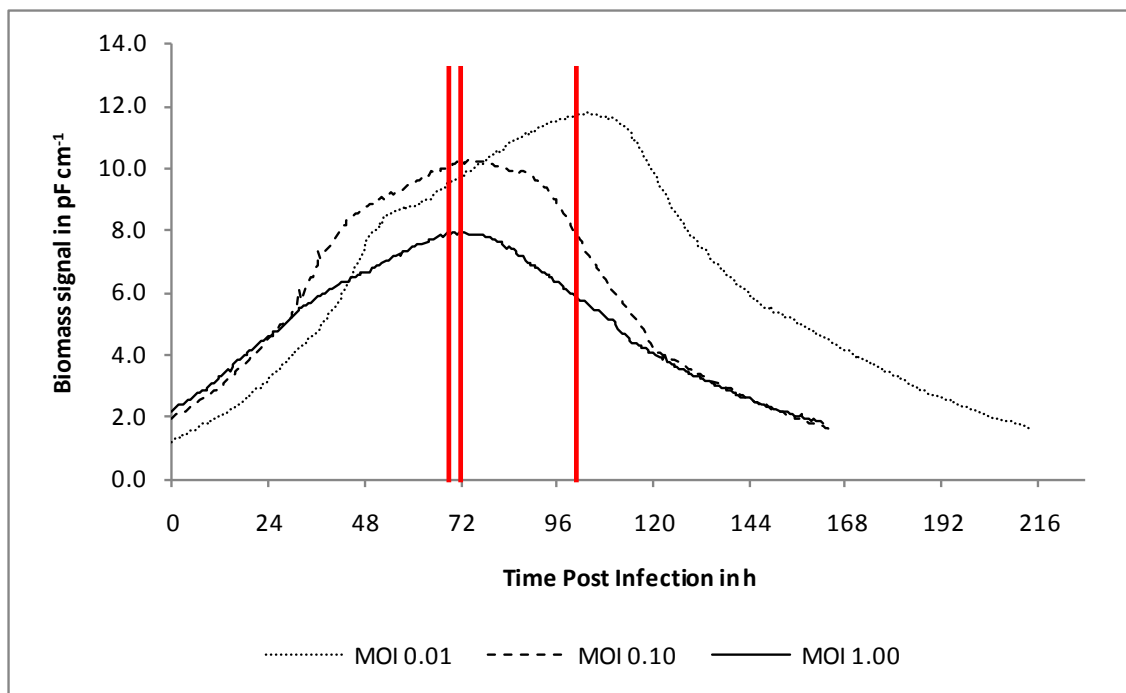


Figure 4.47. Comparison of Biomass Signal with the time of peak recombinant baculovirus concentration at the three MOI. The peak in recombinant baculovirus concentration was achieved at approximately the occurrence of the peak in the Biomass signal and is indicated by the red vertical lines.

The agreement in these two parameters can be explained with the changes and processes in a *Spodoptera frugiperda* insect cell post infection. Once the cell is infected, it starts replicating the recombinant baculovirus and production thereof peaks around 17 to 20 h post infection. The cell also starts swelling. Therefore, the peak in baculovirus concentration can reasonable be expected approximately 20 h after the culture was completely infected. Additionally at this time approximately the peak in viable biovolume should be reached due to the induced cell swelling before significant amounts of the cells have died due to cell lysis.

Especially the connection of the Biomass signal and the baculovirus concentration could be very useful in the routine monitoring and operation of industrial scale baculovirus expression vector system processes. Working seed stocks of the recombinant baculovirus have to be produced regularly for subsequent recombinant protein production. Production of high quality virus seed with a minimum number of defective virus particles is usually performed at very low

MOI below 0.10. As already mentioned earlier, the process becomes prone to fluctuations at these low MOI and therefore optimal harvest time to achieve maximum baculovirus titer may shift considerably. With the use of the dielectric spectroscopy, the time of harvest could be detected in-line and in real-time without the need of sampling the reactor or relying on pre-established fixed harvest time criteria, which may result in premature harvest with sub-optimum baculovirus concentration. On the other hand, a harvest too late may also affect baculovirus quality in terms of infectivity and recombinant protein expression capability and could be avoided when using the dielectric spectroscopy as a real-time monitoring device. Obviously, and maybe even more importantly, the same approach could also be applied in bioprocesses where the baculovirus itself is the desired product and not some recombinant protein. It should be noted that validity of these statements should be checked for each specific application and (downstream) procedure. In cases where the produced baculovirus seed is not directly harvested and frozen without further processing to remove any cells but rather filtered or centrifuged, the extracellular only baculovirus concentration may peak slightly delayed. Nevertheless, even in such a case a criterion based on dielectric spectroscopy could be developed.

An additional observation made during the low MOI experiments was the occurrence of a plateau region in the Biomass signal, which was especially prominent in the cases of an infection at MOI 0.01 and 0.10. While the exact cause for this plateau could not be identified due to the limited sampling frequency for off-line analysis, it occurred at approximately the same time as the L-glutamine depletion in the cultures. Since the Biomass signal is supposedly, and confirmed by experimental data in this work, a measurement of the volume fraction of viable cells (viable biovolume) it seems appropriate to say that the increase in biovolume leveled off during the time of the observed plateau phase. The fact that the plateau was nearly invisible in MOI 1.00 cultures may be explained by the fact that the depletion in L-glutamine occurred later in these cultures when the Biomass signal already had reached its peak and was starting to decrease again, therefore being somehow being overlaid. Interestingly such a plateau could also be observed in the uninfected control culture indicating it was not necessarily limited to infected cultures and the accompanying changes in the cell's physiological and dielectric properties. Even in this case the plateau coincided with the depletion of L-glutamine in the medium. These observations triggered another subset of feeding experiments, which are described in Chapter 4.3.

4.2.8 Recombinant PCV2 ORF2 Protein Yield Prediction

It was shown earlier, that the recombinant PCV2 ORF2 protein harvest concentration was prone to significant variations, especially at the lowest MOI. These variations were presumably due to the less reproducible process at the lower MOI but daily samples and accompanying off-line analyses were not able to explain the observed differences in recombinant PCV2 ORF2 protein production. The dielectric spectroscopy measurements on the other hand were performed very frequently (every 30 minutes) and potentially also give more insight into the cell's physiological state. It was proposed that this information might lead to a better understanding of the process state, and while it may not always be completely clear if and how the cell's dielectric properties changed during the early phases of the process, the obtained dielectric spectroscopy signals still represent the cell cultures state at the time of measurement. It was suggested that this could be used to predict the recombinant PCV2 ORF2 protein harvest concentration early in the process, since the late stage protein expression phase is generally dependent on the early infection phase in the cell culture and deviations in the latter will carry on into the former.

While due to the approximately 24 h sampling interval no samples were taken exactly at the time of the observed peak in the Biomass signal, it was found that the maximum Biomass signal obtained at the actual sampling points (which generally occurred right before the peak in this signal) correlated with the obtained recombinant PCV2 ORF2 protein yield. This was usually approximately the point of maximum viable biovolume in the respective process and occurred approximately 24 h after the infection of the culture was completed. This also meant that the peak in budded baculovirus production occurred at this time and that the expression of recombinant PCV2 ORF2 protein had just started, usually 72 to 96 h (day 3 to 4) post infection. Additionally, only a minor fraction of the cells was determined as dead by the Vi-CELL XR trypan blue staining at this time. Assuming each unit of viable biovolume or viable cell contributes the same mean amount to both, the Biomass signal at the time of sampling and the overall recombinant PCV2 ORF2 protein yield, it should be possible to establish a linear correlation between these two parameters. The obtained correlations are shown in Figure 4.48 and Figure 4.49.

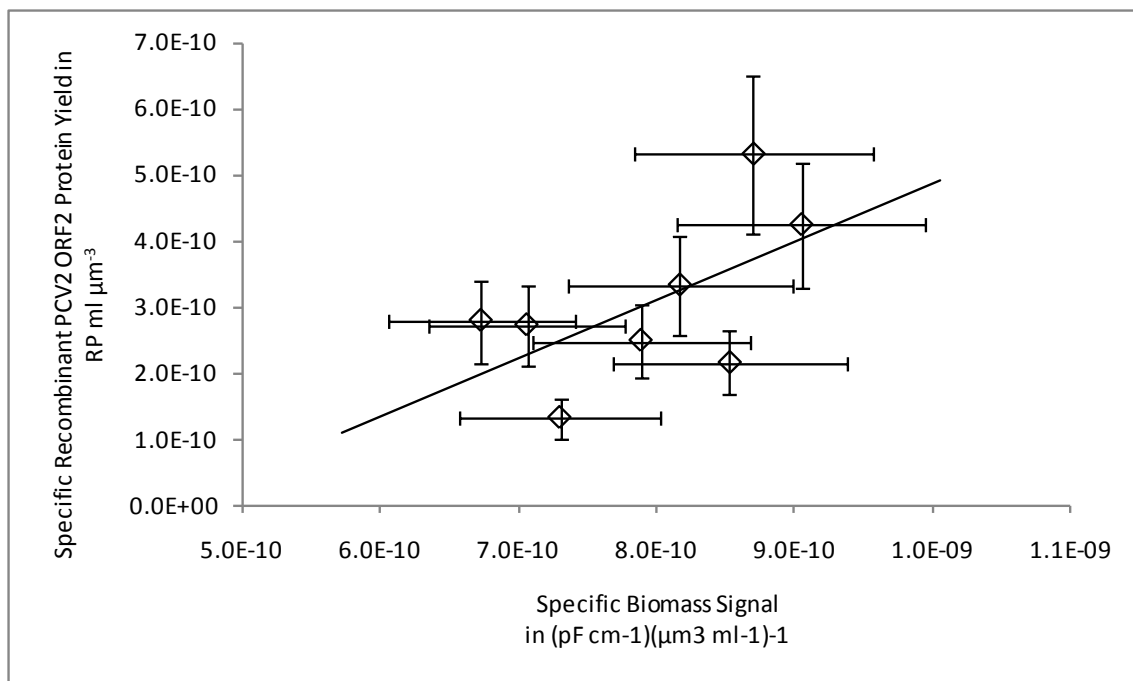


Figure 4.48. Correlation specific recombinant PCV2 ORF2 yield vs. specific Biomass signal at the time of signal peak based on viable biovolume.

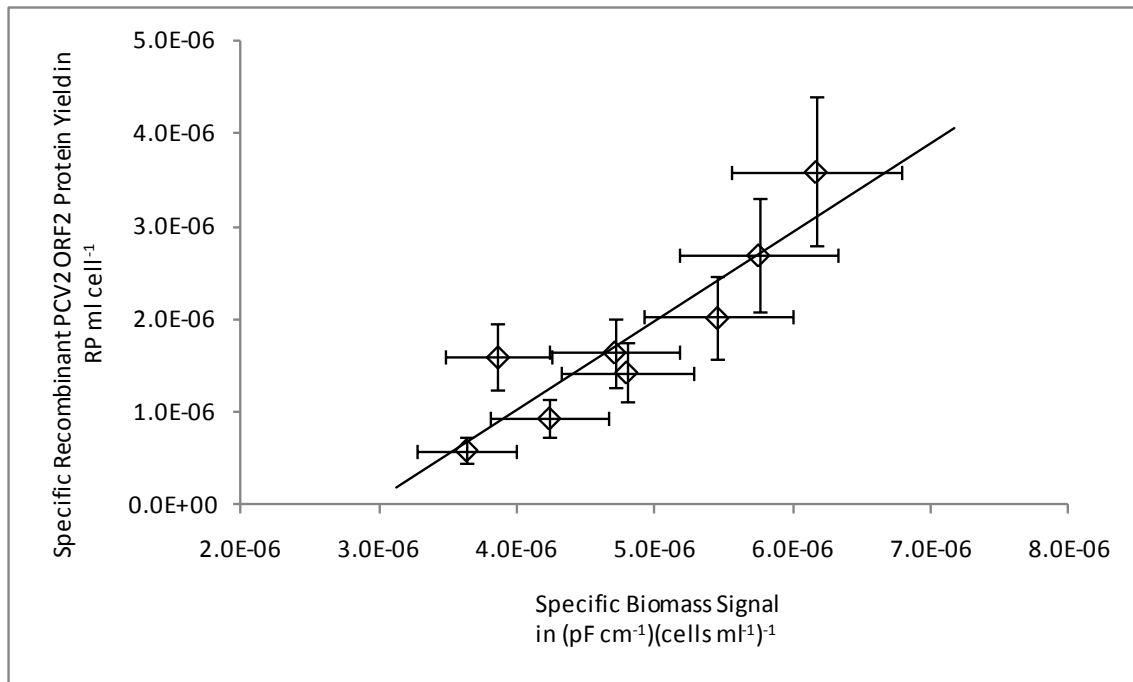


Figure 4.49. Correlation specific recombinant PCV2 ORF2 yield vs. specific Biomass signal at the time of signal peak based on viable cell density.

The obtained correlations show, that a higher specific PCV2 ORF2 protein productivity usually was indicated by a higher specific Biomass signal. Interestingly the correlation based on the viable cell count is much better than the one based on the viable biovolume and can be described by Equation 27. Knowing the cell concentration at the time of the Biomass signal peak, either by sampling and off-line analyses or estimation through the DS data, would then allow a prediction of the final harvest PCV2 ORF2 protein concentration.

Specific Recombinant PCV2 ORF2 Protein Yield

Equation 27

$$= \left(0.9634 \times \text{Specific Biomass Signal per Viable Cell} \frac{\frac{\text{cells}}{\text{ml}}}{\frac{\text{pF}}{\text{cm}}} - 2.83 \right) \times 10^{-6} \frac{\text{RP ml}}{\text{cell}}$$

The viable biovolume based correlation is of a lower quality and may be explained with the assumption, that the calculated parameter viable biovolume is prone to a larger error than the viable cell density alone. This may have led to the less accurate correlation. Nevertheless, since the Biomass signal overall reflects the viable biovolume, and a higher specific Biomass signal per cell therefore means a larger mean volume of this cell, the obtained correlations basically indicate, that a larger cell was equal to a higher specific PCV2 ORF2 protein production. A similar behavior was observed before for the production of other recombinant proteins in insect cells and confirms the observations made in this work^{142, 160}. Interestingly the correlation obtained was valid over the whole range of utilized MOI from 0.01 to 1.00 and was even able to predict the observed variations in the specific yield at MOI 0.01. It is expected that the correlation would become better if samples were taken at the actual peak in the Biomass signal. The obtained correlations could be very useful in the routine industrial scale recombinant protein production utilizing the baculovirus expression vector system. Obtaining a reliable prediction for the yield early in the process would allow early judgment about the success of a specific production run and may allow decisions and planning for the subsequent downstream processing procedures, including any concentration or dilution steps, before the specific process is even finished. With current technology, the first measurement of the recombinant PCV2 ORF2 protein concentration is not obtained until days after the end of the process.

4.2.9 Infection Phase Modeling with Dielectric Spectroscopy Data

As described earlier, the infection of insect cell cultures at low MOIs in the range from 0.01 to 1.00 generally means that the infection is non-synchronous and therefore the process is strongly dependent on subsequent (secondary) infections by newly produced virus particles. This led to significant variations in various cell parameters kinetics and even recombinant baculovirus and protein yields between, but also sometimes within, each MOI. The dielectric spectroscopy performed with the FOGALE iBiomass 465 instrument allowed to follow the process during the infection phase in terms several cell culture parameters by utilizing a multivariate modeling approach. A multivariate approach was chosen because the two other types of models generally proposed, linear and Cole-Cole, were not suitable for this application. The first is only valid as long as the viable cell size does not change, which was clearly the case in these cultures post infection with the recombinant PCV2 ORF2 baculovirus. The Cole-Cole model can only be used to calculate viable cell density and viable cell size when one can assume a constant specific cell membrane capacitance C_m and intracellular conductivity σ_i during the process. It has been shown that this assumption is not valid in a variety of situations, one of them virus infection and release^{12, 73, 139}.

The multivariate models developed were based on partial least squares (PLS) regression and built using the software JMP 8 (SAS Institute Inc). While PLS is commonly used to analyze spectroscopic data in a variety of applications⁸⁸, several studies used PLS regression models specifically for the analysis of dielectric spectroscopy data in cell culture processes involving mammalian or yeast cell cultures^{77, 88, 161} but no application in insect cell cultures has been reported. This technique builds a model based on linear combinations to find the fundamental relations between the independent variables and responses. In this case, the capacitance spectra at 16 frequencies (corrected by subtracting the background capacitance at 10000 kHz) as provided by the FOGALE iBiomass 465 instrument were the independent variables. All measurements obtained off-line were the dependent parameters, or so called responses. These included cell parameters like volume fraction of viable cells, viable cell density, or average cell size.

The peak in the Biomass signal served as the end point of the infection and therefore modeling phase, because at this time (day 3 or 4 post infection depending on the MOI) generally all cells were infected, the baculovirus concentration did not change significantly anymore thereafter and no significant amounts of the PCV2 ORF2 protein had been produced. Additionally off-line analyses performed with the Vi-CELL XR analyzer became less accurate after this point therefore compromising the model quality. Model calibration was performed using the data generated during the low MOI experiments. Dielectric spectroscopy data generated in experiment MOI 1.00 #3 and a few other data points were excluded due to apparent issues during those sampling points. Overall, the calibration set for the infection phase contained 35 data points. To avoid over-fitting a standard cross validation procedure was performed by the software. Cross validation is a standard procedure in PLS modeling and would also allow estimation of the predictive power of the model for new data even in the absence of an independent validation data set¹⁶². Details on the obtained models can be found in Appendix G - .

The performance of the calibration models was evaluated by calculating the root mean standard error of calibration RMSEC according to Equation 28:

$$RMSEC = \sqrt{\frac{\sum_{i=1}^n (\hat{y}_i - y_i)^2}{n}} \quad \text{Equation 28}$$

The RMSEC for each variable is given in Table 4.7. The given percent error of calibration (PEC) was calculated by dividing the RMSEC by the mean of the respective data set⁷⁷.
88, 128 .

Table 4.7. Performance of calibration models.

	P	Viable Cell Density in cells ml ⁻¹	Average Cell Diameter in μm	Medium Glutamine Concentration in mmol L ⁻¹	Baculovirus Produced in log ₁₀ TCID50 ml ⁻¹
RMSEC	0.0009	3.25E+05	0.70	0.47	0.45
PEC	9.5	15.8	3.5	21.0	22.0

Clearly, the developed PLS model fit well for the volume fraction of viable cells P (viable biovolume) and the average cell diameter with 9.5 and 3.5 % error, respectively. The error for the viable cell density was slightly higher with 15.8 %. The “indirectly” related variables medium L-glutamine concentration and baculovirus produced had model calibration errors of 21.0 and 22.0 %, respectively. It is not surprising that these values are higher, because they can only be related indirectly to the dielectric spectroscopy measurements through the measured cell’s dielectric properties.

While the PRESS statistic as calculated by the cross-validation principally gives an estimation of the predictive power for the developed PLS models, an additional validation experiment was performed to verify the models with an independent data set. Target viable cell density at the time of infection was 1.00×10^6 cells ml⁻¹ and the MOI 0.10. It has to be noted that the experiment performed was slightly different. Specifically a different lot of Sf-9 clone cells and recombinant PCV2 ORF2 baculovirus seed we used. Additionally the cells to be infected were not grown in a preculture as described before, but instead scaled up externally in spinner flasks to allow a so-called concurrent infection directly at 15 L working volume. Raw data collected is presented in Appendix H - .

Figure 4.50 to Figure 4.53 compare the experimental results of the validation experiment with the model-predicted values for several variables.

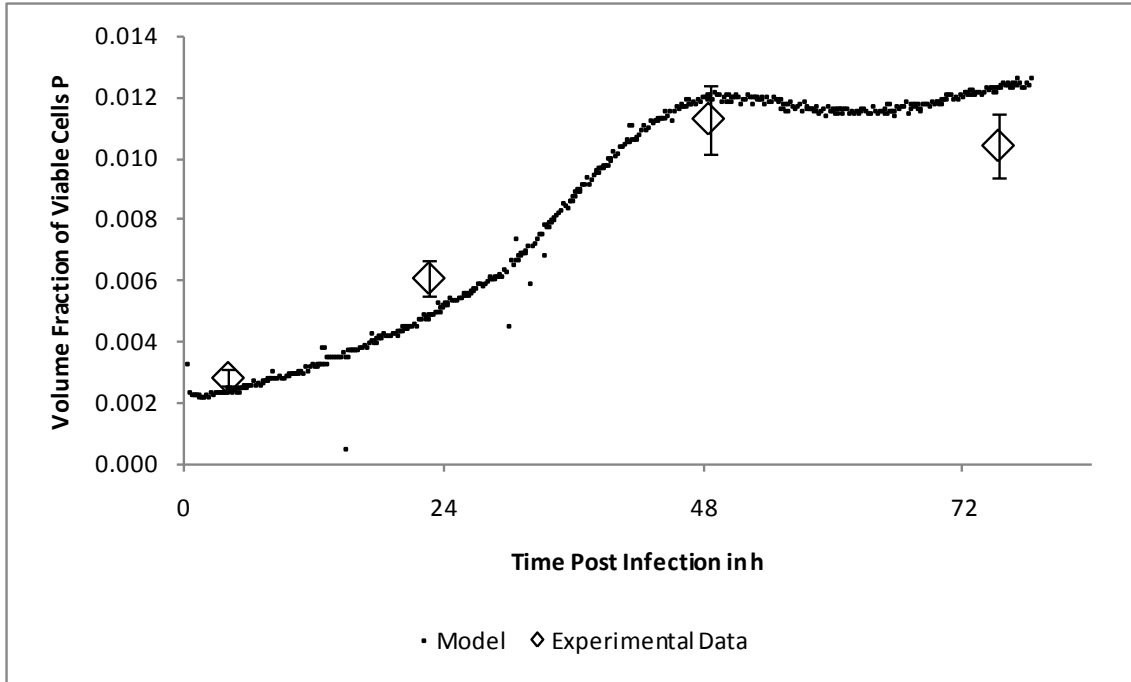


Figure 4.50. Model validation for volume fraction of viable cells P.

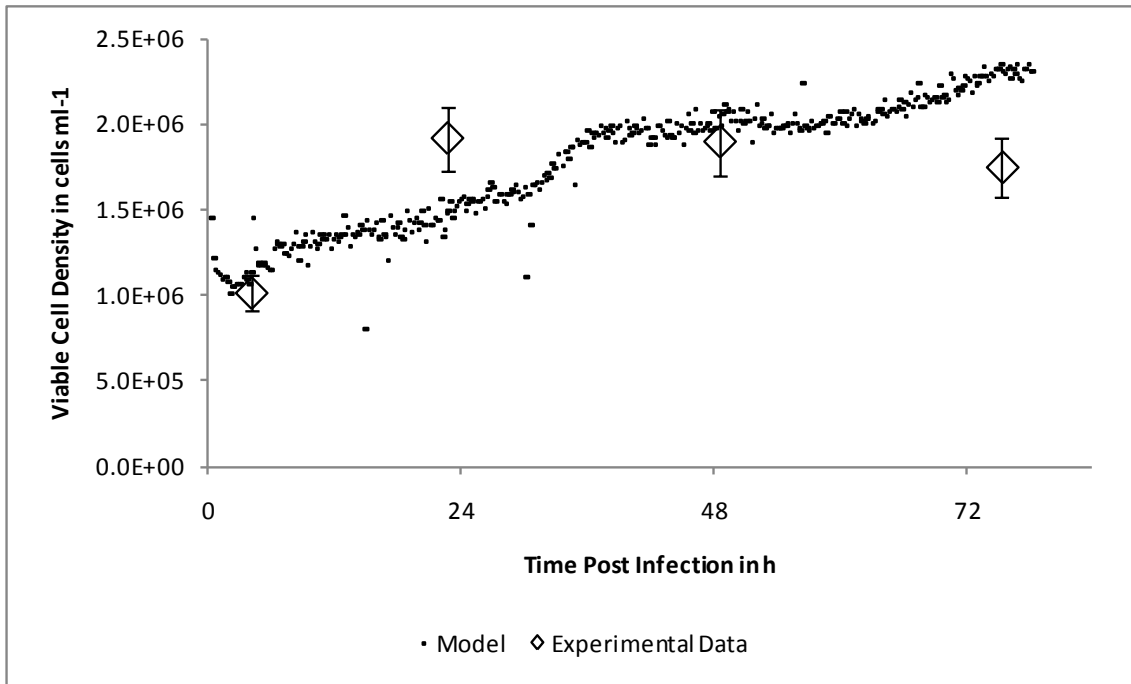


Figure 4.51. Model validation for viable cell density.

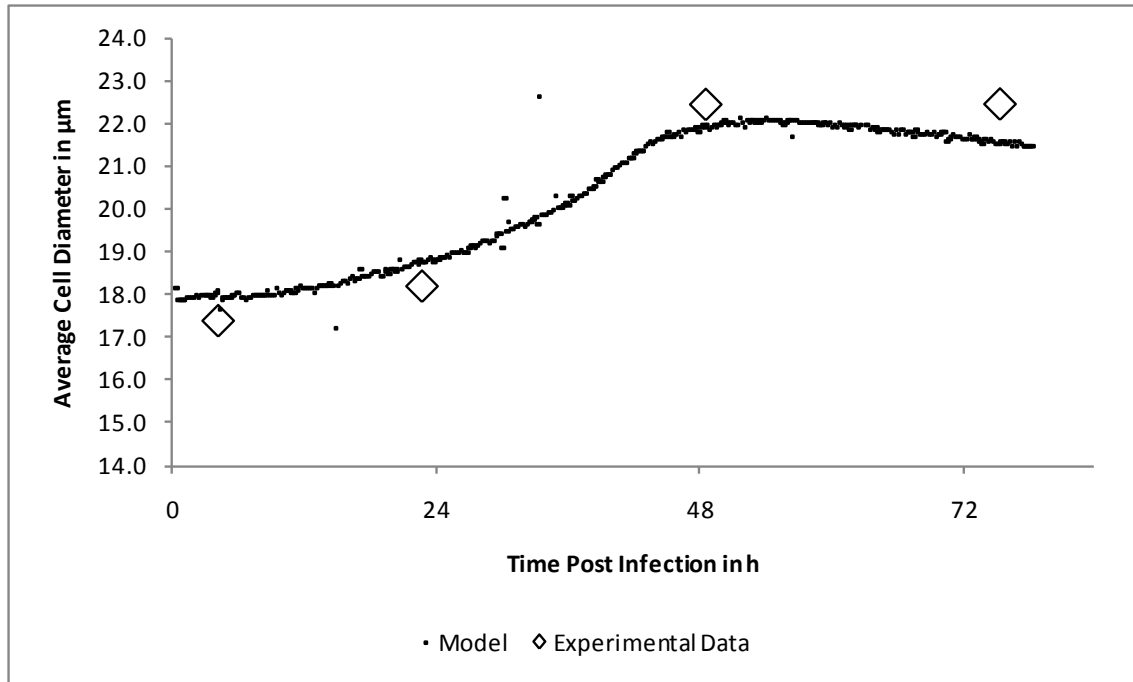


Figure 4.52. Model validation for average cell diameter.

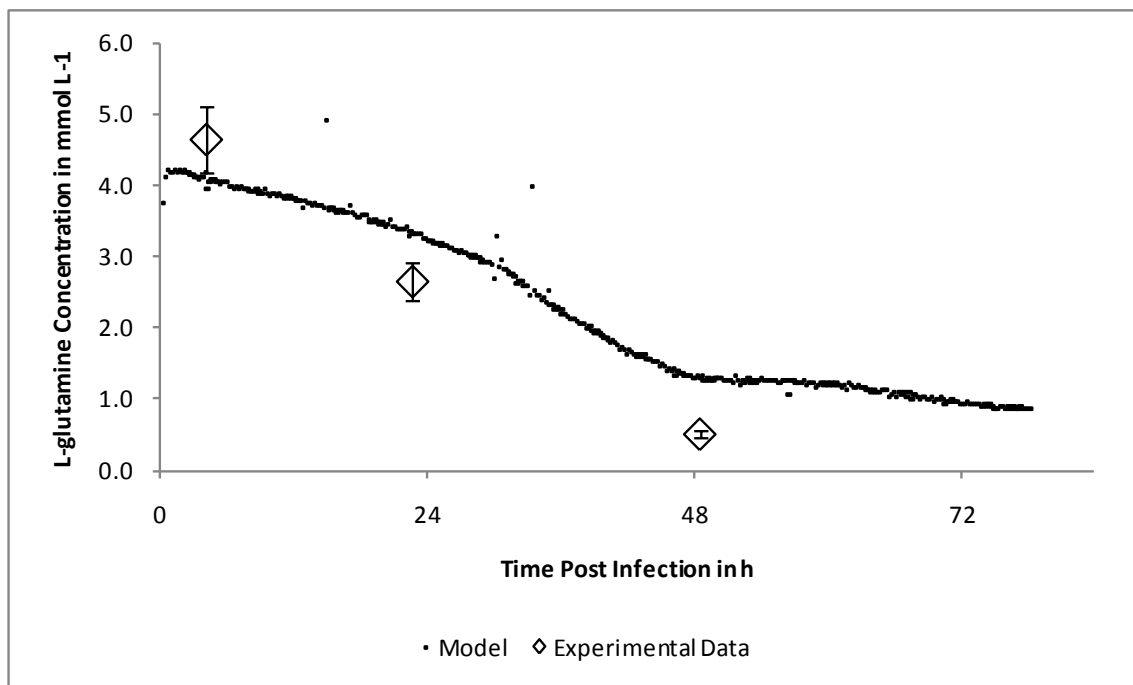


Figure 4.53. Model validation for medium glutamine concentration.

The predictive power of the models was evaluated by calculating the root mean standard error of prediction RMSEP according to Equation 29:

$$RMSEP = \sqrt{\frac{\sum_{i=1}^n (\hat{y}_i - y_i)^2}{n}} \quad \text{Equation 29}$$

The RMSEP for each variable is given in Table 4.8. The given percent error of prediction (PEP) was calculated by dividing the RMSEP by the mean of the respective data set^{77, 88, 128}.

Table 4.8. Model predictive power (RMSEP).

	P	Viable Cell Density in cells ml ⁻¹	Average Cell Diameter in μm	Medium Glutamine Concentration in mmol L ⁻¹
RMSEP	0.0013	4.16E+05	0.58	0.78
% Error	16.5	25.2	2.9	29.8

Again, the volume fraction of viable cells P and the average cell diameter were predicted best by the respective PLS model with errors of 16.5 and 2.9 %, respectively. These values are acceptable and allow reasonable estimation of these variables by the developed PLS models for independent data sets. The error for the viable cell density increased strongly compared to the calibration data set and was calculated to be 25.2 %. This is a rather higher error and reasonable estimation of the viable cell density with the developed PLS model may be not very accurate. The same is true for the prediction of the medium L-glutamine concentration with an error of 29.8 %. While these two models could still give good estimations of the general trend in the culture, the predicted absolute values should be treated with caution.

While an increase in the errors is not surprising if one uses independent data, one reason for the particular large changes for some of the variables may be the slightly different process in this case. While the target MOI was chosen to be 0.10 and therefore well within the range used for model calibration, the process behaved slightly different. More specifically the viable cell density leveled off after already one day post infection and cells starting dying earlier than observed for the same MOI in the low MOI experiments described earlier. The cells also

consumed L-glutamine slightly faster and therefore the predicted values were generally higher than the experimentally determined ones (except the initial measurement).

While the errors observed seem rather large at first sight one needs to remember that the techniques used to analyze off-line samples generally do not provide much better estimations with errors of at least 10 % for the parameters investigated here. Therefore, application of such PLS models to obtain real-time information about the process state without the need of sampling, and so reducing the risk of contamination and labor required, should still be considered a very useful and acceptable alternative. In addition, the PLS models developed in this work are based on a calibration data set for infection at a wide range of MOI from 0.01 to 1.00. While it was the goal of this work to obtain a “universal” model valid over the whole MOI range to account for substantial variations in the process due to “real MOI” deviations, an industrial process would generally be performed at an optimized MOI. This should result in a less variable process and therefore a more accurate prediction.

4.2.10 Conclusions

Industrial scale bioprocesses based on the BEVS are preferably performed under low MOI conditions. While this saves costly virus seed, it makes the process also dependent on subsequent production of new virus particles and subsequent infection processes to completely infect the culture and induce recombinant protein expression in all the cells. Small deviations in cell density, virus to cell ratio or time of infection may be amplified under such situations causing variability in the processes and yields. It was hypothesized that DS could be a useful tool for real-time on-line monitoring of such cultures allowing detection of culture events and may even serve as a predictive tool for process success and eventually yield. DS was applied to a total of nine multi-liter bioreactor cultures focusing on process behavior at three different low MOI, 0.01, 0.10 and 1.00, and DS data was related to information obtained by off-line sample analyses.

Cultures infected at the three different MOI showed significantly different profiles and kinetics post infection for several parameters. Generally the process was delayed with decreasing

MOI in terms of infection kinetics, cell related parameters like growth, swelling and lysis, recombinant virus and eventually PCV2 ORF2 protein production.

Increasing MOI generally led to decreasing cell growth and eventually lower maximum viable cell densities post infection when compared to the uninfected control culture. This behavior could qualitatively be explained with the amount of virus particles added to the culture at the time of infection and the subsequent infection kinetics as summarized in Figure 4.54 and Figure 4.55. A baculovirus infected cell stops dividing. The more virus particles were added initially at the time of infection, the more were produced by the cells primarily infected early in the process, the quicker secondary infections were facilitated and eventually the earlier the stop in cell division due to infection outlasted the cell division. Determined initial infection rates for the specific recombinant baculovirus used in this work were comparable to theoretical values (Poisson distribution) and reports in the literature.

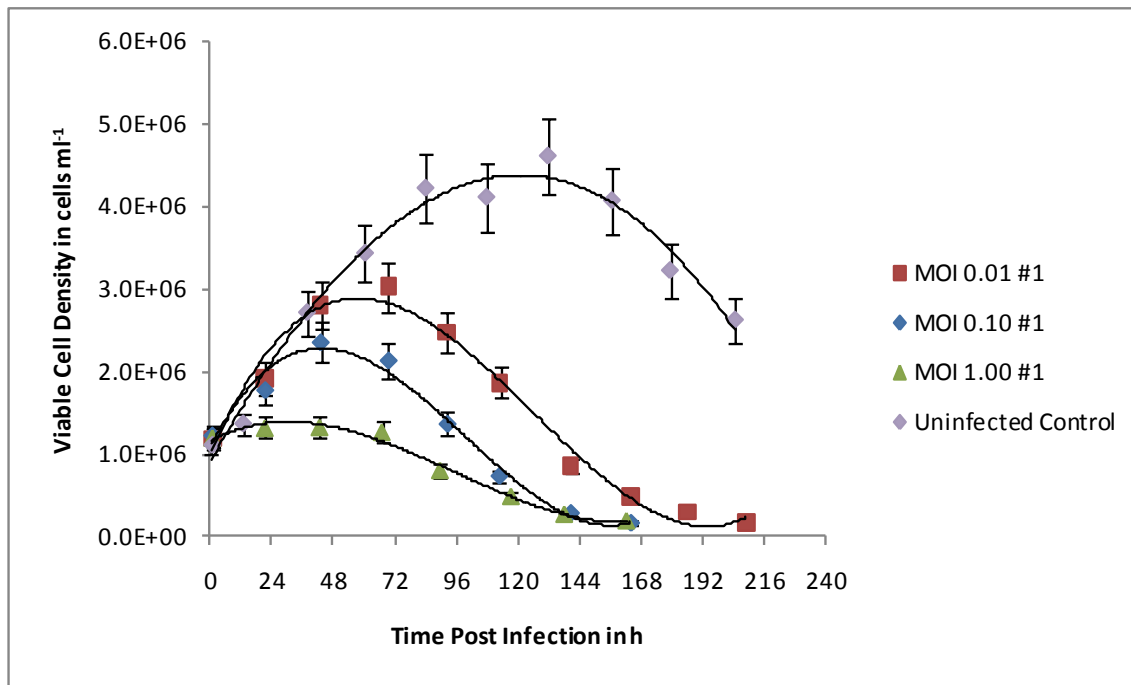


Figure 4.54. Viable cell density post infection at the three different MOI compared to an uninfected control culture. Initial values were approximately 1.0×10^6 cells ml^{-1} . The viable cell density increased for up to 72 h post infection depending on the MOI. Decreasing maximum viable cell densities were observed with increasing MOI with peak values of

approximately 3.0 , 2.2 , and 1.2×10^6 cells ml^{-1} for MOI 0.01, 0.10, and 1.00, respectively. Afterwards the viable cell density decreased continuously until the end of the process. Trendlines are intended to guide the eye only.

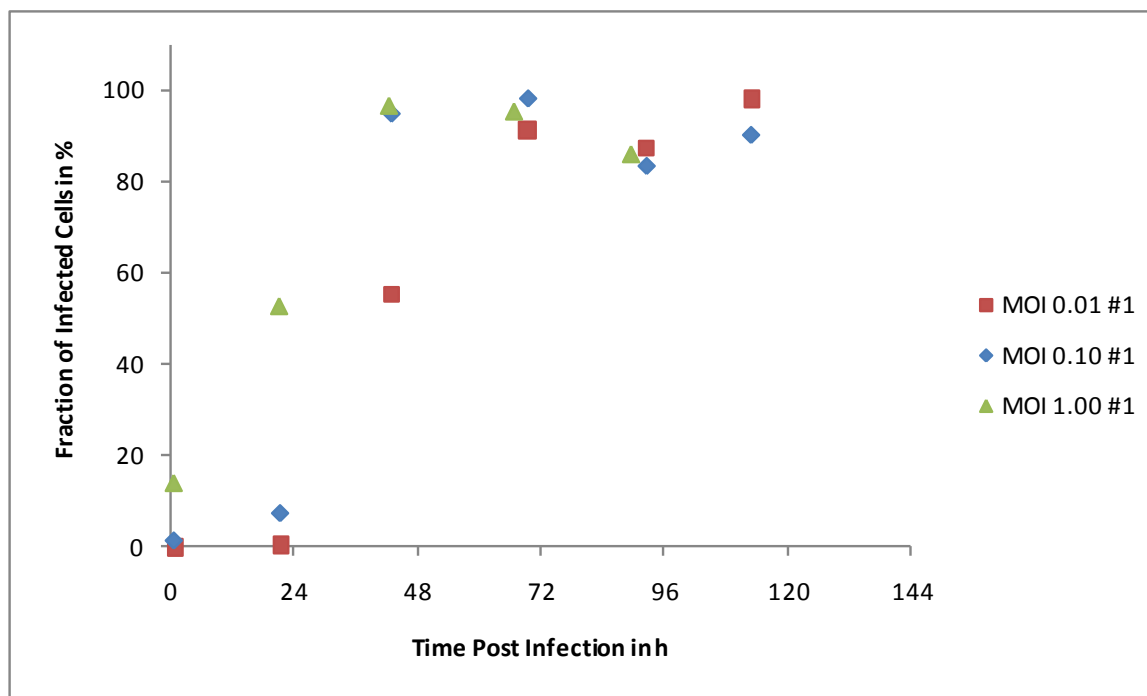


Figure 4.55. Fraction of infected cells post infection at the three different MOI. A higher initial MOI resulted in faster infection kinetics and eventually earlier complete infection of the culture at approximately 48 to 72 h post infection. Trendlines are intended to guide the eye only.

Despite the fact that recombinant PCV2 ORF2 protein production could be achieved at all three MOI, results indicated that mean PCV2 ORF2 harvest concentrations increased with the MOI (see Figure 4.56). While differences observed were not always statistically significant at the $\alpha = 0.95$ level, the trend described seems reasonable. Maybe even more importantly, variations in the yield were greatly reduced, when the MOI was increased, indicating lower variability in the process under those conditions. Interestingly, the specific productivity in terms of recombinant PCV2 ORF2 protein per cell also greatly varied with MOI (see Figure 4.57). Overall, an increasing specific productivity per biovolume or cell was observed with increasing MOI. This may be due to the fact that more of the resources available to the culture (nutrients, but also cell

apparatus) were channeled into the production of recombinant PCV2 ORF2 protein instead used up for cell growth purposes.

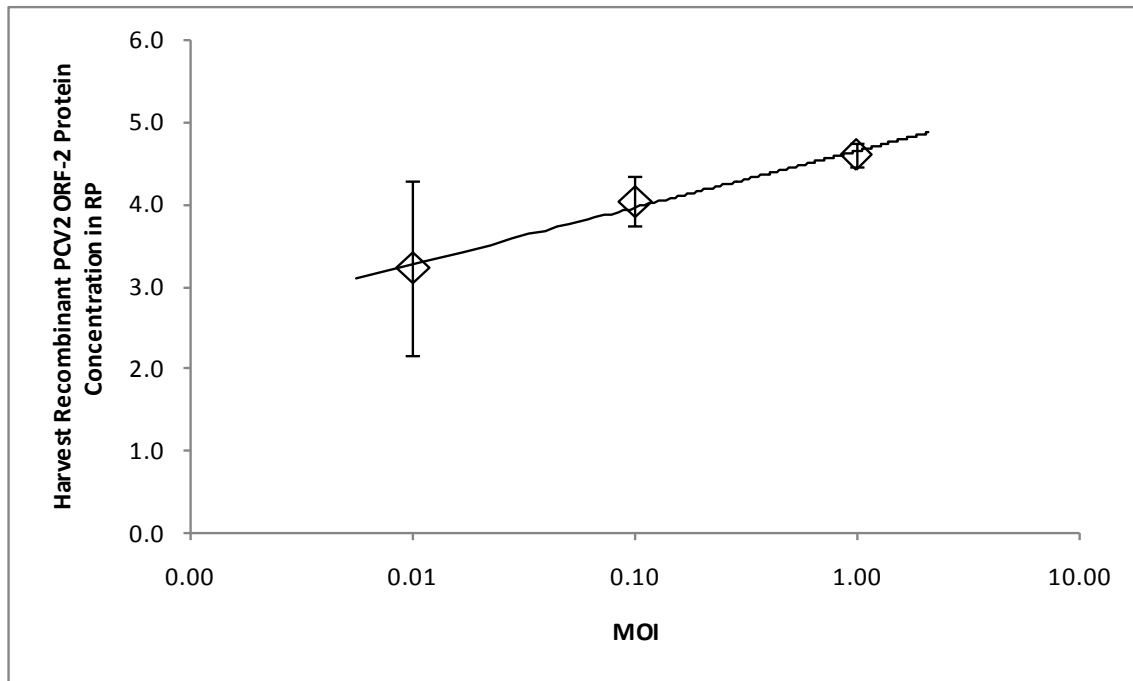


Figure 4.56. Dependency of harvest recombinant PCV2 ORF2 protein concentration on MOI. Variability in the harvest PCV2 ORF2 concentration decreased greatly with increasing MOI. Values shown are mean \pm standard deviation based on the three replicates performed at each MOI.

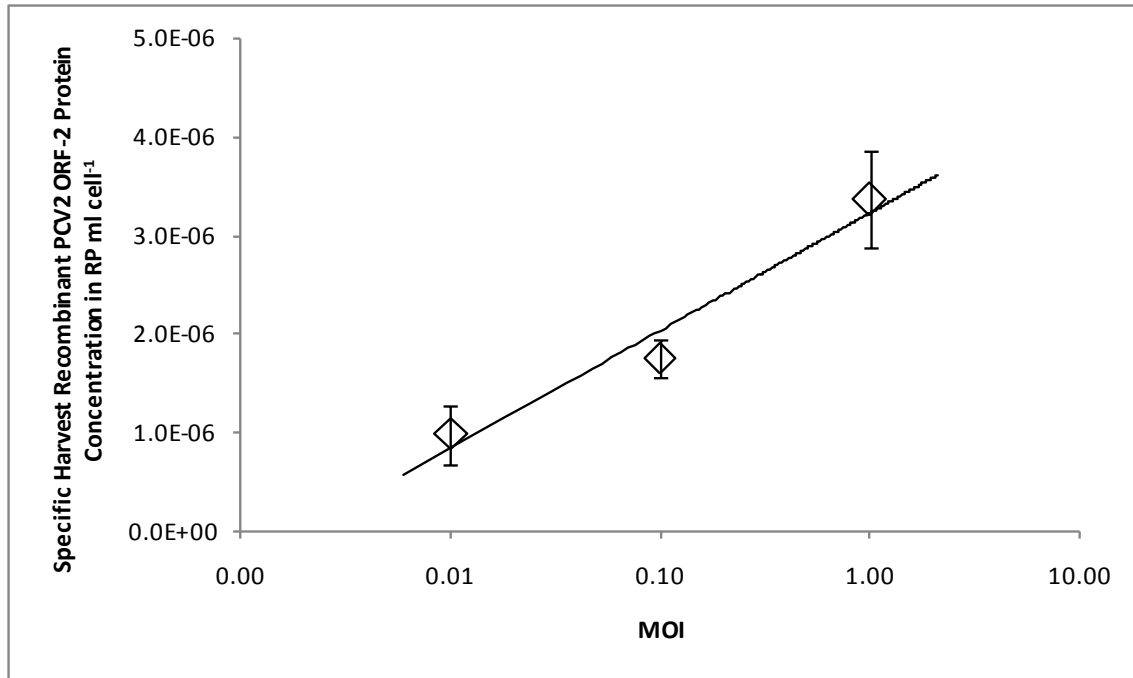


Figure 4.57. Dependency of the specific recombinant PCV2 ORF2 protein productivity per observed maximum viable cell density on MOI. Mean specific yields were approximately 3 times higher at MOI 1.00 than at 0.01. Values shown are mean \pm standard deviation based on the three replicates performed at each MOI.

DS was used to monitor the cultures infected in the low MOI range in-line and in real-time. DS proved to be able to distinguish between the different MOI conditions by providing significantly different profiles for the specific DS signals ($\Delta\epsilon$, f_c , α , Biomass, σ_s). The differences could generally be explained with the MOI dependent progress of the culture in terms of culture parameters like viable cell density or diameter, but late in the process deviations occurred. Nevertheless, DS allowed detecting of important culture events and even early prediction of recombinant protein production seems to be possible based on the real-time data. The peak in the Biomass signal for example occurred at approximately the same time as the maximum recombinant baculovirus concentration was achieved (see Figure 4.58). This would allow real-time initiation of the harvest procedure in baculovirus seed expansion.

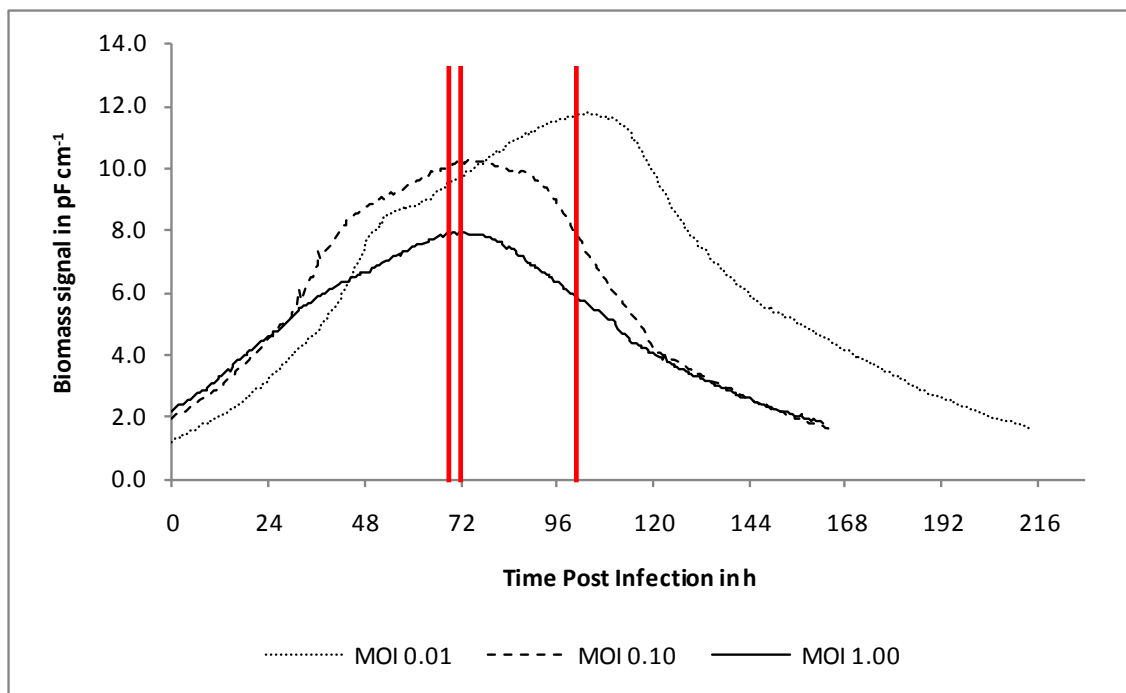


Figure 4.58. Comparison of Biomass Signal with the time of peak recombinant baculovirus concentration at the three MOI. The peak in recombinant baculovirus concentration was achieved at approximately the occurrence of the peak in the Biomass signal and is indicated by the red vertical lines.

Based on the assumption, that a larger cell was equal to a higher specific PCV2 ORF2 protein production^{142, 160}, a linear correlation could be obtained between the specific Biomass signal per viable cell at the time of the signal peak, indicating an increasing volume of the cell with an increasing specific PCV2 ORF2 protein yield per viable cell (see Figure 4.59). The correlation obtained was valid over the whole range of MOI from 0.01 to 1.00 and was even able to predict the observed large variations in the specific yield at MOI 0.01. The obtained correlations could be very useful in the routine industrial scale recombinant protein production with the BEVS. Obtaining a reliable prediction for the yield early in the process would allow early judgment about the success of a specific production run and may allow decisions and planning for the subsequent downstream processing procedures, including any concentration or dilution steps, before the specific process is even finished. With current technology, the first measurement of the recombinant PCV2 ORF2 protein concentration is not obtained until hours to days after the end of the process.

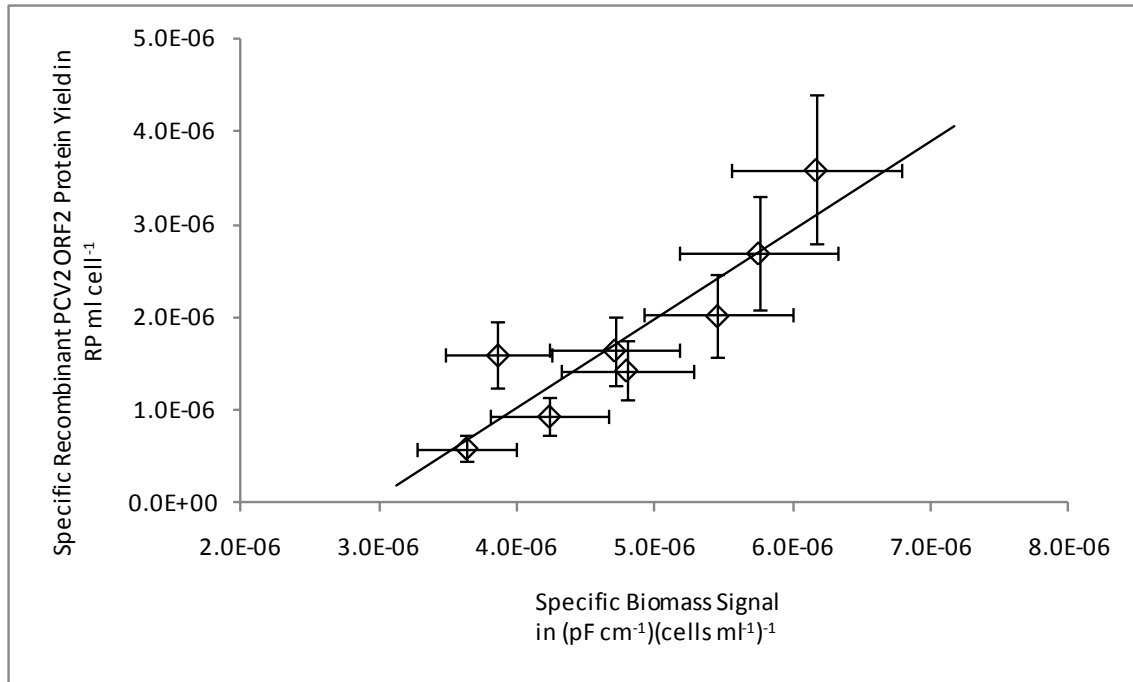


Figure 4.59. Correlation specific recombinant PCV2 ORF2 yield vs. specific Biomass signal at the time of signal peak based on viable cell density.

A multivariate model was developed to follow the infection process in the cultures within the MOI range investigated here. Using the data from the low MOI study as a calibration data set allowed developing PLS models (one for each response) for the estimation of several variables in real-time based on the DS data. The obtained models were successfully validated in an independent experiment (MOI 0.10). Figure 4.60 and Figure 4.61 as well as Table 4.9 summarize the findings and model quality in terms of its predictive power.

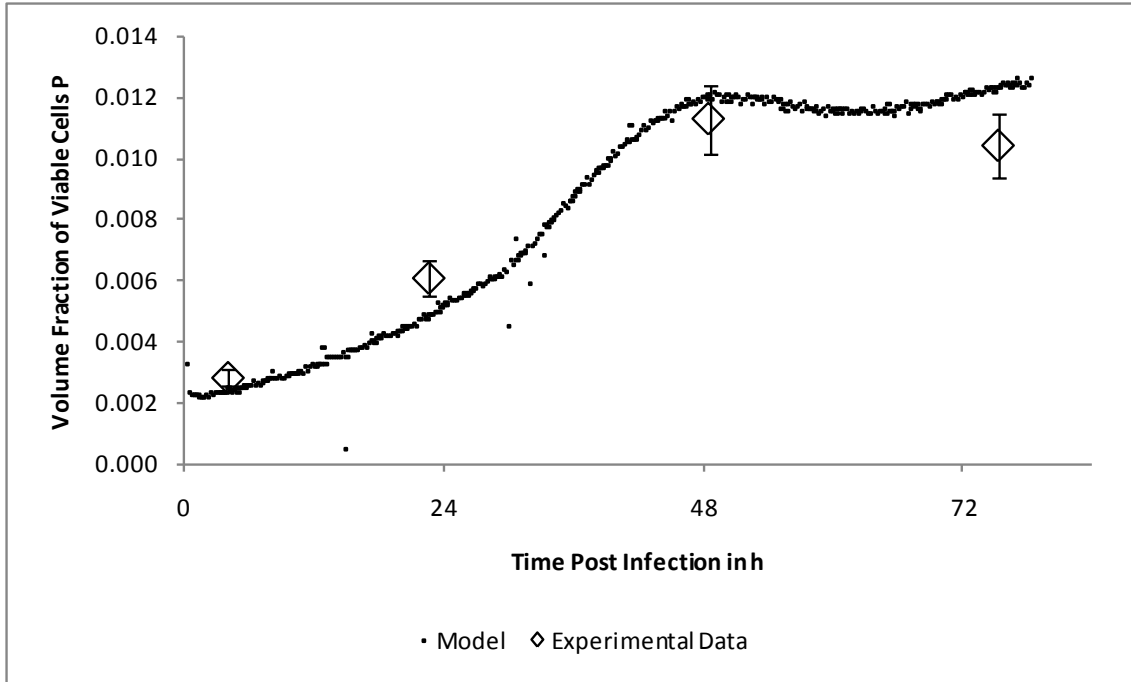


Figure 4.60. Model validation for volume fraction of viable cells P.

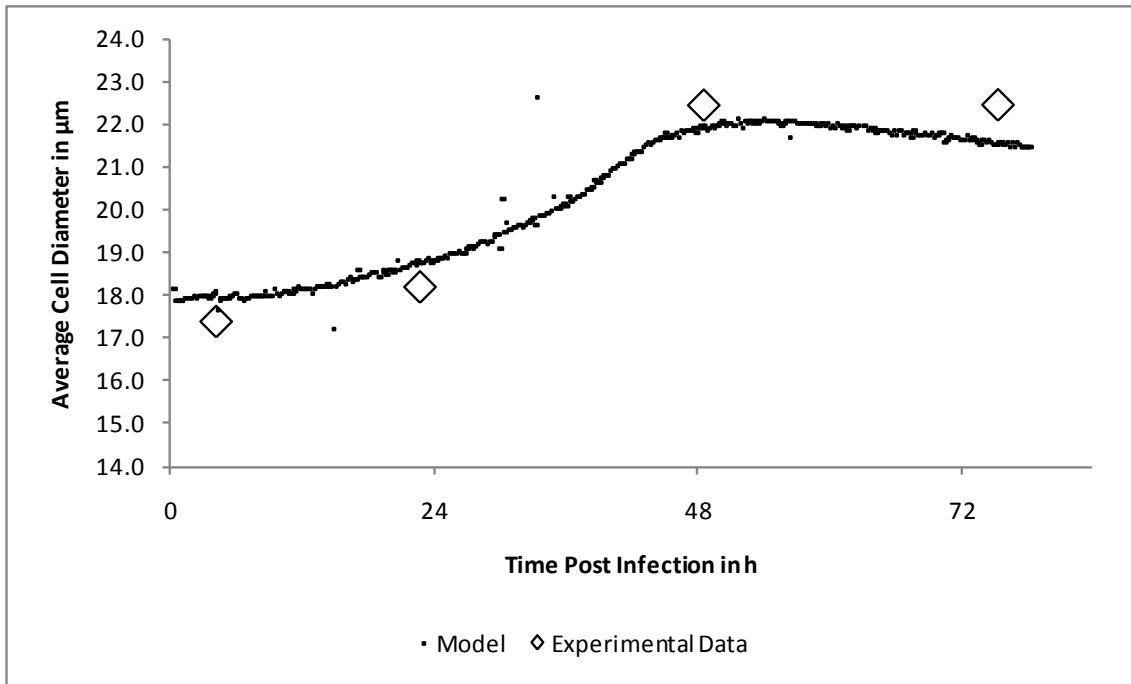


Figure 4.61. Model validation for average cell diameter.

Table 4.9. Model predictive power (RMSEP).

	P	Viable Cell Density in cells ml ⁻¹	Average Cell Diameter in μm	Medium Glutamine Concentration in mmol L ⁻¹
RMSEP	0.0013	4.16E+05	0.58	0.78
% Error	16.5	25.2	2.9	29.8

While the models developed here were based on calibration experiments in the range of MOI 0.01 to 1.00 to cover all potential process variations due to inconsistent “real MOI”, an industrial bioprocess based on the BEVS would generally be performed at an optimized MOI. Ideally, this should result in a process with a smaller range of “real MOI” than used here, and therefore a further improvement of the predictive power of the model can be expected. To the authors' knowledge this is the first time PLS modeling has been successfully applied to a bioprocess based on the BEVS for the production of a recombinant protein. With a better understanding of the processes late in the cultures, it should also be possible to extend the PLS model throughout the whole culture until the time of harvest. With the knowledge obtained, potentially otherwise unidentified causes for observed problems in the large scale and under different vessel configurations, e.g. an insufficient infection early in the process, could be identified and therefore tackled.

4.3 Medium Supplementation for Uninfected Sf-9 Clone Cell Growth

During the uninfected control culture, it was observed, that a specific nutrient, namely L-glutamine, was rapidly depleted in the culture medium. With L-glutamine being a major carbon and energy source for insect cells and this depletion happening relatively early in the processes, usually after approximately 48 h, it was proposed that this could potentially have a significant negative impact on the cultures in terms of cell growth and achievable maximum cell densities¹⁶³. Interestingly, DS signals recorded showed specific behavior around the time of L-glutamine depletion. Both, the dielectric increment $\Delta\epsilon$ and the Biomass signal, showed a distinct plateau phase at approximately the time L-glutamine was depleted (see Figure 4.62, compare Figure 4.27 for time of L-glutamine depletion). In case of the $\Delta\epsilon$ signal the plateau lasted about 24 h before another subsequent increase was observed, but the Biomass signal plateau lasted only about 12 h. Since samples had only been taken approximately every 24 h from the culture with none taken during the plateau phase, no immediate explanation for these plateaus in the signals could be found.

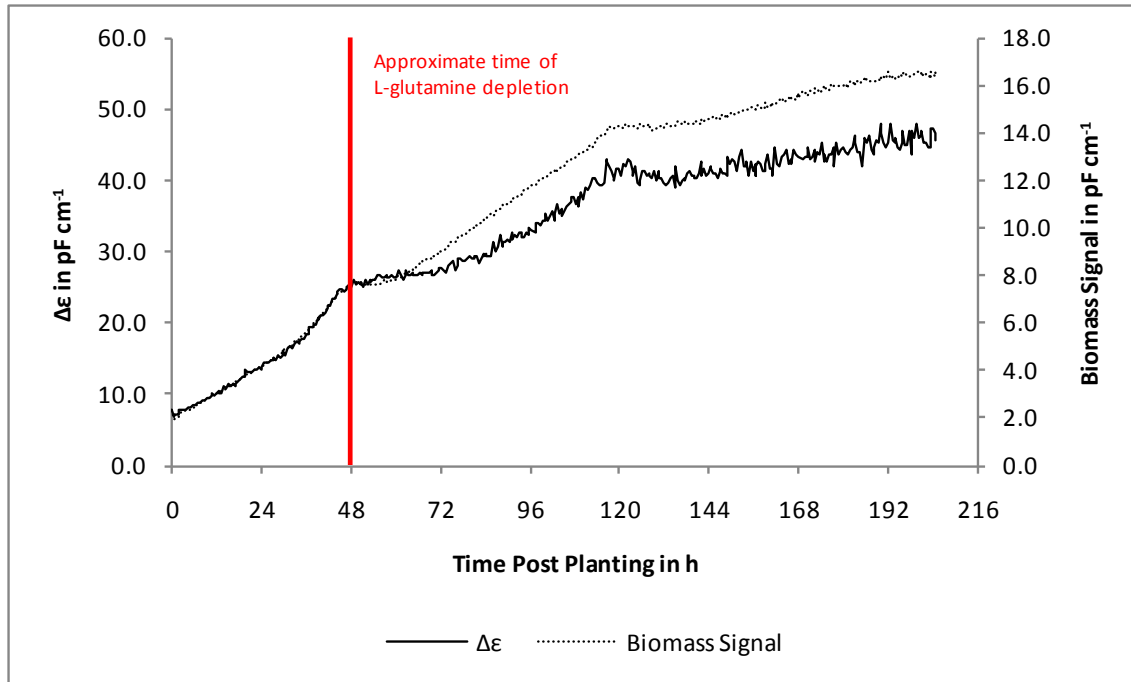


Figure 4.62. $\Delta\epsilon$ and Biomass signal from the uninfected control culture in the low MOI study. The first plateau occurred at approximately the same time L-glutamine was depleted in the culture medium.

Based on the theoretical dielectric cell model, several factors could have influenced these signals. $\Delta\epsilon$ is dependent on the volume fraction of viable cells P and the cell radius, but also the specific cell membrane capacitance C_m . P increased from the sample taken immediately prior the plateau phase to the first sample after, but it was not clear how P behaved during the actual plateau phase. Because the cell size independent Biomass signal also showed the same plateau, even though it was only about half as long, it was speculated that a change in viable cell radius alone was probably not the cause for the observed plateaus. In fact, no significant cell size change could be observed for the samples taken immediately prior to and after the observed plateau phase, but again, data during the plateau phase was not available. Assuming an increasing P during the plateau phase the only factor left potentially influencing the signals could have been C_m . To cause the changes in the signal as observed, C_m would have had to decrease during the plateau phase. Since the characteristic frequency is also dependent on C_m , changes in the latter should have also been reflected there with an increasing f_c . A significant increase in f_c was observed approximately from 60 h into the process but this change came much later than the

initial onset of the plateau phases in both, $\Delta\varepsilon$ and the Biomass signal, making it unlikely that this alone caused the plateaus. Additionally the values for f_c were still much lower than the working frequency for the Biomass signal (1000 kHz), which would ideally mean, that the latter would not have been influenced much by the increase in f_c .

To get more insight into the plateau phase and its possible causes and also to investigate the effect of L-glutamine depletion, two more uninfected cell growth experiments were performed in parallel, utilizing precultures #12 and #13. One culture was a repetition of the uninfected control culture while the second culture was fed multiple times with a 200 mM L-glutamine solution in order to prevent depletion. This culture was supplemented every time the L-glutamine concentration in the media had dropped below approximately 2.0 mmol L^{-1} and L-glutamine levels were brought back up to approximately 6.0 mmol L^{-1} . Care was taken not to exceed this level to avoid any other potential side effects on cell metabolism. Samples were taken from the culture approximately every 8 h starting from approximately 24 h into the process to obtain more information about changes in the culture during the plateau phase accompanying the L-glutamine depletion. Raw data collected is presented in Appendix I - .

Figure 4.63 and Figure 4.64 below illustrate the results of these experiments. Significant differences in the $\Delta\varepsilon$ and Biomass profiles between the control and feeding culture were observed. In general the L-glutamine fed culture showed a faster increase in the respective signals even early in the process after around 24 h when L-glutamine depletion had not yet occurred in the control culture. Interestingly the plateau phase was not observed during the L-glutamine supplemented culture and the values of the measured parameters $\Delta\varepsilon$ and Biomass were about twice as high in the supplemented culture at around this time. In contrast to the control culture, the supplemented culture reached its respective maximum values and leveled off relatively soon after this, at approximately 66 h into the process, while the control culture showed slow but steady increases until eventually leveling off at around 114 h into the process.

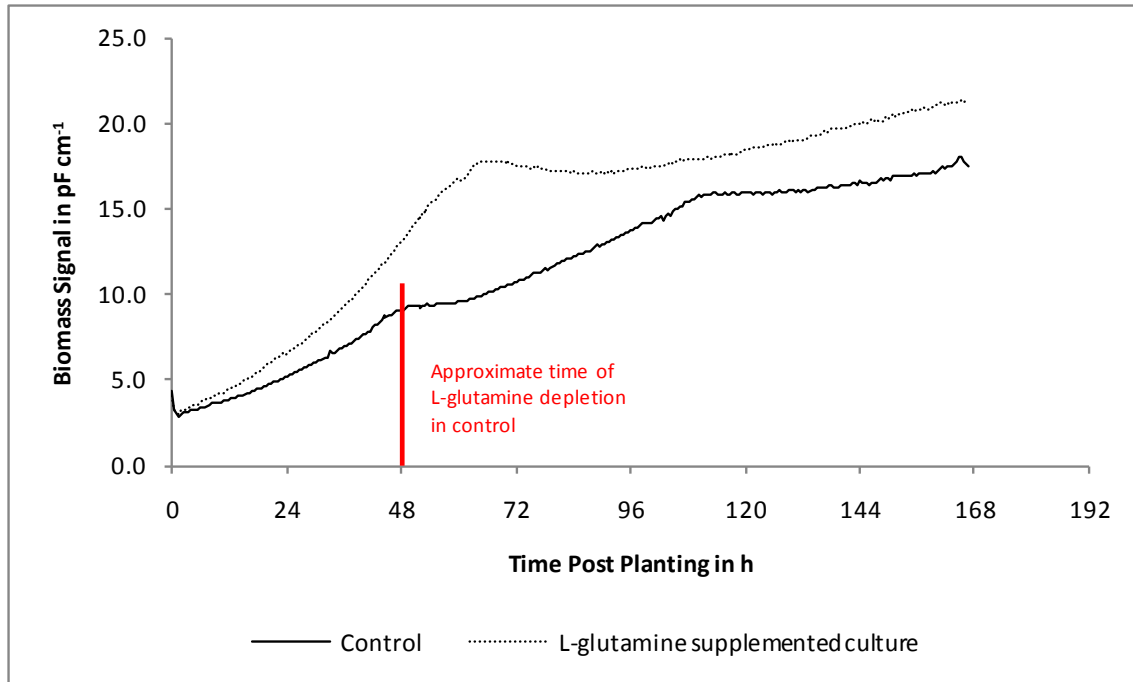


Figure 4.63. Comparison of the Biomass signal for a L-glutamine supplemented culture with a control culture without any supplementation. The supplemented culture does not show the same plateau phase as the control culture around 48 h post planting.

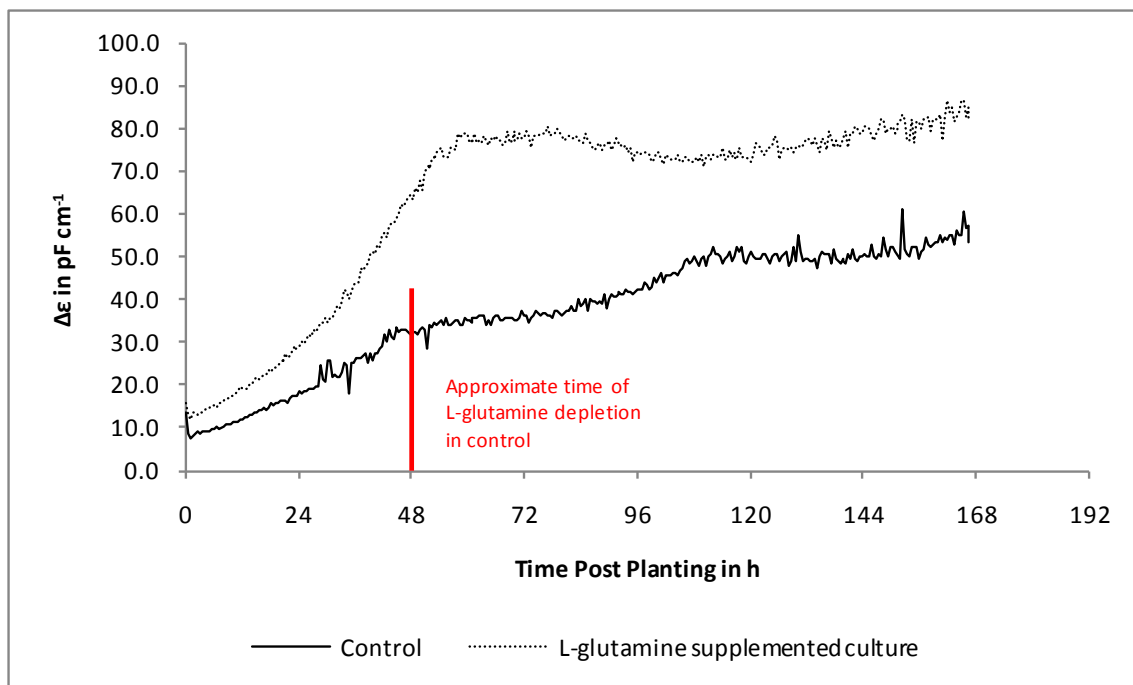


Figure 4.64. Comparison of $\Delta\epsilon$ for a L-glutamine supplemented culture with a control culture without any supplementation.

While the supplementation of the uninfected Sf-9 clone cell culture with L-glutamine seems to be the fundamental cause for the differences in the $\Delta\epsilon$ and Biomass signals, the off-line analyses of the samples revealed why these differences were observed. Figure 4.65 shows the profile for the viable cell density during the two processes, as determined with the Vi-CELL XR instrument. The L-glutamine supplemented culture exhibited significantly higher values in both parameters from approximately 48 h into the process, indicating that the observed L-glutamine depletion indeed slowed down, but did not cease, cell growth. The depleted culture seemed to switch its metabolism to a more D-Glucose and L-glutamate based consumption and continued growing at a slower rate and in a non-exponential fashion. Regarding the plateau phase, itself observed at the time of L-glutamine depletion, it seems reasonable to explain this with a slow-down in the cell propagation during the metabolic switch. The off-line data for the volume fraction of viable cells and viable cell density seems to support this theory but a complete stop in the growth was not detected. One has to keep in mind though, that the sampling was still only performed at approximately every 8 h and while the values obtained during this phase seem to

indicate a continuous increase the values are not necessarily significantly differently based on the instruments error.

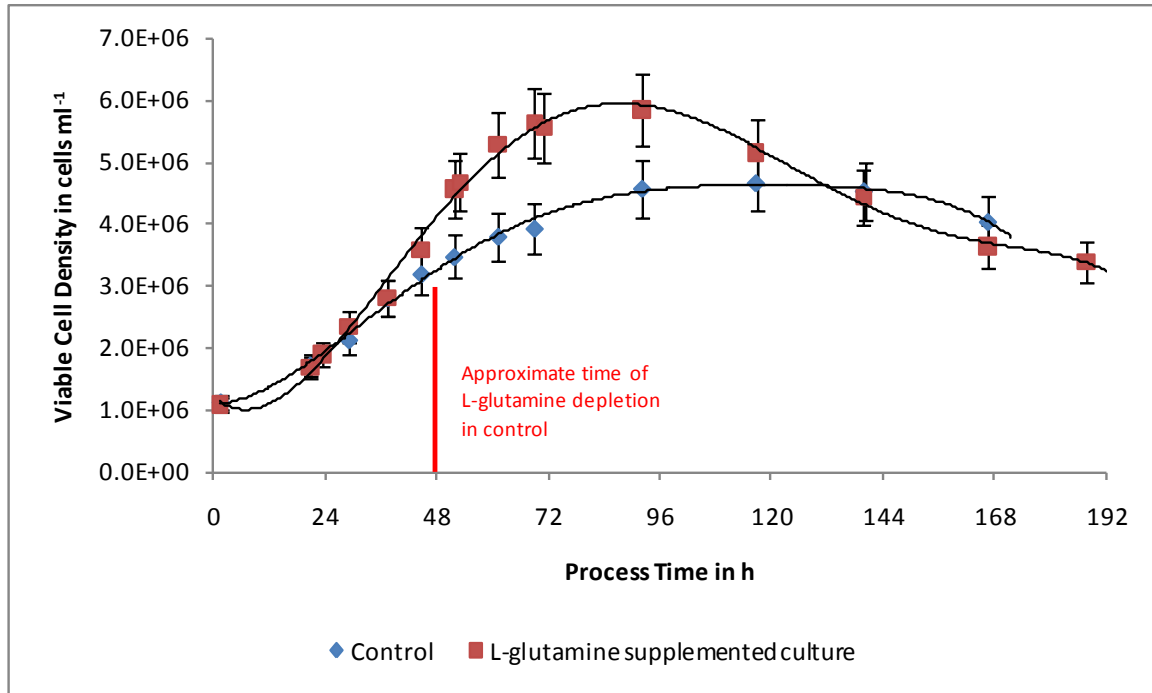


Figure 4.65. Comparison of the viable cell density for an L-glutamine supplemented culture with a control culture without any supplementation. The supplemented culture shows increased cell growth reaching an approximately 45 % higher maximum viable cell density at 72 h post planting. Trendlines are intended to guide the eye only.

According to Equation 4 the viable cell radius r and the specific cell membrane capacitance C_m also have an influence on $\Delta\varepsilon$. Off-line data supported the assumption made earlier, that cell size changes did not cause the plateau observed. While the changes in the viable cell size were very small and probably not even significant (data not shown), the trend was a conflictive increase of the cell size during this time. C_m could not be measured directly in this work and therefore its potential influence is unknown at this point. Based on these observations it seems reasonable to say, that the plateau phase in $\Delta\varepsilon$ and the Biomass signal seems to be mainly caused by a temporary stop in cell propagation during a metabolic switch due to a depletion of a main nutrient, namely L-glutamine. Once the switch was completed, the culture started growing again, but at a slower pace.

While the supplementation of the uninfected *Spodoptera frugiperda* cell culture with L-glutamine significantly accelerated growth and increased the achieved cell densities even early in the process, it remains unclear what caused this culture to enter the stationary phase at around 66 h into the process. L-glutamine was still left in sufficient quantities in the supplemented growth media but other media nutrients not measured in this work may have been depleted around this time. It is also possible that undetected byproducts of the cell culture had accumulated to inhibiting levels at this point but at least one research found that this is usually not a problem in insect cell culture¹⁶⁴. At around 53 h into the process, the dissolved oxygen concentration in the culture dropped to 0 % for a few seconds due to a backpressure problem in the vessel during one of the L-glutamine addition steps. While the dissolved oxygen concentration completely recovered eventually over the next 2 hours this may have caused or contributed to the subsequent stop in cell propagation. Additional experiments would be needed to investigate and eventually confirm or reject these hypotheses.

In general, the cell densities achieved in this work, even with feeding of L-glutamine, are still well below values reported earlier for comparable *Spodoptera frugiperda* insect cell cultures. Depending on the specific feeding strategy utilized (one time addition, multiple feeds) cell densities in fed-batch cultures reached ranged from 1.2 to 5.2 x 10⁷ cells ml⁻¹ for Sf-9 and Sf-21 cell cultures^{13, 123, 165}. Cultures in perfusion mode yielded approximately the same cell densities between 1.5 to 5.5 x 10⁷ cells ml⁻¹ for the same two cell lines^{166, 167}.

Therefore, further investigation in both, feeding components and alternative process modes, should be considered. Especially in the industrial production environment one would have to weigh the potential benefits of a higher cell yield with the disadvantages of a more complex process and control strategy. But it is reasonable to assume, that a significant improvement in the cell yield could lead to a reduction in time and cost of the large-scale cell production. The proposed potential feeding or media replacement strategies could be improved and controlled very accurately by utilizing the available real-time DS data. Based on the on-line estimation of the viable cell density within the culture, together with knowledge about the specific consumption or production rates of e.g. L-glutamine, would allow to automatically

calculate and control the optimal rate of feeding or perfusion to keep the concentrations of the nutrients and metabolites in question at acceptable levels. Figure 4.66 sketches such a control strategy.

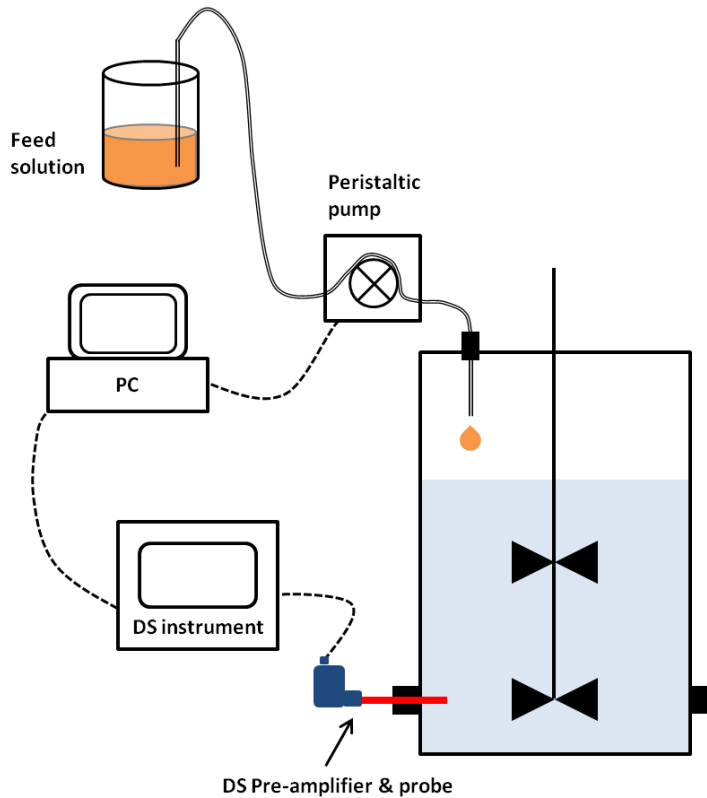


Figure 4.66. Schematic of a proposed feed-rate control based on DS measurements in-line of a bioreactor.

While this approach of a controlled continuous feeding would definitively be more cumbersome than a simple one-time addition at the beginning of the process or pulse additions during the process, it may also be very beneficial. It has been shown that feeding strategies based on step additions often lead to significant changes in the media osmolality which could be not only be attributed to decreases in the maximum achieved viable cell density in uninfected cultures but also recombinant protein productivity of infected cells, when compared to cultures with a semi-continuous feed^{13, 168}.

4.3.1 Conclusions

During the uninfected control culture it was observed, that a specific nutrient, namely L-glutamine, was rapidly depleted in the culture medium. It was proposed that this could have had a significant negative impact on cell growth because of the fact that L-glutamine is a major nutrient in insect cell culture. DS data, specifically $\Delta\varepsilon$ and the Biomass signal, exhibited distinct plateaus from approximately the time of L-glutamine depletion in the culture medium lasting approximately 12 and 24 h. A set of two experiments including a non-fed control culture and a second culture supplemented with L-glutamine to avoid depletion of this nutrient was conducted. It was found, that the depletion in L-glutamine indeed had a significant negative impact on Sf-9 clone cell growth. An improvement of approximately 45 % in viable cell density after 72 h, approximately the beginning of the stationary phase in the supplemented culture, was achieved when L-glutamine was fed to the culture. At this point it is still unclear what eventually caused the supplemented culture to enter the stationary phase with sufficient L-glutamine still available in the medium. DS data reflected the observed large differences in terms of viable cell density and growth. Based on these results it was proposed to use DS as a tool to control either feed or perfusion rates in more sophisticated process modes, potentially yielding even higher cell yields.

Chapter 5 - Conclusion and Outlook

This PhD research project focused on the application of DS in an industrial bioprocess at the multi-liter scale utilizing *Spodoptera frugiperda* derived Sf-9 clone cells and the BEVS with a recombinant baculovirus to produce a protein of the VLP class that serves as the immunostimulating agent in a vaccine. A newly developed DS instrument specialized for the use in the biopharmaceutical field was used together with a range of off-line sample analyses to quantify key process parameters. It was proposed that the use of DS as an on-line tool would allow insight into intricate processes within the cultures under low MOI conditions, allowing not only evaluation of the current state of a process but also prediction of the success of production formation already at an early stage.

DS could successfully be implemented into the growth process of uninfected cells. Developed linear correlations now allow the real-time estimation of viable biovolume and cell density on-line without the need for sampling. This greatly eliminates the contamination risk associated with the sampling procedure itself but also greatly reduces the time and effort usually required to perform the discrete sampling and any subsequent off-line analysis. Having such a tool has the potential to improve the repeatability of subsequent baculovirus infection and recombinant protein production processes because of more consistent “real MOI”.

DS proved also to be able to monitor and differentiate cultures infected in the low MOI range (0.01 to 1.00). Significantly different profiles for DS related parameters were obtained at the different MOI, allowing the qualitative monitoring of the infection and recombinant protein production process. Differences in the DS data could generally be explained with the different behavior of culture parameters like viable cell density or cell diameter, but some questions remain, especially late in the process. Nevertheless, DS did not only allow detection of important culture events in real-time, e.g. the peak in baculovirus production/concentration, but also seems to be able to serve as a predictive tool for the overall recombinant protein yield early in the process. Additionally, PLS models were developed to follow the infection phase in the low MOI range quantitatively for specific culture parameters. The obtained models provide information about the progress in viable biovolume, cell diameter, and even L-glutamine concentration in the

culture medium with a sufficient accuracy. It is expected that the quality of the models can be further improved when an optimized, narrower MOI range is utilized, which is usually the case in an industrial application. A potential extension of the model to include the lysis phase of the cultures should also be investigated. To the knowledge of the author, this is the first time PLS modeling has been successfully applied to a BEVS based bioprocess.

During the experiments performed in this work it was observed, that a specific nutrient, namely L-glutamine, was depleted early in the process in both, uninfected and infected, cultures. This depletion was accompanied by a significant plateau in some of the DS signals. Additional supplementation experiments identified the L-glutamine depletion as ultimately causing those plateaus by temporarily ceasing cell growth before a switch in the cells metabolism had occurred. An improvement of approximately 45 % in maximum viable cell density was achieved by a simple feeding strategy. It is proposed that more sophisticated processed modes like continuous fed-batch or even perfusion will allow further improvement of the cell yield but further research is required to identify potentially limiting nutrients or inhibiting metabolites. DS would allow implementation of an adequate control of the feed or perfusion rate to ensure optimum process conditions by providing real-time information about the viable cell density.

A similar depletion of the same nutrient was observed for the case of baculovirus infected cultures, regardless of the virus concentration added used. Preliminary experiments with a one-time addition of an L-glutamine and L-cystein feed at the beginning of the culture gave promising results in terms of increased yield but DS data also showed distinct differences compared to a non-supplemented control culture (see Figure 5.1) . In general, the DS data seemed to indicate an extended culture, despite the fact that off-line analysis showed a comparable drop in cell viability. This again indicates that “dead” cells (as determined by trypan blue) may still contribute significantly to the DS signals in some cases. Further research is required to investigate the effect of medium specific nutrient supplementation and its effects on the PCV2 ORF2 production process and yield. DS could be a valuable tool in those investigations providing additional data and insight into the culture’s progress.

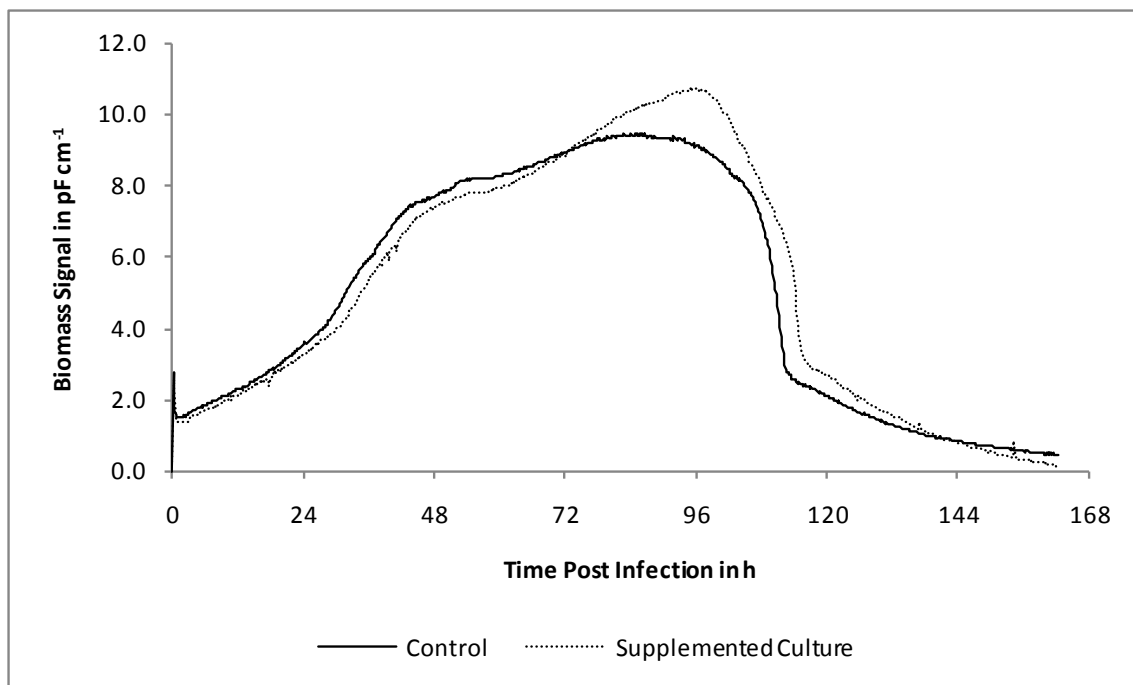


Figure 5.1. Comparison of Biomass signals for a supplemented infected culture (MOI 0.10, L-glutamine and L-cystein supplementation) with a control culture without any supplementation. The supplemented culture seems to be extended slightly and exhibits a higher Biomass signal peak.

Summarized, DS along with the information derived in this work will contribute to satisfy the increased requirements for on-line process monitoring as delineated in the PAT initiative by the FDA. It allows non-invasive and non-destructive continuous monitoring of suspension as well as adherent cell cultures but continuous research is required. The influence of all the cells dielectric properties like the specific membrane capacitance or the intracellular conductivity is not fully understood yet and dedicated research in this area could potentially greatly improve the understanding of DS data and its application. Additionally, improved methods to estimate the biovolume from a cell size distribution taking into account more than just one representative parameter like the mode or mean should be considered¹⁶⁹. Nevertheless, routine process monitoring to follow culture parameters by PLS models, detection of deviations from the normal and specific events in the culture's progress as well as yield prediction have been successfully established in this work. Transfer of the DS technology into the multi-m³

routine production has the potential to greatly improve process understanding in the production scale as well as to simplify but also increase repeatability of the processes.

References

1. Weber, W.; Fussenegger, M. In *Insect Cell-Based Recombinant Protein Production*; Eibl, R., Eibl, D., Pörtner, R., Catapano, G. and Czermak, P., Eds.; Cell and Tissue Reaction Engineering; Springer Berlin Heidelberg: 2009; pp 263-277.
2. FDA Guidance for Industry PAT — A Framework for Innovative Pharmaceutical Development, Manufacturing, and Quality Assurance. **2004**.
3. Clementschitsch, F.; Bayer, K. Improvement of bioprocess monitoring: development of novel concepts. *Microbial Cell Factories* **2006**, *5*, 19.
4. Teixeira, A. P.; Oliveira, R.; Alves, P. M.; Carrondo, M. J. T. Advances in on-line monitoring and control of mammalian cell cultures: Supporting the PAT initiative. *Biotechnol. Adv.* **2009**, *27*, 726-732.
5. Carvell, J. P.; Dowd, J. E. On-line measurements and control of viable cell density in cell culture manufacturing processes using radio-frequency impedance. *Cytotechnology* **2006**, *50*, 35-48.
6. Carvell, J. P. Viable Biomass Sensor for Bioreactors. *BIOforum Europe* **2008**, 54-55.
7. Ducommun, P.; Bolzonella, I.; Rhiel, M.; Pugeaud, P.; von Stockar, U.; Marison, I. W. On-line determination of animal cell concentration. *Biotechnol. Bioeng.* **2001**, *72*, 515-522.
8. Fehrenbach, R.; Comberbach, M.; Pêtre, J. O. On-line biomass monitoring by capacitance measurement. *J. Biotechnol.* **1992**, *23*, 303-314.
9. Noll, T.; Biselli, M. Dielectric spectroscopy in the cultivation of suspended and immobilized hybridoma cells. *J. Biotechnol.* **1998**, *63*, 187-198.
10. Sarra, M.; Ison, A. P.; Lilly, M. D. The relationships between biomass concentration, determined by a capacitance-based probe, rheology and morphology of *Saccharopolyspora erythraea* cultures. *J. Biotechnol.* **1996**, *51*, 157-165.
11. Zeiser, A.; Bedard, C.; Voyer, R.; Jardin, B.; Tom, R.; Kamen, A. A. On-line monitoring of the progress of infection in Sf-9 insect cell cultures using relative permittivity measurements. *Biotechnol. Bioeng.* **1999**, *63*, 122-126.
12. Ansorge, S.; Esteban, G.; Schmid, G. On-line monitoring of infected Sf-9 insect cell cultures by scanning permittivity measurements and comparison with off-line biovolume measurements. *Cytotechnology* **2007**, *55*, 115-124.

13. Elias, C. B.; Zeiser, A.; Bedard, C.; Kamen, A. A. Enhanced growth of Sf-9 cells to a maximum density of 5.2×10^7 cells per mL and production of beta-galactosidase at high cell density by fed batch culture. *Biotechnol. Bioeng.* **2000**, *68*, 381-388.
14. Negrete, A.; Esteban, G.; Kotin, R. M. Process optimization of large-scale production of recombinant adeno-associated vectors using dielectric spectroscopy. *Appl. Microbiol. Biotechnol.* **2007**, *76*, 761-772.
15. Zeiser, A.; Elias, C. B.; Voyer, R.; Jardin, B.; Kamen, A. A. On-line monitoring of physiological parameters of insect cell cultures during the growth and infection process. *Biotechnol. Prog.* **2000**, *16*, 803-808.
16. Hitchman, R. B.; Possee, R. D.; King, L. A. Baculovirus Expression Systems for Recombinant Protein Production in Insect Cells. *Recent Patents on Biotechnology* **2009**, *3*, 46-54.
17. Kost, T. A.; Condreay, J. P.; Jarvis, D. L. Baculovirus as versatile vectors for protein expression in insect and mammalian cells. *Nat. Biotechnol.* **2005**, *23*, 567-575.
18. Smith, G. E.; Summers, M. D.; Fraser, M. J. Production of Human Beta Interferon in Insect Cells Infected with a Baculovirus Expression Vector. *Mol. Cell. Biol.* **1983**, *3*, 2156-2165.
19. Kelly, B. J.; King, L. A.; Possee, R. D. In *Introduction to Baculovirus Molecular Biology*; Murhammer, D. W., Ed.; Baculovirus and Insect Cell Expression Protocol; 2007; pp 25-54.
20. Possee, R. D.; King, L. A. In *Baculovirus Transfer Vectors*; Murhammer, D. W., Ed.; Baculovirus and Insect Cell Expression Protocol; 2007; pp 55-76.
21. Maranga, L.; Cruz, P.; Aunins, J.; Carrondo, M. In *Production of Core and Virus-Like Particles with Baculovirus Infected Insect Cells*; Tools and Applications of Biochemical Engineering Science; Springer Berlin / Heidelberg: 2002; Vol. 74, pp 183-206.
22. Harrison, R. L.; Jarvis, D. L. In *Transforming Lepidopteran Insect Cells for Improved Protein Processing*; Murhammer, D. W., Ed.; Baculovirus and Insect Cell Expression Protocol; 2007; pp 341-356.
23. Harwood, S. In *Small-Scale Protein Production with the Baculovirus Expression Vector System*; Murhammer, D. W., Ed.; Baculovirus and Insect Cell Expression Protocol; 2007; pp 211-223.
24. Murhammer, D. W. In *Useful Tips, Widely Used Techniques, and Quantifying Cell Metabolic Behavior*; Murhammer, D. W., Ed.; Baculovirus and Insect Cell Expression Protocols; Humana Press: 2007; pp 3-22.

25. Jantafong, T.; Boonsoongnern, A.; Poolperm, P.; Urairong, K.; Lekcharoensuk, C.; Lekcharoensuk, P. Genetic characterization of porcine circovirus type 2 in piglets from PMWS-affected and -negative farms in Thailand. *Virology Journal* **2011**, *8*, 88.
26. Kiupel, M.; Stevenson, G. W.; Galbreath, E. J.; North, A.; HogenEsch, H.; Mittal, S. K. Porcine Circovirus type 2 (PCV2) causes apoptosis in experimentally inoculated BALB/c mice. *BMC Veterinary Research* **2005**, *1*.
27. Guo, L. J.; Lu, Y. H.; Wei, Y. W.; Huang, L. P.; Liu, C. M. Porcine circovirus type 2 (PCV2): genetic variation and newly emerging genotypes in China. *Virology Journal* **2010**, *7*, 273.
28. Segales, J.; Allan, G. M.; Domingo, M. In *Porcine Circovirus Diseases*; Barbara E. Straw, B. E., Zimmerman, J. J., D'Allaire, S. and Taylor, D. J., Eds.; Diseases of Swine; Wiley-Blackwell: 2006; pp 299-308.
29. Opriessnig, T.; Meng, X.; Halbur, P. G. Porcine circovirus type 2-associated disease: Update on current terminology, clinical manifestations, pathogenesis, diagnosis, and intervention strategies. *Journal of Veterinary Diagnostic Investigation* **2007**, *19*, 591-615.
30. Tischer, I.; Rasch, R.; Tochterman, G. Characterization of Papovavirus-Like and Picornavirus-Like Particles in Permanent Pig Kidney-Cell Lines. *Zentralblatt Fur Bakteriologie Mikrobiologie Und Hygiene Series A-Medical Microbiology Infectious Diseases Virology Parasitology* **1974**, *226*, 153-167.
31. John C.S. Harding, J. C. S.; Clark, E. G. Recognizing and diagnosing postweaning multisystemic wasting syndrome (PMWS). *Swine Health and Production* **1996**, *5*, 201-203.
32. Harding, J. C. S.; Clark, E. G. Recognizing and diagnosing postweaning multisystemic wasting syndrome (PMWS). *Swine Health and Production* **1997**, *5*, 201-203.
33. Harding, J. C. S. The clinical expression and emergence of porcine circovirus 2. *Vet. Microbiol.* **2004**, *98*, 131-135.
34. Blanchard, P.; Mahe, D.; Cariolet, R.; Keranflec'h, A.; Baudouard, M. A.; Cordioli, P.; Albina, E.; Jestin, A. Protection of swine against post-weaning multisystemic wasting syndrome (PMWS) by porcine circovirus type 2 (PCV2) proteins. *Vaccine* **2003**, *21*, 4565-4575.
35. Nawagitgul, P.; Harms, P. A.; Morozov, I.; Thacker, B. J.; Sorden, S. D.; Lekcharoensuk, C.; Paul, P. S. Modified indirect porcine circovirus (PCV) type 2-based and recombinant capsid protein (ORF2)-based enzyme-linked Immunosorbent assays for detection of antibodies to PCV. *Clin. Diagn. Lab. Immunol.* **2002**, *9*, 33-40.

36. Allan, G. M.; Ellis, J. A. Porcine circoviruses: a review. *Journal of Veterinary Diagnostic Investigation* **2000**, *12*, 3-14.
37. Meehan, B. M.; McNeilly, F.; Todd, D.; Kennedy, S.; Jewhurst, V. A.; Ellis, J. A.; Hassard, L. E.; Clark, E. G.; Haines, D. M.; Allan, G. M. Characterization of novel circovirus DNAs associated with wasting syndromes in pigs. *J. Gen. Virol.* **1998**, *79*, 2171-2179.
38. Mahe, D.; Blanchard, P.; Truong, C.; Arnauld, C.; Le Cann, P.; Cariolet, R.; Madec, F.; Albina, E.; Jestin, A. Differential recognition of ORF2 protein from type 1 and type 2 porcine circoviruses and identification of immunorelevant epitopes. *J. Gen. Virol.* **2000**, *81*, 1815-1824.
39. Nawagitgul, P.; Morozov, I.; Bolin, S. R.; Harms, F. A.; Sorden, S. D.; Paul, P. S. Open reading frame 2 of porcine circovirus type 2 encodes a major capsid protein. *J. Gen. Virol.* **2000**, *81*, 2281-2287.
40. Li, F.; Hashimura, Y.; Pendleton, R.; Harms, J.; Collins, E.; Lee, B. A systematic approach for scale-down model development and characterization of commercial cell culture processes. *Biotechnol. Prog.* **2006**, *22*, 696-703.
41. Butler, M. Animal cell cultures: recent achievements and perspectives in the production of biopharmaceuticals. *Appl. Microbiol. Biotechnol.* **2005**, *68*, 283-291.
42. Baldi, L.; Hacker, D. L.; Adam, M.; Wurm, F. M. Recombinant protein production by large-scale transient gene expression in mammalian cells: state of the art and future perspectives. *Biotechnol. Lett.* **2007**, *29*, 677-684.
43. Czermak, P.; Pörtner, R.; Brix, A. In *Special Engineering Aspects*; Eibl, R., Eibl, D., Pörtner, R., Catapano, G. and Czermak, P., Eds.; Cell and Tissue Reaction Engineering; Springer Berlin Heidelberg: 2009; pp 83-172.
44. Vojinovic, V.; Cabral, J. M. S.; Fonseca, L. P. Real-time bioprocess monitoring Part I: In situ sensors. *Sensors and Actuators B-Chemical* **2006**, *114*, 1083-1091.
45. Gnoth, S.; Jenzsch, M.; Simutis, R.; Luebbert, A. Process Analytical Technology (PAT): Batch-to-batch reproducibility of fermentation processes by robust process operational design and control. *J. Biotechnol.* **2007**, *132*, 180-186.
46. Ducommun, P.; Kadouri, A.; von Stockar, U.; Marison, I. W. On-line determination of animal cell concentration in two industrial high-density culture processes by dielectric spectroscopy. *Biotechnol. Bioeng.* **2002**, *77*, 316-323.
47. Rudolph, G.; Brückerhoff, T.; Bluma, A.; Korb, G.; Scheper, T. Optische In-line-Messverfahren zur Zellzahl- und Zellgrößenbestimmung in der Bioprozesstechnik. *Chemie Ingenieur Technik* **2007**, *79*, 42-51.

48. Myers, M. A. Direct measurement of cell numbers in microtitre plate cultures using the fluorescent dye SYBR green I. *J. Immunol. Methods* **1998**, *212*, 99-103.
49. Rengarajan, K.; Cristol, S. M.; Mehta, M.; Nickerson, J. M. Quantifying DNA concentrations using fluorometry: A comparison of fluorophores. *Molecular Vision* **2002**, *8*, 416-421.
50. Zipper, H.; Brunner, H.; Bernhagen, J.; Vitzthum, F. Investigations on DNA intercalation and surface binding by SYBR Green I, its structure determination and methodological implications. *Nucleic Acids Res.* **2004**, *32*, e103.
51. Cook, J. A.; Mitchell, J. B. Viability Measurements in Mammalian-Cell Systems. *Anal. Biochem.* **1989**, *179*, 1-7.
52. Folly, R. O. M.; Valdman, B.; Valero, F.; Sola, C. Potentiometric sensor for on line glucose determination. *Biotechnol. Tech.* **1996**, *10*, 867-870.
53. Huang, Y. L.; Li, S. Y.; Dremel, B. A. A.; Bilitewski, U.; Schmid, R. D. On-line Determination of Glucose-Concentration Throughout Animal-Cell Cultures Based on Chemiluminescent Detection of Hydrogen-Peroxide Coupled with Flow-Injection Analysis. *J. Biotechnol.* **1991**, *18*, 161-172.
54. Male, K. B.; Gartu, P. O.; Kamen, A. A.; Luong, J. H. T. On-line monitoring of glucose in mammalian cell culture using a flow injection analysis (FIA) mediated biosensor. *Biotechnol. Bioeng.* **1997**, *55*, 497-504.
55. Pickup, J. C.; Hussain, F.; Evans, N. D.; Rolinski, O. J.; Birch, D. J. S. Fluorescence-based glucose sensors. *Biosens. Bioelectron.* **2005**, *20*, 2555-2565.
56. Renneberg, R.; Lisdat, F. In *Biosensing for the 21st Century*; Springer: 2008; .
57. Boudreau, M.; Benton, T. Bioprocess Control: What the Next 15 Years Will Bring. *Pharmaceutical Manufacturing* **2008**, *7*, 18-20.
58. Riley, M. R.; Rhiel, M.; Zhou, X. J.; Arnold, M. A.; Murhammer, D. W. Simultaneous measurement of glucose and glutamine in insect cell culture media by near infrared spectroscopy. *Biotechnol. Bioeng.* **1997**, *55*, 11-15.
59. Lee, H. L. T.; Boccazzi, P.; Gorret, N.; Ram, R. J.; Sinskey, A. J. In situ bioprocess monitoring of Escherichia coli bioreactions using Raman spectroscopy. *Vibrational Spectroscopy* **2004**, *35*, 131-137.
60. Kussow, C. M.; Zhou, W. C.; Gryte, D. M.; Hu, W. S. Monitoring of Mammalian-Cell Growth and Virus Production Process using On-line Oxygen-Uptake Rate Measurement. *Enzyme Microb. Technol.* **1995**, *17*, 779-783.

61. Baker, K. N.; Rendall, M. H.; Patel, A.; Boyd, P.; Hoare, M.; Freedman, R. B.; James, D. C. Rapid monitoring of recombinant protein products: a comparison of current technologies. *Trends Biotechnol.* **2002**, *20*, 149-156.
62. Cannizzaro, C.; Rhiel, M.; Marison, I.; von Stockar, U. On-line monitoring of *Phaffia rhodozyma* fed-batch process with in situ dispersive Raman spectroscopy. *Biotechnol. Bioeng.* **2003**, *83*, 668-680.
63. De Beer, T. R. M.; Baeyens, W. R. G.; Ouyang, J.; Vervaet, C.; Remon, J. P. Raman spectroscopy as a process analytical technology tool for the understanding and the quantitative in-line monitoring of the homogenization process of a pharmaceutical suspension. *Analyst* **2006**, *131*, 1137-1144.
64. Rathore, A. S.; Yu, M.; Yeboah, S.; Sharma, A. Case study and application of process analytical technology (PAT) towards bioprocessing: Use of on-line high-performance liquid chromatography (HPLC) for making real-time pooling decisions for process chromatography. *Biotechnol. Bioeng.* **2008**, *100*, 306-316.
65. Dünnebier, G.; Tups, H. FDA PAT Initiative - Eine Anwendersicht zu technischen Möglichkeiten und aktueller industrieller Umsetzung. *Chemie Ingenieur Technik* **2007**, *79*, 2019-2028.
66. Kourti, T. The process analytical technology initiative and multivariate process analysis, monitoring and control. *Analytical and Bioanalytical Chemistry* **2006**, *384*, 1043-1048.
67. Chew, W.; Sharratt, P. Trends in process analytical technology. *Analytical Methods* **2010**, *2*, 1412-1438.
68. Austin, G. D.; Watson, R. W. J.; Damore, T. Studies of On-line Viable Yeast Biomass with a Capacitance Biomass Monitor. *Biotechnol. Bioeng.* **1994**, *43*, 337-341.
69. Heggart, H.; Margaritis, A.; Stewart, R. J.; Pilkington, M.; Sobezak, J.; Russell, I. Measurement of brewing yeast viability and vitality: A review of methods. *Technical quarterly quarterly - Master Brewers Association of the Americas* **2000**, *37*, 409-430.
70. Florian, M. In *Electrochemical Impedance Spectroscopy*; Analytical Methods In Corrosion Science and Engineering; CRC Press: 2005; pp 463-505.
71. Ellis, K. J. Human body composition: In vivo methods. *Physiol. Rev.* **2000**, *80*, 649-680.
72. Markx, G. H.; Davey, C. L. The dielectric properties of biological cells at radiofrequencies: Applications in biotechnology. *Enzyme Microb. Technol.* **1999**, *25*, 161-171.
73. Ansorge, S.; Esteban, G.; Schmid, G. Multifrequency Permittivity Measurements Enable On-Line Monitoring of Changes in Intracellular Conductivity Due to Nutrient Limitations During Batch Cultivations of CHO Cells. *Biotechnol. Prog.* **2010**, *26*, 272-283.

74. Patel, P.; Markx, G. H. Dielectric measurement of cell death. *Enzyme Microb. Technol.* **2008**, *43*, 463-470.
75. Pilwat, G.; Zimmermann, U. Determination of Intracellular Conductivity from Electrical Breakdown Measurements. *Biochim. Biophys. Acta* **1985**, *820*, 305-314.
76. Arnold, W. M. Monitoring of biological cell collection by dielectric spectroscopy. *Conference on Electrical Insulation and Dielectric Phenomena, 2001 Annual Report* **2001**, 40-44.
77. Cannizzaro, C.; Gugerli, R.; Marison, I.; von Stockar, U. On-line biomass monitoring of CHO perfusion culture with scanning dielectric spectroscopy. *Biotechnol. Bioeng.* **2003**, *84*, 597-610.
78. Davey, C. L.; Davey, H. M.; Kell, D. B.; Todd, R. W. Introduction to the Dielectric Estimation of Cellular Biomass in Real-Time, with Special Emphasis on Measurements at High-Volume Fractions. *Anal. Chim. Acta* **1993**, *279*, 155-161.
79. Esteban, G.; Luong, B.; Ossart, F. US2008/0312843A1, 2008.
80. Markx, G. H.; Davey, C. L.; Kell, D. B. To what Extent is the Magnitude of the Cole-Cole-Alpha of the Beta-Dielectric Dispersion of Cell-Suspensions Explicable in Terms of the Cell-Size Distribution. *Bioelectrochem. Bioenerget.* **1991**, *25*, 195-211.
81. Guan, Y.; Kemp, R. In *The Viable Cell Monitor: A Dielectric spectroscope for Growth and Metabolic Studies of Animal Cells on Macroporous Beads*; New Developments and New Applications in Animal Cell Technology; Springer Netherlands: 2002; pp 321-328.
82. Ehret, R.; Baumann, W.; Brischwein, M.; Schwinde, A.; Wolf, B. On-line control of cellular adhesion with impedance measurements using interdigitated electrode structures. *Med. Biol. Eng. Comput.* **1998**, *36*, 365-370.
83. Ron, A.; Fishelson, N.; Croitoriu, N.; Benayahu, D.; Shacham-Diamand, Y. Theoretical examination of aggregation effect on the dielectric characteristics of spherical cellular suspension. *Biophys. Chem.* **2009**, *140*, 39-50.
84. Fricke, H. A Mathematical Treatment of the Electric Conductivity and Capacity of Disperse Systems ii. The Capacity of a Suspension of Conducting Spheroids Surrounded by a Non-Conducting Membrane for a Current of Low Frequency. *Phys. Rev.* **1925**, *26*, 678.
85. Fricke, H. The Complex Conductivity of a Suspension of Stratified Particles of Spherical Or Cylindrical Form. *J. Phys. Chem.* **1955**, *59*, 168-170.
86. Fricke, H. The Electric Permittivity of a Dilute Suspension of Membrane-Covered Ellipsoids. *J. Appl. Phys.* **1953**, *24*, 644-646.

87. Schwan, H. P. Electrical properties of tissue and cell suspensions. *Adv Biol Med Phys* **1957**, 14-209.
88. Opel, C. F.; Li, J.; Amanullah, A. Quantitative Modeling of Viable Cell Density, Cell Size, Intracellular Conductivity, and Membrane Capacitance in Batch and Fed-Batch CHO Processes Using Dielectric Spectroscopy. *Biotechnol. Prog.* **2010**, *26*, 1187-1199.
89. Höber, R. Eine Methode, die elektrische Leitfähigkeit im Innern von Zellen zu messen. *Pflugers Arch - Eur J Physiol* **1910**, *133*, 237-253.
90. Hildebrandt, C.; Bueth, H.; Cho, S.; Impidjati; Thielecke, H. Detection of the osteogenic differentiation of mesenchymal stem cells in 2D and 3D cultures by electrochemical impedance spectroscopy. *J. Biotechnol.* **2010**, *148*, 83-90.
91. Ceriotti, L.; Ponti, J.; Colpo, P.; Sabbioni, E.; Rossi, F. Assessment of cytotoxicity by impedance spectroscopy. *Biosens. Bioelectron.* **2007**, *22*, 3057-3063.
92. Ehret, R.; Baumann, W.; Brischwein, M.; Schwinde, A.; Stegbauer, K.; Wolf, B. Monitoring of cellular behaviour by impedance measurements on interdigitated electrode structures. *Biosens. Bioelectron.* **1997**, *12*, 29-41.
93. Guo, M. L.; Chen, J. H.; Yun, X. B.; Chen, K.; Nie, L. H.; Yao, S. Z. Monitoring of cell growth and assessment of cytotoxicity using electrochemical impedance spectroscopy. *Biochimica Et Biophysica Acta-General Subjects* **2006**, *1760*, 432-439.
94. Qiu, Y.; Liao, R.; Zhang, X. Real-time monitoring primary cardiomyocyte adhesion based on electrochemical impedance spectroscopy and electrical cell-substrate impedance sensing. *Anal. Chem.* **2008**, *80*, 990-996.
95. Rahman, A. R. A.; Register, J.; Vuppala, G.; Bhansali, S. Cell culture monitoring by impedance mapping using a multielectrode scanning impedance spectroscopy system (CellMap). *Physiol. Meas.* **2008**, *29*, S227-S239.
96. Yu, N. C.; Atienza, J. M.; Bernard, J.; Blanc, S.; Zhu, J.; Wang, X. B.; Xu, X.; Abassi, Y. A. Real-time monitoring of morphological changes in living cells by electronic cell sensor arrays: An approach to study G protein-coupled receptors. *Anal. Chem.* **2006**, *78*, 35-43.
97. Ceriotti, L.; Ponti, J.; Broggi, F.; Kob, A.; Drechsler, S.; Thedinga, E.; Colpo, P.; Sabbioni, E.; Ehret, R.; Rossi, F. Real-time assessment of cytotoxicity by impedance measurement on a 96-well plate. *Sensors and Actuators B-Chemical* **2007**, *123*, 769-778.
98. Lee, R. M.; Choi, H.; Shin, J.; Kim, K.; Yoo, K. Distinguishing between apoptosis and necrosis using a capacitance sensor. *Biosens. Bioelectron.* **2009**, *24*, 2586-2591.

99. Liu, Q.; Yu, J.; Xiao, L.; On Tang, J. C.; Zhang, Y.; Wang, P.; Yang, M. Impedance studies of bio-behavior and chemosensitivity of cancer cells by micro-electrode arrays. *Biosens. Bioelectron.* **2009**, *24*, 1305-1310.
100. Malleo, D.; Nevill, J. T.; Lee, L. P.; Morgan, H. Continuous differential impedance spectroscopy of single cells. *Microfluidics and Nanofluidics* **2010**, *9*, 191-198.
101. Huang, X.; Greve, D. W.; Nguyen, D. D.; Domach, M. M. Impedance based biosensor array for monitoring mammalian cell behavior. *Sensors 2003, Proceedings of IEEE* **2003**, *1*, 304-309.
102. Dziong, D.; Bagnaninchi, P.; Kearney, R. E.; Tabrizian, M. In *In A Highly Responsive System for On-line in vitro Assessment of Tissue Growth within MicroPorous Polymer Scaffolds*; 2006; , pp 1043-1046.
103. Bragos, R.; Sarro, E.; Fontova, A.; Soley, A.; Cairo, J.; Bayes-Genis, A.; Resell, J. In *In Four Versus Two-Electrode Measurement Strategies for Cell Growing and Differentiation Monitoring Using Electrical Impedance Spectroscopy*; 2006; , pp 2106-2109.
104. Miller, J. H.; Warmflash, D. Martian Soil Biosensors Based on Dielectric Spectroscopy. *Institute for Space Systems Operations Annual Report* **2006**, 21-26.
105. Blute, T.; Gillies, R. J.; Dale, B. E. Cell-Density Measurements in Hollow Fiber Bioreactors. *Biotechnol. Prog.* **1988**, *4*, 202-209.
106. Ansorge, S.; Esteban, G.; Ghommidh, C.; Schmid, G. In *Monitoring Nutrient Limitations by On-line Capacitance Measurements in Batch & Fed-batch CHO Fermentations*; Smith, R., Ed.; Proceedings of the 19th ESACT Meeting: Cell Technology for Cell Products; Springer Netherlands: 2007; pp 723-726.
107. Rourou, S.; Gaumon, S.; Kallel, H. On-Line Monitoring of Vero Cells Cultures During the Growth and Rabies Virus Process Using Biomass Spectrometer. *Cells and Culture: ESACT Proceedings* **2010**, *4*, 829-832.
108. FOGALE nanotech Inc. In *Biomass System User Manual V02*; 2009; .
109. YSI Incorporated In *2700 Select Biochemistry Analyzer User's Manual*; Yellow Springs, Ohio, 2007; .
110. Sweeny, D. J.; Diasio, R. In *The isolated hepatocyte and isolated perfused liver as models for studying drug and chemical-induced hepatotoxicity*; Meeks, R. G., Harrison, S. D. and Bull, R. J., Eds.; Hepatotoxicology; 1991; pp 215-240.
111. Altman, S. A.; Randers, L.; Rao, G. Comparison of trypan blue dye exclusion and fluorometric assays for mammalian cell viability determinations. *Biotechnol. Prog.* **1993**, *9*, 671-674.

112. Morera, C.; Villanueva, M. Heat treatment and viability assessment by Evans blue in cultured *Symbiodinium kawagutii* cells. *World Journal of Microbiology and Biotechnology* **2009**, *25*, 1125-1128.
113. Jarvis, D. L.; Garcia, A. Biosynthesis and Processing of the Autographa-Californica Nuclear Polyhedrosis-Virus Gp64 Protein. *Virology* **1994**, *205*, 300-313.
114. Mulvania, T.; Hayes, B.; Hedin, D. A Flow Cytometric Assay for Rapid, Accurate Determination of Baculovirus Titers. *BioProcess J* **2004**, *3*, 47-53.
115. Pettman, G. R. In *Analysis of Baculovirus Infected Sf9 Cells Using Flow Cytometry*; Bernard, A., Griffiths, B., Noé, W. and Wurm, F., Eds.; Proceedings of the 16th ESACT Meeting: Animal cell technology: products from cells, cells as products; Springer: 2002; pp 363-366.
116. eBioscience, I. Technical datasheet Anti-Baculovirus Envelope gp64 Protein PE (12-6991). **2009**.
117. Johansson, U. In *Immunological Studies of Human Cells*; Macey, M. G., Ed.; Flow Cytometry: Principles and Applications; Humana Press: 2007; pp 181-208.
118. Hensler, W.; Singh, V.; Agathos, S. N. Sf9 Insect-Cell Growth and Beta-Galactosidase Production in Serum and Serum-Free Media. *Biochemical Engineering VIII* **1994**, *745*, 149-166.
119. King, G. A.; Daugulis, A. J.; Faulkner, P.; Goosen, M. F. A. Recombinant Beta-Galactosidase Production in Serum-Free Medium by Insect Cells in a 14-L Airlift Bioreactor. *Biotechnol. Prog.* **1992**, *8*, 567-571.
120. Rhiel, M.; MitchellLogean, C. M.; Murhammer, D. W. Comparison of *Trichoplusia ni* BTI-Tn-5B1-4 (High Five(TM)) and *Spodoptera frugiperda* Sf-9 insect cell line metabolism in suspension cultures. *Biotechnol. Bioeng.* **1997**, *55*, 909-920.
121. SAFC Biosciences, I. Technical Bulletin EX-CELL™ 420 EX-CELL™ 420 Frequently Asked Questions. **2006**.
122. Mendonca, R. Z.; Palomares, L. A.; Ramirez, O. T. An insight into insect cell metabolism through selective nutrient manipulation. *J. Biotechnol.* **1999**, *72*, 61-75.
123. Chiou, T. W.; Hsieh, Y. C.; Ho, C. S. High density culture of insect cells using rational medium design and feeding strategy. *Bioprocess Eng.* **2000**, *22*, 483-491.
124. Drews, M.; Paalme, T.; Vilu, R. The Growth and Nutrient Utilization of the Insect-Cell Line *Spodoptera-Frugiperda* Sf9 in Batch and Continuous-Culture. *J. Biotechnol.* **1995**, *40*, 187-198.

125. Harris, C. M.; Todd, R. W.; Bungard, S. J.; Lovitt, R. W.; Morris, J. G.; Kell, D. B. Dielectric Permittivity of Microbial Suspensions at Radio Frequencies - a Novel Method for the Real-Time Estimation of Microbial Biomass. *Enzyme Microb. Technol.* **1987**, *9*, 181-186.
126. Junker, B. H.; Wang, H. Y. Bioprocess monitoring and computer control: Key roots of the current PAT initiative. *Biotechnol. Bioeng.* **2006**, *95*, 226-261.
127. Esteban, G.; Ansorge, S.; Schmid, G. On-Line Viable Cell Density and Physiological States Monitoring by Dielectric Spectroscopy Sf9 Growth and Infection Process. , *2011*.
128. Dabros, M.; Dennewald, D.; Currie, D. J.; Lee, M. H.; Todd, R. W.; Marison, I. W.; von Stockar, U. Cole-Cole, linear and multivariate modeling of capacitance data for on-line monitoring of biomass. *Bioprocess and Biosystems Engineering* **2009**, *32*, 161-173.
129. Ivorra, A.; Genesca, M.; Sola, A.; Palacios, L.; Villa, R.; Hotter, G.; Aguilo, J. Bioimpedance dispersion width as a parameter to monitor living tissues. *Physiol. Meas.* **2005**, *26*, S165-S173.
130. Kell, D. B.; Harris, C. M. On the Dielectrically Observable Consequences of the Diffusional Motions of Lipids and Proteins in Membranes .1. Theory and Overview. *European Biophysics Journal with Biophysics Letters* **1985**, *12*, 181-197.
131. Ryabov, Y. E.; Feldman, Y. Novel approach to the analysis of the non-Debye dielectric spectrum broadening. *Physica A-Statistical Mechanics and its Applications* **2002**, *314*, 370-378.
132. Asami, K.; Hanai, T.; Koizumi, N. Dielectric Properties of Yeast-Cells. *J. Membr. Biol.* **1976**, *28*, 169-180.
133. Soley, A.; Lecina, M.; Gamez, X.; Cairo, J. J.; Riu, P.; Rosell, X.; Bragos, R.; Godia, F. On-line monitoring of yeast cell growth by impedance spectroscopy. *J. Biotechnol.* **2005**, *118*, 398-405.
134. Chin, S.; Hughes, M. P.; Coley, H. M.; Labeed, F. H. Rapid assessment of early biophysical changes in K562 cells during apoptosis determined using dielectrophoresis. *International Journal of Nanomedicine* **2006**, *1*, 333-337.
135. Dopp, E.; Jonas, L.; Nebe, B.; Budde, A.; Knippel, E. Dielectric changes in membrane properties and cell interiors of human mesothelial cells in vitro after crocidolite asbestos exposure. *Environ. Health Perspect.* **2000**, *108*, 153-158.
136. Gimsa, J.; Schnelle, T.; Zechel, G.; Glaser, R. Dielectric-Spectroscopy of Human Erythrocytes - Investigations Under the Influence of Nystatin. *Biophys. J.* **1994**, *66*, 1244-1253.

137. Hölzel, R. Nystatin-induced changes in yeast monitored by time-resolved automated single cell electrorotation. *Biochimica et Biophysica Acta (BBA) - General Subjects* **1998**, 1425, 311-318.
138. Labeed, F. H.; Coley, H. M.; Hughes, M. P. Differences in the biophysical properties of membrane and cytoplasm of apoptotic cells revealed using dielectrophoresis. *Biochimica Et Biophysica Acta-General Subjects* **2006**, 1760, 922-929.
139. Archer, S.; Morgan, H.; Rixon, F. J. Electrorotation studies of baby hamster kidney fibroblasts infected with herpes simplex virus type 1. *Biophys. J.* **1999**, 76, 2833-2842.
140. Kurschner, M.; Nielsen, K.; Andersen, C.; Sukhorukov, V. L.; Schenk, W. A.; Benz, R.; Zimmermann, U. Interaction of lipophilic ions with the plasma membrane of mammalian cells studied by electrorotation. *Biophys. J.* **1998**, 74, 3031-3043.
141. Janakiraman, V.; Forrest, W. F.; Chow, B.; Seshagiri, S. A rapid method for estimation of baculovirus titer based on viable cell size. *J. Virol. Methods* **2006**, 132, 48-58.
142. Palomares, L. A.; Pedroza, J. C.; Ramirez, O. T. Cell size as a tool to predict the production of recombinant protein by the insect-cell baculovirus expression system. *Biotechnol. Lett.* **2001**, 23, 359-364.
143. Eichmeyer, M.; Nitzel, G.; Schaeffer, M. 7,833,707, 2010.
144. Bernal, V.; Carinhas, N.; Yokomizo, A. Y.; Carrondo, M. J. T.; Alves, P. M. Cell Density Effect in the Baculovirus-insect Cells System: A Quantitative Analysis of Energetic Metabolism. *Biotechnol. Bioeng.* **2009**, 104, 162-180.
145. Ikonomou, L.; Schneider, Y. J.; Agathos, S. N. Insect cell culture for industrial production of recombinant proteins. *Appl. Microbiol. Biotechnol.* **2003**, 62, 1-20.
146. Dee, K. U.; Shuler, M. L. Optimization of an assay for baculovirus titer and design of regimens for the synchronous infection of insect cells. *Biotechnol. Prog.* **1997**, 13, 14-24.
147. Licari, P.; Bailey, J. E. Modeling the Population-Dynamics of Baculovirus-Infected Insect Cells - Optimizing Infection Strategies for Enhanced Recombinant Protein Yields. *Biotechnol. Bioeng.* **1992**, 39, 432-441.
148. Palomares, L. A.; Estrada-Mondaca, S.; Ramirez, O. T. In *Principles and Applications of the Insect Cell-Baculovirus Expression Vector System*; Ozturk, S., Hu, W., Eds.; CRC Press: 2006; pp 627-692.
149. Mena, J. A.; Ramirez, O. T.; Palomares, L. A. Population kinetics during simultaneous infection of insect cells with two different recombinant baculoviruses for the production of rotavirus-like particles. *Bmc Biotechnology* **2007**, 7, 39.

150. Enden, G.; Zhang, Y. H.; Merchuk, J. C. A model of the dynamics of insect cell infection at low multiplicity of infection. *J. Theor. Biol.* **2005**, *237*, 257-264.
151. Hu, Y. C.; Bentley, W. E. Effect of MOI ratio on the composition and yield of chimeric infectious bursal disease virus-like particles by baculovirus co-infection: Deterministic predictions and experimental results. *Biotechnol. Bioeng.* **2001**, *75*, 104-119.
152. Roldao, A.; Carrondo, M. J. T.; Alves, P. M.; Oliveira, R. Stochastic simulation of protein expression in the baculovirus/insect cells system. *Comput. Chem. Eng.* **2008**, *32*, 68-77.
153. Zhang, Y. H.; Merchuk, J. C. A mathematical model of baculovirus infection on insect cells at low multiplicity of infection. *Acta Biochimica Et Biophysica Sinica* **2004**, *36*, 729-740.
154. Liebman, J. M.; LaSala, D.; Wang, W.; Steed, P. M. When less is more: enhanced baculovirus production of recombinant proteins at very low multiplicities of infection. *Biotechniques* **1999**, *26*, 36-42.
155. Huang, C.; Chen, A.; Wang, L.; Guo, M.; Yu, J. Electrokinetic measurements of dielectric properties of membrane for apoptotic HL-60 cells on chip-based device. *Biomed. Microdevices* **2007**, *9*, 335-343.
156. Pethig, R.; Talary, M. S. Dielectrophoretic detection of membrane morphology changes in Jurkat T-cells undergoing etoposide-induced apoptosis. *Iet Nanobiotechnology* **2007**, *1*, 2-9.
157. Wang, X. J.; Becker, F. F.; Gascoyne, P. R. C. Membrane dielectric changes indicate induced apoptosis in HL-60 cells more sensitively than surface phosphatidylserine expression or DNA fragmentation. *Biochimica Et Biophysica Acta-Biomembranes* **2002**, *1564*, 412-420.
158. Bonincontro, A.; Di Ilio, V.; Pedata, O.; Risuleo, G. Dielectric properties of the plasma membrane of cultured murine fibroblasts treated with a nonterpenoid extract of *Azadirachta indica* seeds. *J. Membr. Biol.* **2007**, *215*, 75-79.
159. Bai, W.; Zhao, K.; Asami, K. Effects of copper on dielectric properties of E. coli cells. *Colloids and Surfaces B-Biointerfaces* **2007**, *58*, 105-115.
160. Sandhu, K. S.; Naciri, M.; Al-Rubeai, M. Prediction of recombinant protein production in an insect cell-baculovirus system using a flow cytometric technique. *J. Immunol. Methods* **2007**, *325*, 104-113.
161. Ansorge, S.; Henry, O.; Aucoin, M.; Voyer, R.; Carvell, J. P.; Kamen, A. Monitoring the Cell Size Distribution of Mammalian Cell Cultures Using On-Line Capacitance Measurements. *Cells and Culture: ESACT Proceedings* **2010**, *4*, 853-859.

162. Wold, S.; Sjoström, M.; Eriksson, L. PLS-regression: a basic tool of chemometrics. *Chemometrics Intellig. Lab. Syst.* **2001**, *58*, 109-130.
163. Benslimane, C.; Elias, C. B.; Hawari, J.; Kamen, A. Insights into the central metabolism of *Spodoptera frugiperda* (Sf-9) and *Trichoplusia ni* BTI-Tn-5B1-4 (Tn-5) insect cells by radiolabeling studies. *Biotechnol. Prog.* **2005**, *21*, 78-86.
164. Wang, M. Y.; Kwong, S.; Bentley, W. E. Effects of Oxygen Glucose Glutamine Feeding on Insect-Cell Baculovirus Protein Expression - a Study on Epoxide Hydrolase Production. *Biotechnol. Prog.* **1993**, *9*, 355-361.
165. Nguyen, B.; Jarnagin, K.; Williams, S.; Chan, H.; Barnett, J. Fed-Batch Culture of Insect Cells - a Method to Increase the Yield of Recombinant Human Nerve Growth-Factor (Rhngf) in the Baculovirus Expression System. *J. Biotechnol.* **1993**, *31*, 205-217.
166. Caron, A. W.; Tom, R. L.; Kamen, A. A.; Massie, B. Baculovirus Expression System Scaleup by Perfusion of High-Density Sf-9 Cell-Cultures. *Biotechnol. Bioeng.* **1994**, *43*, 881-891.
167. Deutschmann, S. M.; Jager, V. Optimization of the Growth-Conditions of Sf21 Insect Cells for High-Density Perfusion Culture in Stirred-Tank Bioreactors. *Enzyme Microb. Technol.* **1994**, *16*, 506-512.
168. Zhang, J. L.; Kalogerakis, N.; Behie, L. A.; Iatrou, K. A 2-Stage Bioreactor System for the Production of Recombinant Proteins using a Genetically-Engineered Baculovirus-Insect Cell System. *Biotechnol. Bioeng.* **1993**, *42*, 357-366.
169. Sokolenko, S.; Cheng, Y.; Aucoin, M. G. Getting More from Cell Size Distributions: Establishing More Accurate Biovolumes by Estimating Viable Cell Populations. *Biotechnol. Prog.* **2010**, *26*, 1787-1795.

Appendix A - Composition of PCV2 ORF2 ELISA Buffers

Carbonate Coating Buffer, 0.05 M, pH 9.6

2.93 g NaHCO₃
1.59 g Na₂CO₃
100 ml Deionized Water

PCV2 10x D-PBS, pH 7.3

80.0 g NaCl
11.5 g Na₂HPO₄
2.0 g KCl
2.0 g KH₂HPO₄
QS to 1000 ml with Deionized Water

Blocking Solution, pH 7.3

50.0 g Non-Fat Dry Milk
0.5 ml Tween 20
100 ml 10x D-PBS, pH 7.3
QS to 1000 ml with Deionized Water

Wash/Diluent Solution, pH 7.3

1000 ml 10x D-PBS, pH 7.3
5 ml Tween 20
8995 ml Deionized Water

Appendix B - Precultures – Raw Data

Table B.1. Raw data precultures – off-line analyses.

Preculture #	Time Post Planting in h	pH	Total Cell Density in cells ml ⁻¹	Viable Cell Density in cells ml ⁻¹	Viability in %	Mean Average Cell Diameter in µm	Mean Viable Cell Diameter in µm	D-glucose in mmol L ⁻¹	L-lactate in mmol L ⁻¹	L-glutamine in mmol L ⁻¹	L-glutamate in mmol L ⁻¹
1	0.89	6.41	5.1E+05	4.7E+05	92.3	17.4	17.8	32.64	1.12	5.24	6.64
	27.95	6.37	1.2E+06	1.1E+06	96.0	18.0	18.2	31.92	1.23	4.71	7.76
	49.18	6.27	2.2E+06	2.1E+06	97.2	18.2	18.3	30.03	1.90	3.31	8.35
2	2.01	6.39	4.8E+05	4.5E+05	93.6	17.7	17.8	32.42	1.13	5.68	7.01
	27.48	6.37	1.0E+06	9.8E+05	96.8	18.5	18.7	31.86	1.33	4.97	8.01
	49.39	6.25	2.2E+06	2.1E+06	96.9	18.2	18.3	29.81	2.00	3.51	8.20
3	0.76	6.53	4.6E+05	4.4E+05	95.8	17.9	18.0	31.42	1.07	5.46	7.25
	25.23	6.48	8.2E+05	7.9E+05	96.2	18.3	18.5	31.25	1.12	5.13	7.40
	49.80	6.32	2.0E+06	1.9E+06	96.9	18.2	18.3	30.03	1.65	3.33	8.19
	53.70	6.29	2.4E+06	2.3E+06	97.0	18.2	18.3	28.70	1.70	2.88	8.41
4	0.89	6.51	4.7E+05	4.5E+05	94.8	17.2	17.4	31.53	1.12	5.48	6.85
	25.33	6.46	8.9E+05	8.4E+05	94.6	18.3	18.6	31.08	1.14	5.11	7.36
	50.68	6.31	1.9E+06	1.8E+06	95.7	18.3	18.5	29.86	1.77	3.80	8.00
	53.71	6.27	2.3E+06	2.3E+06	96.8	18.3	18.5	29.09	1.89	3.29	8.18
5	0.53	6.51	4.6E+05	4.3E+05	94.4	17.2	17.3	31.75	1.11	5.81	6.77
	26.01	6.42	1.0E+06	9.9E+05	96.5	17.9	18.1	31.92	1.15	5.11	7.70
	47.20	6.27	1.8E+06	1.7E+06	96.5	17.9	18.1	29.20	1.55	2.78	8.63
6	0.57	6.49	4.4E+05	4.0E+05	92.0	16.9	17.3	32.14	1.14	5.80	6.96
	26.15	6.43	1.2E+06	1.2E+06	95.5	17.9	18.1	31.31	1.17	4.80	7.49
	47.34	6.28	2.1E+06	2.0E+06	96.5	17.9	18.0	29.31	1.85	2.60	8.68
7	0.59	6.53	3.6E+05	3.3E+05	92.3	17.5	17.9	32.58	1.13	5.83	7.14
	30.56	6.45	6.9E+05	6.6E+05	94.8	18.0	18.3	32.75	1.22	4.85	7.67
	52.47	6.30	1.7E+06	1.6E+06	96.6	17.9	18.0	30.86	1.84	3.43	8.10
8	0.71	6.52	5.3E+05	4.8E+05	90.2	17.5	17.9	31.58	1.14	5.62	7.24
	30.64	6.41	9.7E+05	8.8E+05	91.7	17.6	18.0	31.75	1.33	4.18	7.82
	52.73	6.23	2.2E+06	2.1E+06	96.6	17.8	18.0	28.75	2.23	2.53	8.52
9	0.58	6.48	5.0E+05	4.7E+05	93.4	16.8	17.1	32.47	1.10	5.40	7.25
	25.50	6.41	8.3E+05	7.8E+05	93.9	17.7	17.9	32.53	1.08	4.44	7.62
	50.74	6.25	2.2E+06	2.2E+06	96.5	17.7	17.8	30.08	1.83	2.57	8.71
10	0.69	6.55	3.9E+05	3.6E+05	90.3	17.9	18.3	32.53	0.98	5.40	7.13
	25.67	6.53	9.8E+05	9.1E+05	93.7	17.8	18.1	32.19	1.05	4.44	7.79
	50.92	6.39	2.3E+06	2.2E+06	96.0	18.0	18.1	29.70	1.79	2.71	8.47
11	0.72	6.50	3.7E+05	3.3E+05	87.8	16.8	17.3	33.86	1.11	4.79	7.46
	23.05	6.44	5.7E+05	5.4E+05	94.4	17.6	17.9	32.69	1.10	3.94	7.64
	48.95	6.29	1.6E+06	1.5E+06	95.2	17.8	18.0	30.36	1.62	2.76	8.37
	55.46	6.24	2.1E+06	2.0E+06	95.1	18.0	18.2	30.20	1.90	2.12	8.51
12	0.60	6.55	4.3E+05	4.0E+05	92.9	17.5	17.9	33.58	1.07	4.05	7.19
	22.32	6.47	7.3E+05	7.0E+05	95.5	17.8	17.9	33.03	1.09	3.49	7.33
	48.67	6.29	1.7E+06	1.6E+06	96.2	18.0	18.1	31.42	1.72	2.02	7.98
	53.81	6.24	2.1E+06	2.0E+06	95.2	18.0	18.2	31.19	1.95	1.72	8.34
13	0.74	6.51	5.3E+05	5.0E+05	92.9	17.7	17.9	32.92	1.09	4.06	7.15
	22.45	6.43	9.2E+05	8.7E+05	95.2	18.0	18.2	33.19	1.27	3.46	7.78
	48.81	6.25	1.9E+06	1.8E+06	96.5	18.1	18.2	31.19	2.21	1.77	7.98
	53.95	6.21	2.4E+06	2.3E+06	95.8	17.9	18.1	31.03	2.39	1.41	8.15

Table B.2. Raw data precultures – dielectric spectroscopy.

Preculture #	Time Post Planting in h	Biomass (1000 kHz) in pF cm ⁻¹	Suspension Conductivity in mS cm ⁻¹	Δε in pF cm ⁻¹	f _ε in kHz	alpha in -	C(300kHz) in pF	C(373kHz) in pF	C(465kHz) in pF	C(578kHz) in pF	C(720kHz) in pF	C(897kHz) in pF	C(1117kHz) in pF	C(1391kHz) in pF	C(1732kHz) in pF	C(2156kHz) in pF	C(2684kHz) in pF	C(3342kHz) in pF	C(4161kHz) in pF	C(5181kHz) in pF	C(6451kHz) in pF	C(8031kHz) in pF	C(10000kHz) in pF
1	0.89	1.04	15.38	3.10	760	0.102	3.77	3.27	2.93	2.54	2.16	1.88	1.59	1.35	1.14	0.98	0.85	0.75	0.69	0.61	0.56	0.51	0.47
	27.95	2.19	15.54	7.62	677	0.099	6.87	6.27	5.61	4.92	4.22	3.57	2.97	2.45	2.01	1.60	1.37	1.17	1.04	0.85	0.82	0.77	0.69
	49.18	4.38	15.33	19.14	554	0.104	14.45	12.90	11.16	9.42	7.77	6.30	5.00	3.88	2.95	2.23	1.68	1.27	0.98	0.81	0.58	0.44	0.35
2	2.01	0.69	15.44	2.22	702	0.100	2.43	2.34	2.13	1.96	1.75	1.56	1.38	1.25	1.13	0.98	0.90	0.86	0.82	0.77	0.75	0.74	0.69
	27.48	1.77	15.59	7.01	606	0.094	6.06	5.57	4.93	4.32	3.69	3.13	2.60	2.19	1.81	1.43	1.25	1.12	1.00	0.90	0.87	0.84	0.79
	49.39	3.79	15.45	15.80	590	0.088	13.57	11.89	10.31	8.66	7.14	5.79	4.57	3.56	2.84	1.99	1.61	1.21	0.99	0.89	0.70	0.59	0.53
3	0.76	0.84	15.32	2.57	768	0.100	2.37	2.14	1.87	1.63	1.38	1.14	0.93	0.73	0.57	0.43	0.32	0.21	0.17	0.12	0.09	0.07	0.05
	25.23	1.92	15.24	6.24	720	0.099	6.54	5.71	4.89	4.20	3.53	2.91	2.37	1.91	1.52	1.15	0.93	0.75	0.60	0.44	0.42	0.39	0.33
	49.80	4.32	15.27	16.46	627	0.098	18.05	14.99	12.36	10.11	8.17	6.46	5.06	3.86	2.89	2.06	1.52	1.10	0.77	0.54	0.38	0.27	0.19
4	53.70	4.90	15.27	18.93	614	0.099	20.45	16.95	13.98	11.38	9.13	7.23	5.62	4.28	3.19	2.26	1.66	1.16	0.81	0.57	0.36	0.23	0.14
	0.89	0.80	15.45	2.63	704	0.100	2.11	1.99	1.73	1.53	1.29	1.08	0.89	0.70	0.51	0.39	0.31	0.25	0.18	0.12	0.11	0.10	0.07
	25.33	1.80	15.36	6.57	658	0.094	5.02	4.67	4.17	3.67	3.10	2.56	2.11	1.68	1.29	0.92	0.72	0.60	0.45	0.34	0.31	0.30	0.27
5	50.68	3.20	15.39	16.16	521	0.085	10.75	9.75	8.35	6.98	5.68	4.49	3.45	2.57	1.87	1.18	0.85	0.55	0.34	0.19	0.12	0.07	0.03
	53.71	3.55	15.40	15.88	568	0.077	12.18	10.80	9.26	7.70	6.23	4.96	3.82	2.83	1.95	1.30	0.94	0.61	0.37	0.22	0.12	0.07	0.04
	0.53	0.97	15.32	3.24	680	0.102	2.96	2.59	2.22	1.85	1.53	1.22	0.97	0.73	0.55	0.39	0.27	0.19	0.10	0.07	0.01	-0.02	-0.04
6	26.01	2.08	15.34	7.71	634	0.100	7.53	6.40	5.40	4.48	3.65	2.91	2.28	1.75	1.31	0.91	0.69	0.47	0.32	0.21	0.13	0.08	0.04
	47.20	4.33	15.31	16.78	609	0.104	15.77	13.47	11.36	9.44	7.67	6.15	4.85	3.72	2.82	2.01	1.52	1.08	0.76	0.52	0.37	0.26	0.17
	0.57	1.23	15.38	4.06	696	0.102	3.63	3.27	2.84	2.43	2.07	1.68	1.38	1.10	0.81	0.65	0.51	0.36	0.29	0.22	0.16	0.12	0.10
7	26.15	2.10	15.41	7.69	651	0.096	6.02	5.50	4.88	4.22	3.56	2.90	2.35	1.86	1.34	1.03	0.80	0.58	0.45	0.33	0.25	0.21	0.18
	47.34	3.51	15.39	13.15	639	0.092	10.04	9.25	8.16	7.06	5.96	4.85	3.90	3.06	2.23	1.67	1.30	0.96	0.73	0.54	0.42	0.34	0.28
	0.59	0.59	15.21	2.21	635	0.100	1.68	1.51	1.29	1.11	0.92	0.73	0.55	0.41	0.29	0.19	0.12	0.06	0.02	0.01	-0.03	-0.05	-0.06
8	30.56	1.26	15.27	4.68	648	0.097	3.35	3.08	2.77	2.38	2.03	1.64	1.29	0.99	0.73	0.46	0.37	0.24	0.14	0.08	0.05	0.03	0.01
	52.47	2.95	15.24	10.92	644	0.095	8.42	7.63	6.75	5.76	4.81	3.91	3.08	2.37	1.75	1.20	0.91	0.60	0.40	0.26	0.16	0.09	0.04
	0.71	0.80	15.35	2.73	684	0.100	2.38	2.13	1.87	1.59	1.35	1.10	0.88	0.70	0.55	0.40	0.31	0.22	0.16	0.12	0.10	0.07	0.06
9	30.64	1.65	15.35	6.79	606	0.096	4.54	4.23	3.81	3.31	2.75	2.23	1.76	1.38	1.06	0.68	0.50	0.34	0.24	0.16	0.13	0.08	0.06
	52.73	3.74	15.32	14.58	633	0.084	11.59	10.44	9.12	7.75	6.44	5.19	4.05	3.11	2.29	1.56	1.15	0.78	0.53	0.37	0.26	0.17	0.12
	0.58	1.14	15.27	3.20	788	0.101	3.90	3.24	2.77	2.27	1.93	1.53	1.20	1.00	0.74	0.54	0.43	0.32	0.23	0.15	0.10	0.06	0.04
10	25.50	0.98	15.35	2.13	1087	0.098	0.36	0.71	0.92	0.94	0.95	0.86	0.74	0.61	0.40	0.25	0.19	0.07	-0.01	-0.08	-0.08	-0.11	-0.13
	50.74	4.54	15.25	18.19	608	0.094	17.90	14.97	12.44	10.14	8.14	6.38	4.86	3.61	2.54	1.67	1.19	0.92	0.35	0.10	-0.04	-0.11	-0.18
	0.69	0.92	15.41	2.77	770	0.101	2.62	2.32	2.06	1.73	1.46	1.19	0.97	0.75	0.64	0.43	0.31	0.22	0.15	0.10	0.06	0.03	0.02
11	25.67	1.77	15.40	5.85	708	0.098	5.29	4.63	4.09	3.49	2.91	2.38	1.89	1.46	1.13	0.78	0.59	0.41	0.29	0.19	0.13	0.09	0.04
	50.92	3.85	15.37	13.91	660	0.094	12.02	10.59	9.23	7.88	6.50	5.25	4.15	3.19	2.40	1.69	1.25	0.87	0.60	0.42	0.26	0.15	0.09
	0.72	0.69	15.31	2.29	710	0.100	2.35	2.06	1.77	1.53	1.30	1.05	0.87	0.70	0.57	0.44	0.36	0.28	0.24	0.17	0.17	0.15	0.13
12	23.05	1.36	15.41	4.50	706	0.100	4.35	3.80	3.28	2.81	2.33	1.91	1.53	1.22	0.94	0.65	0.53	0.38	0.29	0.20	0.17	0.13	0.09
	48.95	3.18	15.41	11.73	638	0.102	10.10	8.89	7.63	6.44	5.30	4.28	3.39	2.60	1.93	1.33	1.02	0.69	0.46	0.31	0.18	0.09	0.02
	55.46	4.02	15.41	14.41	656	0.102	12.60	11.12	9.58	8.15	6.74	5.45	4.35	3.37	2.52	1.78	1.36	0.95	0.67	0.46	0.29	0.18	0.08
13	0.60	0.96	15.37	3.00	733	0.101	2.81	2.50	2.17	1.87	1.58	1.28	1.04	0.82	0.64	0.48	0.37	0.26	0.19	0.14	0.10	0.07	0.05
	22.32	1.63	15.36	5.86	655	0.100	5.68	4.86	4.12	3.41	2.80	2.24	1.75	1.34	1.00	0.69	0.51	0.34	0.21	0.14	0.07	0.03	0.00
	48.67	4.39	15.33	17.12	608	0.104	15.75	13.54	11.44	9.50	7.77	6.23	4.89	3.76	2.83	2.02	1.52	1.08	0.75	0.52	0.35	0.24	0.16
13	53.81	5.27	15.32	20.78	604	0.103	19.14	16.37	13.84	11.50	9.39	7.47	5.85	4.50	3.38	2.41	1.82	1.28	0.88	0.61	0.40	0.26	0.16
	0.74	1.44	15.36	3.02	1009	0.112	5.70	5.04	4.47	3.97	3.55	3.18	2.85	2.59	2.37	2.19	2.04	1.93	1.83	1.72	1.61	1.49	1.31
	22.45	2.64	15.41	6.69	854	0.129	9.90	8.73	7.65	6.76	5.93	5.22	4.60	4.05	3.61	3.25	2.96	2.72	2.55	2.36	2.18	1.98	1.74
13	48.81	5.09	15.39	17.64	636	0.145	18.03	15.75	13.74	11.90	10.14	8.65	7.30	6.15	5.21	4.44	3.84	3.36	3.01	2.68	2.42	2.13	1.85
	53.95	5.82	15.37	22.35	564	0.152	20.35	17.77	15.43	13.29	11.35	9.60	7.73	6.73	5.64	4.77	4.07	3.50	3.11	2.75	2.45	2.14	1.86

Appendix C - Precultures - Kinetics

Table C.1. Kinetics precultures.

Preculture #	μ in h ⁻¹	t_D in h	q_{Glc} in mmol cell ⁻¹ s ⁻¹	q_{Gln} in mmol cell ⁻¹ s ⁻¹	q_{Lac} in mmol cell ⁻¹ s ⁻¹	q_{Glu} in mmol cell ⁻¹ s ⁻¹
1	0.031	22.3	-1.37E-14	-1.02E-14	4.09E-15	9.01E-15
2	0.033	21.1	-1.42E-14	-1.18E-14	4.70E-15	6.46E-15
3	0.031	22.1	-1.27E-14	-1.20E-14	2.94E-15	5.40E-15
4	0.031	22.7	-1.15E-14	-1.03E-14	3.59E-15	6.24E-15
5	0.030	23.1	-1.62E-14	-1.92E-14	2.82E-15	1.18E-14
6	0.034	20.1	-1.69E-14	-1.91E-14	4.24E-15	1.03E-14
7	0.030	22.9	-1.15E-14	-1.60E-14	4.75E-15	6.41E-15
8	0.028	24.4	-1.37E-14	-1.50E-14	5.28E-15	6.21E-15
9	0.030	22.9	-1.20E-14	-1.42E-14	3.67E-15	7.32E-15
10	0.036	19.1	-1.53E-14	-1.45E-14	4.38E-15	7.25E-15
11	0.032	21.4	-2.04E-14	-1.49E-14	4.39E-15	5.84E-15
12	0.030	22.8	-1.25E-14	-1.22E-14	4.65E-15	6.02E-15
13	0.029	24.2	-8.38E-15	-1.18E-14	5.76E-15	4.44E-15
Mean	0.031	22.2	-1.38E-14	-1.39E-14	4.25E-15	7.13E-15
STDEV	0.002	1.4	2.88E-15	2.85E-15	8.10E-16	1.98E-15

Appendix D - Infection at Low MOI - Raw Data

Table D.1. Raw data infection at low MOI – off-line analyses (1 of 2).

Process ID	Time Post Planting in h	pH	Total Cell Density in cells ml ⁻¹	Viable Cell Density in cells ml ⁻¹	Viability in %	Mean Average Cell Diameter in µm	Mean Viable Cell Diameter in µm	D-glucose in mmol L ⁻¹	L-lactate in mmol L ⁻¹	L-glutamine in mmol L ⁻¹	L-glutamate in mmol L ⁻¹	PCF2 ORF2 Concentration in RP	Baculovirus Concentration in log ₁₀ TCID50 ml ⁻¹	Fraction of Infected Cells in %	
MOI 0.10 #1	0.90	6.32	1.28E+06	1.23E+06	95.6	18.1	18.3	31.47	1.44	4.69	7.87	0.0	3.7	1.3	
	21.50	6.26	1.84E+06	1.78E+06	96.7	18.3	18.4	27.31	1.71	3.55	8.07	0.0	4.2	7.3	
	43.12	6.23	2.46E+06	2.36E+06	95.8	21.8	21.9	26.59	1.79	1.65	7.93	0.0	6.4	94.9	
	69.59	6.27	2.43E+06	2.14E+06	88.0	23.2	23.4	24.64	0.67	0.97	8.19	0.5	8.5	98.3	
	92.56	6.29	2.21E+06	1.37E+06	62.1	21.5	23.2	22.92	0.77	0.82	8.38	1.8	8.0	83.4	
	112.80	6.07	2.44E+06	7.40E+05	30.3	21.2	25.4	21.43	1.27	1.09	8.44	3.3	8.2	90.3	
	140.61	5.96	2.44E+06	2.90E+05	12.0	18.3	22.5	20.20	2.15	0.34	9.50	2.6	8.5	-	
	164.05	5.92	2.46E+06	1.70E+05	7.1	16.5	19.2	20.09	2.51	0.44	9.57	3.9	7.8	-	
	MOI 0.01 #1	1.00	6.33	1.23E+06	1.19E+06	96.7	18.1	18.3	31.75	1.47	4.66	7.70	0.0	2.7	0.1
		21.57	6.27	1.97E+06	1.92E+06	97.7	18.4	18.5	29.75	2.11	3.75	7.00	0.0	2.6	0.5
43.09		6.23	2.91E+06	2.80E+06	96.4	19.7	19.8	26.87	2.13	1.69	8.33	0.0	4.6	55.4	
69.56		6.35	3.23E+06	3.03E+06	94.0	22.1	22.2	24.15	1.02	0.72	8.08	0.1	7.5	91.3	
92.53		6.35	2.89E+06	2.48E+06	85.8	22.3	22.6	21.15	0.75	0.81	7.78	0.7	8.4	87.5	
113.06		6.27	3.12E+06	1.87E+06	60.0	22.4	24.4	17.71	1.09	1.03	7.52	1.8	8.8	98.3	
140.75		6.17	3.23E+06	8.60E+05	26.7	19.4	23.1	15.10	2.50	0.30	8.49	3.2	8.3	-	
164.16		6.16	3.15E+06	4.90E+05	15.7	17.0	21.1	13.88	3.41	0.44	8.93	4.3	8.4	-	
186.04		6.05	3.03E+06	3.00E+05	10.0	15.7	19.1	12.99	3.82	0.33	8.89	6.0	8.0	-	
209.34		6.02	3.07E+06	1.70E+05	5.5	14.4	16.8	12.71	4.12	0.40	8.96	4.3	8.0	-	
MOI 1.00 #1	0.76	6.33	1.24E+06	1.20E+06	96.2	18.2	18.3	30.75	1.38	4.58	7.46	0.0	5.4	14.2	
	21.27	6.28	1.38E+06	1.32E+06	95.9	20.3	20.4	29.47	1.61	3.07	8.20	0.0	6.0	52.9	
	42.66	6.30	1.43E+06	1.33E+06	92.7	23.0	23.1	28.14	1.34	1.91	8.64	0.2	7.6	96.9	
	67.00	6.28	1.47E+06	1.27E+06	86.0	23.5	23.8	26.64	0.79	1.53	8.73	1.2	7.8	95.6	
	89.78	6.11	1.36E+06	8.00E+05	58.7	21.5	23.4	26.14	0.94	1.05	9.11	2.4	8.4	86.3	
	117.54	5.91	1.80E+06	4.80E+05	26.4	20.2	24.4	25.53	1.62	1.22	9.25	5.3	8.6	-	
	138.38	5.86	1.82E+06	2.60E+05	14.4	18.8	22.6	24.98	2.01	1.10	9.33	5.1	8.0	-	
	162.69	5.84	1.75E+06	1.80E+05	10.2	17.6	19.6	25.03	2.29	1.30	9.14	4.8	8.6	-	
	MOI 0.10 #2	0.95	6.33	1.20E+06	1.14E+06	95.0	18.2	18.4	30.69	1.59	4.68	7.58	0.0	3.6	1.4
		21.42	6.24	1.87E+06	1.80E+06	96.5	18.3	18.4	29.81	1.99	3.65	7.84	0.0	3.5	4.8
42.92		6.28	2.32E+06	2.17E+06	93.8	20.8	21.1	27.59	2.16	2.09	8.08	0.0	5.8	94.1	
67.29		6.36	2.20E+06	1.99E+06	90.2	23.1	23.3	25.26	1.20	1.11	8.39	0.5	7.8	97.5	
90.02		6.34	2.34E+06	1.57E+06	67.0	21.8	23.4	24.03	0.95	0.85	8.44	2.7	8.8	93.3	
117.70		6.08	2.23E+06	6.30E+05	28.2	20.2	25.1	22.70	1.78	0.72	8.62	6.0	8.3	-	
138.54		6.00	2.47E+06	3.80E+05	15.6	17.9	22.5	21.76	2.48	0.95	8.80	5.2	8.5	-	
163.65		5.95	2.54E+06	2.10E+05	8.2	16.2	19.3	21.43	2.90	1.23	8.65	4.4	8.2	-	
MOI 1.00 #2		0.75	6.28	1.32E+06	1.27E+06	96.3	18.0	18.1	31.14	1.42	3.96	8.43	0.0	4.7	12.0
		22.97	6.07	1.44E+06	1.38E+06	95.9	19.4	19.5	29.53	1.74	2.48	8.61	0.0	5.0	38.4
	46.66	6.23	1.74E+06	1.63E+06	93.8	22.4	22.5	26.81	1.09	0.68	9.14	0.1	7.6	96.5	
	71.91	6.02	1.96E+06	1.67E+06	85.4	22.6	23.0	25.37	0.52	0.19	9.43	1.0	7.7	96.0	
	96.24	5.81	1.78E+06	1.12E+06	62.6	21.4	22.8	24.20	1.13	0.60	8.80	2.2	8.6	91.4	
	117.27	5.73	2.03E+06	8.00E+05	39.2	21.5	24.4	22.76	1.85	0.59	8.70	3.9	7.6	76.1	
	147.09	5.68	2.10E+06	3.70E+05	17.4	18.8	22.1	21.43	2.91	0.81	8.86	4.4	7.8	-	
	170.39	5.67	2.18E+06	2.10E+05	9.8	17.3	19.1	21.43	3.33	0.80	8.74	4.5	7.5	-	

Table D.2. Raw data infection at low MOI – off-line analyses (2 of 2).

MOI 0.01 #2	0.87	6.30	1.17E+06	1.13E+06	96.5	17.9	18.0	31.25	1.48	4.02	8.13	0.0	2.7	0.2	
	23.11	6.17	2.34E+06	2.26E+06	96.9	17.7	17.8	29.25	2.13	2.84	8.34	0.0	2.7	0.4	
	46.81	6.15	3.58E+06	3.38E+06	94.6	18.8	19.0	25.42	2.34	0.50	8.53	0.0	5.5	47.3	
	72.05	6.28	3.46E+06	3.26E+06	94.1	20.4	20.5	23.31	0.83	0.16	8.25	0.0	7.5	95.3	
	96.40	6.27	3.02E+06	2.73E+06	90.6	21.0	21.2	19.21	0.57	0.61	7.68	0.4	8.3	96.9	
	117.39	6.29	3.07E+06	1.97E+06	64.0	20.8	22.7	15.04	0.94	0.53	7.76	1.3	8.3	97.4	
	147.19	6.04	3.39E+06	1.23E+06	36.3	18.8	22.3	11.60	2.40	0.67	7.84	2.8	8.3	-	
	170.49	6.05	3.38E+06	8.40E+05	25.0	16.9	21.3	9.99	3.54	0.75	8.07	4.0	8.3	-	
	190.47	6.02	3.48E+06	5.80E+05	16.6	15.3	20.1	8.88	4.02	0.79	8.18	3.1	8.8	-	
	214.54	5.89	3.46E+06	3.40E+05	9.8	13.9	18.6	8.44	4.61	0.96	8.39	3.2	8.2	-	
MOI 0.01 #3	0.67	6.32	1.61E+06	1.55E+06	96.3	17.6	17.7	31.14	1.69	4.10	7.83	0.0	2.6	0.1	
	21.51	6.19	1.99E+06	1.94E+06	97.5	18.0	18.1	29.81	2.31	3.10	7.87	0.0	2.7	0.4	
	45.43	6.20	3.71E+06	3.61E+06	97.2	18.8	18.9	26.03	2.74	0.68	8.14	0.0	5.6	42.4	
	69.50	6.33	3.93E+06	3.72E+06	94.8	20.3	20.4	23.04	0.90	0.32	7.64	0.0	7.5	92.3	
	93.16	6.32	3.71E+06	3.35E+06	90.5	21.0	21.2	18.93	0.62	0.39	7.53	0.4	8.4	94.7	
	117.66	6.25	3.97E+06	2.40E+06	60.4	20.2	22.3	13.99	1.15	0.32	7.46	0.9	7.8	95.3	
	138.36	6.25	3.93E+06	1.70E+06	43.2	18.8	22.2	11.05	2.03	0.39	7.61	1.1	8.3	-	
	165.28	6.05	4.09E+06	1.11E+06	27.2	16.9	21.8	8.55	3.43	0.51	7.90	2.1	8.4	-	
	190.81	6.07	3.91E+06	6.30E+05	16.0	15.0	20.1	7.33	4.34	0.54	8.09	2.5	8.0	-	
	216.18	5.93	4.01E+06	4.60E+05	4.0	13.8	19.1	6.55	4.97	0.67	8.12	2.2	8.5	-	
MOI 0.10 #3	0.86	6.29	1.25E+06	1.19E+06	95.5	17.9	18.1	31.42	1.47	4.17	8.04	0.0	4.4	0.7	
	22.43	6.22	2.01E+06	1.93E+06	96.0	18.0	18.2	29.92	1.73	2.94	8.08	0.0	4.5	3.9	
	50.16	6.25	2.60E+06	2.42E+06	93.3	21.8	22.0	26.09	1.32	1.07	7.68	0.0	7.4	-	
	72.47	6.28	2.72E+06	2.41E+06	88.8	22.2	22.2	24.70	0.63	0.78	8.00	0.4	8.4	-	
	94.87	6.23	2.69E+06	1.82E+06	67.6	21.4	22.3	22.31	0.74	0.51	8.67	1.3	8.5	95.4	
	118.45	6.13	2.77E+06	1.00E+06	36.2	20.2	23.5	20.09	1.15	0.41	8.69	2.5	8.7	-	
	140.93	6.03	2.89E+06	5.80E+05	20.0	17.8	21.8	18.59	1.92	0.54	8.81	3.1	8.0	-	
	167.79	5.98	2.86E+06	3.10E+05	11.0	15.7	18.7	18.04	2.42	0.55	9.13	3.9	8.5	-	
	MOI 1.00 #3	0.86	6.42	1.26E+06	1.19E+06	94.6	17.9	18.1	31.14	1.35	4.31	7.95	0.0	4.7	6.7
		22.53	6.32	1.28E+06	1.19E+06	93.3	19.7	19.9	29.97	1.84	3.11	8.16	0.0	5.7	33.0
50.16		6.36	1.21E+06	1.04E+06	86.1	22.8	23.0	28.03	1.63	1.79	8.72	0.2	7.8	-	
72.60		6.33	1.48E+06	1.19E+06	80.4	23.0	23.4	27.42	1.27	1.02	8.94	1.5	8.2	-	
94.98		6.15	1.40E+05	7.20E+05	51.0	21.0	22.8	26.75	1.69	1.01	9.16	2.6	8.4	95.2	
118.55		5.95	1.65E+06	4.30E+05	26.0	19.8	24.2	25.98	2.69	0.88	9.08	3.0	7.7	-	
141.01		5.89	1.60E+06	2.50E+05	15.4	18.4	22.0	25.64	3.42	0.90	9.15	3.6	8.3	-	
168.03		5.86	1.79E+06	1.60E+05	8.7	16.7	18.0	25.81	3.77	0.83	9.35	4.6	7.8	-	
Uninfected Control		0.52	6.34	1.16E+06	1.10E+06	95.3	17.9	18.1	30.58	1.48	3.07	7.83	-	-	-
		12.58	6.06	1.43E+06	1.36E+06	95.4	18.0	18.1	32.25	1.80	2.64	7.87	-	-	-
	37.55	6.19	2.83E+06	2.71E+06	95.7	17.4	17.6	28.86	1.84	1.22	8.25	-	-	-	
	60.28	6.33	3.60E+06	3.43E+06	95.5	17.8	18.0	26.20	0.98	0.48	8.02	-	-	-	
	83.92	6.31	4.55E+06	4.22E+06	92.6	17.8	18.0	23.26	0.56	0.46	7.34	-	-	-	
	107.76	6.28	5.16E+06	4.11E+06	79.6	17.6	17.9	17.76	0.54	0.43	6.99	-	-	-	
	131.76	6.25	5.94E+06	4.61E+06	77.7	18.0	18.3	12.77	0.36	0.66	6.47	-	-	-	
	156.84	6.22	5.71E+06	4.07E+06	71.2	17.9	18.3	7.44	0.30	1.13	5.66	-	-	-	
	179.55	6.21	5.50E+06	3.22E+06	58.5	17.8	18.4	3.33	0.48	0.78	5.16	-	-	-	
	205.01	6.27	5.34E+06	2.62E+06	49.0	17.5	17.5	0.08	0.82	0.58	4.39	-	-	-	

Table D.3. Raw data infection at low MOI – dielectric spectroscopy (1 of 2).

Process ID	Time Post Planting in h	Biomass (1000 kHz) in pF cm ⁻¹	Suspension Conductivity in mS cm ⁻¹	Δε in pF cm ⁻¹	ε _t in kHz	alpha in -	C(300kHz) in pF	C(373kHz) in pF	C(465kHz) in pF	C(578kHz) in pF	C(720kHz) in pF	C(897kHz) in pF	C(1117kHz) in pF	C(1391kHz) in pF	C(1732kHz) in pF	C(2156kHz) in pF	C(2684kHz) in pF	C(3342kHz) in pF	C(4161kHz) in pF	C(5181kHz) in pF	C(6451kHz) in pF	C(8031kHz) in pF	C(10000kHz) in pF
MOI 0.10 #1	0.90	2.05	15.54	8.11	603	0.095	6.59	5.91	5.23	4.48	3.75	3.08	2.49	1.98	1.54	1.13	0.96	0.76	0.64	0.56	0.46	0.40	0.34
	21.50	4.14	15.32	16.72	602	0.091	14.07	12.33	10.73	9.03	7.44	6.03	4.76	3.65	2.76	2.00	1.56	1.18	0.89	0.75	0.54	0.41	0.32
	43.12	8.14	15.28	42.68	500	0.083	33.66	28.91	24.25	19.84	15.91	12.47	9.58	7.23	5.66	4.11	2.96	2.16	1.61	1.50	0.90	0.70	0.54
	69.59	10.07	15.23	49.70	501	0.111	37.70	32.66	27.75	23.05	18.74	14.95	11.75	9.07	6.93	5.13	3.99	3.02	2.31	1.79	1.36	1.04	0.80
	92.56	9.45	15.26	37.05	609	0.098	29.98	26.71	23.51	20.03	16.65	13.55	10.77	8.42	6.49	4.83	3.81	2.94	2.28	1.79	1.41	1.13	0.89
	112.80	5.61	15.41	22.67	581	0.110	16.91	15.25	13.52	11.60	9.71	7.94	6.38	5.04	3.92	2.91	2.40	1.86	1.47	1.24	0.93	0.72	0.55
	140.61	2.80	15.50	6.26	1034	0.118	6.18	5.85	5.51	5.04	4.51	3.98	3.47	2.99	2.57	2.01	1.87	1.59	1.36	1.17	0.97	0.81	0.66
	164.05	1.58	15.57	2.67	1540	0.108	2.95	2.86	2.84	2.69	2.49	2.28	2.10	1.90	1.69	1.32	1.34	1.18	1.03	0.92	0.76	0.64	0.51
	1.00	1.63	15.68	7.91	528	0.089	6.15	5.44	4.73	4.02	3.35	2.70	2.17	1.73	1.38	0.97	0.85	0.68	0.61	0.60	0.50	0.46	0.44
	21.57	3.59	15.45	14.48	606	0.085	12.75	11.17	9.67	8.17	6.71	5.31	4.32	3.37	2.69	1.84	1.49	1.13	0.93	0.84	0.64	0.55	0.49
43.09	7.03	15.42	29.14	593	0.083	26.11	22.62	19.29	16.06	13.13	10.49	8.20	6.31	4.83	3.41	2.66	1.96	1.51	1.24	0.95	0.76	0.63	
69.56	10.59	15.37	56.50	485	0.098	44.48	38.00	31.86	26.03	20.94	16.47	12.72	9.78	7.43	5.39	4.17	3.13	2.41	1.92	1.47	1.17	0.95	
92.53	11.89	15.38	50.35	572	0.101	41.84	36.65	31.59	26.54	21.79	17.55	13.90	10.83	8.32	6.19	4.86	3.73	2.90	2.30	1.81	1.46	1.18	
113.06	10.17	15.47	40.96	593	0.101	33.49	29.66	25.70	21.86	18.12	14.68	11.63	9.10	7.03	5.17	4.07	3.09	2.41	1.97	1.48	1.15	0.93	
140.75	4.82	15.58	15.72	699	0.114	14.55	13.09	11.59	10.07	8.63	7.25	5.99	4.94	4.11	3.06	2.66	2.18	1.84	1.58	1.34	1.17	1.02	
164.16	3.07	15.65	8.28	838	0.112	9.75	8.58	7.57	6.59	5.71	4.88	4.14	3.54	3.00	2.26	2.09	1.76	1.54	1.37	1.18	1.04	0.92	
186.04	1.66	15.73	3.95	954	0.104	5.80	5.07	4.50	3.97	3.50	3.06	2.69	2.39	2.11	1.60	1.59	1.43	1.29	1.18	1.08	1.01	0.91	
209.34	1.02	15.81	3.54	978	0.104	4.00	3.51	3.11	2.75	2.47	2.22	2.03	1.90	1.77	1.30	1.38	1.28	1.20	1.11	1.05	1.00	0.92	
0.76	2.30	15.56	9.17	604	0.097	12.67	9.92	7.83	6.13	4.79	3.71	2.80	2.09	1.51	1.00	0.74	0.50	0.31	0.21	0.10	0.04	0.00	
21.27	4.34	15.27	19.86	549	0.090	23.08	18.48	14.78	11.71	9.19	7.07	5.37	4.01	2.95	2.04	1.52	1.07	0.74	0.52	0.36	0.26	0.19	
42.66	6.32	15.20	37.41	447	0.101	33.65	27.21	21.89	17.31	13.49	10.38	7.86	5.90	4.35	3.10	2.33	1.71	1.21	0.89	0.62	0.44	0.31	
67.00	7.83	15.17	33.14	569	0.105	33.23	27.68	22.90	18.66	15.01	11.92	9.25	7.09	5.33	3.85	2.93	2.18	1.59	1.17	0.85	0.62	0.45	
89.78	6.86	15.22	27.58	595	0.103	27.57	23.07	19.23	15.83	12.77	10.14	7.91	6.09	4.56	3.26	2.49	1.82	1.31	0.98	0.65	0.44	0.29	
117.54	4.21	15.31	17.20	619	0.127	21.89	17.13	13.47	10.52	8.16	6.20	4.63	3.32	2.28	1.33	0.92	0.37	-0.05	-0.35	-0.57	-0.79	-0.87	
138.38	2.88	15.36	10.58	706	0.131	18.10	13.68	10.47	8.01	6.07	4.57	3.41	2.48	1.72	0.97	0.74	0.30	-0.02	-0.31	-0.45	-0.64	-0.71	
162.69	1.80	15.43	6.05	834	0.120	15.06	10.92	8.00	5.84	4.26	3.06	2.18	1.51	0.95	0.38	0.29	-0.05	-0.30	-0.50	-0.63	-0.80	-0.84	
0.95	1.24	15.69	12.64	349	0.074	4.40	4.17	3.48	2.81	2.19	1.62	1.16	0.76	0.38	0.09	0.02	-0.09	-0.16	-0.16	-0.19	-0.19	-0.17	
21.42	2.85	15.42	14.37	525	0.081	9.17	8.41	7.26	6.04	4.92	3.90	2.97	2.20	1.58	0.91	0.64	0.38	0.21	0.11	0.03	-0.01	-0.02	
42.92	5.97	15.37	29.00	534	0.077	21.92	19.32	16.37	13.54	10.89	8.56	6.54	4.88	3.60	2.36	1.71	1.16	0.77	0.50	0.33	0.23	0.15	
67.29	8.29	15.33	45.45	481	0.090	32.47	28.22	23.85	19.58	15.67	12.25	9.44	7.13	5.29	3.74	2.82	2.04	1.47	1.05	0.75	0.54	0.38	
90.02	8.56	15.34	36.43	578	0.091	26.88	24.37	21.18	17.95	14.83	11.93	9.33	7.14	5.38	3.75	2.86	2.06	1.50	1.08	0.77	0.55	0.40	
117.70	4.03	15.47	18.76	536	0.096	12.16	11.26	9.92	8.48	7.06	5.71	4.55	3.53	2.71	1.86	1.55	1.18	0.91	0.71	0.56	0.45	0.35	
138.54	1.80	15.55	7.24	584	0.108	4.18	4.30	3.94	3.51	3.02	2.58	2.17	1.81	1.51	1.00	0.97	0.82	0.69	0.56	0.50	0.44	0.37	
163.65	0.41	15.64	-	-	-	0.06	0.62	0.69	0.66	0.61	0.56	0.52	0.48	0.42	0.16	0.33	0.29	0.27	0.28	0.22	0.20	0.17	
0.75	2.75	15.55	10.45	626	0.101	10.87	9.08	7.50	6.19	4.98	3.93	3.06	2.32	1.73	1.19	0.89	0.61	0.39	0.24	0.13	0.07	0.01	
22.97	5.15	15.32	21.24	589	0.099	20.79	17.42	14.43	11.84	9.47	7.49	5.80	4.35	3.21	2.22	1.64	1.12	0.72	0.48	0.26	0.12	0.02	
46.66	7.97	15.24	49.02	428	0.107	37.51	31.15	25.37	20.32	15.98	12.32	9.38	7.01	5.19	3.67	2.73	1.94	1.34	0.94	0.58	0.35	0.18	
71.91	9.60	15.18	43.64	524	0.121	37.29	31.59	26.42	21.78	17.62	14.02	10.99	8.46	6.44	4.70	3.61	2.65	1.92	1.38	0.98	0.69	0.46	
96.24	8.67	15.29	36.34	559	0.126	30.85	26.53	22.50	18.79	15.41	12.40	9.82	7.67	5.89	4.32	3.37	2.51	1.84	1.35	0.97	0.69	0.46	
117.27	7.21	15.36	27.00	609	0.136	24.38	20.98	17.90	15.10	12.48	10.18	8.18	6.48	5.06	3.76	3.03	2.29	1.71	1.26	0.92	0.67	0.44	
147.09	4.44	15.46	12.74	788	0.138	15.23	12.85	10.85	9.15	7.63	6.31	5.18	4.24	3.42	2.56	2.17	1.69	1.31	1.00	0.74	0.54	0.36	
170.39	2.78	15.52	6.05	1078	0.121	10.27	8.37	6.92	5.79	4.82	4.05	3.35	2.80	2.32	1.72	1.55	1.24	0.96	0.75	0.55	0.41	0.26	

Table D.4. Raw data infection at low MOI – dielectric spectroscopy (2 of 2).

MOI 0.01 #2	0.87	1.35	15.81	5.11	616	0.095	2.43	2.63	2.48	2.26	2.01	1.67	1.37	1.09	0.74	0.54	0.45	0.33	0.26	0.19	0.14	0.13	0.11
	23.11	3.11	15.43	10.15	713	0.093	6.54	6.52	6.00	5.34	4.66	3.90	3.16	2.48	1.85	1.29	1.00	0.68	0.49	0.37	0.23	0.16	0.11
	46.81	7.12	15.39	26.36	643	0.095	20.28	18.52	16.33	14.10	11.77	9.55	7.61	5.92	4.46	3.18	2.40	1.69	1.22	0.89	0.59	0.42	0.30
	72.05	9.73	15.32	39.71	589	0.102	31.08	27.75	24.09	20.49	16.95	13.67	10.85	8.46	6.33	4.70	3.59	2.65	1.99	1.46	1.09	0.83	0.62
	96.40	11.56	15.32	39.86	673	0.109	30.52	28.14	25.19	21.94	18.65	15.40	12.46	9.84	7.57	5.62	4.35	3.22	2.40	1.78	1.30	0.97	0.71
	117.39	10.44	15.36	32.98	733	0.099	24.33	23.09	21.24	18.85	16.28	13.63	11.07	8.84	6.78	5.05	3.94	2.94	2.23	1.67	1.23	0.91	0.67
	147.19	5.60	15.53	14.75	867	0.104	10.74	10.59	10.08	9.26	8.23	7.09	5.94	4.91	3.87	2.88	2.39	1.84	1.45	1.12	0.84	0.66	0.50
	170.49	3.98	15.60	9.31	982	0.109	6.49	6.72	6.56	6.19	5.64	4.98	4.30	3.64	2.92	2.23	1.94	1.53	1.24	0.99	0.77	0.61	0.48
	190.47	2.69	15.68	5.67	1106	0.104	4.02	4.27	4.26	4.14	3.84	3.43	3.03	2.66	2.18	1.64	1.52	1.24	1.04	0.85	0.70	0.59	0.49
	214.54	1.62	15.74	3.21	1168	0.097	2.80	2.72	2.69	2.62	2.45	2.17	1.96	1.72	1.39	1.00	1.01	0.84	0.73	0.62	0.52	0.46	0.39
MOI 0.01 #3	0.67	0.99	15.34	5.52	500	0.088	2.74	2.64	2.44	2.09	1.75	1.40	1.08	0.82	0.58	0.31	0.25	0.17	0.12	0.08	0.09	0.08	0.08
	21.51	3.13	15.36	11.49	662	0.085	8.76	8.07	7.19	6.22	5.22	4.28	3.39	2.63	1.98	1.31	1.01	0.71	0.50	0.35	0.28	0.22	0.16
	45.43	7.44	15.29	24.14	725	0.067	25.05	21.53	18.60	15.62	12.87	10.33	8.10	6.19	4.63	3.22	2.38	1.54	1.15	0.74	0.56	0.34	0.35
	69.50	10.01	15.26	39.17	620	0.088	35.48	30.64	26.31	22.03	17.97	14.34	11.19	8.61	6.50	4.61	3.45	2.48	1.79	1.29	0.93	0.66	0.47
	93.16	12.17	15.26	40.95	700	0.090	36.76	32.54	28.62	24.59	20.53	16.71	13.31	10.34	7.91	5.72	4.35	3.16	2.31	1.68	1.21	0.86	0.61
	117.66	8.98	15.34	26.60	785	0.083	24.49	21.95	19.74	17.23	14.68	12.15	9.76	7.70	5.96	4.32	3.36	2.49	1.86	1.37	1.03	0.76	0.57
	138.36	6.18	15.40	17.37	814	0.086	16.09	14.42	13.12	11.52	9.82	8.21	6.67	5.32	4.14	2.94	2.36	1.77	1.33	0.99	0.76	0.57	0.43
	165.28	3.50	15.51	8.91	913	0.092	8.34	7.54	7.02	6.28	5.53	4.68	3.89	3.17	2.57	1.78	1.52	1.17	0.92	0.72	0.57	0.43	0.33
	190.81	1.70	15.61	3.63	1111	0.094	3.64	3.22	3.13	2.93	2.65	2.30	1.97	1.69	1.46	0.89	0.90	0.72	0.60	0.49	0.42	0.34	0.28
	216.18	0.57	15.71	1.11	1271	0.097	1.13	0.88	0.99	1.02	0.95	0.89	0.79	0.72	0.60	0.28	0.41	0.36	0.32	0.28	0.26	0.23	0.20
MOI 0.10 #3	0.86	1.72	15.78	8.65	532	0.086	9.01	7.05	5.54	4.19	3.12	2.26	1.57	0.95	0.48	0.03	-0.11	-0.32	-0.45	-0.50	-0.56	-0.57	-0.56
	22.43	4.09	15.30	17.60	580	0.086	17.75	14.59	11.80	9.38	7.35	5.62	4.15	2.97	1.96	1.11	0.68	0.22	-0.08	-0.27	-0.41	-0.46	-0.50
	50.16	8.96	15.23	45.04	521	0.082	40.05	33.41	27.38	22.06	17.24	13.22	9.92	7.26	5.11	3.36	2.33	1.40	0.76	0.33	0.02	-0.16	-0.29
	72.47	9.30	15.23	44.55	524	0.101	38.65	32.43	26.84	21.74	17.21	13.46	10.22	7.66	5.50	3.75	2.67	1.70	1.00	0.50	0.17	-0.04	-0.20
	94.87	9.29	15.24	37.92	591	0.098	33.83	28.85	24.30	20.01	16.15	12.68	9.79	7.37	5.31	3.57	2.57	1.61	0.93	0.44	0.11	-0.12	-0.28
	118.45	6.13	15.33	23.98	617	0.092	22.04	18.77	15.78	12.98	10.46	8.21	6.28	4.69	3.31	2.10	1.53	0.86	0.40	0.09	-0.13	-0.27	-0.35
	140.93	3.22	15.46	10.97	685	0.100	11.70	9.74	8.17	6.78	5.45	4.29	3.33	2.60	1.87	1.12	0.94	0.56	0.30	0.10	-0.01	-0.08	-0.15
	167.79	1.67	15.54	5.18	719	0.104	6.34	5.17	4.25	3.39	2.77	2.13	1.67	1.31	0.94	0.48	0.49	0.28	0.13	0.04	-0.07	-0.11	-0.16
MOI 1.00 #3	0.86	1.42	15.86	4.62	731	0.096	4.00	3.49	3.13	2.72	2.24	1.83	1.42	1.09	0.87	0.48	0.38	0.24	0.14	0.07	0.01	-0.03	-0.04
	22.53	2.95	15.40	11.66	615	0.091	10.01	8.68	7.56	6.35	5.19	4.14	3.25	2.48	1.88	1.25	0.97	0.68	0.48	0.35	0.23	0.16	0.11
	50.16	4.77	15.37	24.13	500	0.103	18.74	16.05	13.61	11.19	8.97	7.07	5.50	4.21	3.20	2.23	1.73	1.27	0.93	0.68	0.48	0.33	0.23
	72.60	5.75	15.34	21.88	629	0.103	17.04	15.33	13.58	11.69	9.72	7.91	6.27	4.88	3.89	2.66	2.09	1.53	1.13	0.83	0.59	0.40	0.28
	94.98	4.79	15.41	15.91	701	0.101	12.12	11.17	10.30	9.07	7.70	6.41	5.14	4.11	3.27	2.30	1.87	1.43	1.08	0.83	0.62	0.45	0.34
	118.55	2.94	15.48	7.15	950	0.101	5.39	5.24	5.13	4.81	4.29	3.72	3.13	2.61	2.17	1.52	1.34	1.06	0.83	0.65	0.49	0.37	0.29
	141.01	1.60	15.54	2.73	1572	0.099	1.13	1.48	1.88	2.05	2.02	1.94	1.79	1.63	1.47	1.03	1.02	0.86	0.72	0.59	0.48	0.40	0.32
	168.03	0.67	15.57	1.00	5367	0.097	-1.47	-0.93	-0.29	0.15	0.43	0.64	0.76	0.82	0.85	0.55	0.67	0.59	0.51	0.44	0.34	0.28	0.23
Uninfected	0.52	1.99	15.14	7.09	654	0.101	5.92	5.32	4.63	3.92	3.28	2.67	2.15	1.68	1.26	0.85	0.70	0.50	0.35	0.25	0.18	0.12	0.06
Control	12.58	3.08	15.44	10.25	700	0.101	9.43	8.36	7.29	6.28	5.24	4.31	3.49	2.79	2.15	1.55	1.25	0.93	0.72	0.52	0.43	0.35	0.26
	37.55	5.88	15.35	19.39	703	0.105	17.77	15.66	13.64	11.66	9.74	7.99	6.41	5.03	3.87	2.77	2.14	1.55	1.11	0.78	0.57	0.40	0.26
	60.28	7.91	15.27	26.33	695	0.105	24.17	21.25	18.53	15.78	13.21	10.79	8.69	6.83	5.23	3.79	2.93	2.13	1.56	1.11	0.82	0.60	0.41
	83.92	10.41	15.24	29.84	801	0.103	28.03	25.20	22.23	19.37	16.58	13.83	11.31	8.99	7.01	5.16	4.00	2.92	2.17	1.55	1.17	0.87	0.62
	107.76	12.96	15.21	37.71	792	0.102	35.00	31.45	27.89	24.20	20.69	17.23	14.06	11.23	8.68	6.39	4.90	3.57	2.64	1.89	1.41	1.05	0.75
	131.76	14.25	15.17	39.76	830	0.092	38.86	34.68	30.63	26.67	22.74	18.90	15.43	12.22	9.35	6.85	5.20	3.77	2.71	1.91	1.37	0.97	0.65
	156.84	15.09	15.07	41.95	830	0.084	39.99	36.09	32.06	28.19	24.02	20.04	16.32	12.93	9.95	7.30	5.56	4.06	2.96	2.11	1.61	1.22	0.88
	179.55	16.03	15.02	44.32	831	0.082	42.27	38.23	34.03	29.81	25.46	21.30	17.30	13.73	10.54	7.76	5.88	4.29	3.18	2.28	1.74	1.35	1.00
	205.01	16.61	15.15	45.71	830	0.081	44.02	39.52	34.91	30.46	25.98	21.52	17.29	13.60	10.38	7.47	5.53	3.92	2.71	1.86	1.25	0.83	0.51

Appendix E - Infection at Low MOI – Complete Plots

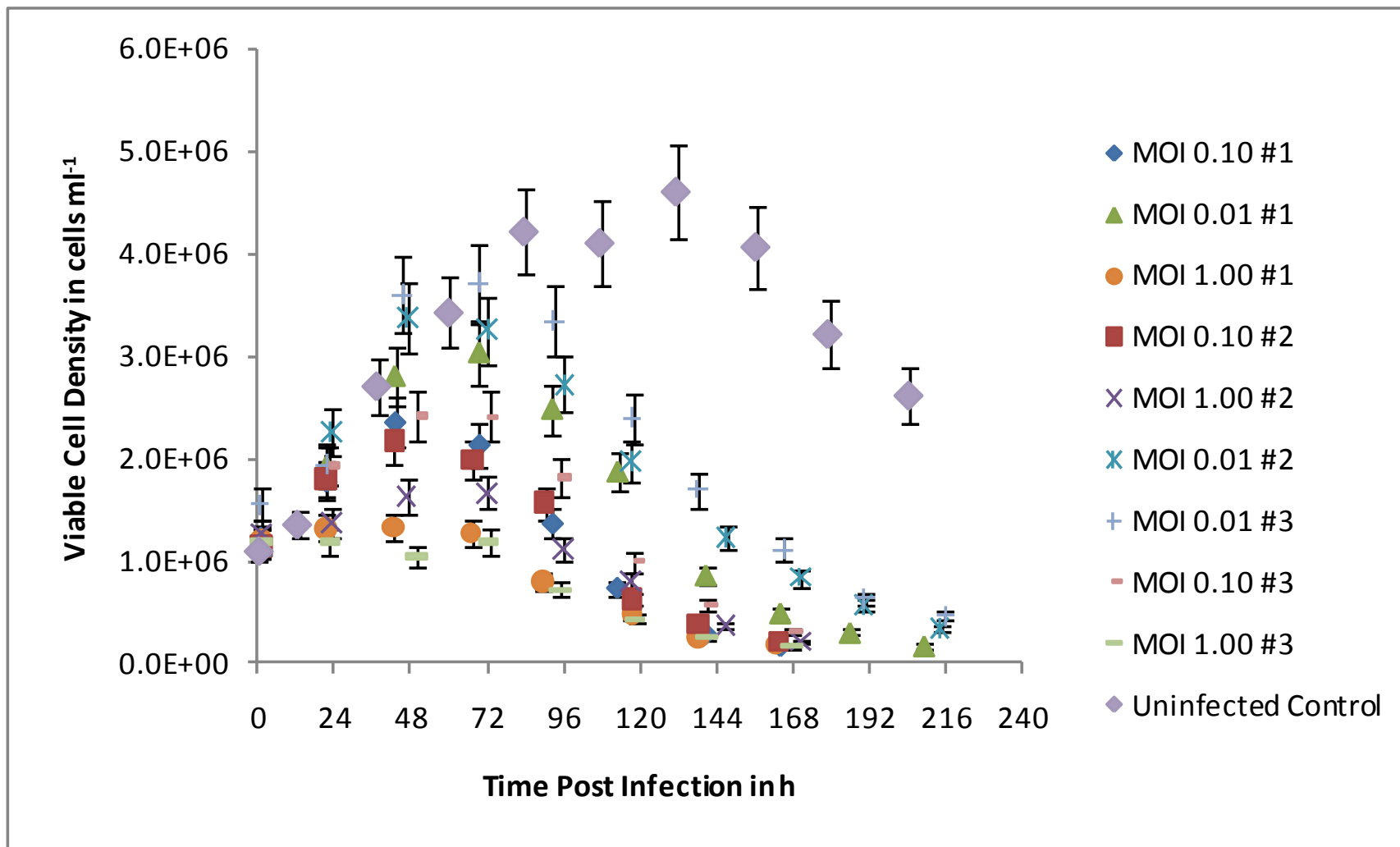


Figure E.1. Viable cell density post infection.

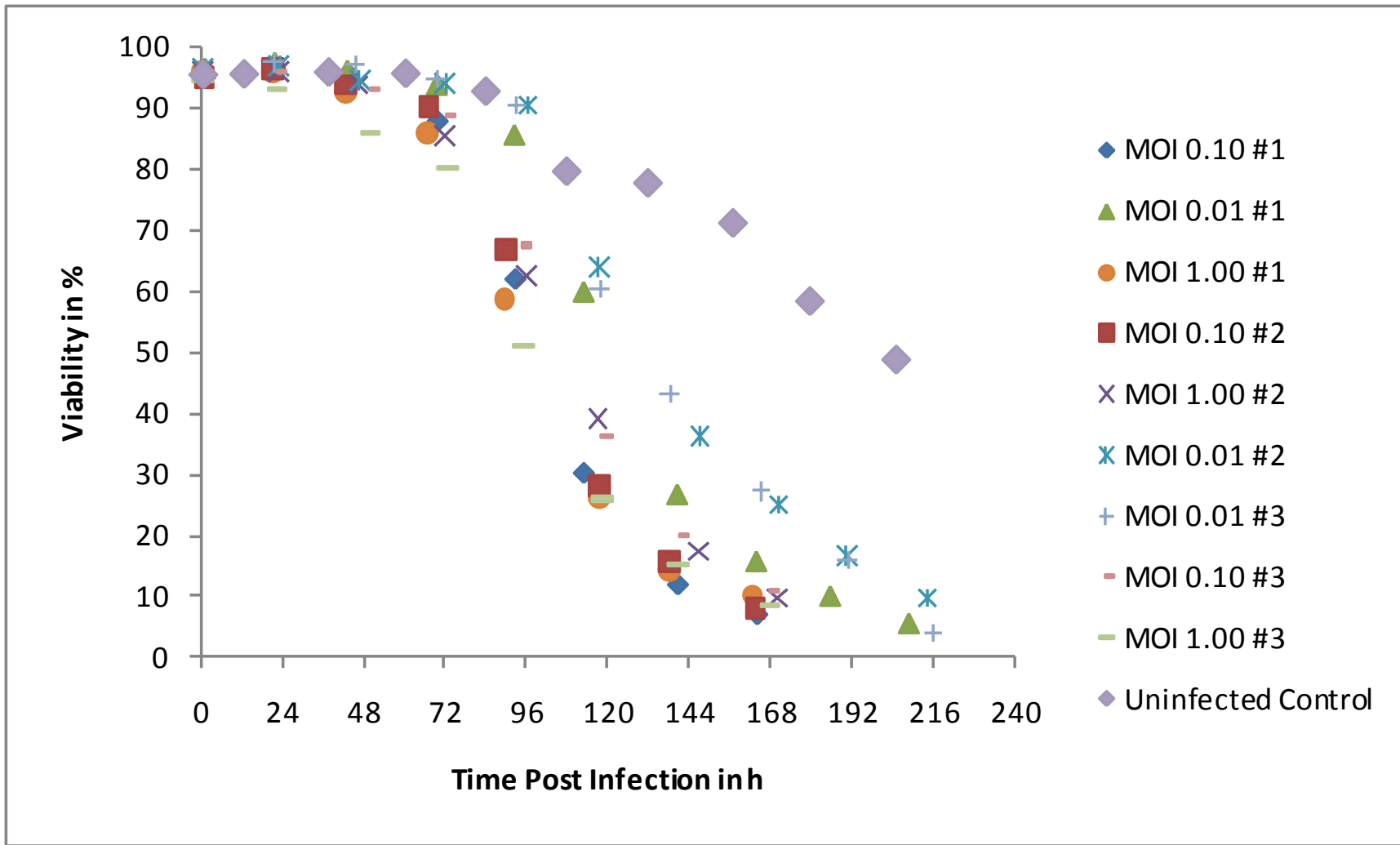


Figure E.2. Viability post infection.

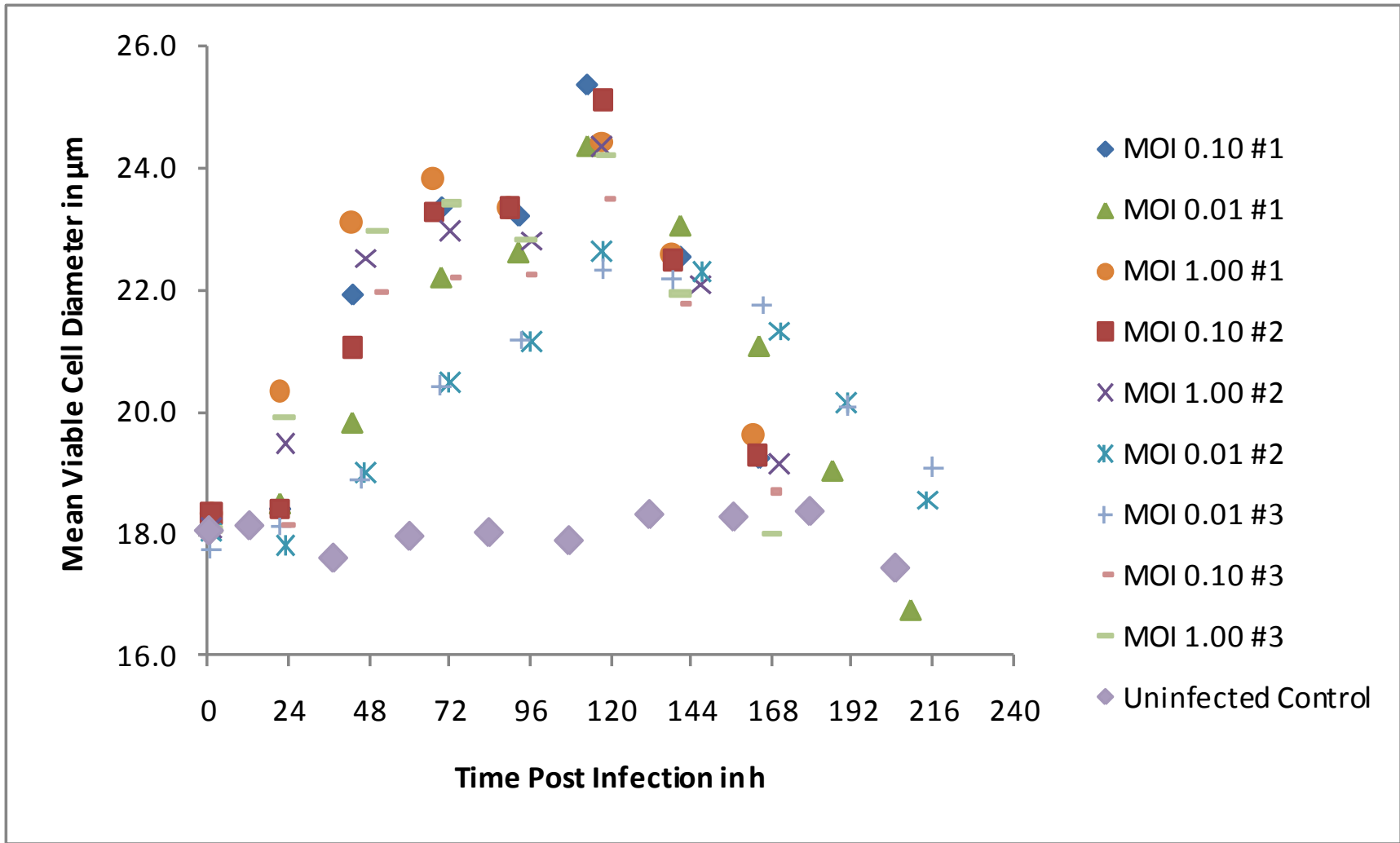


Figure E.3. Mean viable cell diameter post infection.

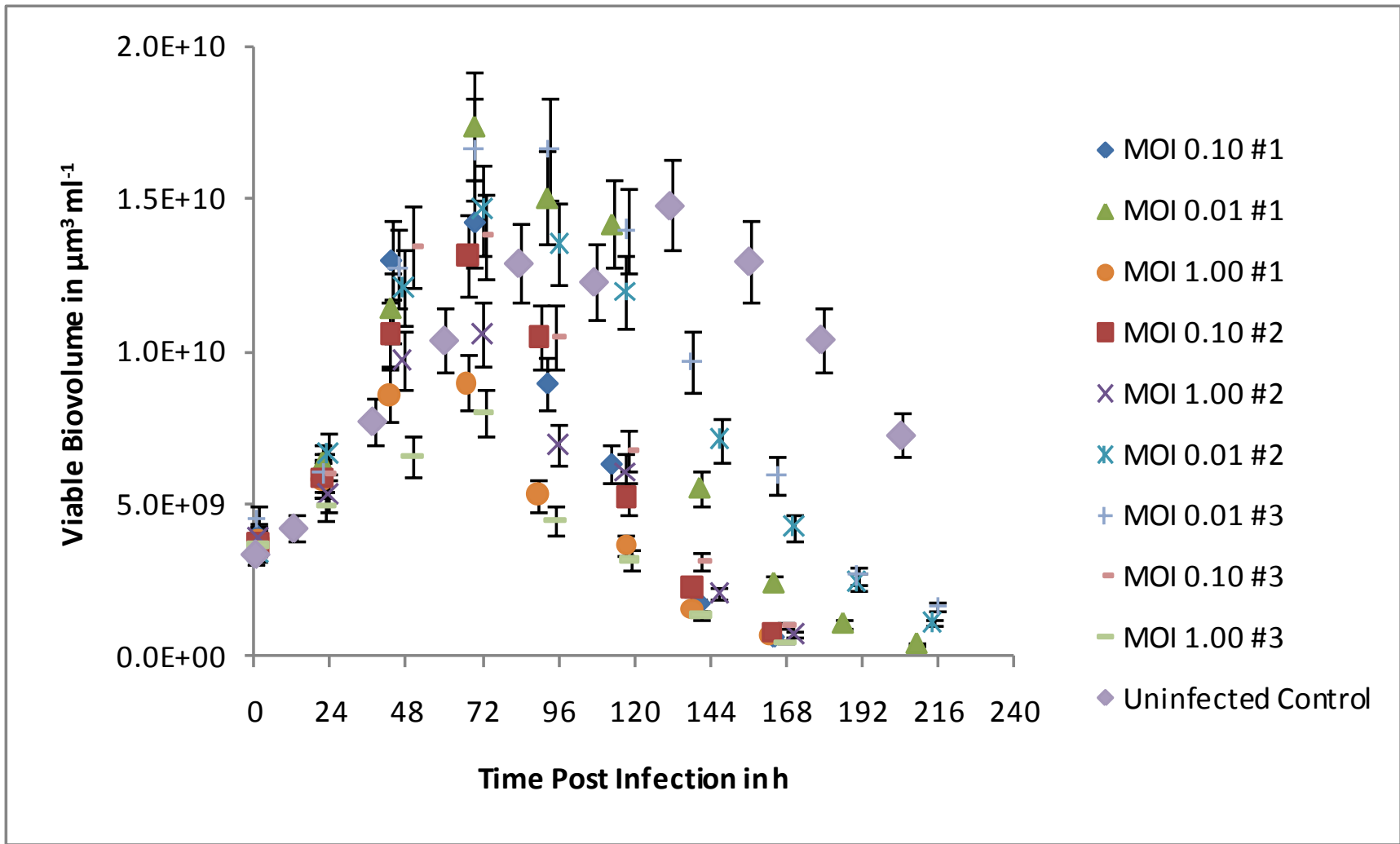


Figure E.4. Viable biovolume post infection.

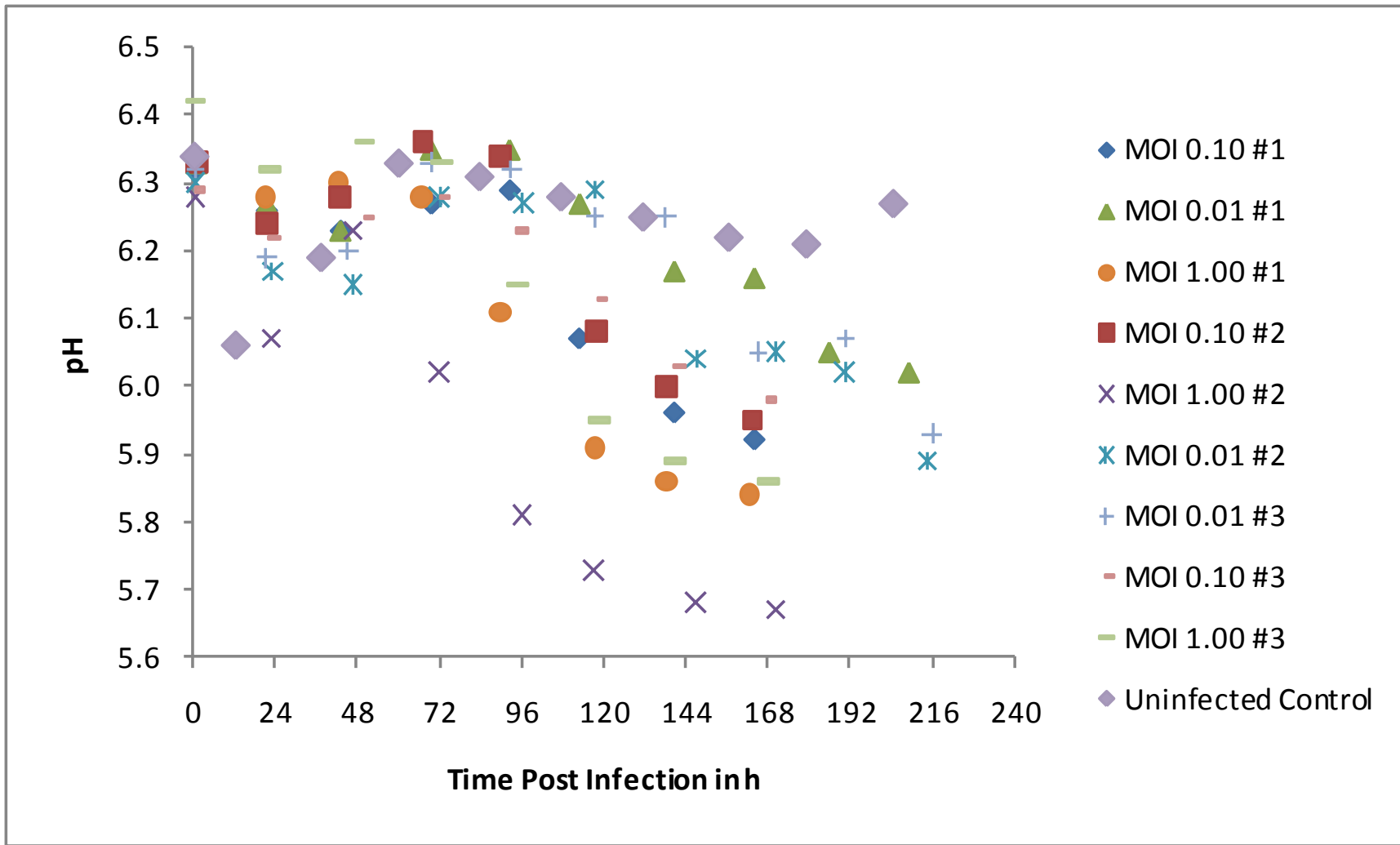


Figure E.5. pH post infection.

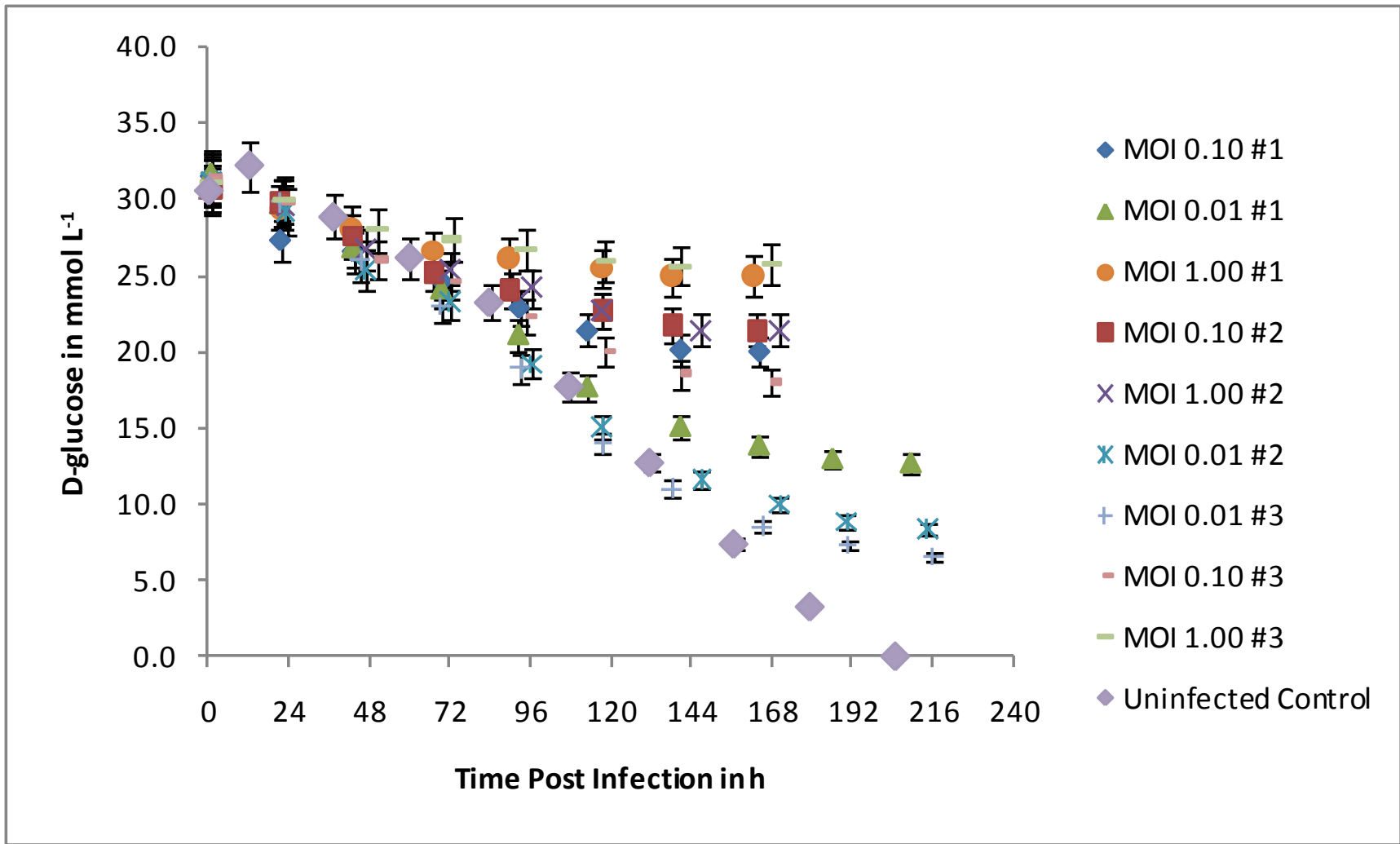


Figure E.6. D-glucose post infection.

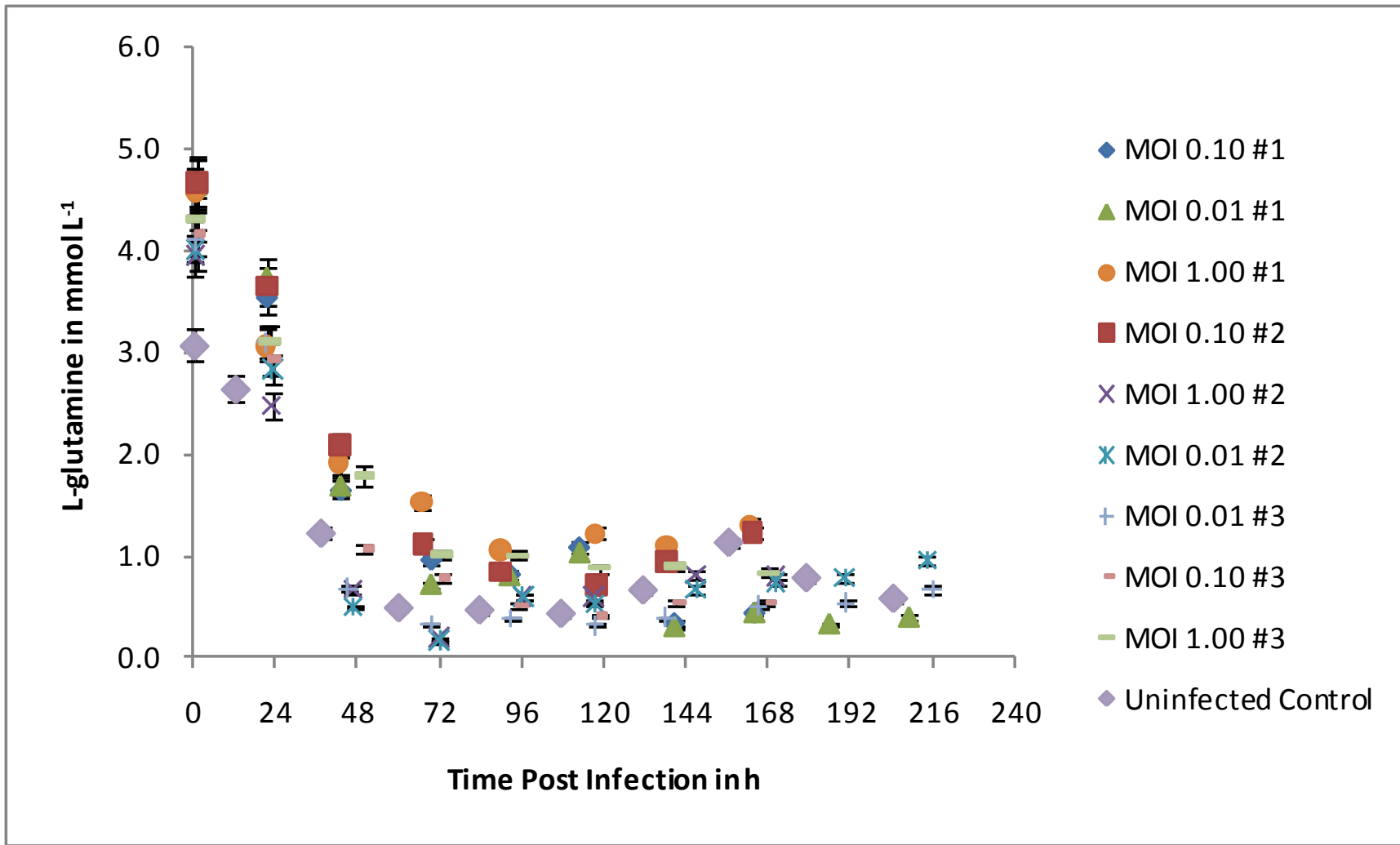


Figure E.7. L-glutamine post infection.

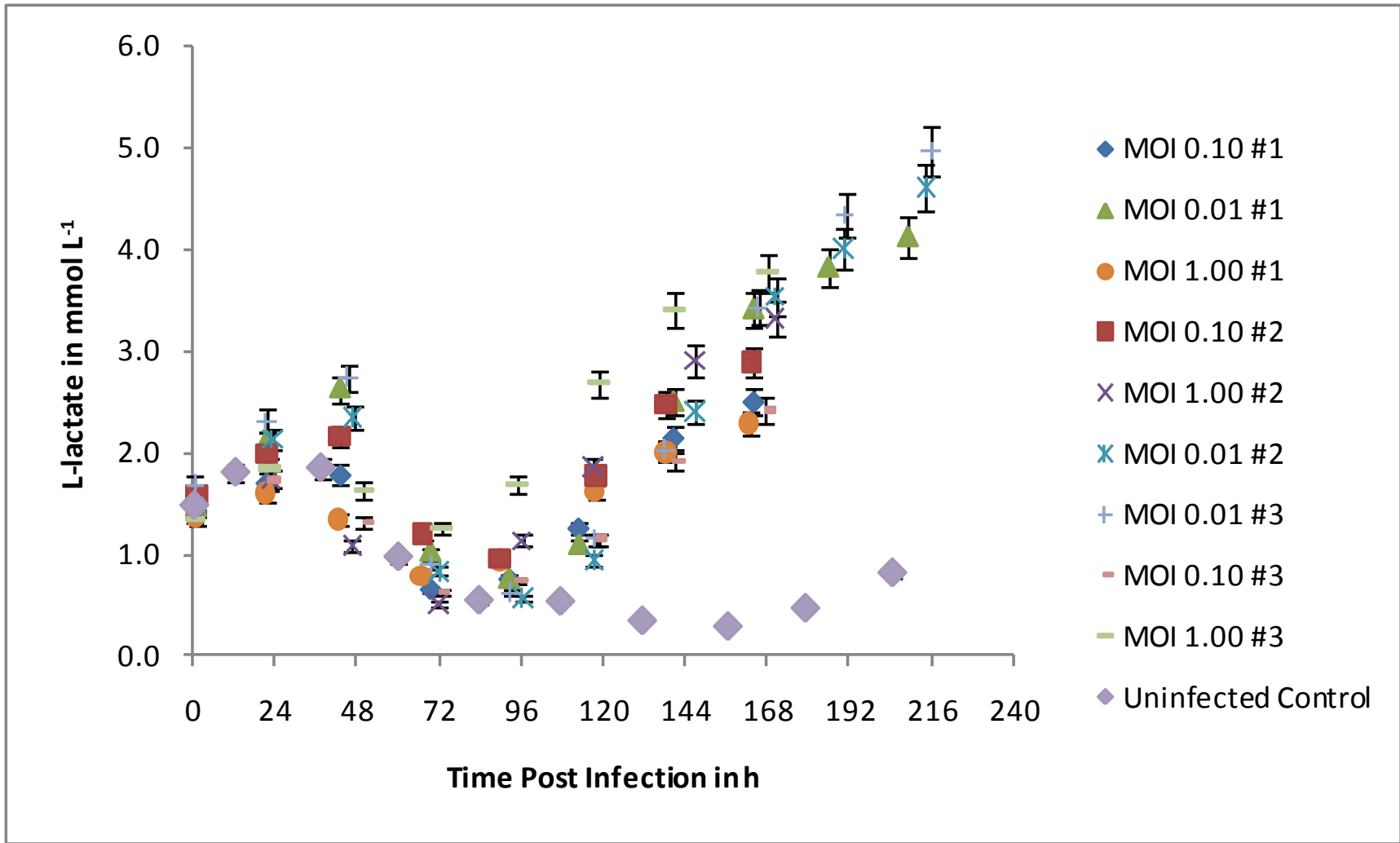


Figure E.8. L-lactate post infection.

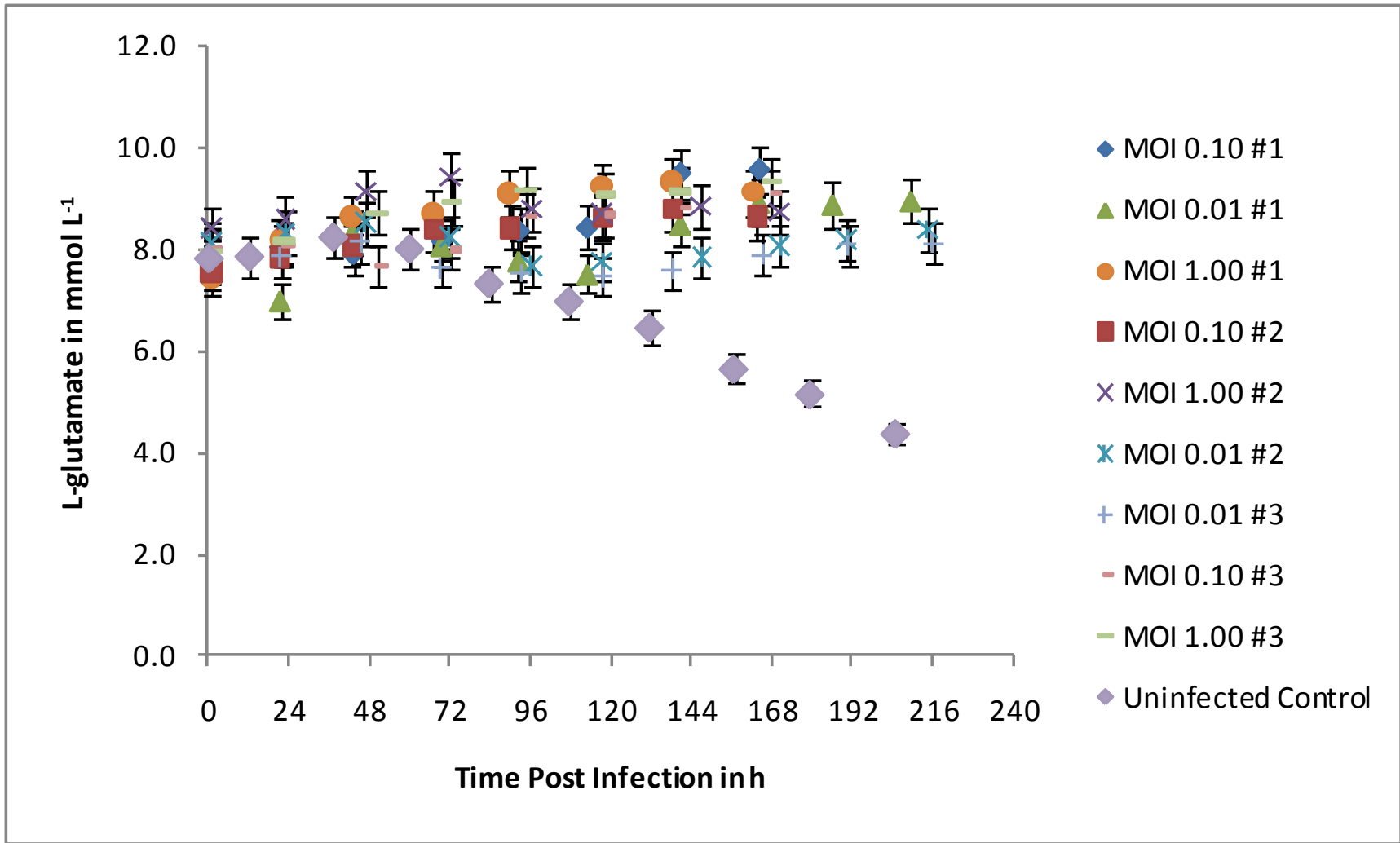


Figure E.9. L-glutamate post infection.

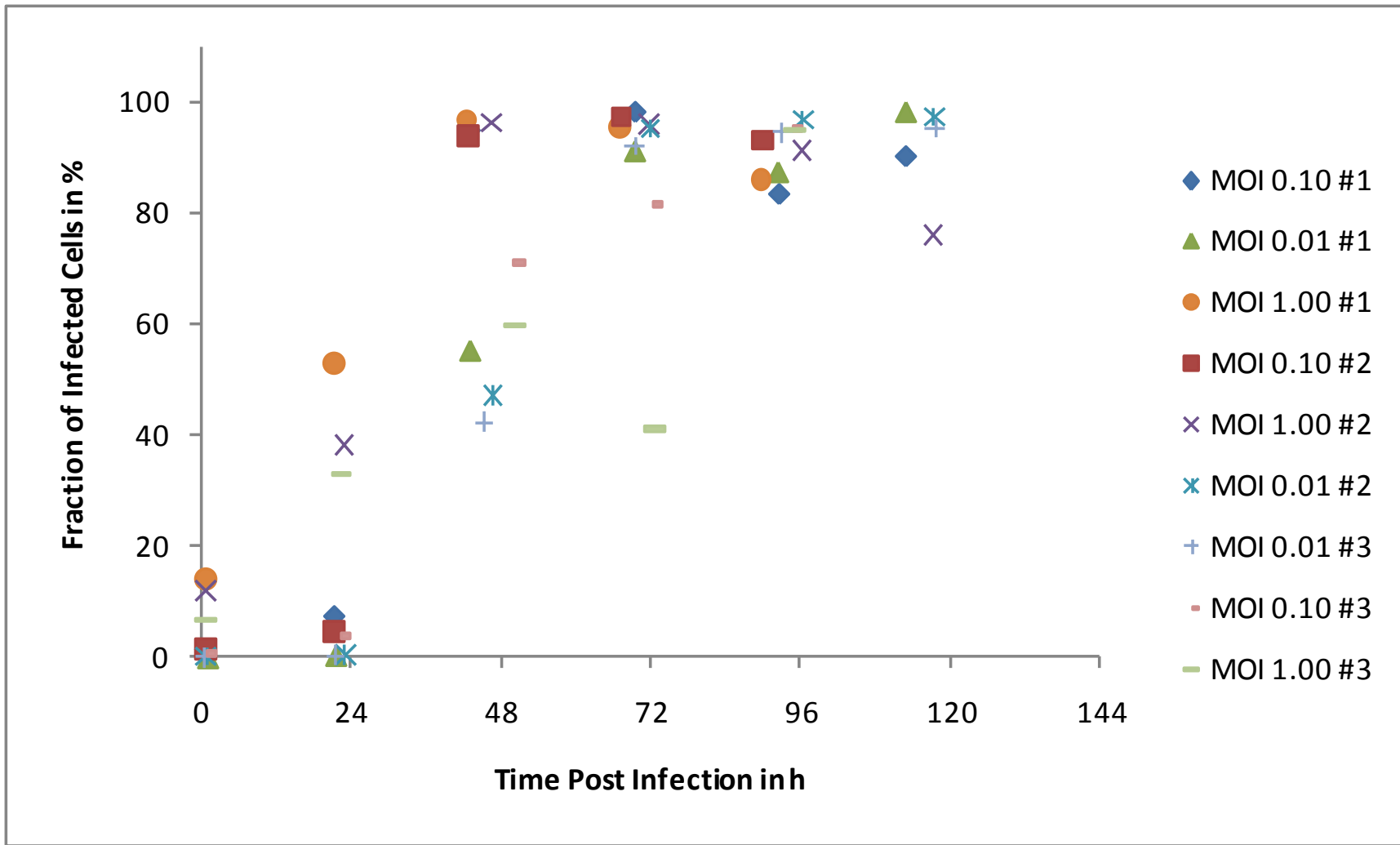


Figure E.10. Fraction of infected cells post infection.

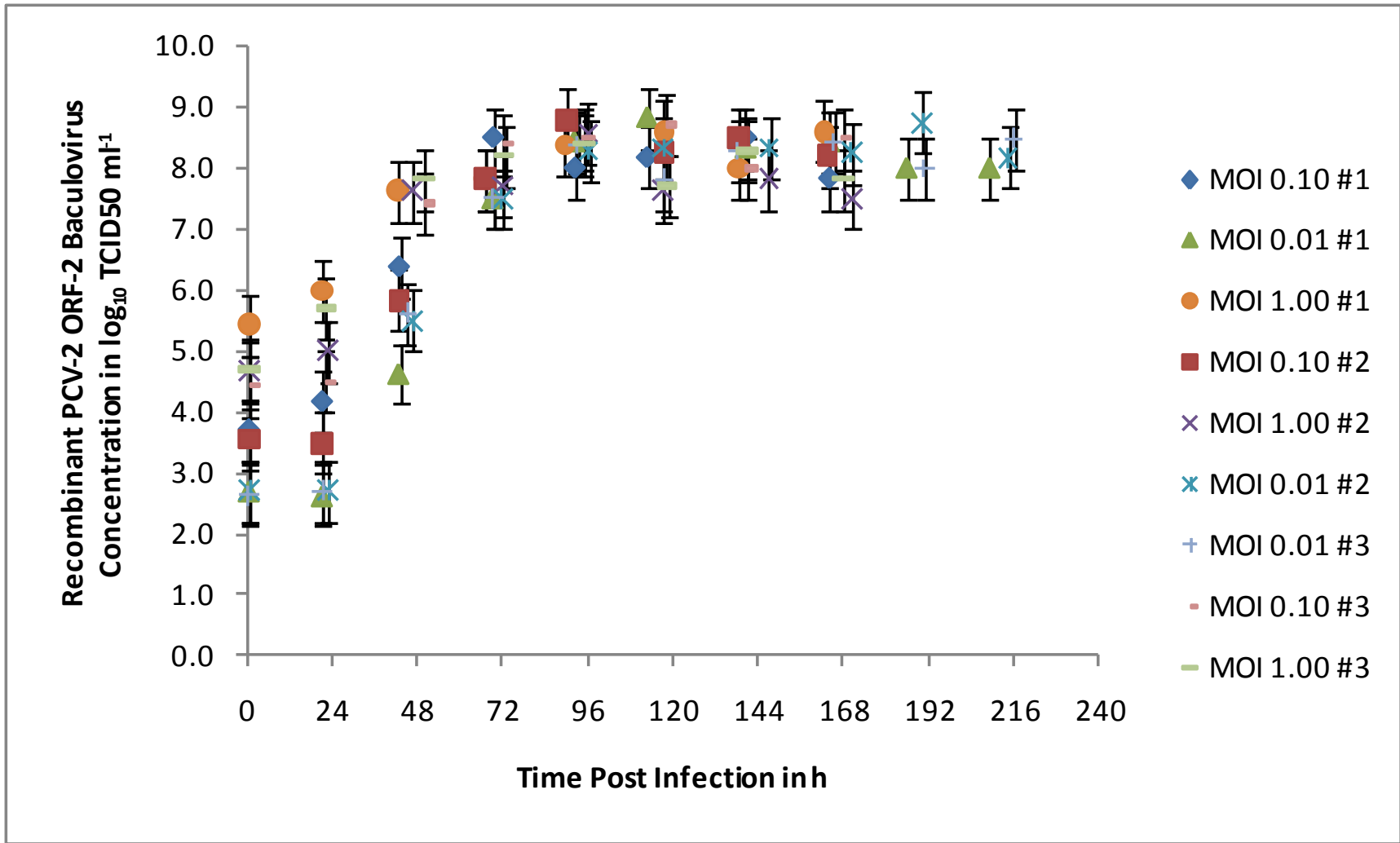


Figure E.11. Recombinant PCV2 ORF2 baculovirus concentration post infection.

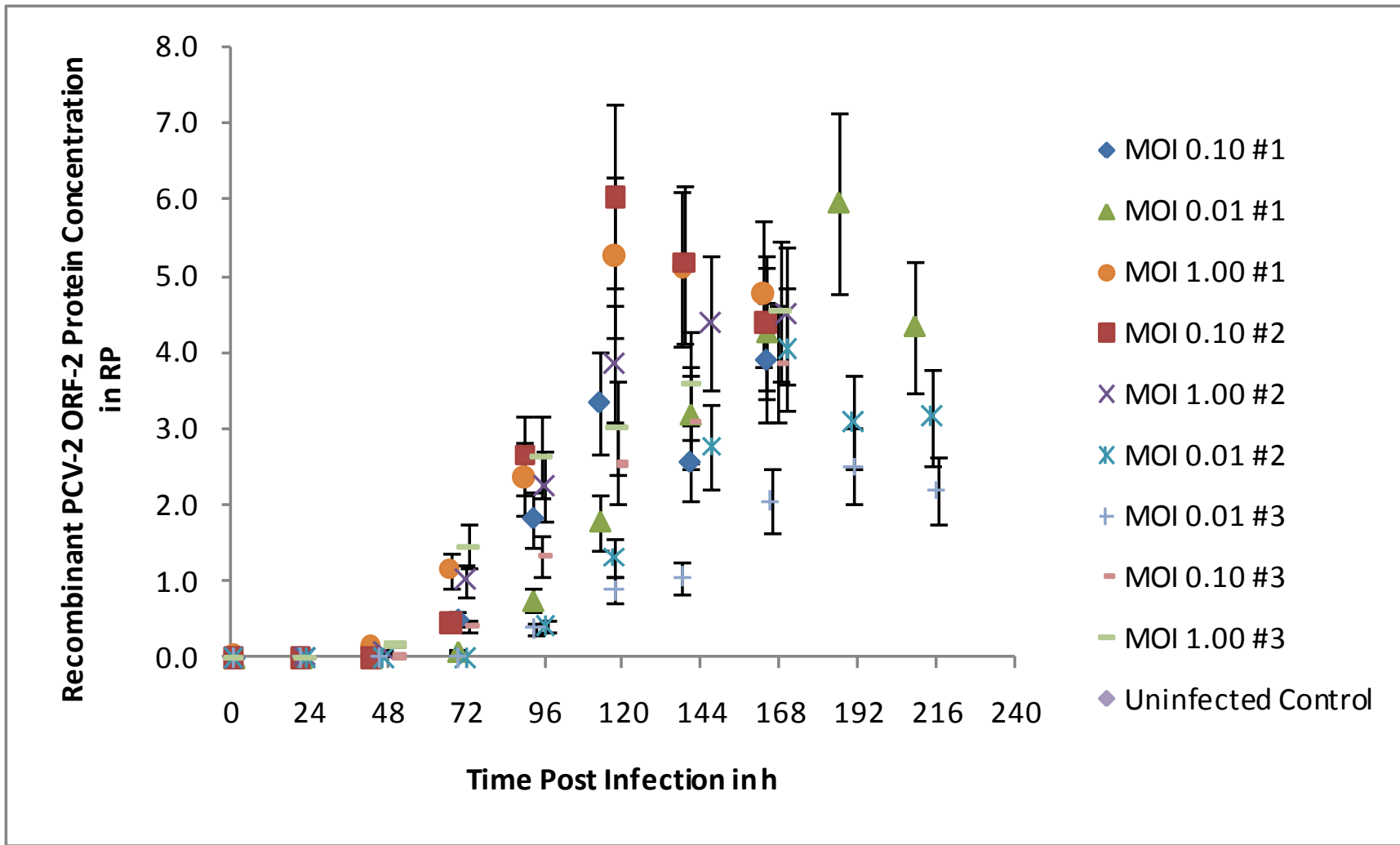


Figure E.12. Recombinant PCV2 ORF2 protein concentration post infection.

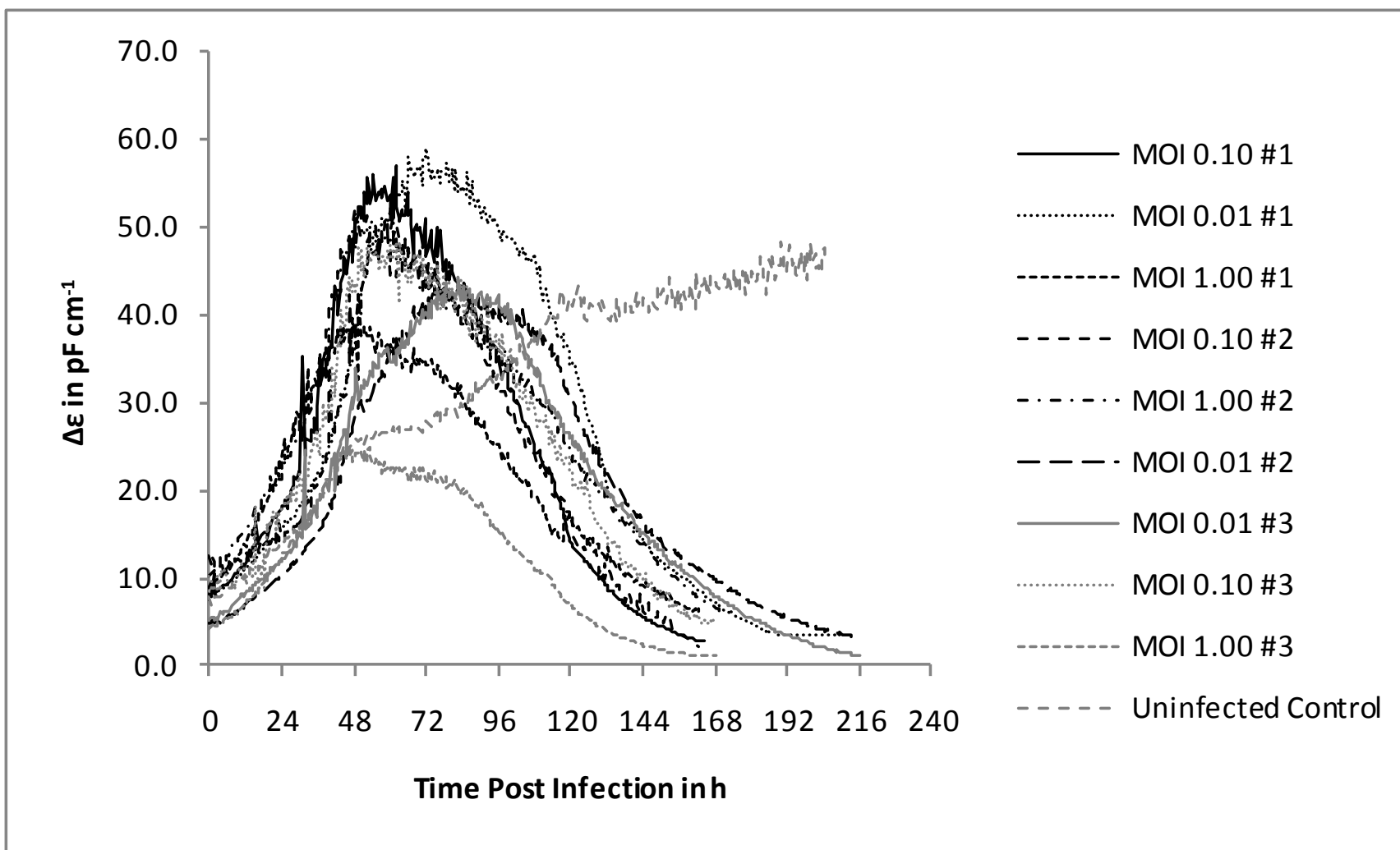


Figure E.13. $\Delta\epsilon$ post infection.

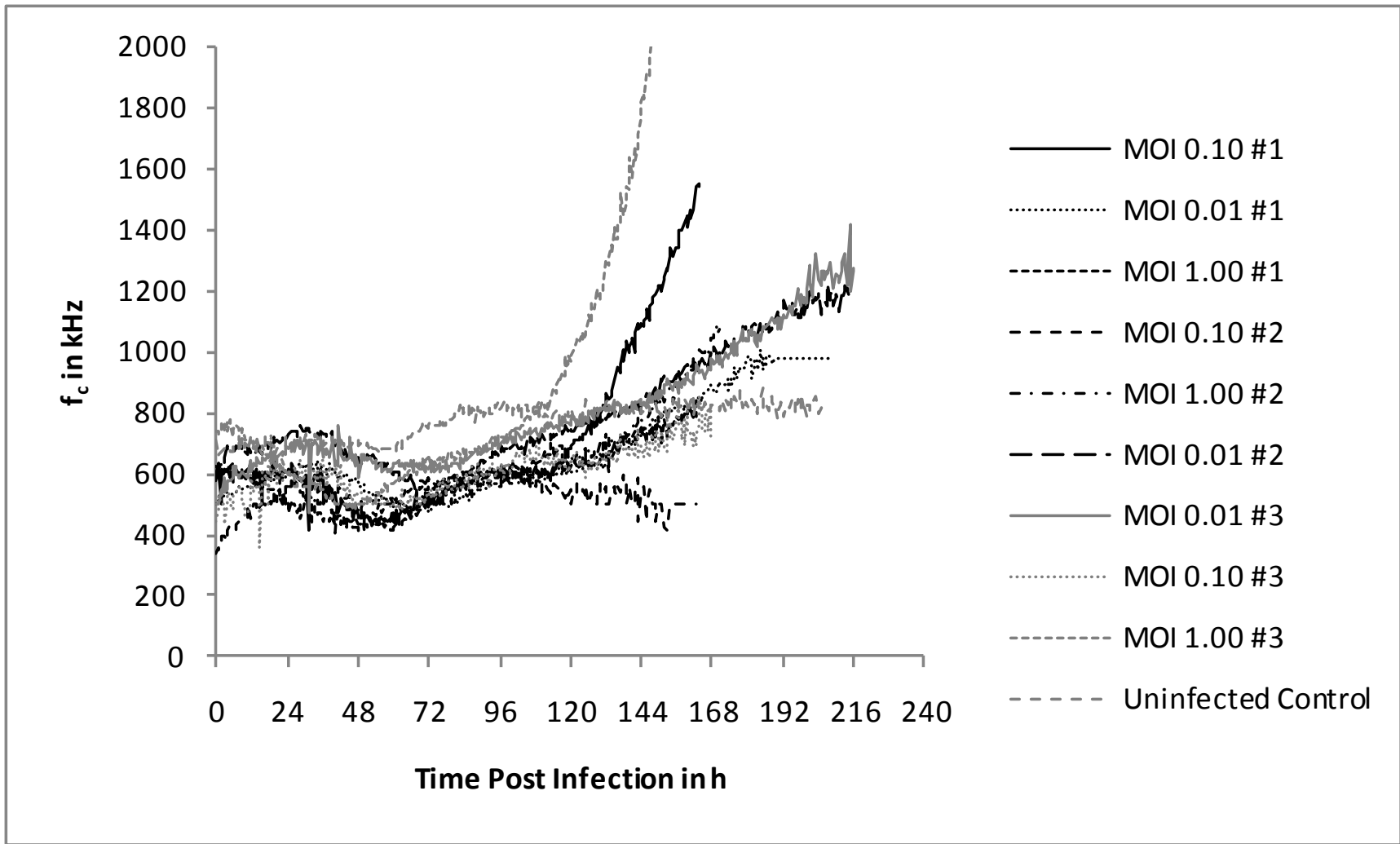


Figure E.14. f_c post infection.

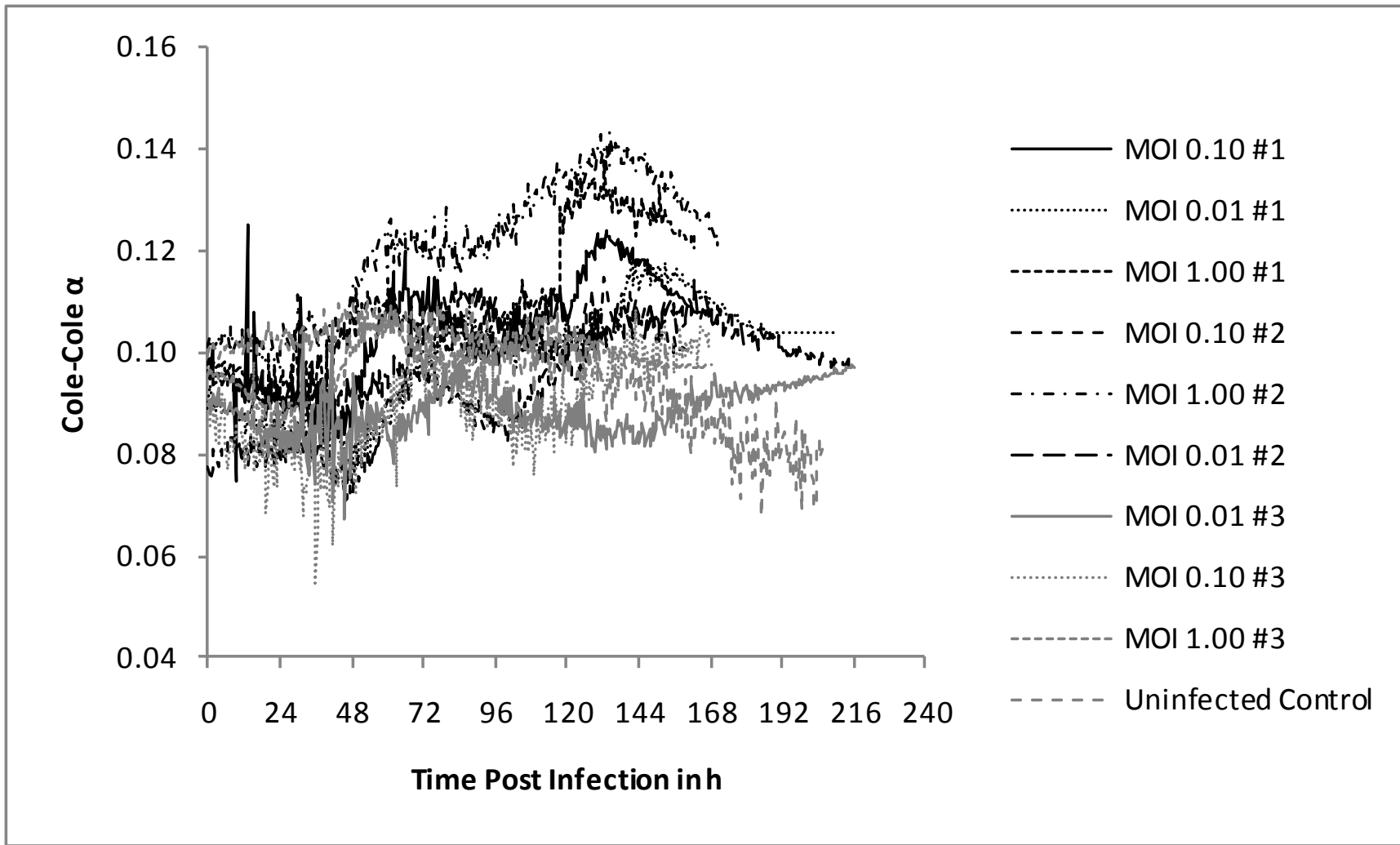


Figure E.15. Cole-Cole α post infection.

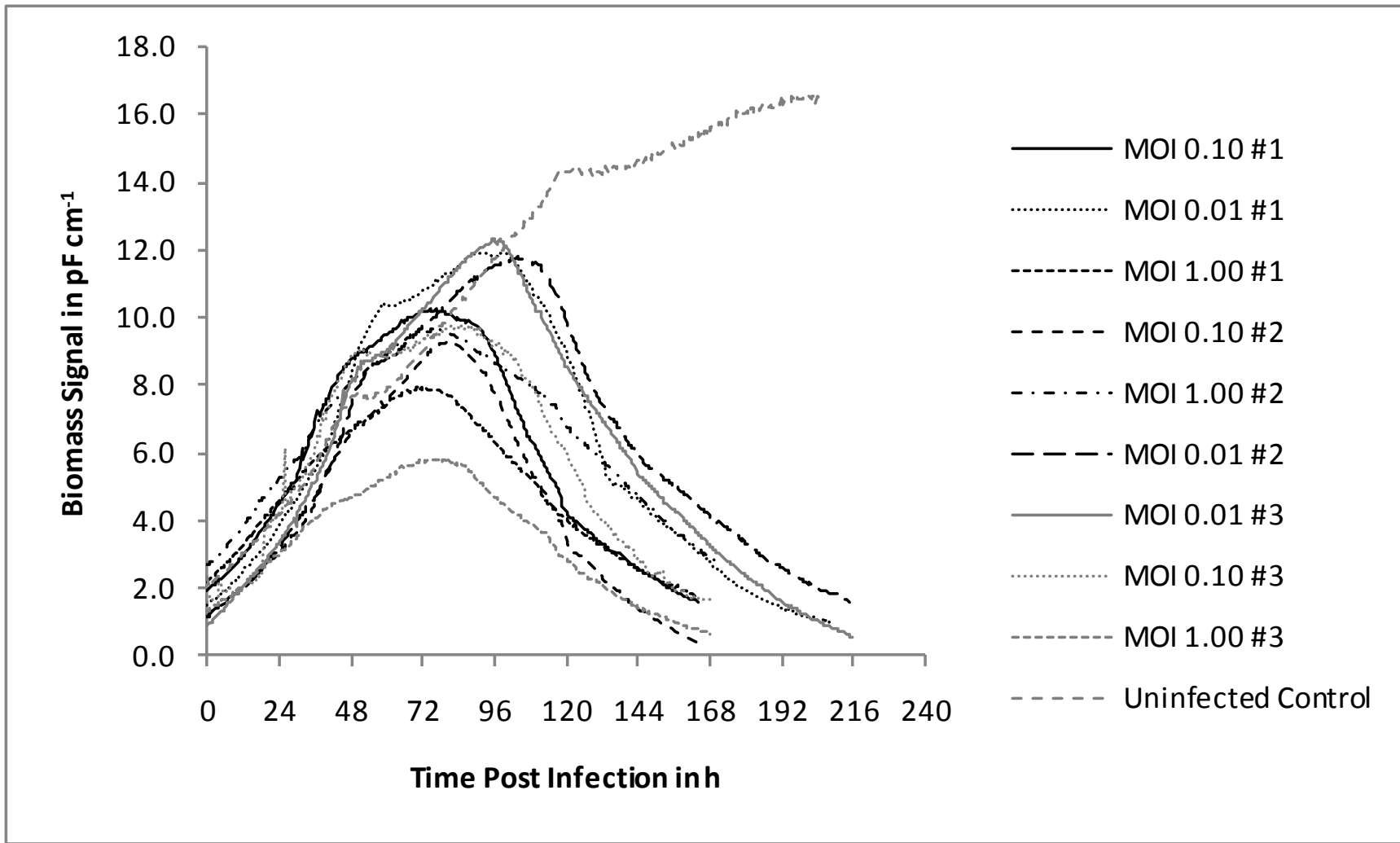


Figure E.16. Biomass signal post infection.

Appendix F - Infection at Low MOI - Tests for Statistical Significance

Table F.1. t-test for parameter RP.

t-Test: Two-Sample Assuming Unequal Variances		
Parameter RP		
	<i>MOI 0.01</i>	<i>MOI 0.10</i>
Mean	3.231111111	4.043333333
Variance	1.148692593	0.086877778
Observations	3	3
Hypothesized Mean Difference	0	
df	2	
t Stat	-1.265615405	
P(T<=t) one-tail	0.166563587	
t Critical one-tail	2.91998558	
P(T<=t) two-tail	0.333127175	
t Critical two-tail	4.30265273	
	<i>MOI 0.01</i>	<i>MOI 1.00</i>
Mean	3.231111111	4.613333333
Variance	1.148692593	0.0223
Observations	3	3
Hypothesized Mean Difference	0	
df	2	
t Stat	-2.212388663	
P(T<=t) one-tail	0.078716075	
t Critical one-tail	2.91998558	
P(T<=t) two-tail	0.15743215	
t Critical two-tail	4.30265273	
	<i>MOI 0.10</i>	<i>MOI 1.00</i>
Mean	4.043333333	4.613333333
Variance	0.086877778	0.0223
Observations	3	3
Hypothesized Mean Difference	0	
df	3	
t Stat	-2.987915821	
P(T<=t) one-tail	0.029113726	
t Critical one-tail	2.353363435	
P(T<=t) two-tail	0.058227452	
t Critical two-tail	3.182446305	

Table F.2. t-test for parameter specific RP per viable biovolume.

t-Test: Two-Sample Assuming Unequal Variances		
Parameter Specific RP per Viable Biovolume		
	<i>MOI 0.01</i>	<i>MOI 0.10</i>
Mean	1.98612E-10	2.94889E-10
Variance	3.62971E-21	1.1007E-21
Observations	3	3
Hypothesized Mean Difference	0	
df	3	
t Stat	-2.42457056	
P(T<=t) one-tail	0.046892181	
t Critical one-tail	2.353363435	
P(T<=t) two-tail	0.093784362	
t Critical two-tail	3.182446305	
	<i>MOI 0.01</i>	<i>MOI 1.00</i>
Mean	1.98612E-10	5.08038E-10
Variance	3.62971E-21	5.58198E-21
Observations	3	3
Hypothesized Mean Difference	0	
df	4	
t Stat	-5.584028734	
P(T<=t) one-tail	0.002522013	
t Critical one-tail	2.131846782	
P(T<=t) two-tail	0.005044026	
t Critical two-tail	2.776445105	
	<i>MOI 0.10</i>	<i>MOI 1.00</i>
Mean	2.94889E-10	5.08038E-10
Variance	1.1007E-21	5.58198E-21
Observations	3	3
Hypothesized Mean Difference	0	
df	3	
t Stat	-4.516144385	
P(T<=t) one-tail	0.010147025	
t Critical one-tail	2.353363435	
P(T<=t) two-tail	0.02029405	
t Critical two-tail	3.182446305	

Table F.3. t-test for parameter specific RP per viable cell.

t-Test: Two-Sample Assuming Unequal Variances		
Parameter Specific RP per Viable Cell		
	<i>MOI 0.01</i>	<i>MOI 0.10</i>
Mean	9.85552E-07	1.75397E-06
Variance	1.78635E-13	5.37397E-14
Observations	3	3
Hypothesized Mean Difference	0	
df	3	
t Stat	-2.760975259	
P(T<=t) one-tail	0.035047556	
t Critical one-tail	2.353363435	
P(T<=t) two-tail	0.070095113	
t Critical two-tail	3.182446305	
	<i>MOI 0.01</i>	<i>MOI 1.00</i>
Mean	9.85552E-07	3.37314E-06
Variance	1.78635E-13	3.56482E-13
Observations	3	3
Hypothesized Mean Difference	0	
df	4	
t Stat	-5.653222493	
P(T<=t) one-tail	0.002411952	
t Critical one-tail	2.131846782	
P(T<=t) two-tail	0.004823903	
t Critical two-tail	2.776445105	
	<i>MOI 0.10</i>	<i>MOI 1.00</i>
Mean	1.75397E-06	3.37314E-06
Variance	5.37397E-14	3.56482E-13
Observations	3	3
Hypothesized Mean Difference	0	
df	3	
t Stat	-4.378697451	
P(T<=t) one-tail	0.011023742	
t Critical one-tail	2.353363435	
P(T<=t) two-tail	0.022047484	
t Critical two-tail	3.182446305	

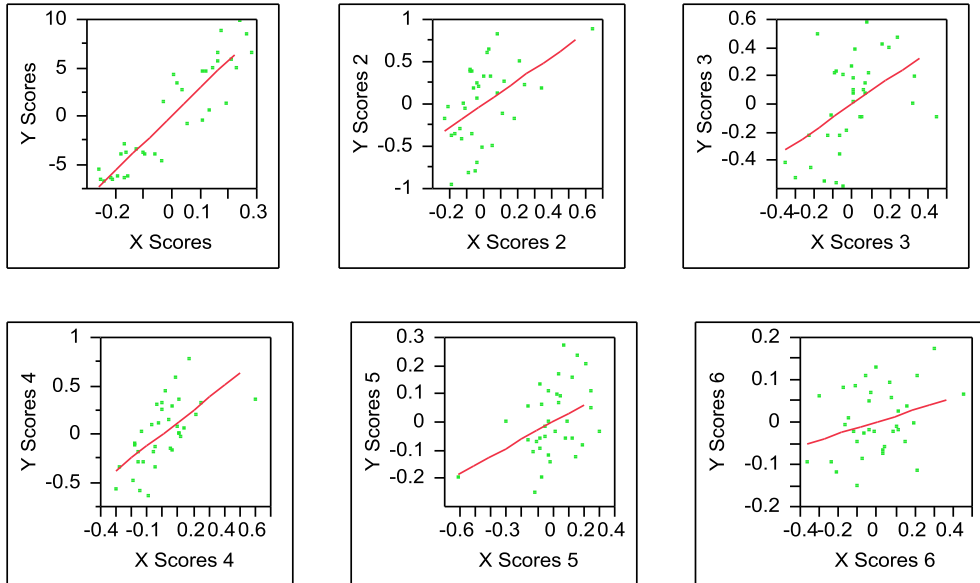
Appendix G - Infection at Low MOI – PLS Model Details

PLS for Variable P

Number of Latent Factors

1 to max=10
6

X-Y Scores Plots



Percent Variation Explained

Number	X X	Cumulative X	Y Y	Cumulative Y
1	97.16	97.16	84.28	84.28
2	1.631	98.79	4.082	88.36
3	0.965	99.76	2.713	91.08
4	0.088	99.85	3.685	94.76
5	0.1	99.94	0.894	95.66
6	0.047	99.99	0.421	96.08
7	0.003	100	0.79	96.87
8	0.002	100	0.533	97.4
9	3e-4	100	0.615	98.02
10	0.001	100	0.224	98.24

















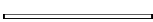
Cross Validation

Number	Prediction RMSE
1	0.412
2	0.37
3	0.345
4	0.271
5	0.255
6	0.252
7	0.348
8	0.464
9	0.635
10	0.664

Press Residuals

P
0.0001964
-0.000931
0.0020402
0.001109
-0.000416
-0.000339
-0.000478
0.0020219
-0.002192
0.0009853
-0.00031
0.0006626
-0.001119
-0.000871
-0.00095
-0.001185
0.000149
0.000376
-0.001727
-0.000557
-0.000519
0.0007641
0.0015208
0.0014021
0.0013628
-0.001755
0.001161
-0.000158
-1.57e-6
0.0017469
-0.000301
-9.319e-5
-0.000659
-0.001111
0.0015752

Model Coefficients for Centered and Scaled Data

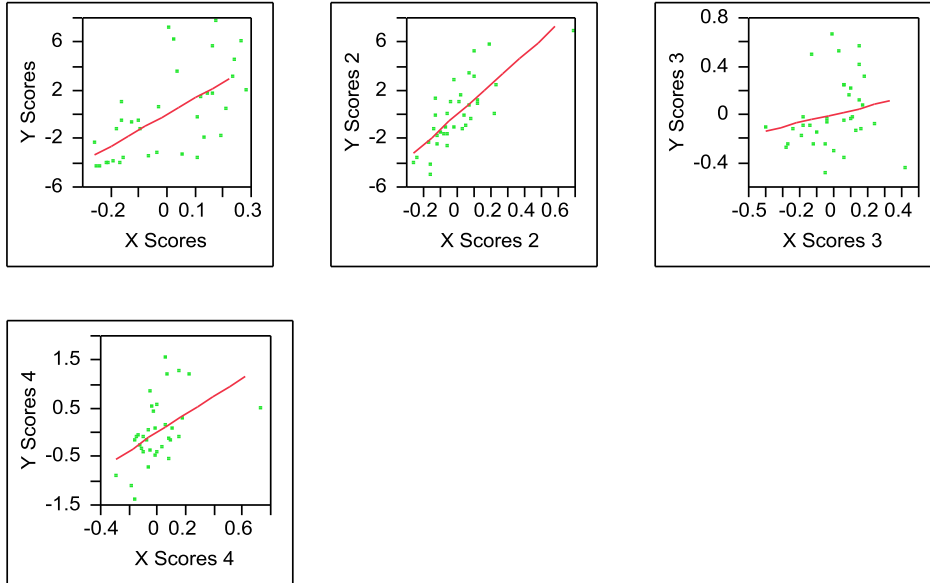
Coefficient	P	P
Intercept	0	
C (300 kHz)	-1.7479	
C (373 kHz)	-0.345821	
C (465 kHz)	0.6265049	
C (578 kHz)	1.0187633	
C (720 kHz)	1.2186472	
C (897 kHz)	0.9978556	
C (1117 kHz)	0.6347587	
C (1391 kHz)	0.6952059	
C (1732 kHz)	0.3973477	
C (2156 kHz)	-0.301553	
C (2684 kHz)	-0.927319	
C (3342 kHz)	-1.551418	
C (4161 kHz)	-0.402807	
C (5181 kHz)	-0.003541	
C (6451 kHz)	0.5536649	
C (8031 kHz)	0.0085567	

PLS for Variable Viable Cell Density

Number of Latent Factors

1 to max=12
4

X-Y Scores Plots



Percent Variation Explained

Number	X X	Cumulative X	Y Y	Cumulative Y
1	97.16	97.16	38.86	38.86
2	0.556	97.71	36.84	75.7
3	2.01	99.72	1	76.7
4	0.142	99.87	5.52	82.22
5	0.088	99.95	1.667	83.89
6	0.038	99.99	0.737	84.63
7	0.002	99.99	3.324	87.95
8	0.003	100	0.984	88.94
9	0.001	100	0.953	89.89
10	5e-4	100	0.818	90.71
11	4e-4	100	0.336	91.04
12	0.001	100	0.054	91.1

Cross Validation

Number	Prediction RMSE
1	0.809
2	0.628
3	0.548
4	0.505
5	0.525
6	0.674
7	0.785
8	0.817
9	1.255
10	1.374
11	1.314
12	1.279

Press Residuals

**Viable cell
density**
99491.596
33806.557
-633685.1
-12989.71
-222019.5
-19971.41
503511.04
685422.31
-280186.1
129698.04
-22415.98
122390.75
-497055.4
-450337.6
-170970.2
-265688.4
-231076.7
68094.863
-358198.3
48731.204
-262400.6
-154775.1
362327.59
687165.66
621186.46
-963300.2
400155.57
306267.16
-375701.9
925156.16
-202407.2
-296228.3
71894.711
-97732.39
-124090.2

Model Coefficients for Centered and Scaled Data

Coefficient	0	1
Intercept	0	
C (300 kHz)	-1.666674	
C (373 kHz)	-0.787904	
C (465 kHz)	-0.061355	
C (578 kHz)	0.4400162	
C (720 kHz)	0.773084	
C (897 kHz)	0.8551709	
C (1117 kHz)	0.8556998	
C (1391 kHz)	0.9254709	
C (1732 kHz)	1.0222318	
C (2156 kHz)	0.3857822	
C (2684 kHz)	-0.126361	
C (3342 kHz)	-0.955815	
C (4161 kHz)	-0.603821	
C (5181 kHz)	0.9613898	
C (6451 kHz)	-0.61458	
C (8031 kHz)	-0.89811	

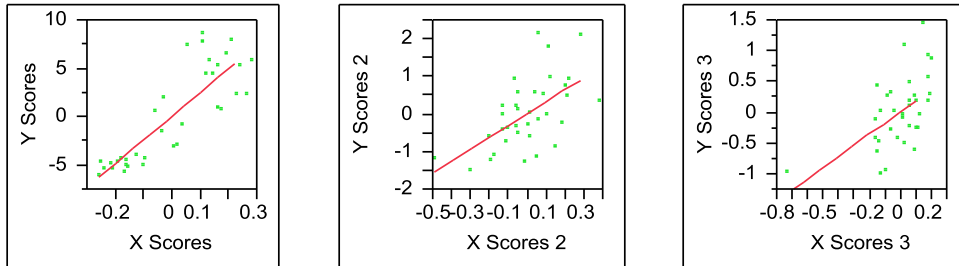
PLS for Variable Mean Cell Diameter

Number of Latent Factors

1 to max=10

3

X-Y Scores Plots



Percent Variation Explained

Number	X X	Cumulative X	Y Y	Cumulative Y
1	97.16	97.16	72.81	72.81
2	1.807	98.97	9.253	82.06
3	0.801	99.77	5.31	87.37
4	0.107	99.87	0.762	88.13
5	0.088	99.96	0.353	88.48
6	0.015	99.98	1.84	90.32
7	0.019	100	0.982	91.31
8	0.002	100	1.685	92.99
9	0.001	100	0.529	93.52
10	3e-4	100	0.76	94.28

Cross Validation

Number	Prediction RMSE
1	0.541
2	0.466
3	0.391
4	0.486
5	0.594
6	0.588
7	0.524
8	0.625
9	0.898
10	0.986

Press Residuals

Average cell
diameter

-0.070888
-0.740546
0.0916772
0.8672353
0.1718468
-0.197373
-0.855563
-1.31983
-0.444092
-0.738003
-0.009591
1.0598301
1.9181619
0.6912232
0.3740192
1.1706226
1.6345426
-0.736536
-0.491167
-0.246605
0.4185478
0.6090689
0.1574571
-0.36931
-0.616984
0.9093612
0.1308802
-0.099146
0.6971393
-1.224755
-0.268862
-0.27814
-1.277148
-0.723341
0.266387

Model Coefficients for Centered and Scaled Data

Coefficient	Average cell diameter	Average cell diameter
Intercept	0	
C (300 kHz)	0.6804086	
C (373 kHz)	0.5232333	
C (465 kHz)	0.3383111	
C (578 kHz)	0.1672908	
C (720 kHz)	0.0217488	
C (897 kHz)	-0.093554	
C (1117 kHz)	-0.193314	
C (1391 kHz)	-0.268585	
C (1732 kHz)	-0.297474	
C (2156 kHz)	-0.262377	
C (2684 kHz)	-0.265311	
C (3342 kHz)	-0.063878	
C (4161 kHz)	-0.089672	
C (5181 kHz)	0.0582055	
C (6451 kHz)	0.1354934	
C (8031 kHz)	0.5355391	

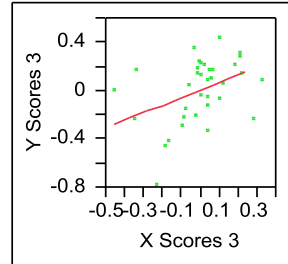
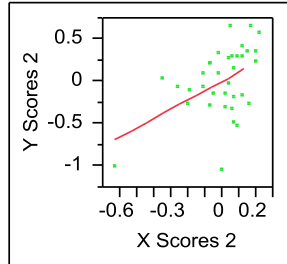
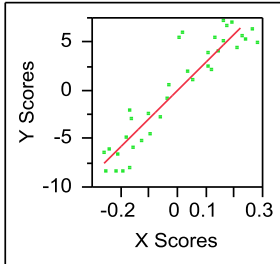
PLS for Variable L-glutamine

Number of Latent Factors

1 to max=8

3

X-Y Scores Plots



Percent Variation Explained

Number	X X	Cumulative X	Y Y	Cumulative Y
1	97.16	97.16	85.69	85.69
2	1.679	98.84	3.26	88.95
3	0.926	99.77	1.827	90.78
4	0.126	99.89	0.245	91.02
5	0.052	99.94	0.291	91.31
6	0.038	99.98	0.39	91.7
7	0.014	100	0.597	92.3
8	0.002	100	0.58	92.88

Cross Validation

Number	Prediction RMSE
1	0.394
2	0.361
3	0.347
4	0.409
5	0.464
6	0.469
7	0.428
8	0.422

Press Residuals

Glutamine concentration

0.5406117
 0.3197288
 0.1040153
 0.1340126
 0.41418
 0.3889714
 -0.319224
 0.325476
 0.8475678
 0.8001815
 0.2072992
 -0.265232
 -0.053673
 0.4904067
 0.1749101
 -0.095197
 -0.27612
 0.249237
 -0.169731
 -0.951199
 -0.799602
 -0.380194
 -0.780813
 -1.394838
 -0.703022
 0.8523726
 -0.427587
 -0.500207
 -0.427079
 -0.231552
 0.9464956
 0.2922589
 0.1135739
 0.4549265
 0.2861434

Model Coefficients for Centered and Scaled Data

Coefficient	Glutamine concentration	Glutamine concentration
Intercept	0	
C (300 kHz)	0.1900551	
C (373 kHz)	0.0881619	
C (465 kHz)	0.0115509	
C (578 kHz)	-0.066452	
C (720 kHz)	-0.130567	
C (897 kHz)	-0.179867	
C (1117 kHz)	-0.2244	
C (1391 kHz)	-0.257632	
C (1732 kHz)	-0.245928	
C (2156 kHz)	-0.244673	
C (2684 kHz)	-0.238004	
C (3342 kHz)	-0.133028	
C (4161 kHz)	-0.138653	
C (5181 kHz)	0.2006627	
C (6451 kHz)	0.1118749	
C (8031 kHz)	0.3615769	

Appendix H - Infection at Low MOI – Raw Data PLS Model Validation

Table H.1. Raw data PLS model validation – off-line analyses.

Process ID	Time Post Planting in h	pH	Total Cell Density in cells ml ⁻¹	Viable Cell Density in cells ml ⁻¹	Viability in %	Mean Average Cell Diameter in μm	D-glucose in mmol L ⁻¹	L-lactate in mmol L ⁻¹	L-glutamine in mmol L ⁻¹	L-glutamate in mmol L ⁻¹
Model	4.12	6.53	1.09E+06	1.02E+06	93.6	17.4	31.52753	1.276643	4.65	7.53
Validation	22.69	6.47	2.04E+06	1.92E+06	94.3	18.2	30.08437	1.054618	2.66	8.15
	48.54	6.42	2.04E+06	1.90E+06	93.0	22.5	27.03153	0.943606	0.52	8.99
	75.34	6.44	2.20E+06	1.75E+06	79.4	22.5	-	-	-	-

Table H.2. Raw data PLS model validation – dielectric spectroscopy.

Process ID	Time Post Planting in h	Biomass (1000 kHz) in pF cm ⁻¹	Suspension Conductivity in mS cm ⁻¹	Δε in pF cm ⁻¹	ε _r in kHz	alpha in -	C(300kHz) in pF	C(373kHz) in pF	C(465kHz) in pF	C(578kHz) in pF	C(720kHz) in pF	C(897kHz) in pF	C(1117kHz) in pF	C(1391kHz) in pF	C(1732kHz) in pF	C(2156kHz) in pF	C(2684kHz) in pF	C(3342kHz) in pF	C(4161kHz) in pF	C(5181kHz) in pF	C(6451kHz) in pF	C(8031kHz) in pF	C(10000kHz) in pF
Model	4.12	1.772037	15.3906231	6.91599	613	0.1	6.618226	5.581463	4.66713	3.782806	3.081171	2.426299	1.8574311	1.3789051	0.9847919	0.6892858	0.4732932	0.2895484	0.1469247	0.094945	-0.022048	-0.086472	-0.0928525
Validation	22.69	3.520216	15.3432503	14.6308	585	0.1	13.13961	11.23397	9.474277	7.829559	6.369656	5.052717	3.9275022	2.9870319	2.1929705	1.5756511	1.1776362	0.8144739	0.5455471	0.3693789	0.2290637	0.1335092	0.06996669
	48.54	8.369818	15.2468033	47.0937	468	0.1	34.74996	29.72658	24.82864	20.27864	16.15495	12.55817	9.611393	7.2206907	5.3465462	3.8561835	2.8636558	2.0535946	1.4513317	1.0276656	0.7158355	0.4905789	0.32089767
	75.34	9.605576	15.2318602	43.99	532	0.11	33.64694	29.32894	25.21212	20.99023	17.1005	13.65582	10.69285	8.1572828	6.1612539	4.4845371	3.4139037	2.481256	1.7880591	1.2813509	0.8961675	0.6105601	0.39529347

Appendix I - Medium Supplementation for Uninfected Sf-9 Clone Cell Cultures – Raw Data

Table I.1. Raw data medium supplementation for uninfected Sf-9 clone cell cultures – off-line analyses.

Process ID	Time Post Planting in h	pH	Total Cell Density in cells ml ⁻¹	Viable Cell Density in cells ml ⁻¹	Viability in %	Mean Average Cell Diameter in µm	D-glucose in mmol L ⁻¹	L-lactate in mmol L ⁻¹	L-glutamine in mmol L ⁻¹	L-glutamate in mmol L ⁻¹	PCF2 ORF2 Concentration in RP	
Control	4.12	6.53	1.09E+06	1.02E+06	93.6	17.4	31.52753	1.276643	4.65	7.53	-	
	22.69	6.47	2.04E+06	1.92E+06	94.3	18.2	30.08437	1.054618	2.66	8.15	-	
	48.54	6.42	2.04E+06	1.90E+06	93.0	22.5	27.03153	0.943606	0.52	8.99	-	
	75.34	6.44	2.20E+06	1.75E+06	79.4	22.5	-	-	-	-	-	
	95.12	6.52	2.11E+06	9.80E+05	46.4	20.7	24.81128	0.477353	0.6	9.17	-	
	117.46	6.60	2.29E+06	4.10E+05	17.9	18.8	24.58925	0	0.57	9.38	2.13	
	145.47	6.52	2.53E+06	1.90E+05	7.5	16.2	21.64742	1.443162	0.71	9.95	3.26	
	165.11	6.47	3.77E+06	4.60E+05	12.2	12.4	21.48091	1.52087	0.79	10.2	3.36	
	Feed	4.01	6.43	1.19E+06	1.06E+06	89.2	17.6	31.69405	1.087922	11.1	7.63	-
		22.55	6.39	1.99E+06	1.85E+06	93.1	17.8	30.3619	0.821492	8.59	8.23	-
48.43		6.13	2.33E+06	2.12E+06	90.8	22.1	27.58659	0.788188	5.94	9.24	-	
75.21		6.04	2.03E+06	1.32E+06	64.9	23.3	-	-	-	-	-	
95.00		6.02	2.05E+06	1.15E+06	56.1	22.2	22.25799	0.377442	3.09	10.7	-	
117.34		6.14	2.73E+06	3.80E+05	13.9	18.5	21.4254	0.643872	3	10.8	4.99	
145.35		6.17	3.16E+06	3.00E+05	9.5	14.5	20.03774	0.854796	2.23	11.1	5.78	
164.99		6.16	6.65E+06	1.53E+06	23.0	10.7	19.92673	0.932504	3.14	11.6	5.62	

Table I.2. Raw data medium supplementation for uninfected Sf-9 clone cell cultures – dielectric spectroscopy.

Process ID	Time Post Planting in h	Biomass (1000 kHz) in pF cm ⁻¹	Suspension Conductivity in mS cm ⁻¹	Δε in pF cm ⁻¹	f _c in kHz	alpha in -	C(300kHz) in pF	C(373kHz) in pF	C(465kHz) in pF	C(578kHz) in pF	C(720kHz) in pF	C(897kHz) in pF	C(1117kHz) in pF	C(1391kHz) in pF	C(1732kHz) in pF	C(2156kHz) in pF	C(2684kHz) in pF	C(3342kHz) in pF	C(4161kHz) in pF	C(5181kHz) in pF	C(6451kHz) in pF	C(8031kHz) in pF	C(10000kHz) in pF	
Control	4.12	1.772037	15.3906231	6.91599	613	0.1	6.618226	5.581463	4.66713	3.782806	3.081171	2.426299	1.8574311	1.3789051	0.9847919	0.6892858	0.4732932	0.2895484	0.1469247	0.094945	-0.022048	-0.086472	-0.0928525	
	22.69	3.520216	15.3432503	14.6308	585	0.1	13.13961	11.23397	9.474277	7.829559	6.369656	5.052717	3.9275022	2.9870319	2.1929705	1.5756511	1.1776362	0.8144739	0.5455471	0.3693789	0.2290637	0.1335092	0.06996669	
	48.54	8.369818	15.2468033	47.0937	468	0.1	34.74996	29.72658	24.82864	20.27864	16.15495	12.55817	9.611393	7.2206907	5.3465462	3.8561835	2.8636558	2.0535946	1.4513317	1.0276656	0.7158355	0.4905789	0.32089767	
	75.34	9.605576	15.2318602	43.99	532	0.11	33.64694	29.32894	25.21212	20.99023	17.1005	13.65582	10.69285	8.1572828	6.1612539	4.4845371	3.4139037	2.481256	1.7880591	1.2813509	0.8961675	0.6105601	0.39529347	
	95.12	8.671052	15.2587042	33.058	619	0.1	26.99294	23.97098	20.92532	17.84129	14.81455	12.03302	9.5526619	7.3948669	5.6394968	4.1365895	3.2161226	2.3872724	1.7606514	1.2872435	0.9501884	0.6875886	0.48140889	
	117.46	4.642787	15.3392248	16.6109	642	0.12	14.33879	12.63733	11.01181	9.386242	7.864574	6.420316	5.1395712	4.0826769	3.1811836	2.3027129	1.9035246	1.4518582	1.0857714	0.8243457	0.5977089	0.4279186	0.29034355	
	145.47	1.55443	15.4455681	3.50682	1014	0.11	4.628018	3.995035	3.502506	3.058959	2.633806	2.241779	1.8916332	1.6158381	1.3418291	0.9709244	0.9631108	0.7803788	0.6319814	0.4976793	0.4160866	0.3391576	0.26114056	
	165.11	0.994966	15.4922056	2.05828	1138	0.1	3.207094	2.714792	2.326603	2.010926	1.71436	1.454457	1.2376629	1.0834	0.9082126	0.601979	0.6714909	0.536634	0.4333783	0.3388367	0.2789753	0.220995	0.15521973	
	Feed	4.01	0.823237	15.4185591	3.27979	646	0.1	2.060111	1.938161	1.749458	1.672286	1.278595	1.171813	0.8385067	0.6300283	0.4582248	0.3109188	0.218081	0.1514564	0.0521164	0.0505116	0.0269404	0.0052156	-0.0029247
		22.55	2.153198	15.3785391	9.53545	564	0.09	7.661045	6.693769	5.702089	4.692727	3.841083	3.052455	2.3560515	1.7721763	1.2958384	0.8550239	0.6030426	0.4117906	0.2656438	0.1656144	0.0993774	0.0577872	0.05167937
48.43		6.455876	15.3095207	41.3147	439	0.09	29.87471	25.33142	20.85945	16.78102	13.2068	10.16756	7.6845012	5.7372232	4.2026281	2.9672279	2.1695633	1.567426	1.117018	0.7877698	0.58375	0.4206245	0.32427764	
75.21		8.506663	15.2577858	47.2624	461	0.11	32.38194	28.20683	23.84612	19.66783	15.83775	12.50804	9.7180367	7.4398599	5.6119099	4.0267444	3.0463443	2.2554195	1.6474712	1.1939297	0.869417	0.6225355	0.4689962	
95.00		9.543404	15.2166681	40.1308	577	0.1	30.83285	27.56336	23.94574	20.3618	16.76596	13.55187	10.676249	8.267273	6.2253094	4.5915389	3.5294318	2.6719401	2.012152	1.4928575	1.139622	0.8695662	0.66611266	
117.34		1.999394	15.3496342	5.78911	769	0.11	5.261179	4.942243	4.419866	3.876546	3.357001	2.877297	2.4349818	2.0647516	1.6845837	1.2482677	1.1475291	0.9662521	0.812916	0.667553	0.5711286	0.4771025	0.40966392	
145.35		-0.27777	15.4431286	1E-08	500	0.1	-0.61087	-0.46169	-0.42877	-0.37647	-0.25173	-0.14917	-0.025417	0.0840559	0.1374669	0.0248504	0.2093968	0.2536871	0.2596424	0.2492704	0.2580044	0.2400136	0.23058367	
164.99		-0.83453	15.5050545	1E-08	500	0.1	-1.85425	-1.60221	-1.50087	-1.36425	-1.1645	-0.92244	-0.692281	-0.471188	-0.306989	-0.377954	-0.114439	-0.015149	0.0396934	0.0736544	0.1029656	0.1165752	0.14023018	